IN-34-CR

Final Report

SRM Internal Flow Tests
and
Computational Fluid Dynamic Analysis

Volume IV
Cold Flow Analyses and CFD Analysis Capability Development

November, 1995

Prepared for:
George C. Marshall Space Flight Center
National Aeronautics and Space Administration
Marshall Space Flight Center, AL 35812

Contract NAS8-39095

Prepared by:
ERC, Incorporated
555 Sparkman Drive, Suite 1622
Huntsville, AL 35816

Table of Contents

Volume II

Volume III

Volume IV

3.3 Cold Flow Analyses

3.3.1 **Checkout Model Analysis**
3.3.2 **ASRM/Technology Model**
3.3.3 **ASRM Aft Section/Nozzle Model**
3.3.4 **ASRM Aft Segment/Nozzle Water Flow Model**
3.3.5 **SAF Loss of Storage Tank Investigation**
3.3.6 **SAF Model Test Plan**
3.3.7 **ASRM Igniter Exhaust Port Model**
3.3.8 **RSRM Nozzle Slag Ejection Precursor Tests**
3.3.9 **RSRM Scaled Nozzle Slag Ejection Model**
3.3.10 **RSRM Inhibitor Dynamics Model**
3.3.11 **RSRM 10% Scale Cold Flow Model**

3.4 CFD Analysis Capability Development

3.4.1 κ–ε **Equation Coefficients Adjustment**

Checkout Model Design and Analysis Work

An evaluation of the effect of model inlet air temperature drift during a test run was performed to aid in the decision on the need for and/or the schedule for including heaters in the SRMAFTE. The Sverdrup acceptance test data was used to determine the drift in air temperature during runs over the entire range of delivered flow rates and pressures. The effect of this temperature drift on the model Reynolds number was also calculated. It was concluded from this study that a 2% change in absolute temperature during a test run could be adequately accounted for by the data analysis program. A handout package of these results was prepared and presented to ED35 management.

During the process of analyzing the Series I test data, it was determined that the pressure ratio, p/p_0, at the model throat was significantly lower than the 1-D theoretical ratio of 0.528. The physical measurement hardware and software were checked first to be sure the pressure measurement was not due to bad calibration or a faulty gauge. The CFD solution for the checkout model was then checked to determine if there was a physical basis for the lower measured pressure ratio. The CFD solution showed that significant 2-D effects were present in the model nozzle throat region where the measurement was taken. The analysis showed that the pressure was not constant across the throat plane of the model nozzle. The pressure at the wall was significantly lower than the motor center line pressure. Since the 2-D effects are of such a large magnitude in the model nozzle, the static pressure measurement at the throat could not be used to accurately determine the model mass flow rate.

A check was made at several other locations throughout the checkout model to determine where significant 2-D effects exist across the model chamber from the centerline to the wall. The pressure across the model port is constant at the spool piece #3 measurement station. This location will provide a very good 1-D pressure measurement in the model. Also, the CFD solution at the metering nozzle throat was checked. It was found that there is a much smaller 2-D effect observed at the metering nozzle throat than at the model nozzle throat. This was due to the smaller entrance angle and larger radius of curvature of the metering nozzle design.

A final report was written by ERC to document the testing and analysis done in Series I testing. The conclusions from that report are included here for reference, as are some of the tables and figures, which follow this discussion. Due to the large size of the report a complete copy is not provided but the report can be referenced by ERCI/HSV-TR92-01.

First, the flow appears to evenly distribute between three of the arms of the model. A comparison cannot be determined for all four arms as the Bottom South arm was not instrumented in such a way as to provide flow rate data.

It is noted that the metering nozzle flowrates are slightly low for the 1200 psi and 900 psi, Mode A test runs. These flowrates were calculated using one-dimensional flow

analysis with a discharge coefficient of 1.00 and are calculated to be less then the facility flowrate. Table 2 lists the calculated discharge coefficients for the Mode A metering nozzle tests for the Series I Data and the Sverdrup Acceptance Data. Some scatter in the data is noted with a high value of 1.003 and a low value of 0.979. The average value for the metering nozzle coefficient is 0.993 for the Series I Test Data.

The discharge coefficients listed in Table 3 for the model nozzle were determined for both the Series I Test Data and the Sverdrup data. The average discharge coefficient for Series I and Sverdrup are 0.977 and 0.973, respectively. This corresponds to an 0.41 percent difference. The Sverdrup data contains two low values of 0.935 and 0.877. These values are not included in the afore mentioned average. In addition, the Series I point of 0.927 was not included in the average.

Comparisons between the calculated model exit static pressure and the actual model exit static pressure for each test condition provided a good indication as to whether or not the flow was attached to the nozzle at the exit plane. The flow remains attached to the nozzle at the exit plane for all cases except the two lowest flowrates of 20 and 40 lbm/sec for both Mode A and B.

Figure 3 is a diffuser performance map in which the ratio of diffuser static pressure to ambient pressure is plotted versus the ratio of model aft total pressure to ambient pressure. It was observed that the diffuser was started for all cases except for mass flowrates of 20 and 40 lbm/sec. This can be seen by examining the data in Table 4.

The paper "Facility For Cold Flow Testing of Solid Rocket Motor Models," co-authored with D. L. Bacchus ED/33 and O. E. Hill ED/35 was successfully presented at the 1992 JANNAF Propulsion Meeting held in Indianapolis, Indiana on February 24th through 27th. Several questions were asked regarding facility availability, instrumentation, and the CFD analysis. The paper is included here for reference.

The Series II Proposed Test Plan Draft was reviewed and approved by ED33 and ED35 personnel. A final, revised version of the Proposed Test Plan was then delivered to NASA. Included in this report are an introduction explaining the history of the Solid Rocket Motor Air Flow Equipment (SRMAFTE) and describing the range of calibration tests that were planned for Checkout Model 538. These calibrations were divided into two groups, Series I and Series II. Series II testing consisted of substantially more instrumentation on Checkout Model 538 than its predecessor Series I. The Series II testing will provide a more detailed knowledge of the test equipment and its operational characteristics. Total, static, differential, dynamic, and velocity pressures as well as static and skin temperatures were measured throughout the system. Performance calculations were made with the test data to quantify the flow characteristics of the SRMAFTE. The pre-test report is included here to provide a detailed discussion of the model.

A request was made by ED35 to divide the existing Proposed Test Plan for Series II calibration into two shorter calibration tests to expedite the initiation of the ASRM Aft Section/Nozzle Model cold flow testing. The two new calibration tests were called Series IIa and Series IIb. The new tests were to be scheduled between the ASRM Aft Section/Nozzle Model testing and the ASRM Technology Model testing. The test objectives from the Proposed Test Plan for Series II calibration were divided according to the requirements of the ASRM Aft Section/Nozzle Model and the ASRM Technology Model tests. Series IIa calibration testing was to be conducted before the proposed ASRM Aft Section/Nozzle Model testing and was designed to include all the test objectives that affect the ASRM Aft Section/Nozzle Model tests. Likewise, Series IIb Calibration testing was to include all of the test objectives that would affect the ASRM Technology Model tests. Both of the new calibration tests required additional skin thermocouples to evaluate the thermal characteristics of the SRMAFTE due to safety considerations.

Series II data was transferred via modem from the NASA/MSFC VAX computer to ERC. As of the end of the month ERC is still waiting for the remaining data to be put on the VAX for modem transfer. The data was run through the data performance program written by ERC. When this was done, some inconsistencies were found in the format of the data files sent to ERC. These problems were worked out with the help of R. Wales, ED35. Some minor changes were made to the Series II Data Performance Program to reflect differences in the instrumentation in different test runs. Meetings were held with NASA/MSFC personnel in order to disseminate the information generated by ERC and possible problems with Series II data. Data plots were provided to NASA/MSFC personnel as they became available. The final report on this model was to be written by NASA/MSFC personnel.

A temperature study was also done on the SRMAFTE test equipment to determine if the reduced temperature of the air flowing trough the facility would pose a safety risk. This analysis was done using the Joule-Thompson effect to determine the temperature drops of the air at different locations as it passes through the facility. This study showed that at an initial tank temperature of 60 °F the air temperature would only drop to approximately 10 °F in the diffuser.

Table 1.   Formulas Used in Performance Calculations

Mach Number	$\dfrac{A}{A^*} = \dfrac{1}{M} \left[\left(\dfrac{2}{K+1}\right)\left(1+\dfrac{K-1}{2}M^2\right)\right]^{\frac{K+1}{2(K-1)}}$
Total Pressure	$\dfrac{Po}{P} = \left(1+\dfrac{K-1}{2}M^2\right)^{\frac{K}{K-1}}$
Total Temperature	$\dfrac{To}{T} = 1 + \dfrac{K-1}{2}M^2 \quad (To = {}^\circ R)$
Flowrate~	$\dfrac{W}{A^*}\dfrac{\sqrt{To}}{Po} = 0.53175 \quad \text{(using a value cd=1)}$

These equations use the values of K=1.4 and R=53.35ft lbf/lbm °R, as corresponds to air.

~This equation uses:

$$W = \frac{lbm}{sec},\ A^* = ft^2 \quad To = {}^\circ R \quad Po = \frac{lbf}{ft^2}$$

Table 2. Metering Nozzle Discharge Coefficients

Manifold Pressure (psia)	Mode	Sverdrup	Series I
1200	A	0.980	0.979
900	A	N/A	0.978
600	A	N/A	0.978
450	A	N/A	0.971
300	A	N/A	0.979
75	A	0.901	**

** Data irregular

Table 3. Model Nozzle Discharge Coefficients

Manifold Pressure (psia)	Mode	Sverdrup	Series I
1200	A	1.010	1.003
900	A	0.976	1.000
600	A	0.965	0.993
450	A	0.962	0.979
300	A	0.959	0.988
75	A	0.935 *	**
610	B	0.980	0.985
300	B	0.990	0.975
150	B	0.877 *	0.978
75	B	0.966	0.968
38	B	0.977	0.927 *

* Not included in average
** Data irregular

Table 4. Model Diffuser Performance Summary

Nominal Flow Rate (lbm/sec)	Mode	Diffuser Pressure/ Model Total Pressure	Diffuser Pressure/ Ambient Pressure
320	A	0.011	0.446
240	A	0.010	0.317
160	A	0.010	0.219
120	A	0.010	0.162
80	A	0.011	0.112
20	A	0.292	0.810
320	B	0.011	0.420
160	B	0.011	0.216
80	B	0.011	0.108
40	B	0.094	0.488
20	B	0.303	0.819

Figure 1. Checkout Model Cutaway Instrumentation Locations
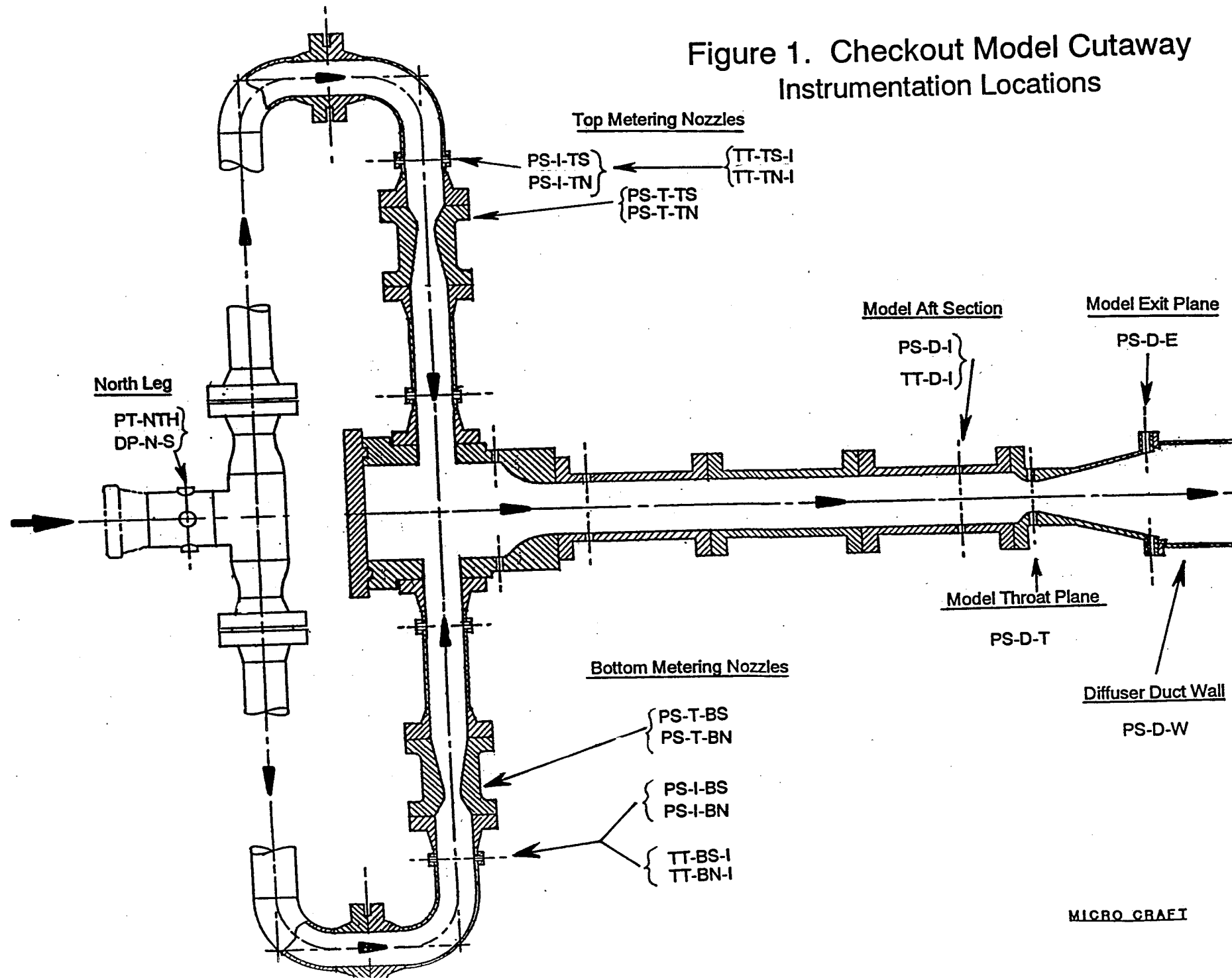
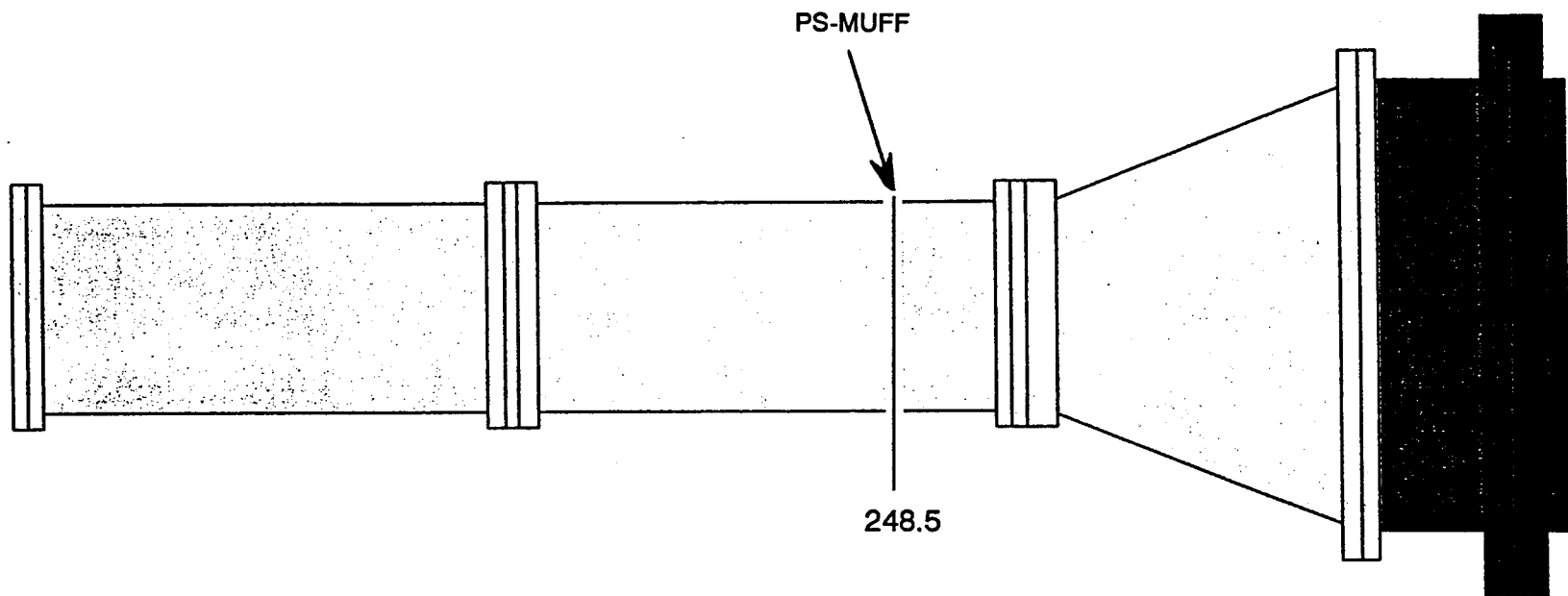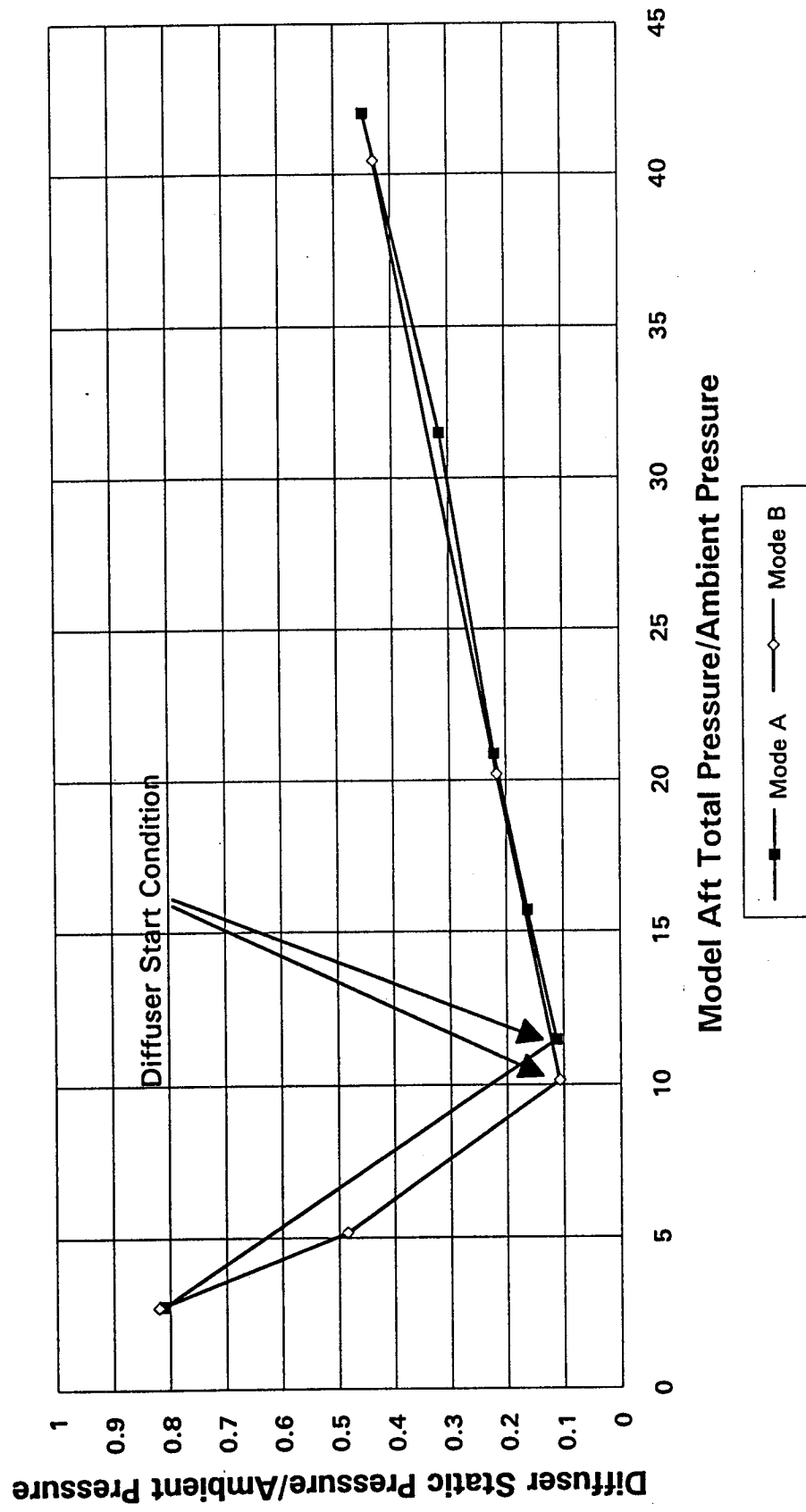# Figure 2. Checkout Model Diffuser
Instrumentation Location

PS-MUFF

248.5

Figure 3. Diffuser Performance Map

ERCI 5/5/92

2-D Effects in the Checkout Model Nozzle

During the process of analyzing the Series I test data, it was determined that the pressure ratio, p/p_o, at the model throat was significantly lower than the 1-D theoretical ratio of 0.528. The physical measurement hardware and software were checked first to be sure the pressure measurement was not due to bad calibration or a faulty gauge. The CFD solution for the checkout model was then checked to determine if there was a physical basis for the lower measured pressure ratio. The CFD solution showed that significant 2-D effects were present in the model nozzle throat region where the measurement was taken. Figure 1 shows the static pressure contours in the model nozzle. The curvature of the pressure contours shows that the pressure is not constant across the throat plane of the model nozzle. The pressure at the wall is significantly lower than the motor center line pressure. Figure 2 shows a plot of the pressure ratio across the model throat from the centerline to the wall. Since the 2-D effects are of such a large magnitude in the model nozzle, the static pressure measurement at the throat cannot be used to accurately determine the model mass flow rate. Also shown on this figure are the Series I, mode A test data point pressure ratios for two tests. The 1200 psi target pressure run and the 75 psi target pressure run from Series I testing are shown.

A check was made at several locations throughout the checkout model to determine where significant 2-D effects exist across the model channel from the centerline to the wall. The pressure across the motor channel is constant at the spool piece #3 measurement station. This is shown in Figure 3. This location will provide a very good 1-D pressure measurement in the model. Also, the CFD solution at the metering nozzle throat was checked. Figure 4 shows that there is a much smaller 2-D effect observed at the metering nozzle throat than at the model nozzle throat. This is due to the smaller entrance angle and larger radius of curvature of the metering nozzle design.
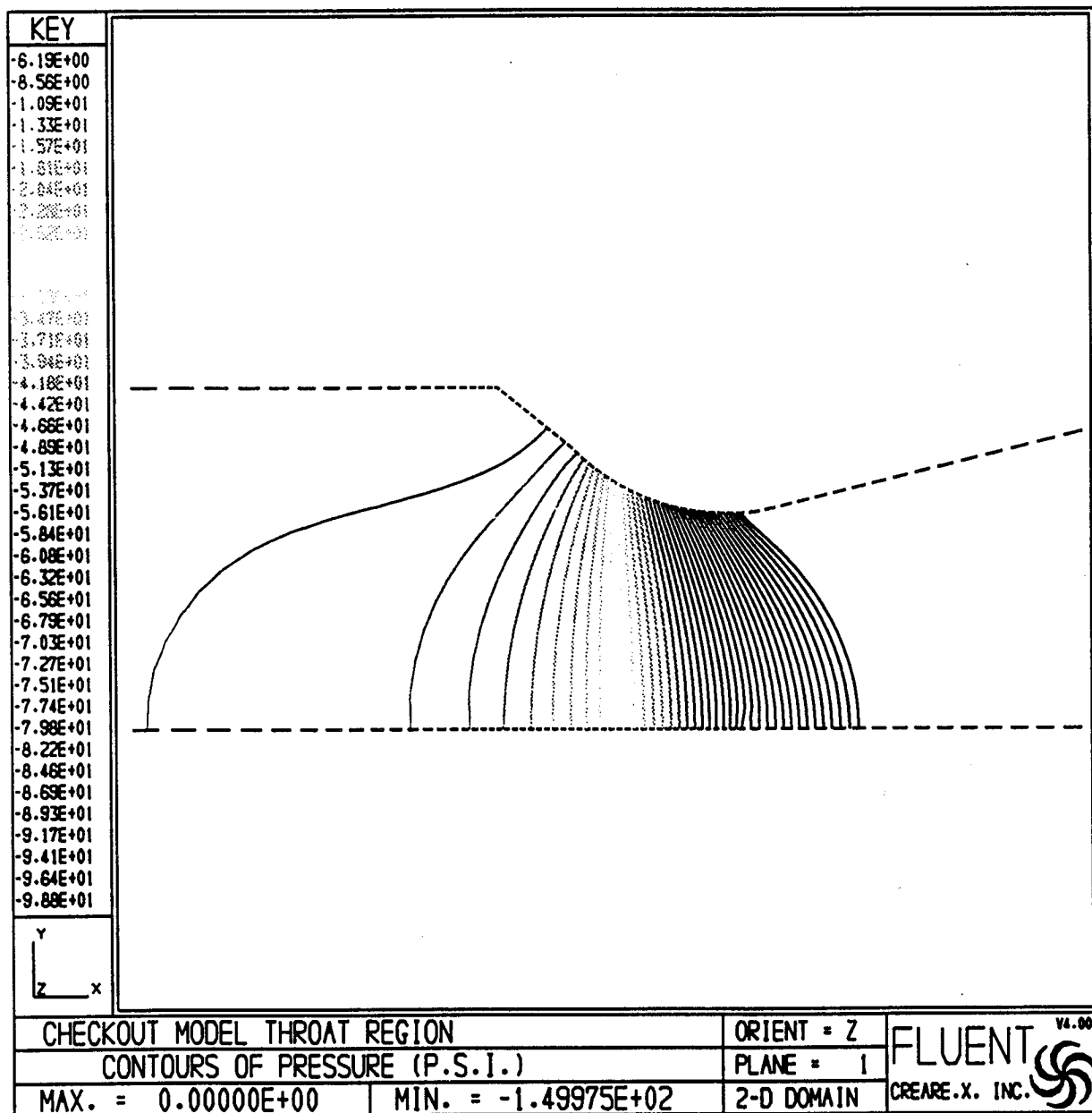
Figure 1. Static Pressure Contours in the Checkout Model Nozzle

Figure 2. Checkout Model Throat Plane CFD Presssure Profile

Entrance Angle = 45 Deg
Radius of Curvature = 1.00
Contraction Ratio = 2.503

Pressure Ratio P/Po (vertical axis, 0.300 to 0.650)

Normalized Radial Distance, r/Rwall (horizontal axis, 0.0 to 1.0)

Legend:
- CFD Prediction
- 1-D Throat Pressure Ratio
- Mode A 1200 psia Run
- Mode A 75 psia Run

ERCI - 10/8/91

Figure 3. Spool Piece Number Three Radial Pressure Profile
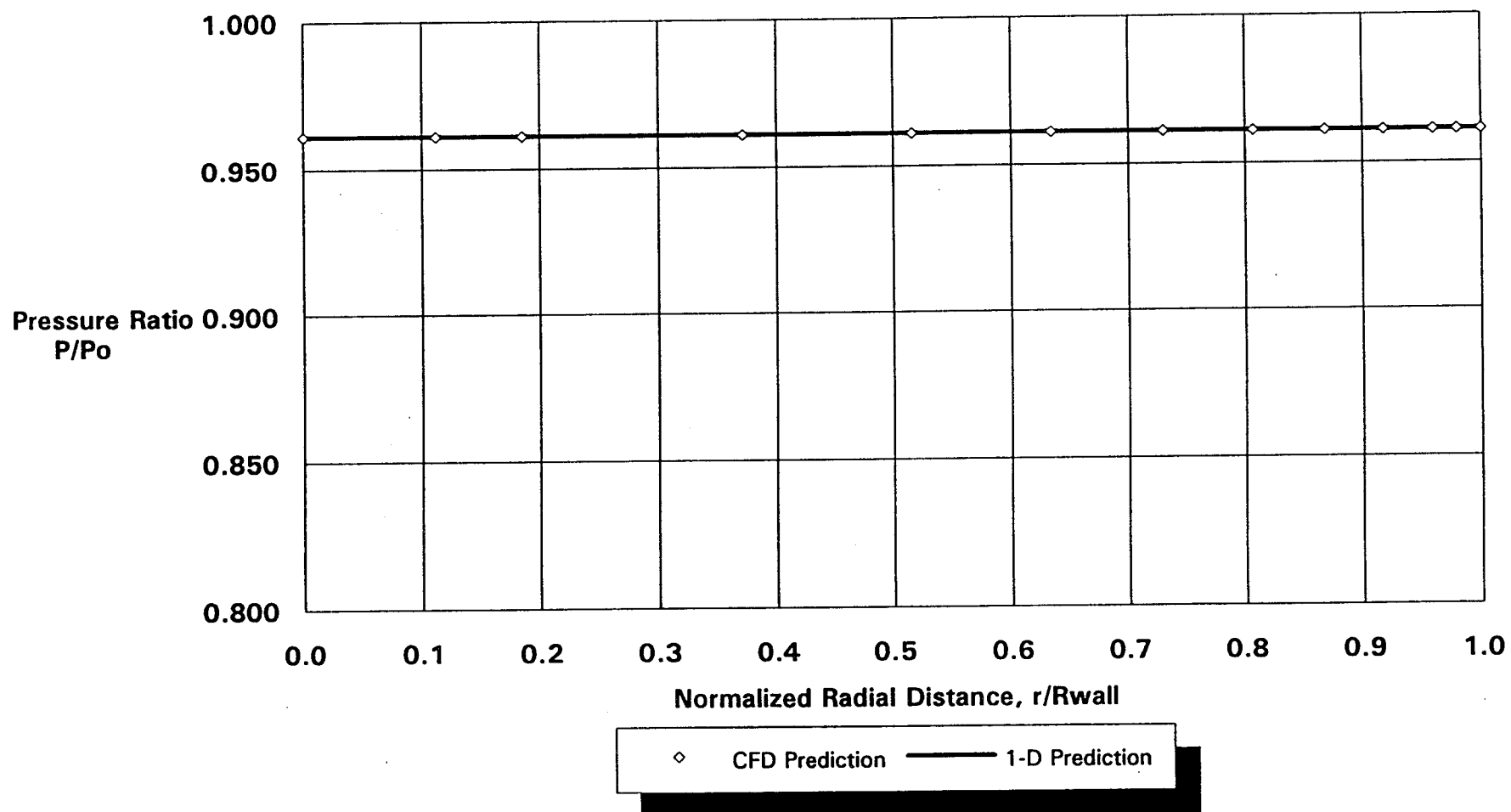
Figure 4. Metering Nozzle Radial Pressure Profile

(Just Upstream of Pressure Tap)

Entrance Angle = 30 Deg
Radius of Curvature = 4.17
Contraction Ratio = 9.003

Pressure Ratio
P/Po

Normalized Radial Distance, r/Rwall

Angle A, 0 Deg   Angle N, 180 Deg   1-D Throat Pressure Ratio
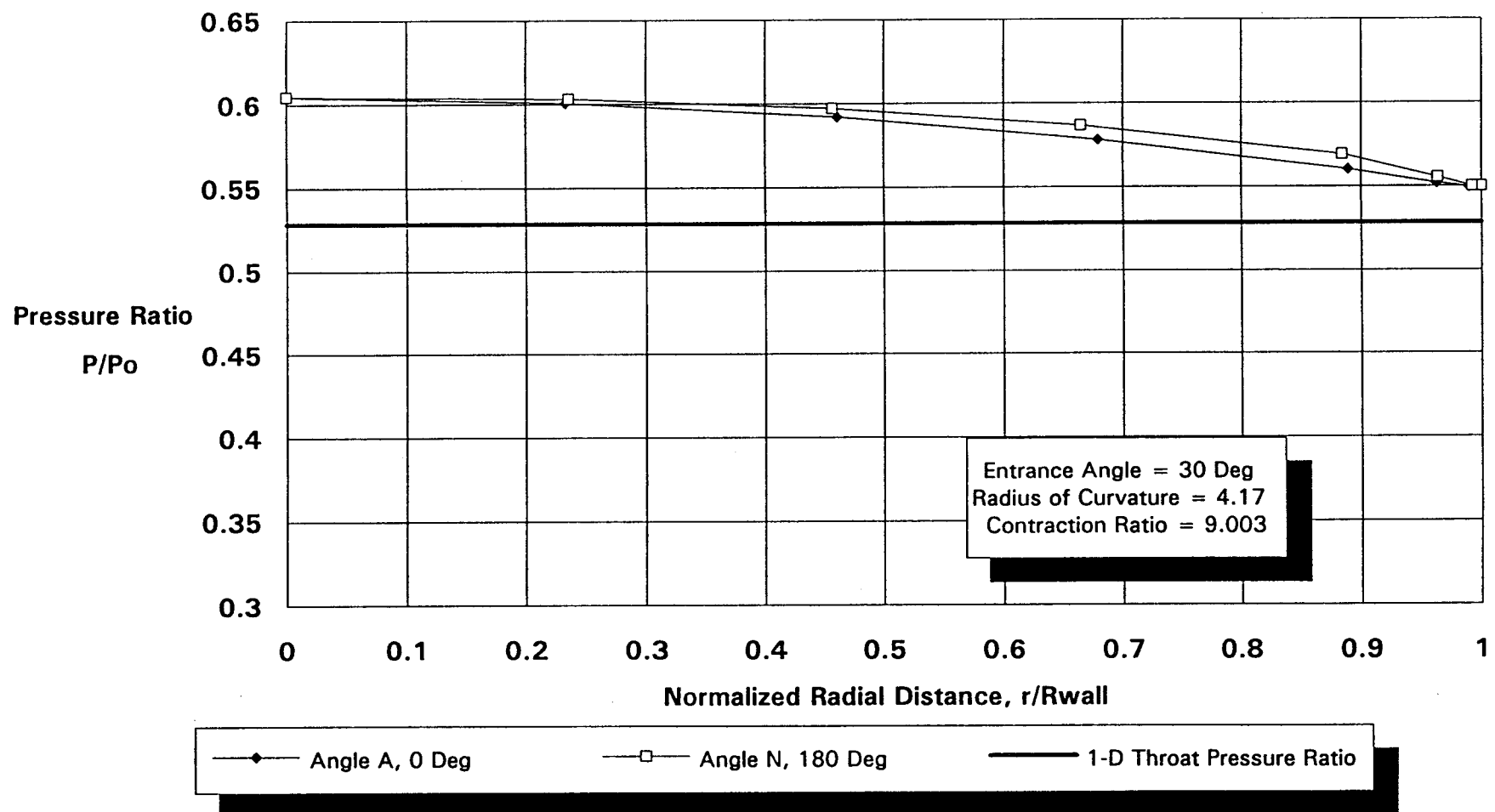
FACILITY FOR COLD FLOW TESTING OF SOLID ROCKET MOTOR MODELS

D. L. Bacchus and O. E. Hill
NASA Marshall Space Flight Center
Huntsville, Alabama
and
R. H. Whitesides
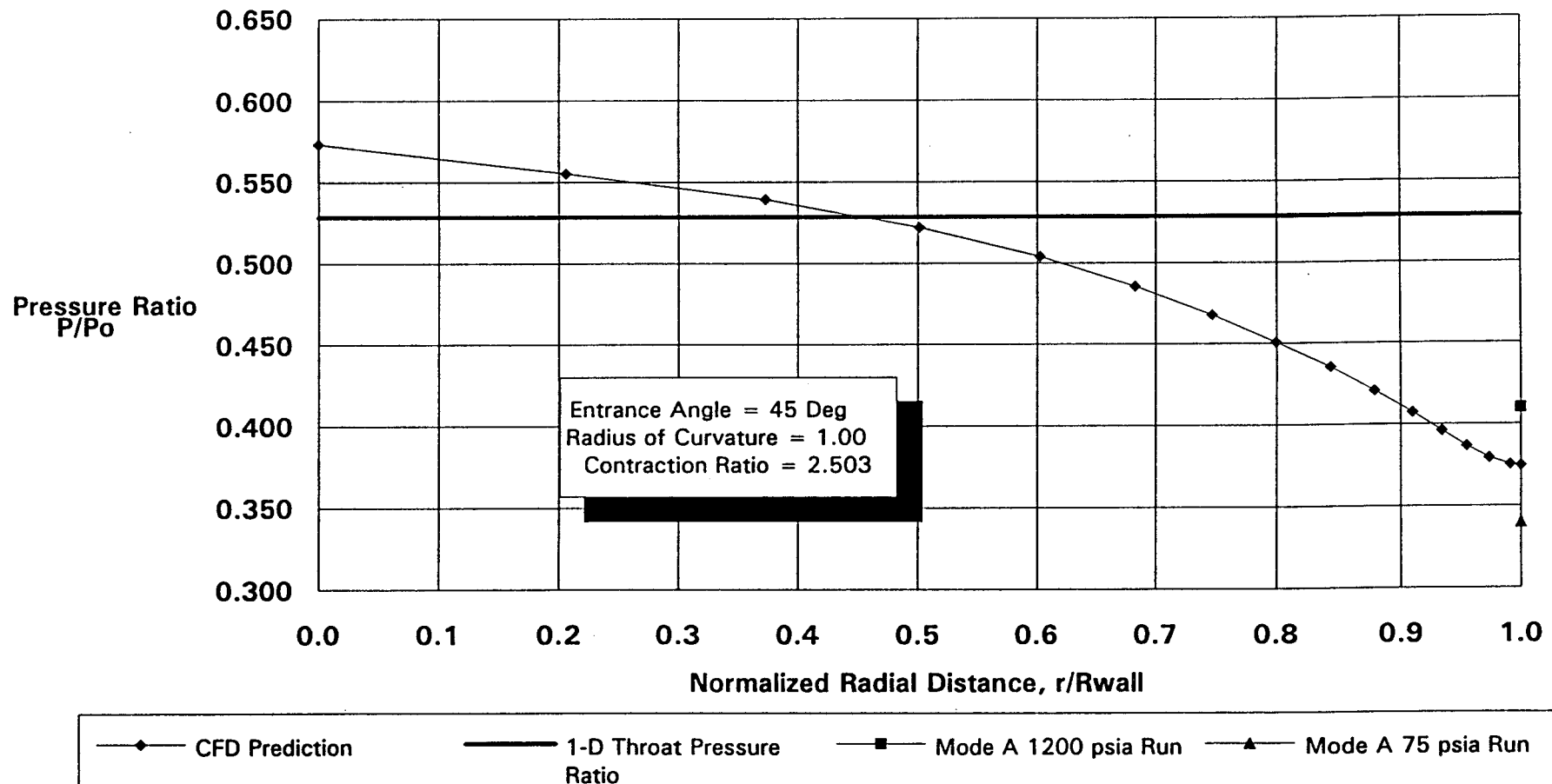ERC, Incorporated
Huntsville, Alabama

ABSTRACT

A new cold flow test facility has been designed and constructed at NASA Marshall Space Flight Center for the purpose of characterizing the flow field in the port and nozzle of solid propellant rocket motors (SRM's). A National Advisory Committee was established to include representatives from industry, government agencies and universities to guide the establishment of design and instrumentation requirements for the new facility. This facility design includes the basic components of air storage tanks, heater, submicron filter, quiet control valve, venturi, model inlet plenum chamber, SRM model, exhaust diffuser, and exhaust silencer. The facility was designed to accommodate a wide range of motor types and sizes from small tactical motors to large space launch boosters. This facility has the unique capability of testing ten percent scale models of large boosters such as the new Advanced Solid Rocket Motor (ASRM), at full scale motor Reynolds Numbers.

Previous investigators have established the validity of studying basic features of solid rocket motor internal flow fields using subscale cold flow models. The purpose of cold flow testing and payoff benefits to solid rocket motor development programs include the acquisition of data to 1) directly evaluate and optimize the design configuration of the propellant grain, insulation, and nozzle and to 2) provide data for validation of the computational fluid dynamics, (CFD), analysis codes and the performance analysis codes.

A facility checkout model was designed, constructed and utilized to evaluate the performance characteristics of the new facility. This model consists of a cylindrical chamber and converging/diverging nozzle with appropriate manifolding to connect it to the facility air supply. It was designed using chamber and nozzle dimensions to simulate the flow in a 10 percent scale model of the ASRM. The checkout model has recently been tested over the entire range of facility flow conditions which include flow rates from 9.07 to 145 kg/sec (20 to 320 lbm/sec) and supply pressures from 5.171×10^5 to 8.274×10^6 Pa (75 to 1200 psia). The performance of the self-pumping exhaust diffuser has been verified down to exhaust pressures of 1.379×10^4 Pa (2 psia). The facility has been successfully operated over the entire range of design pressures and flowrates and is available for national use by industry and government agencies requiring facilities capable of testing SRM cold flow models to support development programs or resolve problems arising on operational flight systems.

INTRODUCTION

Solid propellant rocket motors have historically been developed, produced, and put into service without a detailed knowledge of the structure of the internal flow field and the associated thermal and pressure loads on the bounding surfaces. Motor performance analyses have largely been based on one-dimensional, single phase flow in the port and, in some cases, two-dimensional, two-phase flow in the nozzle. Two- and three-dimensional flow effects in the motor port and nozzle entrance regions have been neglected unless a specific, related design problem occurs during the development program. Multi-dimensional flow field effects can result in pressure loads on the propellant grain and thermal loads on insulation which are significantly different from loads predicted by one-dimensional analyses. Critical design problems can result from incomplete knowledge of these loads.

Approved for public release; distribution is unlimited.

The severe aerothermal environment internal to a solid propellant rocket motor precludes the direct measurement of flow field parameters in a motor test and the direct measurement of propellant surface pressures is precluded by the nature of the live propellant geometry changes during burnback. Computational fluid dynamics (CFD) analyses are becoming available to predict the two- and three-dimensional aspects of the flow field in the rocket motor port. However, the experience base of applying these computer analyses to solid propellant rocket motors is limited and validation of the turbulence models and parameters for solid rocket motor flows is also limited.

The use of subscale cold flow models to study the flow field in the rocket motor chamber and nozzle has gained wide acceptance in the propulsion industry. Flow through various porous wall materials has been used to simulate the flow from the burning propellant gases. Early experiments to simulate the injection driven chamber flow field for a solid rocket motor were conducted by Dunlap, et al., [1]. This experimental work succeeded in verifying the velocity profile predicted by Culick [2] for the inviscid flow in a cylindrical port rocket chamber. It was also shown that Culick's analytical solution satisfies the viscous equations of motion. Beddini [3] predicted the transition of the velocity profile from a Culick laminar type to a steeper turbulent profile at sufficient downstream distances where a critical centerline Reynolds number was exceeded. This phenomena was verified by Dunlap, et al., [4] in a cylindrical port cold flow model. These studies have particular relevance to erosive burning as the near surface mean velocity profile and turbulence characteristics affect heat feedback to the propellant surface and hence burning rate.

The characterization of the flow field in rocket motor ports with specific geometric complexities has also been accomplished with subscale cold flow models. Extensive studies of the flow fields in Titan solid rocket boosters has been performed at United Technologies/Chemical Systems Division with subscale porous wall models using ambient temperature nitrogen [5,6,7,8]. The measured mean velocity and turbulence components provided valuable information for improving the accuracy of ballistic performance, materials erosion and propellant loads analyses. This work has provided significant insights into the role of flow induced instabilities in driving acoustic pressure oscillations and in developing motor design guidelines to avoid these problems. The flow field in the aft end of the Space Shuttle SRM was studied by Waesche, et al., [9] using a water flow model capable of simulating various nozzle gimbal angles and motor burn times. The circumferential flow in the aft end of the Space Shuttle SRM was also studied by Whitesides, et al., [10] using a 7.5 percent scale model with ambient air flow in the NASA/MSFC wind tunnel complex. The same basic model was also used to measure the convective heating around the submerged nozzle nose region at various nozzle gimbal angles [11]. Another version of the same model was further used to study the circumferential flow at the aft field joint of the Space Shuttle SRM due to asymmetric erosion of the propellant inhibitor stubs [12]. Studies at the Atlantic Research Corporation of the effects of various propellant configuration options for the Advanced Solid Rocket Booster on the flow field and motor performance were performed by Waesche, et al., [13,14] using both water and air cold flow models. All of the above studies were invaluable in providing an understanding of complex three-dimensional flow fields and in providing information for improving solid rocket motor design by reducing risk and improving performance.

FACILITY PURPOSE

The development of high performance, cost-effective and reliable solid propellant propulsion systems requires an understanding of the motor internal flow processes. The structural and thermal loads on propellant and insulation components are a direct result of the internal flow processes. In many cases, rocket motor internal flow experiments are prohibitively expensive and cannot be adequately instrumented due to the severe combustion environment. Thus a properly simulated cold flow experiment can give valuable engineering insight into complicated flows occurring in actual motors.

Therefore, a need existed for a national solid rocket motor test facility to evaluate the internal flow fields in a wide variety of rocket motor sizes and types for both industry and government users. The characterization of the internal flow fields in SRM's will provide data for the direct evaluation and optimization of particular design configurations as well as provide validation data for the CFD models. Many typical problems experienced with advanced rocket motor designs can be eliminated if cold flow experiments and accompanying analyses are performed as part of the design development program. Specific benefits to the SRM development program are 1) optimization of the design with respect to a balance between performance, cost effectiveness, and reliability and safety, 2) reduced design risk before commitment to large full scale hardware procurement, and 3) a readily available test model for resolving any design problems that may arise.

Specific data objectives for cold flow model testing can be grouped into the three categories of those affecting 1) motor performance and ballistics, 2) propellant and component structural loads and 3) insulation heating and erosion. Cold flow model data directly related to motor performance issues includes 1) data on flow uniformity and pressure distribution which affects local burn rate including identification of erosive burning zones, 2) slot/port flow interactions, 3) flow separations which affect turbulence generation and combustion chamber pressure oscillation, 4) nozzle flow efficiency, and 5) aerodynamic thrust vector alignment for canted and gimballed nozzles. Cold flow model data

directly useful in structural analyses includes 1) propellant grain pressure loads for slots and aft faces where flow fields are complex, 2) nozzle insulation component pressure loads where significant 2-D and 3-D effects are present, and 3) aerodynamic blowoff loads, side loads, and torque loads on nozzle, bearing and actuator components. Cold flow model data useful in evaluation of insulation heating and erosion includes 1) distribution of wall mass velocity over motor and nozzle insulation surfaces, 2) measurement of convective heat transfer coefficients, boundary layer characteristics, and local turbulence characteristics, and 3) determination of particle impingement trajectories.

FACILITY REQUIREMENTS

The Marshall Space Flight Center has developed a national cold flow test facility which provides a broad range of capabilities to investigate the flow field in SRM's to meet both current and projected needs utilizing state of the art test techniques and instrumentation. In order to assure that this goal was achieved, a SRM Advisory Group was formed and tasked to establish the merits of and the need for such a facility as well as to establish the basic design and instrumentation requirements for the facility. The SRM Advisory Group, chaired by Dr. Leonard H. Caveny, SDIO, is comprised of individuals from industry, government and academic sources with extensive experience in various areas of solid propulsion including analysis, design, testing, and development.

Several features must be considered in the design of cold flow models which are to be utilized in the simulation of a full scale SRM. Failure to incorporate these features and test at the proper conditions can result in misleading data. The model scale factor should be large enough to allow reasonable instrumentation access and maximum Reynolds number characteristics of the full scale motor. Consideration of studying injected particle trajectories for slag retention analyses requires a match of the Froude number for the model and the full scale motor. This results in a model scale factor of 10 percent (the ratio of the square of the sound speeds). The model Reynolds number can be matched to the full scale motor by operating at the correct pressure level. The model flow rate is then determined by the model nozzle size and the chamber pressure.

To effectively represent SRM conditions, the gas evolution from all propellant surfaces must be simulated in a manner which approximates the mass addition from the propellant grain so that the injection-driven flow field which develops along the chamber port is represented. This is best accomplished by admitting the flow through porous walls configured to present the burning propellant surfaces. Relative distribution of the flow rate over the porous surfaces should match that in the SRM by proper use of partitions and external flow rate control.

The above considerations were used to develop specific requirements for maximum and minimum values of model delivered pressures and flow rates for Marshall Space Flight Center's Solid Rocket Motor Air Flow Test Equipment (SRMAFTE). These design requirement values are listed in Table I. The maximum values are based on achieving full scale motor Reynolds number in a 10 percent scale

TABLE I. FACILITY PERFORMANCE REQUIREMENTS

PARAMETER	MAXIMUM		MINIMUM	
1) Flow Rate	145.15 kg/sec	(320 lbm/sec)	1.36 kg/sec	(3.0 lbm/sec)
2) Model Manifold Pressure	8.274x10^6 Pa	(1200 psia)	6.895x10^6 Pa	(100 psia)
3) Model Chamber Pressure	8.274 Pa x10^6	(1200 psia)	.2758x10^6 Pa	(40 psia)
4) Air Inlet Temperature, deg F.	422. deg K	(300 deg F)	Amb/	Amb.
5) Test Duration (Useable)	--	--	30 sec	
6) Tank Re-charge Time	20 minutes		--	--
7) Time To Set Point	6.0 sec			
8) Air Particulate Size	0.3 microns		--	--
9) Air Dewpoint	216. deg K	(-70 deg F)	205.55 K	(-90 deg F)
10) Exhaust Diffuser Duct Press.	--	--	0.3151 Pa	(4.57 psia)
11) Deviation of Pavg From Set Point, %	2.0		--	--
12) Steadiness of Pressure, % p - p	1.0			
13) Steadiness of Temperature, ± % of F	1.0		1.11 deg K	(2 deg F)

Space Shuttle SRM booster. Regulation of the supply air temperature maintains constant air density at a controlled pressure level and minimizes drift in Reynolds number, heat flux and anemometer data. An air filter prevents particles from clogging the porous wall materials in the model. An exhaust diffuser is required to prevent separation in the nozzle due to the higher specific heat ratio and consequently lower nozzle exhaust pressures for the cold air. No thrust stand is required due to the nature of model construction and the heavy supply pipes. Nozzle flow and performance characteristics will be determined from measured wall pressure distributions and velocity traverses at the exit plane.

FACILITY DESCRIPTION

The SRMAFTE configuration is depicted in Figure 1. The air supply for the SRMAFTE is a pressure blowdown system discharging to atmosphere through the solid rocket model. The air storage is comprised of eight storage tanks having a combined capacity of $259.7m^3$ (9100 ft^3).
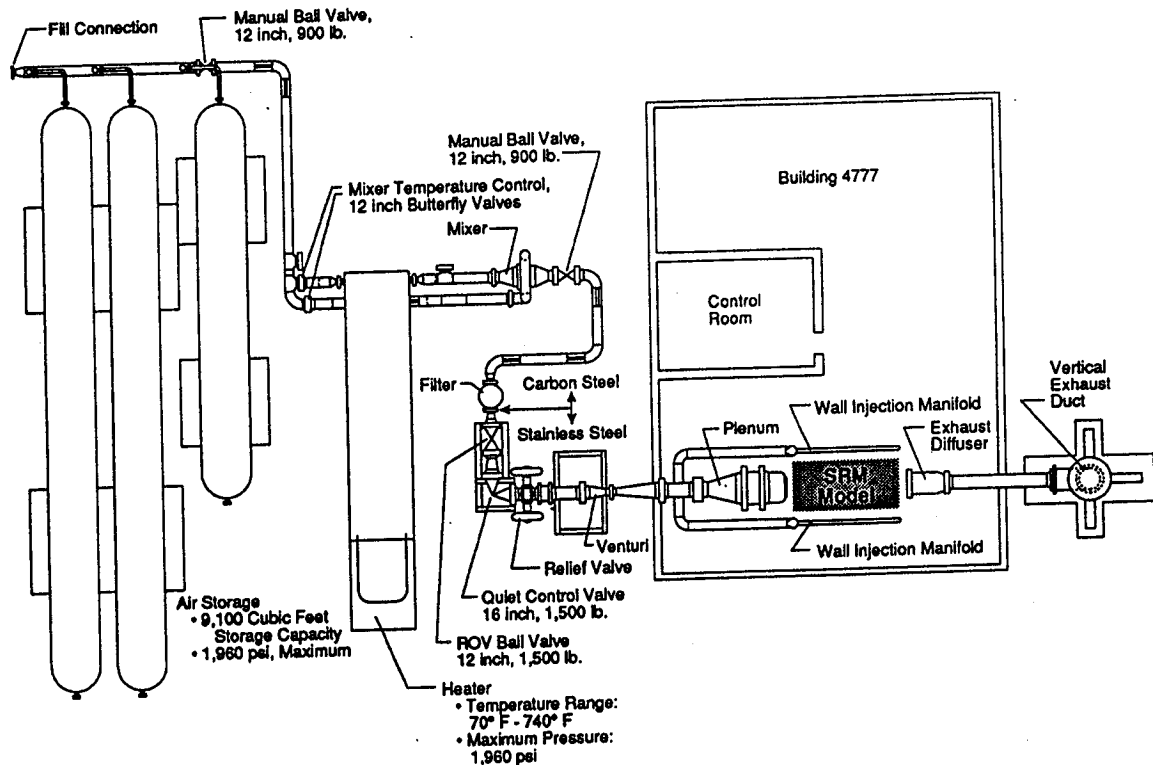

FIGURE 1. SOLID ROCKET MOTOR AIR FLOW TEST EQUIPMENT

The storage tanks are charged up to a maximum pressure of 1.310×10^7 Pa (approximately 1900 psig) from a 2.413×10^7 Pa (3500 psig) dry air supply system. A thermal-mass storage heater with a by-pass mixing loop will be utilized to set the test unit supply air temperature to a near-constant value between 294.4K (530°R) and 422.2K (760°R) during the blowdown interval. This heater unit is not currently in place but planned for the future. The inlet air is filtered through a bonded fiberglass filter with cylindrical cannisters that has a 0.3μ filter rating. The ROV isolation valve is downstream of the filter and is rated for a maximum pressure of 1.351×10^7 Pa (1960 psig). This valve can be shut down at maximum speed in case of emergency. The actual test model inlet pressure is controlled by a quiet trim control valve. The valve uses a hydraulic operator for actuation and will hold the test model stagnation pressure constant at a set-point value as the supply tank pressure decays. Downstream of the quiet valve, a pilot operated safety relief valve is located to discharge 100% of the flow operating at 9.101×10^6 (1320 psia). The nominal air weight flow range for system design is 9.07 to 145 kg/sec (20 to 320 lb/sec) which will be precisely metered by a sub-critical is venturi located at a minimum of 10 equivalent L/D's downstream of the control valve. The filter, control valve, relief valve, and venturi are shown in the Figure 2 photograph. Mass flow through the system is determined by sonic flow through the SRM model nozzle. The checkout model, to be discussed in the following section, is shown in Figure 3. The plenum chamber shown upstream of the model in Figure 1 provides wind tunnel quality conditioned air flow to models with open head end ports. The plenum chamber is not currently in place but is provided for in the facility design pending future model needs.
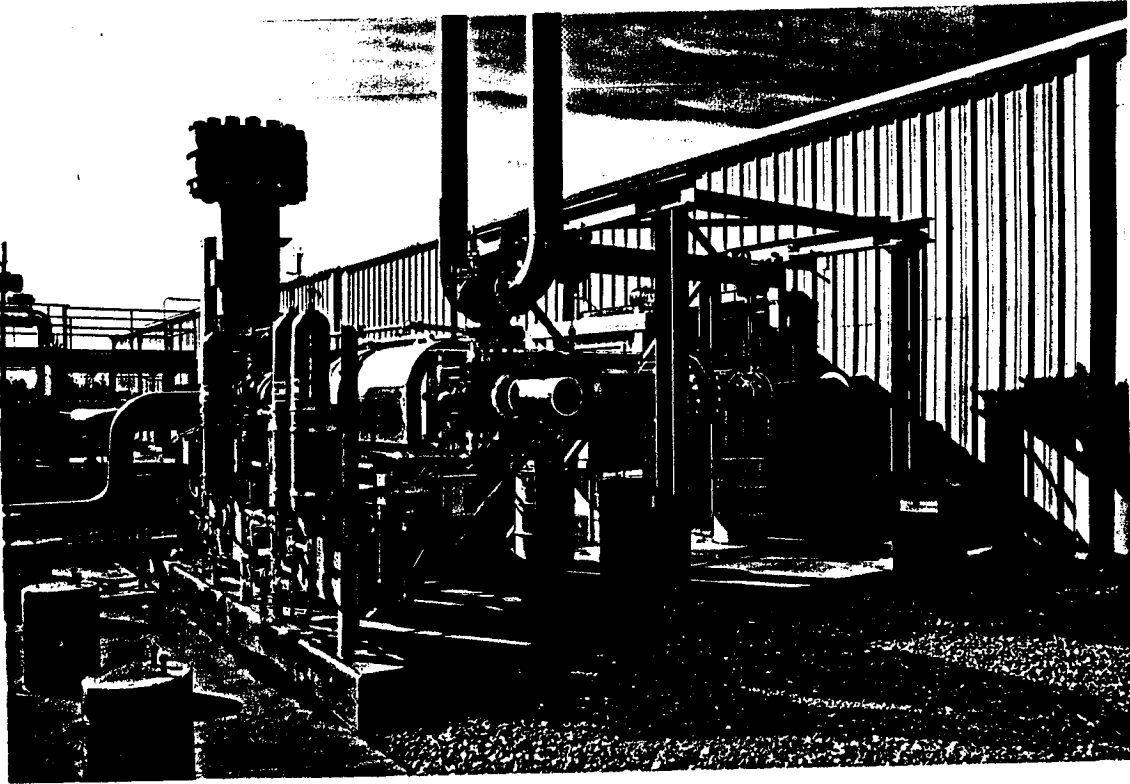
FIGURE 2. SRM AIR FLOW FILTER CONTROL VALVE, AND VENTURI
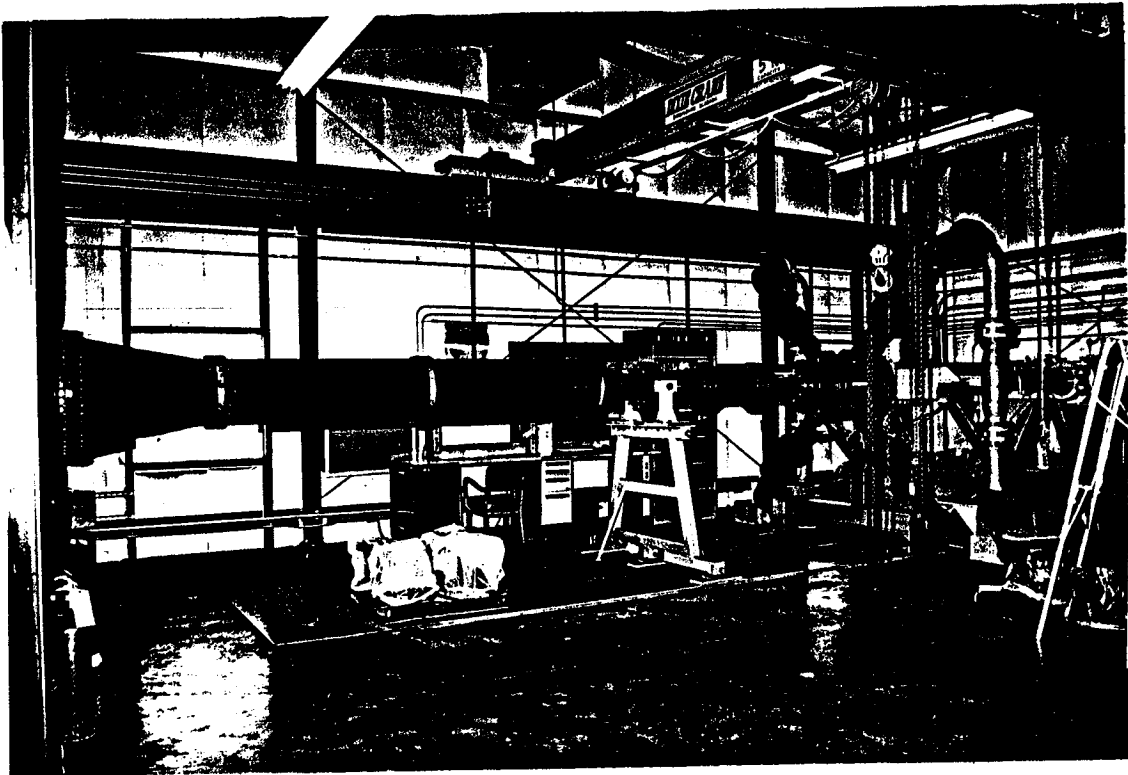

FIGURE 3. SRM AIR FLOW CHECKOUT MODEL, MANIFOLD SYSTEM, AND DIFFUSER

A diffuser shown downstream of the checkout model in Figure 3 enables the test model to operate at full scale booster nozzle expansion ratio without flow separation. Air passes from the diffuser into an exhaust duct which leads to an 85db silencer which is located outside of building 4777 as shown in Figure 4.
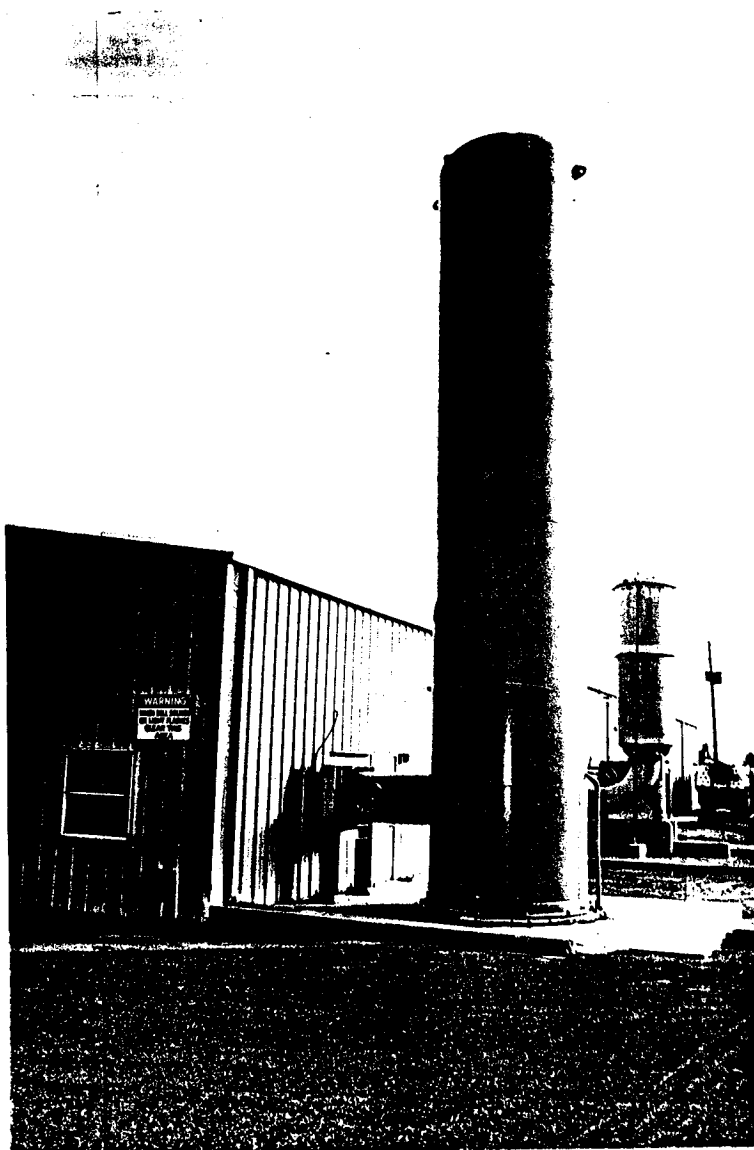
FIGURE 4. SRM AIR FLOW EXHAUST SILENCER

FACILITY CHECKOUT MODEL DESCRIPTION

A simple facility checkout model, as shown in Figure 5, has been designed and fabricated for the primary purpose of evaluating the performance of the solid rocket motor air flow test equipment over the maximum required ranges of flow rate, pressure and temperature. Control and steadiness of flow parameters at limit operating conditions will be monitored at model delivery as well as in the diffuser. The checkout model will also serve as a test bed for advanced instrumentation and flow visualization technology development.

The checkout model consists of three constant diameter chamber spool pieces with a converging/diverging nozzle. The nozzle throat and exit diameters are scaled to 10% RSRM/ASRM size at motor ignition. Also, the nozzle includes a conical exit section with the full RSRM/ASRM expansion ratio in order to verify diffuser and exhaust system performance. The spool pieces will be used in later tests with inserts to simulate propellant grains and could possibly have ports machined to fit windows for flow visualization or LDV measurements. The checkout model, exhaust diffuser, and inlet manifold system are shown in the Figure 3 photograph.

The forward end of the model chamber is bolted to an adapter chamber which in turn attaches to a "dummy plenum" which is needed in the absence of the planned plenum chamber to transmit the thrust load to the facility thrust bed. The model flow is delivered to the adapter chamber through four 6 inch header pipes 90 degrees apart which are fed by the two 8 inch facility manifold pipes.

The checkout model minimum and maximum limit test conditions are shown in Table II. During facility checkout, the model is being operated in two modes. In mode "A", four choked flow metering nozzles will be used in line with the 6 inch header pipes. The 8 inch facility manifold pipes will operate at 8.274×10^6 (1200 psia) and the model chamber will operate at 4.206×10^6 (610 psia) to simulate a distributed flow model with porous walls operating at the maximum facility flow rate. In mode "B", the metering nozzles will be removed and both the model chamber and the manifold system will operate at 4.206×10^6 (610 psia) to simulate an open port model connected to the facility plenum chamber.
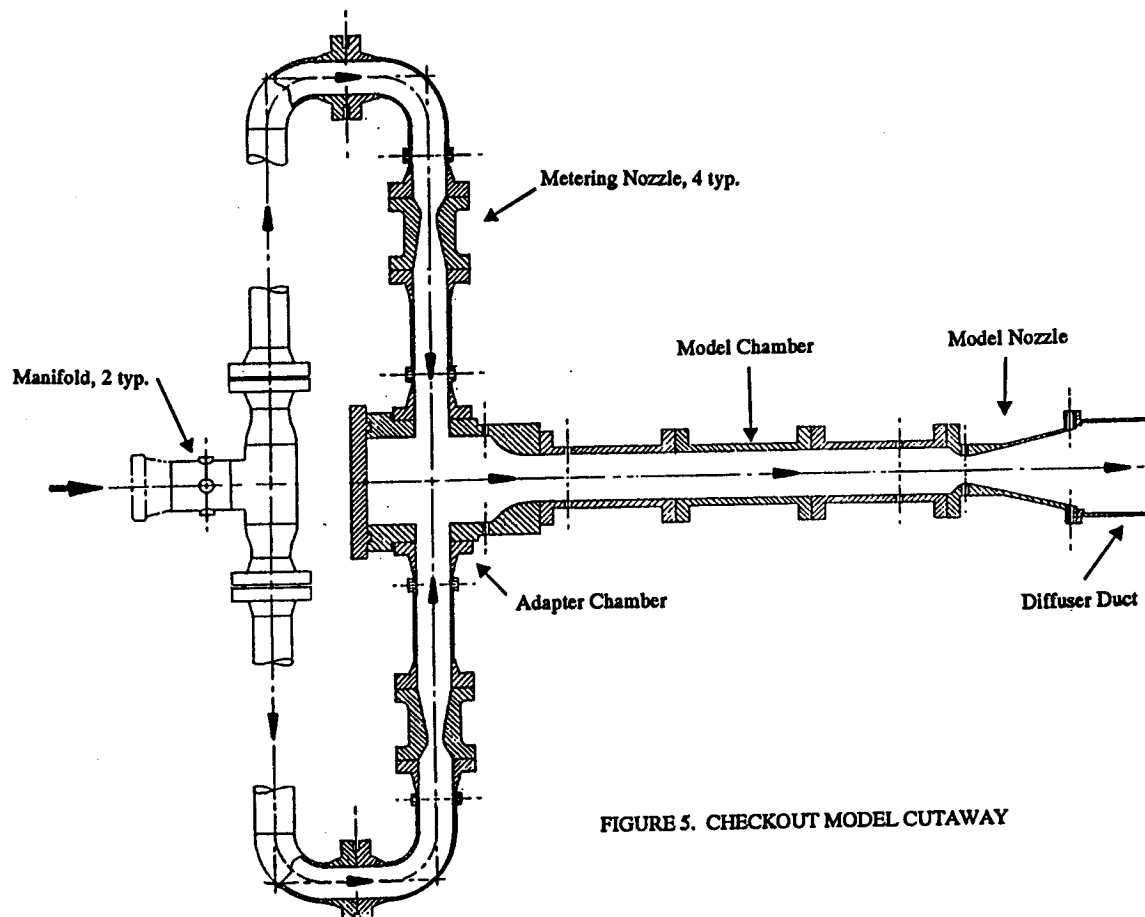
FIGURE 5. CHECKOUT MODEL CUTAWAY

TABLE II. CHECKOUT MODEL TEST CONDITIONS

MODEL TEST MODE	MANIFOLD PRESSURE		CHAMBER PRESSURE		FLOW RATE		AIR TEMP	
	Pa x 10^6	(PSIA)	Pa x 10^6	(PSIA)	KG/S	(LB/S)	DEG K	(DEG R)
"A"	8.274	(1200)	4.206	(610)	145.	(320)	294.	(530)
"A"	0.517	(75)	2.620	(38)	9.07	(20)	294.	(530)
"A"	8.274	(1200)	4.206	(610)	121.	(267)	422.	(760)
"A"	0.620	(90)	0.317	(46)	9.07	(20)	422.	(760)
"B"	4.206	(610)	4.206	(610)	145.	(320)	294.	(530)
"B"	2.620	(38)	2.620	(38)	9.07	(20)	294.	(530)
"B"	5.033	(730)	5.033	(730)	145.	(320)	422.	(760)
"B"	0.317	(46)	0.317	(46)	9.07	(20)	422.	(760)

FACILITY/CHECKOUT MODEL CFD ANALYSIS

A detailed computational fluid dynamic analysis of the SRMAFTE checkout model internal flow geometry was performed in order to verify the design and operational performance of the SRMAFTE model section. The analysis involved the use of a commercially available CFD code referred to as Fluent. The code utilizes the full Navier-Stokes equations cast into a boundary-fitted staggered grid discretization of the

equations of motion. The code also utilizes the standard two-equation k-e turbulence closure model for the Navier-Stokes equations. Both 2-D and 3-D computational techniques were used to analyze the flow field from a position just downstream of the 8 inch manifold pipe, through the checkout model and ending in the diffuser pipe. The region analyzed is shown in Figure 5. The computational results discussed are for a facility pressure of 8.274×10^6 (1200 psia) with the mode "A" metering nozzles installed. A case with the facility pressure at 1.034×10^6 (150 psia) and operating without the metering nozzles installed is also discussed for the diffuser analysis.

As expected, the elbows upstream of the metering nozzle do create some non-uniformity in the flow. However, the non-uniformity does not persist for a prolonged distance aft of the elbow and the pressure variation across the flow field in the header pipes upstream of the metering nozzle is less than one percent. Figure 6 shows the Mach number contours in the metering nozzle. The metering nozzle discharge coefficient computed from the CFD solution was .997. Notice in Figure 6 that the flow shocks down aft of the metering nozzle throat and there is also separation of the flow from the metering nozzle exit walls.
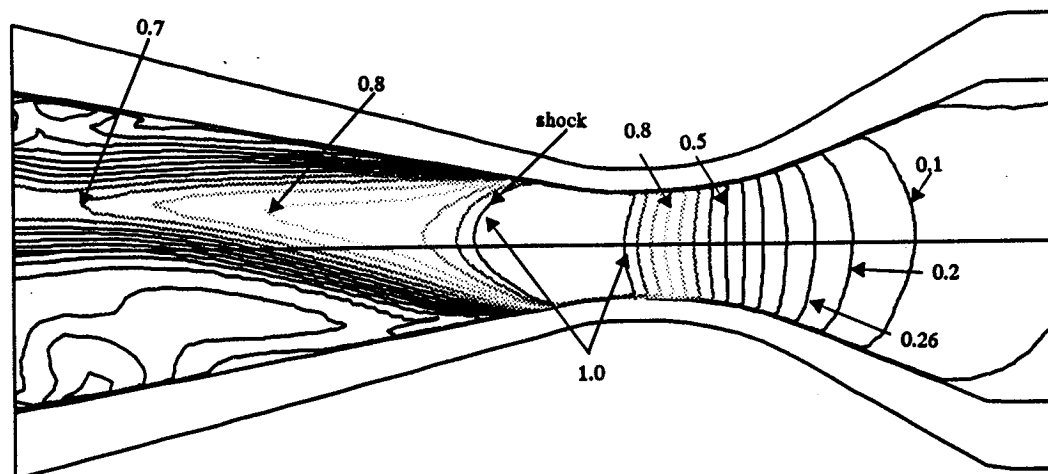
FIGURE 6. METERING NOZZLE MACH NUMBER CONTOURS

Flow is dumped into the adapter chamber from the four symmetric header pipes. The flow field in the adapter chamber is shown in Figure 7. The flow in the adapter chamber is very three-dimensional and non-uniform with maximum transverse velocities of approximately 150 m/s. A hyperbolic spiral design was used for the adapter chamber transition section in an attempt to smoothly transition the non-uniform flow into the checkout model. The CFD solution at the forward end of the model chamber confirms that the adapter transition is performing its function. The velocity profiles are almost completely flat and the magnitude of the transverse velocities have been reduced to a maximum of approximately 20 m/s. The transverse flow velocities continue to decrease down the checkout model length. At the aft end of the model
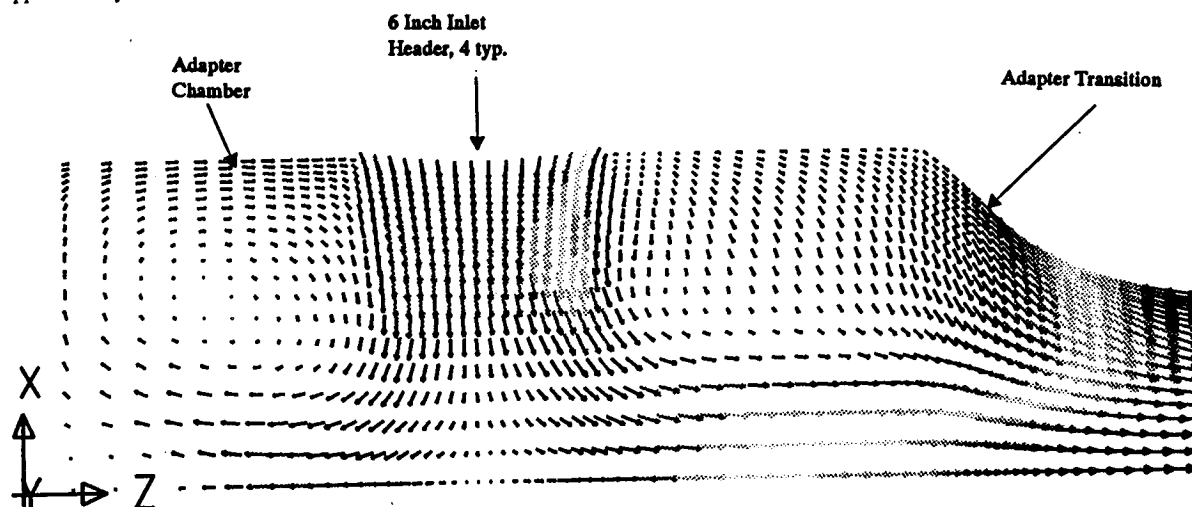
FIGURE 7. VELOCITY FIELD IN THE CHECKOUT MODEL ADAPTER CHAMBER

FIGURE 8. PRESSURE RATIO AND MACH NUMBER PROFILES AT MODEL NOZZLE THROAT PLANE
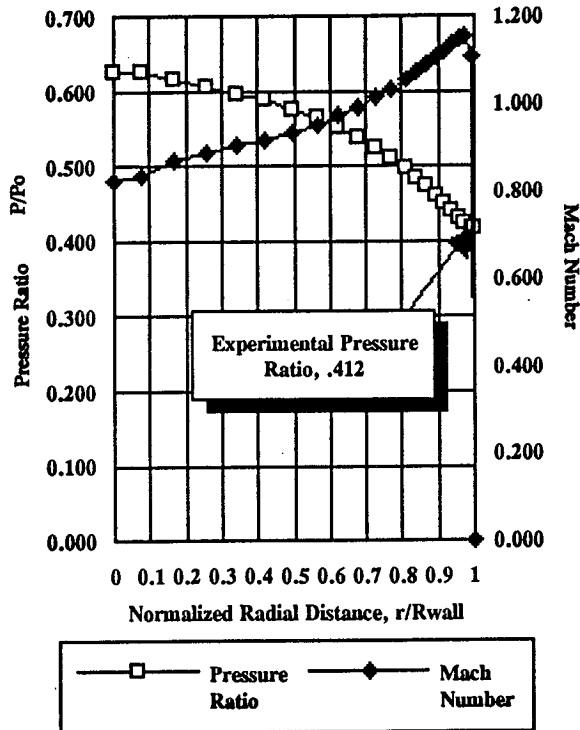
chamber the transverse velocities are less than 1 m/s and there is no measurable pressure gradient across the flow field.

Since the checkout model nozzle was designed using typical solid rocket nozzle parameters, there is a significant 2-D pressure gradient across the model nozzle throat, as shown in Figure 8. The velocity at the nozzle wall is observed to be greater than the sonic velocity while the centerline velocity is still subsonic at this point, as would be expected. The pressure variation across the model nozzle throat is much greater than that observed in the metering nozzle throat due to the differences in the design parameters of the nozzles. The predicted ratio between the static and the total pressure at the wall agrees well with the measured ratio. The calculated discharge coefficient of the model nozzle was 0.993.

The flow field Mach number contours in the diffuser are shown in Figure 9. The figure shows two distinct shocks in the diffuser. One at the corner where the metering nozzle exit cone steps into the larger diameter diffuser and one at the aft end of the diffuser just upstream of the subsonic diffuser transition. This illustrates that the diffuser is operating properly since the flow is shocking down in the diffuser as expected per 1-D design calculations.

FIGURE 9. DIFFUSER DUCT MACH NUMBER CONTOURS

FACILITY/MODEL DATA

Testing with the checkout model was initiated in the fall of 1991 to characterize facility performance and develop optimum operational procedures. Some preliminary results from this testing are shown in Figures 10 - 13. The flowrate data for minimum and maximum pressure runs are shown in Figure 10. The ratio of the model flowrate to the facility flowrate is shown for several test runs in Figure 11. The model flowrate is from the theoretical 1-D equation with a unity discharge coefficient and the facility flowrate is from the calibrated venturi. It appears that a model nozzle discharge coefficient of approximately 0.98 would reduce the ratio to unity except for the lowest flowrate which is currently unexplained. The 16 inch facility supply piping splits into two 8 inch manifold pipes upstream of the model. The division of the flow is shown in the Figure 12 plot of the percentage difference between the pressure in each of the two 8 inch manifold pipes. The maximum difference is less than 0.1 percent which will insure equal flow delivery to each side of future models. The diffuser performance map is shown in Figure 13. The diffuser remains started down to the optimum operating point where the model total pressure to ambient pressure ratio is approximately 8 for mode "B". The flow rates for mode "A" and mode "B" operation are slightly different.
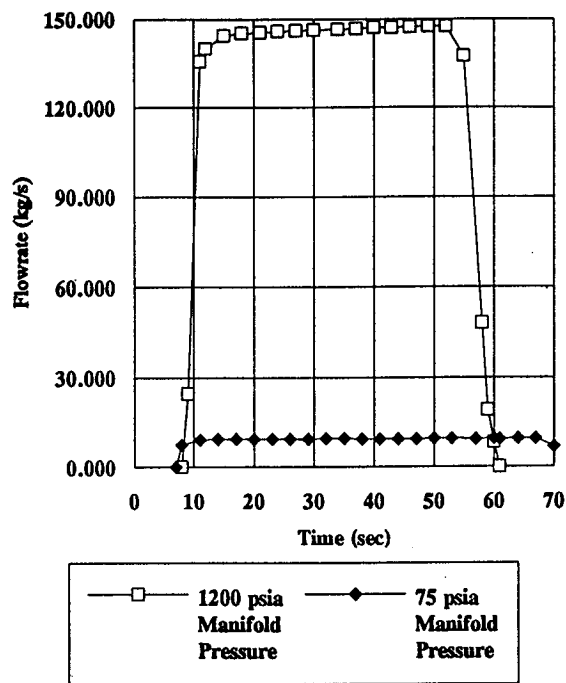
FIGURE 10. MODEL FLOWRATE
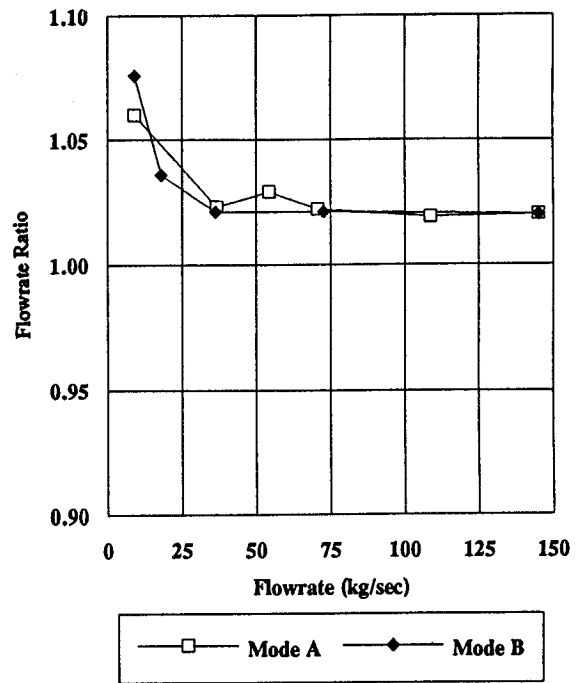
FIGURE 11. RATIO OF MODEL FLOWRATE TO FACILITY FLOWRATE
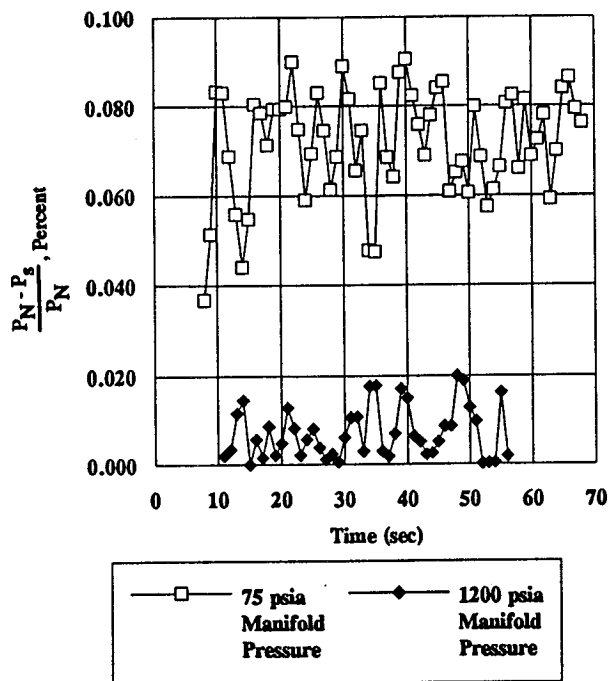
FIGURE 12. MANIFOLD PRESSURE DIFFERENCE
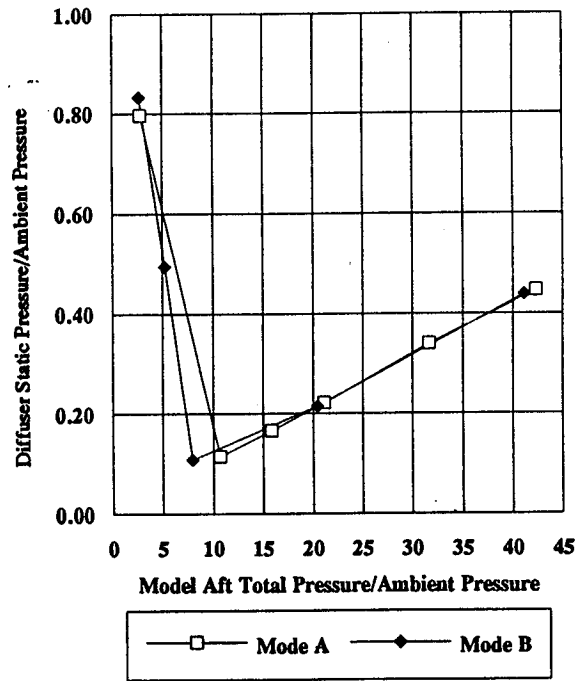
FIGURE 13. DIFFUSER PERFORMANCE MAP

CONCLUSIONS

A facility for the testing of SRM cold flow models has been designed, constructed and checked out at the National Aeronautics and Space Administration's Marshall Space Flight Center in Huntsville, Alabama. The facility is capable of testing 10 percent scale models of large space SRM boosters at full scale Reynolds numbers. The facility is also capable of testing full scale models of small tactical motors at full scale Reynolds numbers. The addition of flow thermal conditioning and upstream plenum chamber flow conditioning will be added as special model needs develop. The facility has been successfully operated over the entire range of design pressures and flowrates. It is available for national use by industry and government agencies requiring facilities capable of testing SRM cold flow models to support development programs or resolve problems arising with operational flight systems.

REFERENCES

1. Dunlap, R., P. G. Willoughby, and R. W. Hermsen, "Flowfield in the Combustion Chamber of a Solid Propellant Rocket Motor," AIAA Journal, Vol. 12, No. 10, 1974, 1440-1442.

2. Culick, F. E. C., "Rotational Axisymmetric Mean Flow and Damping of Acoustic Waves in Solid Propellant Rocket Motors," AIAA Journal, Vol. 4, No. 8, 1966, 1462-1464.

3. Beddini, R. A., "Injection Induced Flows in Porous-Walled Ducts," AIAA Journal, Vol. 24, No. 11, Nov. 1986, 1766-1773; see also, Beddini, R. A., "Analysis of Injection-Induced Flows in Porous-Walled Ducts with Application to the Aerothermochemistry of Solid-Propellant Motors," Ph.D. Thesis, Rutgers University, Oct. 1981.

4. Dunlap, R., A. M. Blackner, R. C. Waugh, R. S. Brown, and P. G. Willoughby, "Internal Flow field Studies in a Simulated Cylindrical Port Rocket Chamber," United Technologies Chemical Division, San Jose, California, Journal of Propulsion and Power, Vol. 6, 1990.

5. Dunlap, R., and P. G. Willoughby, "Cold Flow Study Test Report," CSD4901-78-135, Contract No. F04701-77-C-0060, United Technologies Corporation, Chemical Systems Division, March 1980.

6. Dunlap, R., A. M. Blackner, P. G. Willoughby, T. Jahnsen, "Titan IV Cold Flow Study Report," United Technologies/Chemical Systems Division, CSD 4001-86-89, July 1986, (also CSD 4001-86-89, Change 1, June 1987).

7. Dunlap, R., et al., "Internal Flow Field Investigation," United Technologies/Chemical Systems Division, Air Force Rocket Propulsion Laboratory Report, AFRPL TR-86-104, March 1987.

8. Dunlap, R., A. M. Blackner, and T. Jahnsen, "Titan Recovery Program Phase I, Task V - Internal Flow Field Studies," United Technologies/Chemical Systems Division, CSD 4176-87-100, March 1987.

9. Waesche, R. H. W., W. H. Sargent, and J. F. Marchman, "Space Shuttle Solid Rocket Motor Aft-End Internal Flows," Journal of Propulsion and Power, Vol. 4, 1989.

10. Whitesides, R. H., A. Gosh, S. L. Jenkins, and D. L. Bacchus, "Cold Flow Determination of the Internal Flow Environment Around the Submerged TVC Nozzle for the Space Shuttle SRM," 1989 JANNAF Propulsion Meeting, Cleveland Convention Center, Cleveland, Ohio, May 23 - 25, 1989.

11. Whitesides, R. H., A. Majumdar, S. Jenkins, and D. Bacchus, "Experimental Determination of Convective Heat Transfer Coefficients in the Separated Flow Region of the Space Shuttle Solid Rocket Motor," 28th Aerospace Sciences Meeting, Reno, Nevada, AIAA 90-0043, January 1990.

12. Majumdar, A. K., R. H. Whitesides, S. L. Jenkins, and D. L. Bacchus, "Effect of Idealized Asymmetric Inhibitor Stubs on Circumferential Flow in the Space Shuttle SRM," Journal of Propulsion and Power, Vol. 6, No. 1, January - February 1990.

13. Waesche, R. H. W., J. F. Marchman, and S. Kuppa, "Effects of Grain Slots on Flow in a Solid Rocket Motor," Journal of Propulsion and Power, Vol. 7, 1991.

14. Waesche, R. H. W., J. F. Marchman, and S. Kuppa, "Effects of Grain and Aft-Dome Configuration on Aft-End SRB Internal Flows," Journal of Propulsion and Power, Vol. 7, 1991.

ASRM Technology Model Design

A significant effort was expended to make rapid progress in defining the preliminary requirements for this model. A detailed task list was developed to show the critical steps, technical issues, and decisions to be made in defining the basic model requirements. A refined schedule was developed with Dave Bacchus/ED34 to show how the requirements could be defined with a design layout and a handout listing model operating conditions and design loads. Significant design approach decisions to be made included the model scale factor, the possible use of the existing 8% scale nozzle, and the maximum burn time simulation to be included in the model design. Preliminary layouts of the model were presented based on tentatively selected design guidelines to show overall diameter, lengths, design concepts for joints, partitioning of the model, and flow metering control.

Several basic design approach decisions were made including the selection of a 10% model scale factor and a burn time span of 0 to 60 seconds. Higher burn times could be accommodated by reducing the scale factor and reducing the nozzle throat diameter. Layout drawings of the model were prepared to reflect these decisions. The model was to have a section for each of the three segments of the full scale motor. The forward motor segment containing the longitudinal slots and fins would be represented by two divided cylindrical port sections. The forward section will have a port diameter such that the cross sectional flow area will be equivalent to the flow area in the slots. The aft section of the forward segment is a cylindrical port geometry in the full scale motor and will be scaled to 10 percent in the model.

Analyses were performed on the prediction of acoustic phenomena in the motor port, particularly late in motor burn when vortex shedding occurs from the inhibitor studs protruding into the motor port. An ED33 group was asked to review the need for configuring the ASRM/Technology Model for an 80 second burn time as opposed to a 60 second burn time. This would affect the diameter of the outer pressure vessel.

ASRM and model Reynolds numbers and model operating pressures and flow rates were calculated and presented to NASA/MSFC personnel. The metering nozzles and header pipe sizes for all three model segments were also defined. Also, the full scale ASRM as-cast propellant and nozzle geometry was documented on the ERC AUTOCAD system. These drawings are available as H5101, Aft Case Loaded w/Nozzle, H5102, Center Case Loaded, H5103, Forward Case Loaded, and H5104, Motor Assembly Loaded. The nozzle assembly was also documented separately as H5109. These drawings are assembly level drawings but with detailed internal surface geometry dimensions and are not available at Aerojet or Thiokol. They were used to generate the 10 percent model as-cast geometry, H3101, which will serve as baseline. The deformed, zero burn time geometry was received from Aerojet and was evaluated. The 60 second maximum burn time requirement was changed to 80 seconds as a result of ED33 calculations of the edge tone frequency resonance with the first longitudinal mode at that burn time.

ERC constructed a two-dimensional, axisymmetric, computational grid file to be used to calculate the flow field in the technology model. The drawing used to construct this grid was ERC drawing H3001-1X. The flow field was calculated from the head end of the model a point located at the corner of the port propellant grain at the aft end of the motor. The calculation determined the pressure drop down the entire model length. This was compared to calculations performed for the full scale motor. These calculations were used to set requirements for the ASRM Technology Model flow partitioning.

Detailed analysis work on the model flow phenomena included Δp calculations for the air manifold supply system. Also, analyses of the model axial port pressure gradients were performed. An analysis using both the Culick cosine and the bulk one-dimensional velocity profile was developed and programmed. Also, the 1-D motor port ballistics calculation routine was separated out from a 1-D rocket motor performance program. In addition, a two-dimensional CFD calculation of the model port flow was accomplished. The total axial pressure drop is approximately 100 psi.

An internal MSFC Preliminary Design Review was held and a summary presentation package was complied using material from both the requirements package and the design detail package. This summary package was used for a design review with a National SAF Advisory Group. The group had a number of questions about the facility and a written response to each of the Advisory Group's comments was prepared in memo format and delivered to ED33. All contributors' comments were compiled and presented to Aerophysics Division personnel by Dave Bacchus. Specific actions were discussed and each recommendation was addressed. A concern regarding nitrogen condensation in the model nozzle expansion section was addressed by ERC. Calculations of the static temperature and boiling point temperature at the exit plane for both nitrogen and oxygen were performed and the calculated static temperature was always above the boiling or condensation temperature.

Several codes were further developed and modified to calculate local flow conditions at specific locations in the model chamber and nozzle. These codes include: 1) FLOW - calculates on dimensional flow properties from local area ratio, 2) SHOCK - performs normal and oblique shock calculations, 3) BLOWOFF - calculates nozzle joint blowoff loads, 4) HYPER - calculates hyperbolic nozzle entrance nose contour design, and 5) CHANEL - calculates flow properties down the port of a solid propellant rocket motor with mass addition from propellant burning. These codes were developed/modified by W. C. Aycock for ERC's IBM compatible 486 and 386 personal computers.

An extensive flow analysis was undertaken on the ASRM/Technology Model. The analysis results were presented at several meetings of the Flow Team headed up by Dave Bacchus, ED33. The primary results were presented to the Flow Team and an Update Review was held to follow up on various action items. A final presentation dry run in preparation for an Aerophysics management review was given by Dave Bacchus.

The flow analysis determined the pressure losses that would occur throughout the model. The analysis was set up on a Microsoft Excel spreadsheet to allow flow parameters to be changed. The resulting spreadsheet was used for a number of off design cases and "what if" analyses. The analysis began at the flange at the head of the feed manifold with a stagnation pressure of 1000 psia. The frictional pressure drop down the feed manifold was then calculated. This yielded the pressure at the head end of each of the feeder pipes. The frictional pressure losses were also calculated for each of the feeder pipes down to the metering nozzles. These results enabled a comparison between the stagnation pressures delivered to each metering nozzle. The maximum difference in stagnation pressure was calculated to be 2.32 psi which is a 0.234% difference.

The pressure drop across the metering nozzles was performed with the choked flow equation and the normal shock equations. Pressure downstream of the shock in the expansion section of the metering nozzle must match the required feeder pipe pressures which were calculated as follows.

The flow analysis began with the bore pressure, calculated from CFD analysis, and worked upstream to the metering nozzles. The first pressure drop calculated was that occurring across the porous wall liner. This was done by using an equation supplied by the manufacturer, Krebsoge. This equation was solved by using the iteration scheme present in Excel. This calculated pressure drop varied from section to section due to flow rate and surface area differences. The calculated pressure drop for 25 micron filter rating bronze, the PDR material selection, ranged from 18.3 to 31.2 psi for the various sections. This compared with the requirement of a 50 psi pressure drop across the porous wall liner for the nominal Reynolds number and flow rate..

The next calculation determined the number of drilled holes needed in the plate that would serve as the porous wall in the slot region. The bore pressure was known from CFD and the upstream pressure was known from the porous wall pressure drop. The mass flow for each slot was also given, along with a hole size for the drilled holes. This enabled the calculation of the mass flow per hole which yielded the number of holes needed in each slot. The forward slot was determined to require 115 holes and the aft slot 106 holes with a diameter of 0.0935 inches.

The next pressure drop encountered moving upstream was that across the flow distribution tube. The flow distribution tube was essentially a drilled hole plate, as were the slots in the head end star grain region. For this reason, both were calculated similarly. The pressure drop was calculated using an orifice equation which also required the use of Excel's iterative scheme. The pressure drop was set by the design requirements which call for a 100 psi pressure drop across the star grain slot plates and 25 psi across the flow distribution tube. For the flow distribution tube it was required that all sections have the same hole size and porosity. A porosity was chosen for the flow distribution tube and this determined the number of holes in each section. The pressure drop was then calculated and compared with the 25 psi minimum

requirement. The porosity was then varied until the section with the lowest pressure drop had the required 25 psi pressure drop. Thus, section 3 has the required 25 psi pressure drop where as the highest pressure drop occurs in section 6, 52.3 psi. The total number of 0.0935 in. dia. holes needed was 4712. This same process was carried out for the star grain slot plates, working to a pressure drop of 100 psi. This yielded a requirement of 2242 holes of 0.0935 in. dia. in the star grain region in order to pass the correct flow rate.

Next, the pressure dump pressure loss was calculated for the flow going from the feeder pipes into the plenum ahead of the flow distribution tube. This pressure loss ranges from 2.29 to 5.68 psi.

The frictional pressure loss in the feeder pipes from the plenum to the downstream side of the metering nozzles was calculated and found to be between 0.05 and 2.40 psi. The spreadsheet program also has the ability to calculated some of the pressure recovery in the diverging section of the metering nozzles downstream of the shock.

This spreadsheet program was run for a number of configurations., including the PDR baseline configuration and also for the design as updated by recommendations from the flow team. A number of parametric studies were also performed to determine the effect of hole sizes and porosities on the pressure drops through the model. It was also used to evaluate off-design flow rates and pressures. A copy of the final package is included in this appendix. Similar analyses were completed for off design cases.

The sizes of the drilled holes in the flow distribution tube were addressed a number of times. It was determined that each of the 5 sections of the flow distribution tube did not necessarily have to have the same size drilled holes. A study was done to determine what the drilled hole size in each section would be in order that each section have a pressure drop of 25 psi across the flow distribution tube. Table 1 gives a summary of these results.

Table 1. Flow Distribution Tube Hole Sizes

Section	Hole Dia. (in.)	No. of Holes
2	0.0995	1075
3	0.0935	887
4	0.1040	879
5	0.1065	883
6	0.1130	988

Also, three drilled hole plate samples were designed so that testing could be done to validate the drilled hole pressure drop analysis. The plates were designed so that two of the plates had the same porosity and two of the plates had the same hole size. This would enable the determination of the relation between hole size and pressure drop

and porosity and pressure drop. The data for the drilled hole plates agreed with the ERC predictions, but the data was still somewhat lower than the prediction. An inspection of the plates revealed actual hole sizes larger than designed and rounded edges as opposed to sharp edges which appear to fully explain the difference between data and predictions. The plates were remanufactured and the testing repeated in the same test apparatus with modifications to reduce uncertainty in the sample exposed cross sectional flow areas. After that testing plates 1 and 3 a required a corrected hole diameter to be used in the prediction. These diameters were 0.094 in. for both plates 1 and 3. The prediction for plate 2 used a hole diameter of 0.125 in. When these corrections were made the discharge coefficients for each plate were fine tuned in order to obtain a match between the predicted data and the experimental data. For plates 1 and 3 the discharge coefficient was found to 0.91 where as for plate 2 the discharge coefficient used was 0.88.

Porous material samples were produced by the Krebsoge division in Germany after problems were encountered with the previous samples produced by the American division of Krebsoge. All of the samples tested were stainless steel and the micron ratings were 40, 30, 20, 15, and 10 microns. All the samples were tested at upstream pressures of 600, 500, and 400 psia. The data was analyzed and plots were produced to show the pressure drop for each sample as a function of mass flow per unit area. Also shown on the plots were pressure drop predictions produced using the equation supplied by Krebsoge in their literature. The permeability constants used in the predictions were also taken from the Krebsoge literature. After the data from two samples of 15 micron stainless steel, which were run in both directions, was analyzed, this material was suggested to be the proper material to use for the liner in the ASRM/Technology model. This suggestion was made based on calculations predicting the pressure drop across a half inch wall of the material. The sample test data was used to calculate revised values of the permeability constants for the 15 micron stainless steel material. These revised permeability constants were then used to predicted the pressure drop across a half inch of the 15 micron stainless steel material. The resulting pressure drop met the 50 psid requirement for the ASRM/Technology model porous liner. A package of these results was given to D. Bacchus, ED33. Also included in the package were updated results of calculations done for the star grain and the slot plates for this model. These new calculations arose due to the latest porous material data and the difference on the pressure drop now being calculated.

A set of detailed instrumentation drawings was received from and these were reviewed by ERC and the discrepancies were then addressed. A new set of instrumentation drawings were generated by DEI. These drawings were reviewed and compared to notes on the original set of instrumentation drawings. It was found that all the discrepancies noted earlier had been fixed in this latest set of instrumentation drawings.

ASRM TECHNOLOGY MODEL PRESSURE DROP ANALYSIS

FLOW TEAM UPDATED DESIGN

1000 psia Manifold Pressure

ERC, Inc.
7 October 1992

Constants

Gas Const:	53.353	ft*lbf/lbm*Deg R
Gamma:	1.4	6 in. Sch 120

Initial Conditions

Po:	1000	psia	Temp.:	530.00	Deg. R
Pipe I.D.:	5.761	in.	Sonic Vel.:	1128.58	ft/sec
Pipe Area:	23.767	sq. in.	Density:	5.08	lbm/ft^3
Velocity:	62.96	ft/sec	Mach #	0.0558	
Pressure:	997.82	psia	Rough:	0.00015	ft
Total mass flow:	231.65	lbm/sec	Viscosity:	2.43E-06	ft^2/sec
Mass Flow 1:	103.037	lbm/sec			
Mass Flow 2:	28.046	lbm/sec	Delta P:	0.0392	psi
Mass Flow 3:	19.867	lbm/sec	(Sudden Contraction)		
Mass Flow 4:	24.359	lbm/sec			
Mass Flow 5:	25.458	lbm/sec			
Mass Flow 6:	30.879	lbm/sec			

Station 0 to Station 1

Pipe Dia:	5.501	in.	Pipe Dia:	0.4584	ft.
Pipe Length:	19.646	in.	Pipe Len.:	1.6372	ft.
Mass Flow:	57.91	lbm/sec			
P:	997.79	psia	Re #:	1.30E+07	
Velocity:	69.06	ft/sec	Mach #	0.0612	
Fric. Factor:	0.015268		Sqrt(Fric. Fac.)	0.123564	
Density:	5.08	lbm/ft^3			
Dynamic Press.:	2.61	psi			
Delta P:	0.1426	psi	P1 =	997.68	psia

Station 1 to Station 2

Pipe Dia:	5.501	in.	Pipe Dia:	0.4584	ft.
Pipe Length:	18.732	in.	Pipe Len.:	1.5610	ft.
Mass Flow:	32.15	lbm/sec	Re #:	7.22E+06	
P1:	997.68	psia	Po1:	998.49	psia
Velocity:	38.34	ft/sec	Mach #	0.0340	
Fric. Factor:	0.015314		Density:	5.08	lbm/ft^3
Sqrt(Fric. Fac.)	0.123748		L/D(Tee):	20	
Dynamic Press.:	0.81	psi	Eq. Len:	9.1683	ft.
Delta P =	0.2889	psi	P2 =	997.39	psia

Station 2 to Station 3

Pipe Dia:	5.501	in.	Pipe Dia:	0.4584	ft.
Pipe Length:	26.375	in.	Pipe Len.:	2.1979	ft.
Mass Flow:	25.14	lbm/sec	Re #:	5.65E+06	
P1:	997.39	psia	Po1:	997.89	psia
Velocity:	29.99	ft/sec	Mach #	0.0266	
Fric. Factor:	0.015342		Density:	5.08	lbm/ft^3
Sqrt(Fric. Fac.)	0.123862		L/D(Tee):	20	
Dynamic Press.:	0.49	psi	Eq. Len:	9.1683	ft.
Delta P:	0.1875	psi	P2 =	997.21	psia

Station 3 to Station 4					
Pipe Dia:	5.501	in.	Pipe Dia:	0.4584	ft.
Pipe Length:	17.483	in.	Pipe Len.:	1.4569	ft.
Mass Flow:	20.18	lbm/sec	Re #:	4.53E+06	
P1:	997.21	psia	Po1:	997.52	psia
Velocity:	24.07	ft/sec	Mach #	0.0213	
Fric. Factor:	0.015373		Density:	5.08	lbm/ft^3
Sqrt(Fric. Fac.)	0.123989		L/D(Tee):	20	
Dynamic Press.:	0.32	psi	Eq. Len:	9.1683	ft.
Delta P:	0.1131	psi	P2 =	997.09	psia

Station 4 to Station 5					
Pipe Dia:	5.501	in.	Pipe Dia:	0.4584	ft.
Pipe Length:	26.375	in.	Pipe Len.:	2.1979	ft.
Mass Flow:	14.09	lbm/sec	Re #:	3.16E+06	
P1:	997.09	psia	Po1:	997.25	psia
Velocity:	16.81	ft/sec	Mach #	0.0149	
Fric. Factor:	0.015442		Density:	5.08	lbm/ft^3
Sqrt(Fric. Fac.)	0.124264		L/D(Tee):	20	
Dynamic Press.:	0.15	psi	Eq. Len:	9.1683	ft.
Delta P:	0.0593	psi	P2 =	997.03	psia

Station 5 to Station 6					
Pipe Dia:	5.501	in.	Pipe Dia:	0.4584	ft.
Pipe Length:	18.038	in.	Pipe Len.:	1.5032	ft.
Mass Flow:	7.72	lbm/sec	Re #:	1.73E+06	
P5:	997.03	psia	Po5:	997.08	psia
Velocity:	9.21	ft/sec	Mach #	0.0082	
Fric. Factor:	0.015622		Density:	5.08	lbm/ft^3
Sqrt(Fric. Fac.)	0.124988		L/D(Tee):	20	
Dynamic Press.:	0.05	psi	Eq. Len:	9.1683	ft.
			Po6:	997.06	psia
Delta P:	0.0169	psi	P6 =	997.02	psia

Feeder Pipe #1

Pipe Dia:	3.826	in.	Pipe Dia:	0.3188	ft.	
Pipe Length:	45.500	in.	Pipe Len.:	3.7917	ft.	
Mass Flow:	25.76	lbm/sec	Re #	8.32E+06		
P1:	997.68	psia	Po1:	999.89	psia	
Velocity:	63.50	ft/sec	Mach #1	0.0563		
Fric. Factor:	0.016534		L/D (Tee):	60		
Sqrt(Fric. Fac.)	0.128586		Eq. Len.:	19.13	ft.	
Density:	5.08	lbm/ft^3				
Dynamic Press.:	2.21	psi	Poend =	997.26	psia	
Delta P:	2.6284	psi	Pend =	995.05	psia	

Feeder Pipe #2

Pipe Dia:	1.939	in.	Pipe Dia:	0.1616	ft.	
Pipe Length:	67.680	in.	Pipe Len.:	5.6400	ft.	
Mass Flow:	7.01	lbm/sec	Re #	4.47E+06		
P1:	997.39	psia	Po1:	999.88	psia	
Velocity:	67.32	ft/sec	Mach #	0.0596		
Fric. Factor:	0.019351		L/D (Tee, Elbow):	90		
Sqrt(Fric. Fac.)	0.139109		Eq. Len.:	14.5425	ft.	
Density:	5.08	lbm/ft^3				
Dynamic Press.:	2.48	psi	Poend =	993.86	psia	
Delta P:	6.0042	psi	Pend =	991.39	psia	

Feeder Pipe #3

Pipe Dia:	1.939	in.	Pipe Dia:	0.1616	ft.	
Pipe Length:	67.680	in.	Pipe Len.:	5.6400	ft.	
Mass Flow:	4.97	lbm/sec	Re #	3.17E+06		
P1:	997.21	psia	Po1:	998.45	psia	
Velocity:	47.70	ft/sec	Mach #	0.0423		
Fric. Factor:	0.019382		L/D (Tee, Elbow):	90		
Sqrt(Fric. Fac.)	0.139219		Eq. Len.:	14.5425	ft.	
Density:	5.08	lbm/ft^3				
Dynamic Press.:	1.25	psi	Poend =	995.43	psia	
Delta P:	3.0182	psi	Pend =	994.19	psia	

Feeder Pipe #4

Pipe Dia:	1.939	in.	Pipe Dia:	0.1616	ft.	
Pipe Length:	67.680	in.	Pipe Len.:	5.6400	ft.	
Mass Flow:	6.09	lbm/sec	Re #	3.88E+06		
P1:	997.09	psia	Po1:	998.97	psia	
Velocity:	58.49	ft/sec	Mach #	0.0518		
Fric. Factor:	0.019363		L/D (Tee, Elbow):	90		
Sqrt(Fric. Fac.)	0.139150		Eq. Len.:	14.5425	ft.	
Density:	5.08	lbm/ft^3				
Dynamic Press.:	1.87	psi	Poend =	994.43	psia	
Delta P:	4.5333	psi	Pend =	992.56	psia	

6 in. Sch 120

Feeder Pipe #5					
Pipe Dia:	1.939	in.	Pipe Dia:	0.1616	ft.
Pipe Length:	67.680	in.	Pipe Len.:	5.6400	ft.
Mass Flow:	6.36	lbm/sec	Re #	4.06E+06	
P1:	997.03	psia	Po1:	999.08	psia
Velocity:	61.13	ft/sec	Mach #	0.0542	
Fric. Factor:	0.019359		L/D (Tee, Elbow):	90	
Sqrt(Fric. Fac.)	0.139136		Eq. Len.:	14.5425	ft.
Density:	5.08	lbm/ft^3			
Dynamic Press.:	2.05	psi	Poend =	994.12	psia
Delta P:	4.9509	psi	Pend =	992.08	psia

Feeder Pipe #6					
Pipe Dia:	1.939	in.	Pipe Dia:	0.1616	ft.
Pipe Length:	67.680	in.	Pipe Len.:	5.6400	ft.
Mass Flow:	7.72	lbm/sec	Re #	4.92E+06	
P1:	997.02	psia	Po1:	1000.03	psia
Velocity:	74.15	ft/sec	Mach #	0.0657	
Fric. Factor:	0.019345		L/D (Tee, Elbow):	90	
Sqrt(Fric. Fac.)	0.139085		Eq. Len.:	14.5425	ft.
Density:	5.08	lbm/ft^3			
Dynamic Press.:	3.01	psi	Poend =	992.73	psia
Delta P:	7.2786	psi	Pend =	989.74	psia

ASRM TECHNOLOGY MODEL PRESSURE DROP CALCULATIONS
Downstream of Metering Nozzles

Constants					
Gas Const:	53.353	ft*lbf/lbm*Deg R		Gamma:	1.4

General Conditions					
Total mass flow:	231.650	lbm/sec	Temp.:	530.00	Deg. R
Mass Flow 1:	103.037	lbm/sec	Sonic Vel.:	1128.58	ft/sec
Mass Flow 2:	28.046	lbm/sec	Rough:	0.00015	ft
Mass Flow 3:	19.867	lbm/sec	Viscosity:	2.43E-06	ft^2/sec
Mass Flow 4:	24.359	lbm/sec			
Mass Flow 5:	25.458	lbm/sec			
Mass Flow 6:	30.879	lbm/sec			

Pressure Drop in Metering Nozzle after Shock

Section	Pipe Dia.	Shock Dia.	Throat Dia.	Pipe Area	Shock Ar.	Density 1	Density 2
***	in.	in.	in.	sq. in.	sq. in.	lbm/cu. ft.	lbm/cu. ft.
1	3.826	3.443	1.1976	11.4969	9.3125	3.07	3.08
2	1.939	1.745	0.6248	2.9529	2.3918	2.85	2.86
3	1.939	1.745	0.5259	2.9529	2.3918	2.72	2.72
4	1.939	1.745	0.5823	2.9529	2.3918	2.74	2.75
5	1.939	1.745	0.5953	2.9529	2.3918	2.73	2.74
6	1.939	1.745	0.6556	2.9529	2.3918	2.64	2.66

Section	Velocity 1	Velocity 2	Dyn Press 1	Dyn Press 2	P1	P2	Delta P
***	ft/sec	ft/sec	psi	psi	psia	psia	psi
1	129.70	104.72	5.58	3.65	603.08	605.01	-1.9290
2	148.16	119.51	6.75	4.41	559.49	561.83	-2.3396
3	110.08	88.96	3.55	2.33	533.42	534.65	-1.2270
4	134.02	108.19	5.30	3.47	537.20	539.04	-1.8354
5	140.61	113.47	5.81	3.80	535.12	537.14	-2.0139
6	175.96	141.69	8.83	5.76	518.68	521.75	-3.0692

Friction Loss After Metering Nozzles

Section	Pipe Dia.	Pipe Len.	Pipe Len.	L/D (Elbow)	Eq. Len.	Density	Dyn. Press
***	in.	in.	ft.	***	ft.	lbm/cu. ft.	psi
1	3.826	3.250	0.2708	N/A	N/A	3.08	3.65
2	1.939	10.415	0.8679	16	2.585	2.86	4.41
3	1.939	10.415	0.8679	16	2.585	2.72	2.33
4	1.939	10.415	0.8679	16	2.585	2.75	3.47
5	1.939	10.415	0.8679	16	2.585	2.74	3.80
6	1.939	10.415	0.8679	16	2.585	2.66	5.76

Section	Mach #	Re #	Fric. Fac.	Velocity	P1	P2	Delta P
***	***	***	***	ft/sec	psia	psia	psi
1	0.0928	1.37E+07	0.016775	104.72	605.01	604.96	0.0520
2	0.1059	7.93E+06	0.019572	119.51	561.83	559.98	1.8446
3	0.0788	5.90E+06	0.019669	88.96	534.65	533.67	0.9775
4	0.0959	7.18E+06	0.019602	108.19	539.04	537.59	1.4525
5	0.1005	7.53E+06	0.019587	113.47	537.14	535.55	1.5909
6	0.1255	9.40E+06	0.019527	141.69	521.75	519.35	2.4022

ERCI 10/01/92

Dump Loss into Spool Pieces						
Section	D1	Sec. Len.	D2	Loss Fac.	Density	Mass Flow
***	in.	in.	in.	***	lbm/cu. ft.	ft/sec
1	3.826	19.712	19.353	0.92336	3.08073	103.037
2	1.939	26.387	22.391	0.98506	2.85170	28.046
3	1.939	21.365	20.148	0.98156	2.71770	19.867
4	1.939	21.365	20.148	0.98156	2.73765	24.359
5	1.939	21.645	20.279	0.98180	2.72724	25.458
6	1.939	21.645	20.279	0.98180	2.64478	30.879

Section	Velocity	Dyn. Press.	P1	P2	Delta P
***	ft/sec	psi	psia	psia	psi
1	104.73	3.647	604.96	601.59	3.3671
2	119.90	4.424	559.98	555.63	4.3583
3	89.12	2.330	533.67	531.39	2.2866
4	108.48	3.477	537.59	534.18	3.4125
5	113.80	3.812	535.55	531.80	3.7425
6	142.34	5.783	519.35	513.67	5.6778

ASRM TECHNOLOGY MODEL PRESSURE DROP CALCULATIONS
Star Grain/Flow Distribution Tube

Constants						
Temp:	530.00	Deg. R	Gas Const:	53.353	ft*lbf/lbm*Deg R	
Hole Dia:	0.0935	inches	Hole Porosity:	0.55	%	
Dis. Coeff.:	0.60		Star Grain Hole Size:	0.0935	in.	
			Star Grain Porosity:	0.75	%	

Calculations

Segment	Dw. Area	Up. Area	Density	No. of Holes	Area/Hole	D1	Dia. Ratio
***	sq. in.	sq. in.	lbm/cu. ft.	***	sq. in.	in.	***
1	2052.77	2052.77	3.063581	2242	0.915595	1.079709	0.086597
2	1341.79	1383.72	2.829506	1075	1.287179	1.280190	0.073036
3	1106.75	1141.33	2.706058	887	1.286732	1.279968	0.073049
4	1097.35	1131.64	2.720267	879	1.287415	1.280308	0.073029
5	1102.07	1136.51	2.708186	883	1.287101	1.280152	0.073038
6	1233.62	1272.17	2.615863	988	1.287617	1.280408	0.073024
				Total Holes(2-6): 4712			

Segment	Porosity	Exp. Fact.	Flow Coeff.	Mass Flow	P1	P2	Delta P
***	***	***	***	lbm/sec	psia	psia	psi
1	0.0075	0.95108	0.600017	103.0370	601.59	501.10	100.4913
2	0.0055	0.98269	0.600009	28.0460	555.63	522.78	32.8451
3	0.0055	0.98615	0.600009	19.8670	531.39	506.25	25.1353
4	0.0055	0.97869	0.600009	24.3590	534.18	495.31	38.8618
5	0.0055	0.97663	0.600009	25.4580	531.80	489.37	42.4299
6	0.0055	0.97018	0.600009	30.8790	513.67	461.36	52.3098

*Note: Section 1 is the drilled hole star grain.

ASRM TECHNOLOGY MODEL PRESSURE DROP CALCULATIONS
Porous Wall Liner/Drilled Hole Slot Plates

Constants					
Temp:	530.00	Deg. R	Dyn. Viscosity:	1.237E-05	lbm/ft*sec
Pore Size:	15	microns	Permeability:	7.083E-12	m^2
Wall Thick.:	0.5	in.	Permeability:	1.333E-06	m
Gas Const.:	53.353	ft*lbf/lbm*Deg R	Material:	Bronze	

Calculations for Porous Wall Liner

Segment	Area	Density	Mass Flow	P2	P2
***	sq. in.	lbm/cu. ft.	lbm/sec	psia	pascals
2	507.44	2.44336	24.5234	479.80	3.308E+06
3	412.80	2.35323	19.8670	462.10	3.186E+06
4	434.99	2.29161	20.9560	450.00	3.103E+06
5	424.46	2.12610	25.4580	417.50	2.879E+06
6	630.03	2.09096	30.8790	410.60	2.831E+06

Segment	Area	Density	Vol. Flow	P1	Delta P
***	sq. m	kg/cu. m	cu. m/sec	psia	psi
2	0.32738	39.13889	0.28421	522.78	42.9813
3	0.26632	37.69504	0.23906	506.25	44.1498
4	0.28064	36.70800	0.25895	495.31	45.3135
5	0.27384	34.05687	0.33907	489.37	71.8729
6	0.40647	33.49402	0.41818	461.36	50.7637

Calculations for Slot Plates

Segment	% Flow	Hole Dia.	Porosity	No. of Holes	Area/Hole	D1
***	***	in.	percent	***	sq. in.	in.
2	12.56	0.0935	1.2101	115	0.5674	0.8500
4	13.97	0.0935	1.1390	106	0.6028	0.8761

Segment	Dia. Ratio	Area	Mass Fl./Hole	Mass Flow	Dis. Coeff.	Exp. Fact.
***	***	sq. in.	lbm/sec	lbm/sec	***	***
2	0.110006	65.25	0.03060	3.5226	0.60	0.97254
4	0.106723	63.90	0.03201	3.4030	0.60	0.96607

Segment	Flow Coeff.	Density	P1	P2	Delta P
***	***	lbm/cu. ft.	psia	psia	psi
2	0.600044	2.662244	522.78	473.76	49.0213
4	0.600039	2.522365	495.31	437.94	57.3735

ERCI 10/01/92

ASRM TECHNOLOGY MODEL PRESSURE DROP CALCULATIONS
Analysis Summary

Analysis Assumptions
Incompressible with Density Corrections
Adiabatic
Colebrook Turbulent Friction Factor Correlation

Initial Conditions

Total Mass Flow:	231.65	lbm/sec
Total Pressure:	1000	psia
Temperature:	530.00	Deg. R
Initial Pipe I.D.:	5.761	inches
Pipe Roughness:	0.00015	feet
L/D for Tee(through)	20	
L/D for Tee(branch)	60	
L/D for 90 Degree Elbow	30	
L/D for 45 Degree Elbow	16	

Manifold Pressure Summary

Section	1	2	3	4	5	6
Pressure (psia)	997.68	997.39	997.21	997.09	997.03	997.06
Pipe I.D. (in.)	5.501	5.501	5.501	5.501	5.501	5.501

Feeder Pipe Pressure Summary

Section	1	2	3	4	5	6
Pressure (psia)	995.05	991.39	994.19	992.56	992.08	989.74
Pipe I.D. (in.)	3.826	1.939	1.939	1.939	1.939	1.939

Metering Nozzle Exit

Section	1	2	3	4	5	6
Pressure (psia)	605.01	561.83	534.65	539.04	537.14	521.75

Entrance to Spool Pieces

Section	1	2	3	4	5	6
Pressure (psia)	604.96	559.98	533.67	537.59	535.55	519.35

Spool Piece Plenum

Section	1	2	3	4	5	6
Pressure (psia)	601.59	555.63	531.39	534.18	531.80	513.67

After Flow Distribution Tube

Section	1	2	3	4	5	6
Hole Dia. (in)	0.0935	0.0935	0.0935	0.0935	0.0935	0.0935
Porosity (%)	0.75	0.55	0.55	0.55	0.55	0.55
No. of Holes	2242	1075	887	879	883	988
Delta P (psi)	100.49	32.85	25.14	38.86	42.43	52.31
Pressure (psia)	501.10	522.78	506.25	495.31	489.37	461.36

After Porous Liner

Section	2	3	4	5	6
Pore Size (microns)	15	15	15	15	15
Wall Thick. (in.)	0.5	0.5	0.5	0.5	0.5
Delta P (psi)	42.98	44.15	45.31	71.87	50.76
Pressure (psia)	479.80	462.10	450.00	417.50	410.60

ASRM TECHNOLOGY MODEL FLOW ANALYSIS
SLOT DESIGN STUDY

Aft Slot

Case	Hole Dia.	Bore Pressure	No. of	# Holes/	Slot Flow %
* * *	in.	psia	Holes	Nom. # Holes	* * *
+20% Re #	0.0935	525.53	107	1.00943	14.10
Nominal	0.0935	437.94	106	1.00000	13.97
-20% Re #	0.0935	350.35	105	0.99057	13.84

ASRM Technology Model Analysis

The SAF Technology Model is being designed to provide a 10% scaled model of the ASRM deformed motor geometry operating at full-scale motor Reynolds numbers. The model will be used to assess the internal flow field in the full-scale motor, so the flow in the Technology Model should be as similar as possible to flow field in the full-scale motor. In order to provide a detailed assessment of the design of the Technology model and the internal flow field similarity between the model and the ASRM full-scale motor, CFD analyses are being performed on both the Technology model and the full-scale motor. The analyses are being performed with Fluent/BFC version 3.02. This Navier-Stokes code was validated against the cylindrical port CSD experimental data and the results of this analysis were reported in the May 92 monthly report. The May 92 monthly contains a full discussion of the differences between the standard $\kappa-\varepsilon$ model and the adjusted $\kappa-\varepsilon$ model.

During the month of June, 1992, the CFD analysis of the Technology model was completed. The results of this analysis are reported in this monthly. Results are presented for internal flow fields using both the standard k-e model and the adjusted $\kappa-\varepsilon$ model. In the following discussion the adjusted $\kappa-\varepsilon$ model matches the ballistic and analytical solution data much better than the standard $\kappa-\varepsilon$ model.

The geometry description used to construct the Technology Model computational grid was taken from ERCI drawings H3200-1, revision A and H3200-2, revision A. The dimensions specified in the drawings were used except in the head end region. The drawing H3200-2 shows a star grain propellant configuration in the head end of the model. The star grain propellant flares into the cylindrical port geometry in the transition region shown in the drawing. From the end of the transition at the cylindrical port, upstream to the head end of the model, the propellant grain was modeled as a cylindrical port with a radius equivalent to the star grain configuration flow area. The flow area in the star grain region was calculated and the equivalent cylindrical radius was computed for this area. This equivalent radius was very close to the port radius at the end of the star grain transition so the analysis was simplified by modeling the Technology model head end region as a cylindrical port of radius equal to the radius of the actual port at the end of the star grain transition. This allows the head end to be modeled with a consistent flow area but without the three-dimensional complexity of the actual star grain configuration. This simplification is important since the flow field for the full model chamber from the head end to the nozzle nose is being modeled. If the star grain configuration were modeled the required number of computational cells would increase dramatically. The effects of the star grain propellant configuration on the internal flow in the model will need to be investigated separately.

The computational grid contained 411 axial computational cells and 23 radial computational cells in the port region. The slot regions are resolved using 16 axial cells and 31 radial cells. Figure 5 shows the grid used in this analysis. The y-axis is stretched by a 4x magnification factor in order to show more of the grid structure than

could be shown on an unmagnified grid plot. Figure 6 shows a closeup of the grid in the slot region. This figure readily shows that the grid lines have been clustered near the propellant and solid wall surfaces. The figure also shows that the grid line spacing is smaller in regions where higher flow variable gradients are expected to exist. The two flow field solutions for the technology model, one using the standard κ–ε model (**SKE**) and the other using the adjusted κ–ε model (**AKE**), were calculated using the same computational grid. No analysis has been performed at this point on the sensitivity of the flow solution to the grid resolution. This analysis will be performed as time permits.

The basic thermochemical properties and boundary conditions used in the analysis were:

M, molecular weight	28.97
m, dynamic viscosity(Pa-s)	1.853×10^{-5}
C_p, specific heat(J/kg- K)	1004.5
T_o, Stagnation Temperature(K)	294.4

Figure 7 shows a plot of the Technology Model configuration considered in this analysis. The figure is labeled to show the terminology used in this discussion. A velocity boundary condition was used at the simulated propellant grain surface. Notice that the propellant grain has been divided into six sections. These sections correspond to those shown in ERCI drawing H3200-2, revision A. The correct velocities for the surfaces in the six sections were not known directly. The velocities were obtained by the following iterative process. Since the model geometry is a 10% scaling of the full-scale motor, the six sections shown in Figure 7 can be made to correspond to six sections of the actual rocket motor propellant. The percentage of mass flux injected from the six sections of the full-scale ASRM motor were determined using SPP ballistic calculations for the full-scale ASRM motor. Percentages of the total ASRM mass flux from the propellant surface were computed for each motor section. The total mass flow rate in the Technology Model was determined such that Reynolds number similarity was satisfied between the full-scale motor and the Technology Model in the aft end. Once the total Technology model mass flow rate was computed, the percentages of mass flux for the six sections, (computed from the ASRM full-scale motor), were used to calculate the mass flow rate from each section of the Technology model. The mass flow rate, however, does not directly translate into a velocity boundary condition. A port pressure estimate for the six sections must also be obtained. The initial estimate of the pressure distribution in the port of the model was determined from an analytic code. Given this information, a velocity was obtained from the mass flow rate equation, (m=ρVA) and the ideal gas law. This velocity estimate was then used to converge the flow field to an intermediate convergence level. At this point the calculated mass flow rates based on the initial guess pressure field are compared to the desired mass flow rates for each section. A new velocity boundary condition was computed from this information. This iteration of the velocity boundary condition for the six sections continued until the mass flow rates computed by the CFD code matched the target

mass flow rates which originated from the ASRM full-scale motor run. The final computed velocity boundary conditions associated with the six sections of the Technology Model are shown below.

	SKE model	AKE model
Section 1	4.320 m/s(14.17 ft/s)	4.740 m/s(15.55 ft/s)
Section 2	0.725 m/s(2.38 ft/s)	0.837 m/s(2.75 ft/s)
Section 3	0.827 m/s(2.71 ft/s)	0.905 m/s(2.97 ft/s)
Section 4	0.837 m/s(2.75 ft/s)	0.916 m/s(3.01 ft/s)
Section 5	1.177 m/s(3.01 ft/s)	1.220 m/s(4.00 ft/s)
Section 6	0.974 m/s(3.20 ft/s)	0.976 m/s(3.20 ft/s)

A no-slip velocity boundary condition was utilized along inhibited or non-propellant surfaces located in the model head end and in the slots. A symmetry boundary condition was used along the motor centerline axis of symmetry. All surfaces were considered to be adiabatic. A static pressure boundary conditions was utilized at the aft end outlet of the model. The static pressure was specified as 412.7 psia, which was obtained from similarity calculations associated with reaching the required Aft end full-scale Reynolds number. The total mass flow rate for the propellant surfaces modeled in the Technology model analysis was 101.47 kg/s (223.7 lbm/s). For the SKE model solution, the total computed mass flow rate was 101.33 kg/s (223.4 lbm/s). The computed mass flow rate is within less than 0.2% of the desired mass flow rate for the model. The total computed mass flow rate for the AKE model solution was 101.15 kg/s (223.0 lbm/s). This is within 0.3% of the desired mass flow rate for the model. This problem exhibited a rather slow convergence rate and both solutions required over 10000 iterations to achieve convergence.

As previously mentioned, the standard κ-ε model and the adjusted κ-ε model were used in the CFD code to solve for the Technology model internal flow field. The results will be presented together in a comparative fashion.

A general overview of the flow field results using the SKE model and the AKE model will be given before discussing the actual physics of the internal flow in the Technology model. Figures 8, 9, and 10 show constant axial planes at specific L/D ratios in the Technology model chamber. The ratios are those for which data is plotted in the results section of this report on the Technology model flow field. Figure 8 shows the region of the Technology model from the head end to the first slot while Figure 9 shows the center propellant grain between the forward and aft slots. Figure 10 shows the aft section of the model from the aft slot to a point just upstream of the submerged nose of the nozzle. These figures will be helpful throughout the discussion of the flow field results. These figures may also be referenced as needed to determine the location of a specified L/D ratio mentioned in the text. Figures 11 and 12 show color raster plots of the predicted Mach number in the flow field using the SKE and AKE models, respectively. The most notable observance is that the Mach number plot for the SKE model shows a more concentrated high Mach number region in the aft section of the

model. This means that the centerline Mach number changes more rapidly when using the SKE model than when using the AKE model. Figures 13 and 14 show raster plots of the total pressure in the Technology model using the SKE and AKE models, respectively. The general trend of the total pressure is the same for the two solutions. In the low velocity region of the head end the total pressure is approximately constant. As the mass injection increases, the port Mach number increases and a velocity profile begins to develop. This causes the development of the stratified layers seen in the plot in the radial direction. This is strictly related to the higher dynamic pressure at the model centerline as the flow velocity increases. The SKE model predicts a much greater drop in both the centerline and wall total pressure for the model. As shown in Figure 14, there is only a small loss in total pressure at the centerline at the aft end of the model port using the AKE model. Figures 15 and 16 show raster plots of the pressure in the forward and aft slot regions respectively for the SKE model results. Figures 17 and 18 show the corresponding velocity field for the forward and aft slots predicted using the SKE model. The relative size of the velocity vectors is directly related to the flow Mach number. There is a recirculation region along the downstream face of the slot for both the forward and aft slots. The recirculation region is stronger for the downstream slot since the port Mach number is greater at the aft slot. The stronger port flow at the aft slot causes the flow emanating from the slot to be more restricted than the flow from the forward slot. The recirculation region forms a restriction to the passage of the slot mass flux into the port region. This creates a region of higher velocity flow along the upstream slot face. This is evidenced in the pressure plots, Figures 15 and 16. There is a high pressure region on the downstream slot face and a low pressure region on the upstream slot face. This can also be noted by observing the strength of the flow near the upstream face of the slot in Figures 17 and 18. The AKE model solution does not show a recirculation region in the slots. Figures 19 and 20 show the pressure raster plots for the forward and aft slots respectively and Figures 21 and 22 show the velocity field for the forward and aft slots. The velocity distributions near the wall are different for the solutions using the SKE and the AKE models. This causes the restriction on the flow from the slot to be less for the AKE solution and therefore no recirculation region is generated on the downstream slot face.

The remainder of the discussion of the analytical results will be devoted to a detailed discussion of the physical phenomena existing in the Technology model. Data will be shown and discussed for the static and total pressure in the model and for the axial and radial velocity components at various L/D ratios in the model port. The normalized kinetic energy of turbulence profiles in the model will also be shown. This data will provide a better understanding of the details of what is happening in the model.

Figures 23 and 24 respectively, show a plot of the centerline and average Mach numbers predicted in the technology model port using the SKE model and the AKE model . The Mach number increases very rapidly in the head end section of the model from an L/D of 0 to 4. This is due to the larger amount of mass flow emanating from the head end star grain propellant region. The SKE model predicts transition to turbulent

flow much faster than the AKE model. In reference to the SKE model Mach number prediction, there is a depression in the slope of the centerline Mach number in the region where the velocity profile is changing drastically (L/D from about 10 to 15). Since the SKE model causes a much more rapid transition of the flow, the velocity profiles are much flatter than for the AKE model. This is collaborated by observing that the centerline Mach number is affected less for the AKE model than for the SKE model. The abrupt slope change in the center section of the model (L/D from about 10 to 15) observed in Figure 23 for the SKE model is not present in the AKE model solution. Unlike the SKE model results, the AKE model predicts very little change in the slope of the Mach number for the flow near the centerline of the model. One final comparative note, the sharp drop in the Mach number from an L/D of 18 to 21 is caused by a change in the simulated propellant geometry in the aft section of the model. The area ratio increases rapidly in the aft section of the model due to the divergent propellant geometry. The centerline Mach number for the AKE solution is not as affected by the model geometry change as is centerline Mach number for the SKE model. Again, this is due to a difference in the dissipation of energy predicted when using the two models and this will be illustrated when the velocity and kinetic energy of turbulence profiles are shown.

An analytic model was developed at ERCI and discussed in the May 92 monthly report. This model used a similarity velocity profile assumption to compute the flow characteristics of the Technology model by means of an analytic solution. Either of two velocity profiles may be assumed for the analytic solution. The code can use either a bulk velocity profile, as used in some ballistic codes, or a Culick velocity profile. Figure 25 shows the results from the code using a Culick velocity profile. Figure 26 shows the results using a bulk velocity profile. The head end pressure for these runs was constrained to the head end pressure computed from the CFD runs so that an easy comparison of the results could be made. The plots show the static pressure, the total pressure along the centerline and the average total pressure. The total pressure drop assuming a bulk profile was 55 psi while the total pressure drop assuming the Culick profile was 70 psi. The Culick profile solution predicts more pressure drop down the model port but is more representative of the velocity profile in an actual rocket motor as collaborated by the CSD cold flow experimental test data. The comparison of these results shows that there is a significant difference between using a bulk or a Culick velocity profile assumption.

Figure 27 shows a comparison between the static pressure predicted by the CFD code using the SKE model and the static pressure predicted by the analytic Culick profile solution. The plot shows that the SKE model over predicts the pressure drop down the model port by a substantial amount. From the head end to the forward slot the results of the solutions are close, but downstream of the forward slot at an axial distance of approximately 48 inches the results diverge. This divergence in the solutions is due to two factors. The prediction of transition to turbulent flow upstream of the forward slot is both premature and too rapid. The actual transition of the velocity profiles will be discussed later. Figure 28 shows a comparison between the predicted static pressure

in the model for the CFD solution using the AKE model and the predicted static pressure using the analytic Culick profile solution. The CFD and analytic solutions match closely. The CFD code develops a slightly different slope as the transition process continues down the port. The only other difference exist in the aft section where the port diameter increases rapidly. The differences in the solutions in the aft section of the model are due to drastic changes in the CFD predicted velocity profiles in this region and this will be discussed at a later time. Figures 29 and 30 show the comparison between CFD and analytic total pressure predictions for the SKE and AKE models, respectively. The same observations discussed for the static pressures in the model apply to the total pressure comparison plots. For the SKE model solution the total pressure along the centerline begins to drop rapidly once transition occurs. As shown in Figure 30, the transition phenomenon in the CFD solution using the AKE model is delayed and not as rapid. The total pressure along the centerline is not significantly affected until the aft section of the model.

The normalized axial velocity profiles in the model port illustrate transition of the flow from laminar to turbulent flow. The profiles for the SKE solution will be discussed first. The velocity profiles also show the detailed physical changes in the flow as the air flows down the model port. The normalized axial velocity profiles are plotted in comparative figures for different regions of the Technology model chamber. Figure 31 shows an overall view of how the axial velocity profile changes down the model port. The velocity profiles in the head end of the motor rapidly form profiles very close to a Culick profile. This occurs very near the head end of the model as illustrated in Figure 32. As the flow approaches the forward slot, transition has already begun to occur for the SKE model solution. This is illustrated by the 5.07 L/D velocity profile in Figure 32. As flow continues to move down the model port to the aft end, the velocity profiles become more flattened or turbulent in nature. Figure 33 shows the disturbance of the velocity profiles in the forward slot region. Figure 34 best illustrates the continued transition of the velocity profile to a fully turbulent character. Most of the transition in the axial velocity profiles occur in the center segment of the model coincident with the slope change of the static pressure in the model port noted in the discussion of Figure 27. Figure 35 shows that there is only a small alteration of the axial velocity profile at the aft slot. And Figure 36 shows the velocity profiles in the aft section of the model. The L/D of 17.29 is downstream of the aft slot and just prior to the slope change in the simulated propellant geometry. Notice in Figure 7 how the simulated aft propellant grains flares outward as the model nozzle is approached. This geometry change drastically alters both the axial and radial velocity profile in the model port. The turbulent kinetic energy is also redistributed over the port as will be shown in the sequence of plots for the normalized turbulent kinetic energy. The sequence of figures from Figure 37 to Figure 48 show the normalized turbulent kinetic energy at specified L/D ratios sequentially down the model port. The normalized turbulent kinetic energy level is highest along the centerline of the flow field near the head end of the model just as seen in the experimental data for the CSD cold flow test discussed in the May 92 monthly. The normalized kinetic energy level drops rapidly until an L/D of about 5.07 where a peak begins to develop near the mass injection wall. This peak is very

pronounced by the 6.06 L/D as shown in Figure 40. The peak begins to grow and widen as the flow moves down the model port. A maximum of 8% turbulence level is reached in the aft end of the model. This is much higher than the levels noted in the CSD coldflow test data although test conditions are different. These high levels of turbulence can be associated somewhat with the excessive pressure drop down the model port predicted by the SKE model.

The normalized axial velocity profiles for the AKE model solution are much different when compared with those already presented for the SKE model solution. Figure 49 shows the sequence of velocity profiles at selected L/D ratios from the model head end to the aft end. Figure 50 shows the axial velocity profiles at various L/D ratios in the head end of the model prior to the forward slot. When Figure 50 is compared to Figure 32 it becomes immediately apparent that the AKE model solution is different. The process of transition has not yet started in the AKE model solution for those L/D's plotted in Figure 50. A small growth in the normalized turbulent kinetic energy profile at an L/D of 6.06 signals the possible beginnings of transition upstream of the forward slot but the axial velocity profiles show very little change upstream of the slot region. Figure 51 shows the velocity profiles in the forward slot region where the slot does seem to have a significant effect on the velocity profiles and the transition process. Most of the change in the velocity profiles are concentrated near the mass injection wall in this region of the model. Although the beginnings of transition are evident in the region of the forward slot for the AKE model solution, the transition process is much less rapid than the process predicted by the SKE model. Figure 52 illustrates this well by showing the transition of the velocity profiles along the center section of the model between the forward and aft slots. The transfer of kinetic energy between the model centerline and the wall is much less for the AKE model than for the SKE model. This will again be illustrated when the normalized turbulent kinetic energy profiles are observed for the AKE model solution. The level of turbulence is much lower near the model centerline than for the SKE model solution. Figure 53 shows the velocity profiles in the vicinity of the aft slot and Figure 54 shows the velocity profiles in the aft section of the model. As seen for the SKE model, the simulated propellant grain geometry change has a drastic effect on the velocity profiles in the aft section of the model. Figures 55 to 66 show the normalized turbulent kinetic energy profiles for the AKE model solution at specified L/D ratios from the model head end to the aft end. These are the same L/D's as plotted for the SKE model solution and can be directly compared. The comparative results can be summarized by noting that the growth of a turbulent energy peak near the wall occurs much later for the AKE model solution and the continued growth in turbulence level is slower for the AKE model solution. The maximum turbulence level up to the propellant geometry flare in the aft section of the model is less than 2% for the AKE model solution. This is approximately 5% less than the same level observed for the SKE model solution. Another clearly discernible feature of the AKE model normalized kinetic energy profiles is that the centerline turbulence levels are much lower than for comparative L/D ratios for the SKE model. As previously observed, there is a drastic change in the velocity profiles aft of the propellant geometry flare in the aft section of the model and the normalized turbulent

kinetic energy for the AKE model solution shows a drastic change in the turbulence profile at the L/D of 20.82, Figure 66.

Several concluding observations will now be made to summarize the CFD and analytic solution data presented in this monthly report.

1. As for the analytic solution, the pressure drop generated down the model when assuming a Culick profile is greater than generated when assuming a bulk profile. The difference caused by assuming the Culick profile is significant and the Culick profile is a better choice than the bulk profile. This is backed up by experimental data from the CSD coldflow test which showed velocity profiles much closer to Culick profiles than a bulk profile for the major portion of the model tested. Also, the analytic results based on the assumed Culick velocity profile match the CFD results using the AKE turbulence model which has been validated against the normalized axial velocity and turbulent kinetic energy profile data from the CSD experiment.

2. The AKE turbulence model solution is indicated as the better CFD solution since it matches both the analytic results and the CSD experimental data much better than the SKE solution.

3. Transition of the model axial velocity profiles does not begin until the immediate vicinity of the forward slot. There is evidence of the beginnings of turbulence upstream of the forward slot as observed in the normalized turbulent kinetic energy profiles but the transition is very slow upstream of the forward slot. The forward slot contributes to the onset of turbulence and the transition process speeds up somewhat downstream of the forward slot.

4. Maximum turbulence levels are below 2% for all regions of the model except in the aft section where the simulated propellant grain undergoes slope change causing a drastic increase in area ratio of the model port.

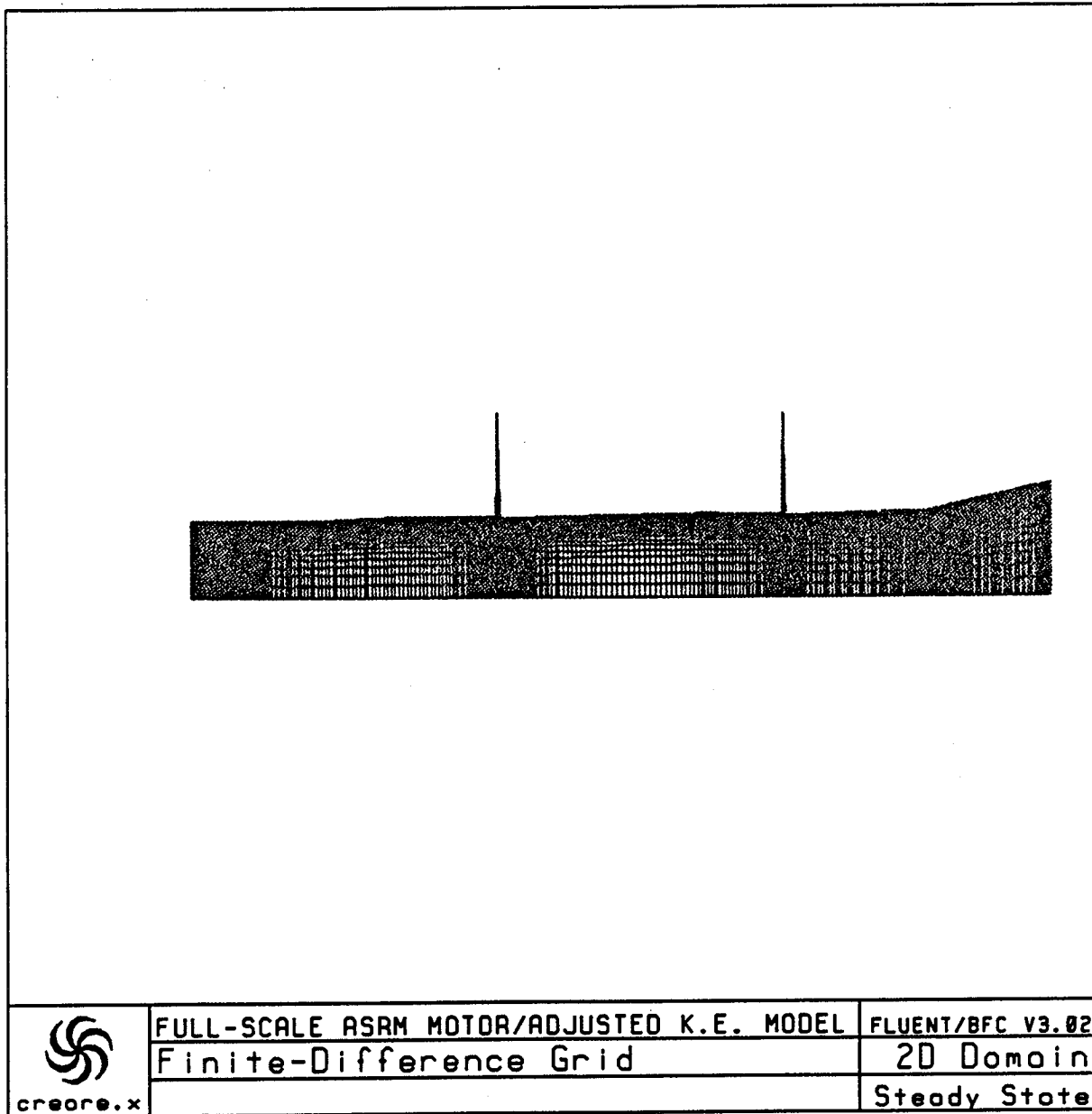| | FULL-SCALE ASRM MOTOR/ADJUSTED K.E. MODEL | FLUENT/BFC V3.02 |
| S | Finite-Difference Grid | 2D Domain |
| creore.x | | Steady State |

Figure 5. Computational Grid for Technology Model

TECHNOLOGY MODEL/DEFORMED GRAIN/410X54 | FLUENT/BFC V3.02
Finite-Difference Grid | 2D Domain
creare.x | | Steady State
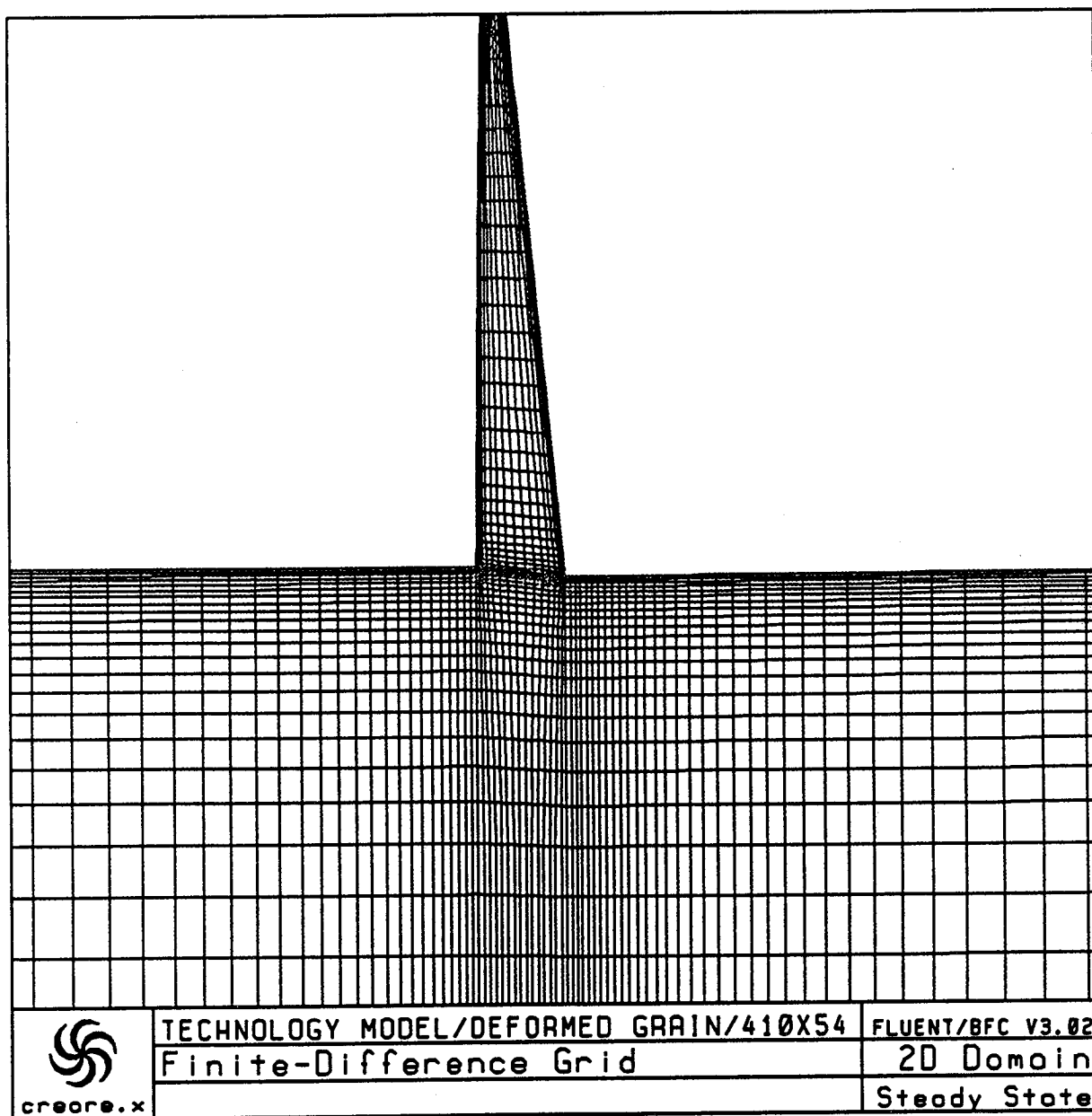
Figure 6. Computational Grid in the Slot Region

End of Head End
Star Grain Transition

Forward Slot

Propellant Surface

Model
Centerline

[L/D]   0.82 1.23 1.74   3.18   4.12   5.07   6.06   7.56
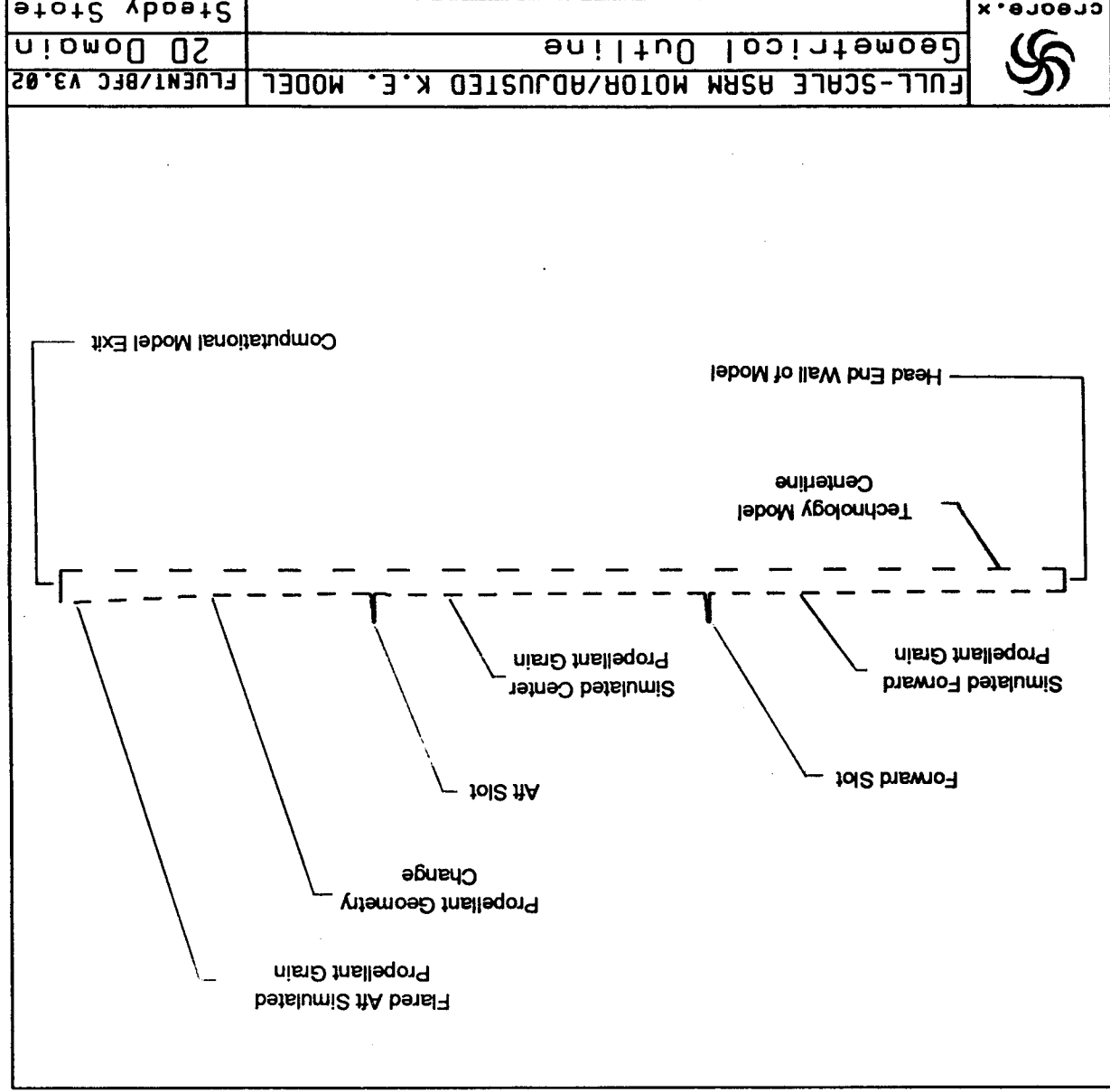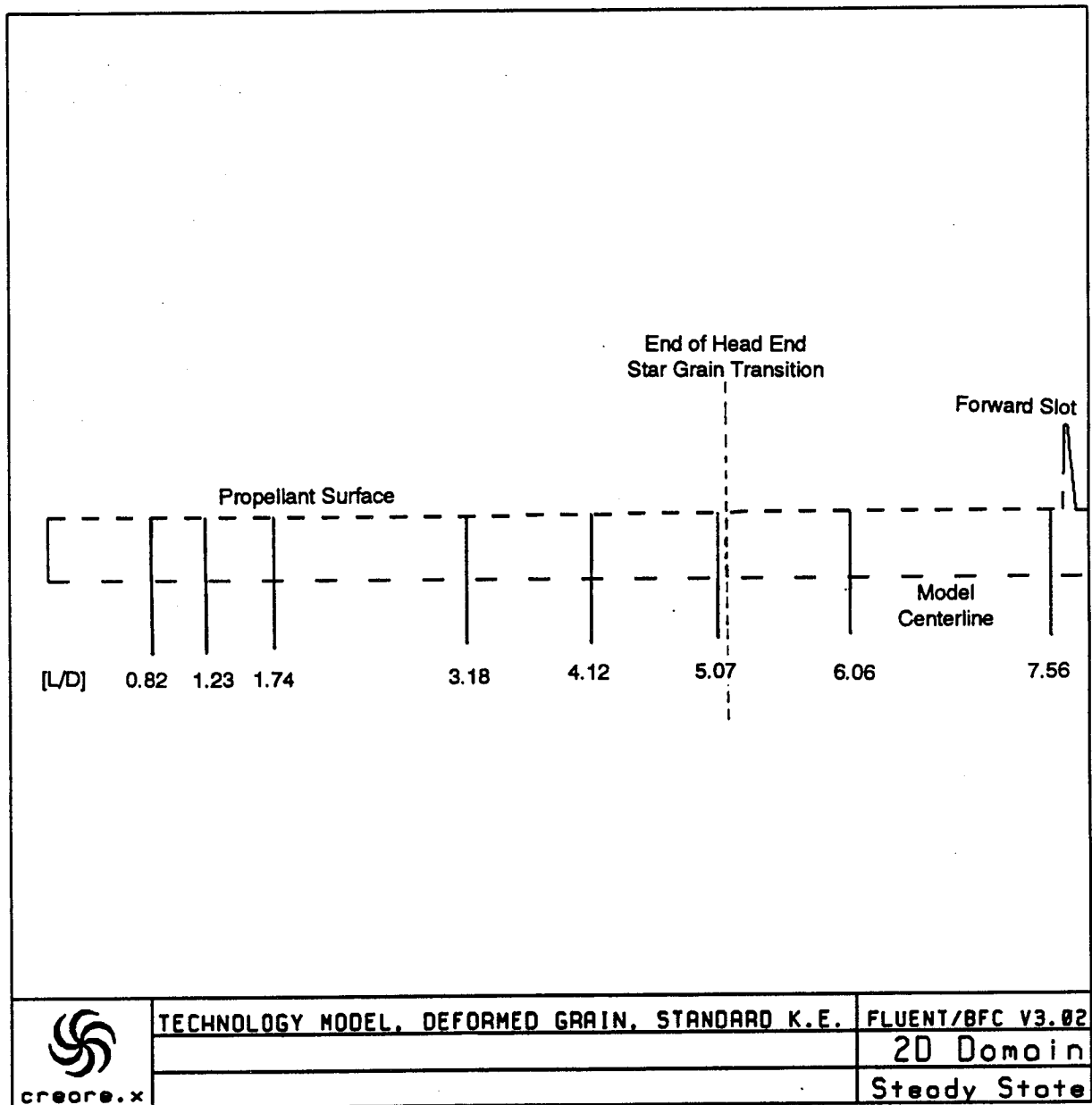
Figure 8. View of the Forward Section

of the Technology Model

TECHNOLOGY MODEL/DEFORMED GRAIN

Forward slot

Propellant grain surface

Aft slot

Model centerline

L/D
7.62
7.66
7.76
8.06
9.37
10.62
11.68
12.77
13.73
14.32
14.60
14.68
14.73
15.34

FLUENT/BFC V3.02
2D Domain
Steady State

creare.x
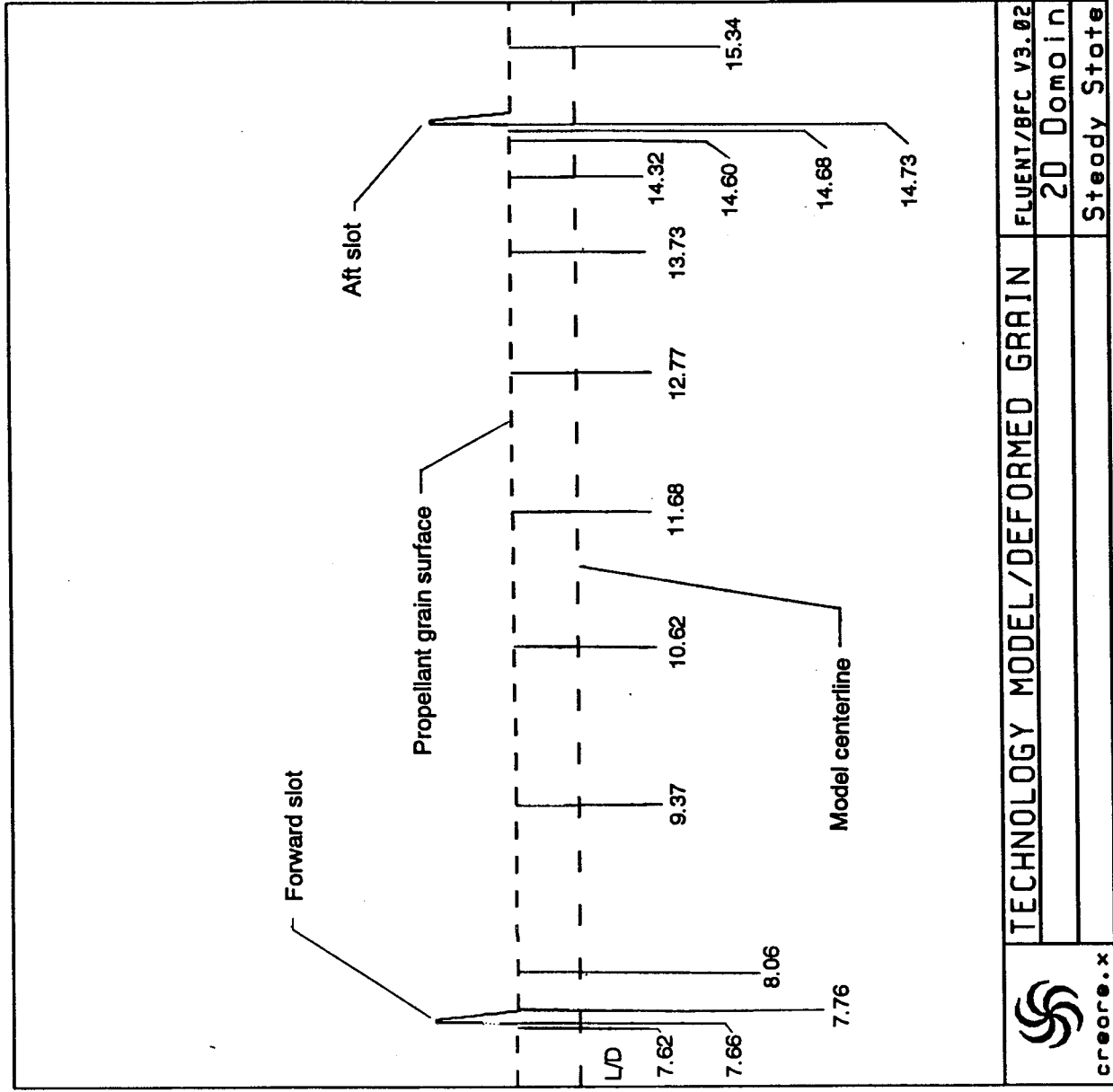
**Figure 9. View of the Center Section
of the Technology Model**

Beginning point of the
submerged nose region

Aft slot

Propellant grain surface

14.73   15.34   16.63   17.29   18.55   19.69   20.82

Model centerline

TECHNOLOGY MODEL/DEFORMED GRAIN   FLUENT/BFC V3.02
                                                    2D Domain
creore.x   Steady State
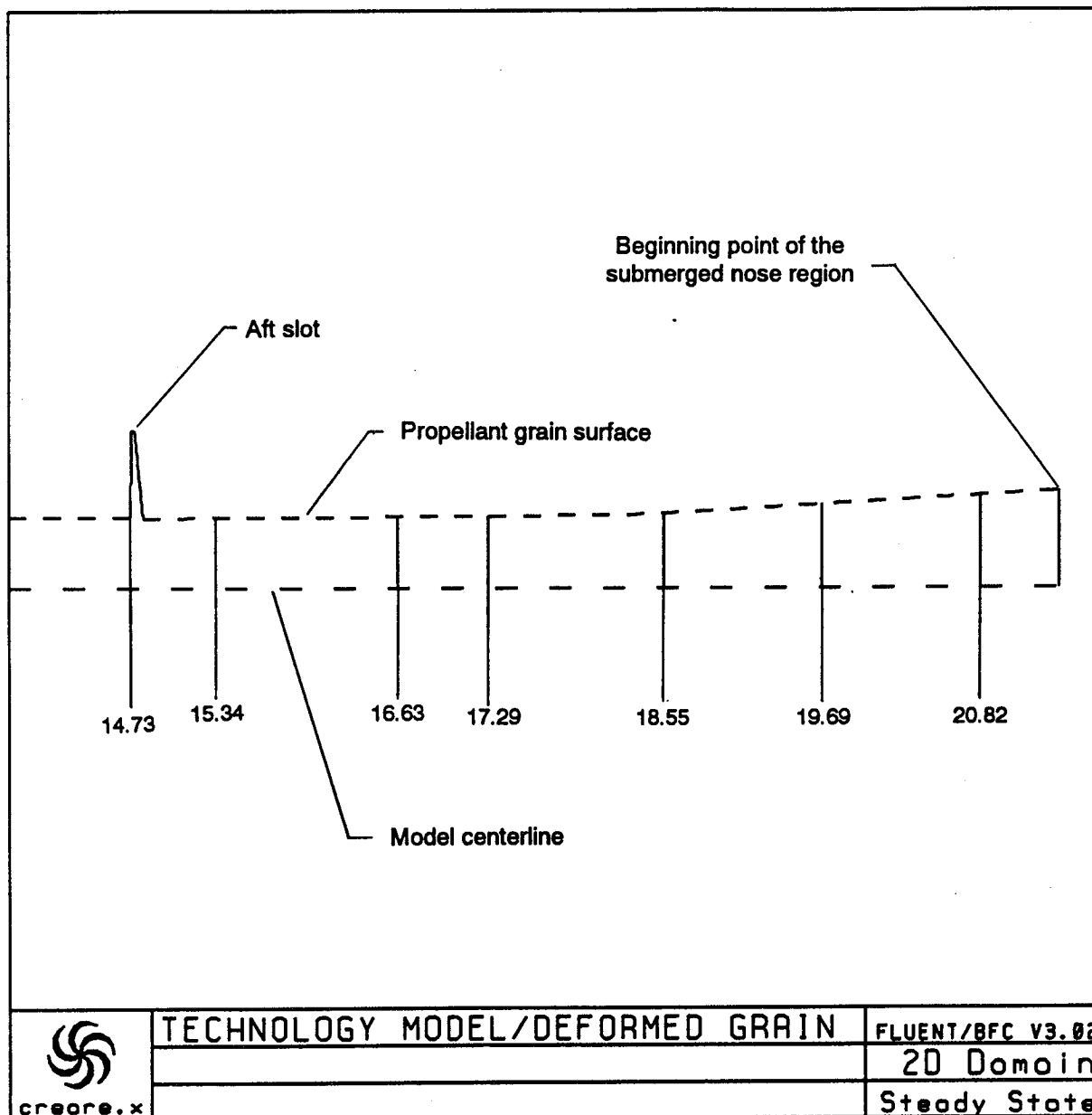
**Figure 10. View of the Aft Section of the
Technology Model**

KEY

Minimum =
0.00E+00

▮	0.00E+00
	3.61E-02
	7.21E-02
	1.08E-01
	1.44E-01
	1.80E-01
	2.16E-01
	2.52E-01
	2.89E-01
	3.25E-01
	3.61E-01
	3.97E-01
	4.33E-01
	4.69E-01
	5.05E-01
▮	5.41E-01

Maximum =
5.41E-01

⟳	TECHNOLOGY MODEL/DEFORMED GRAIN/STANDARD K.E. MODEL	FLUENT/BFC V3.02
	Roster Plot of MACH-NUMBER	2D Domain
creare.x		Steady State
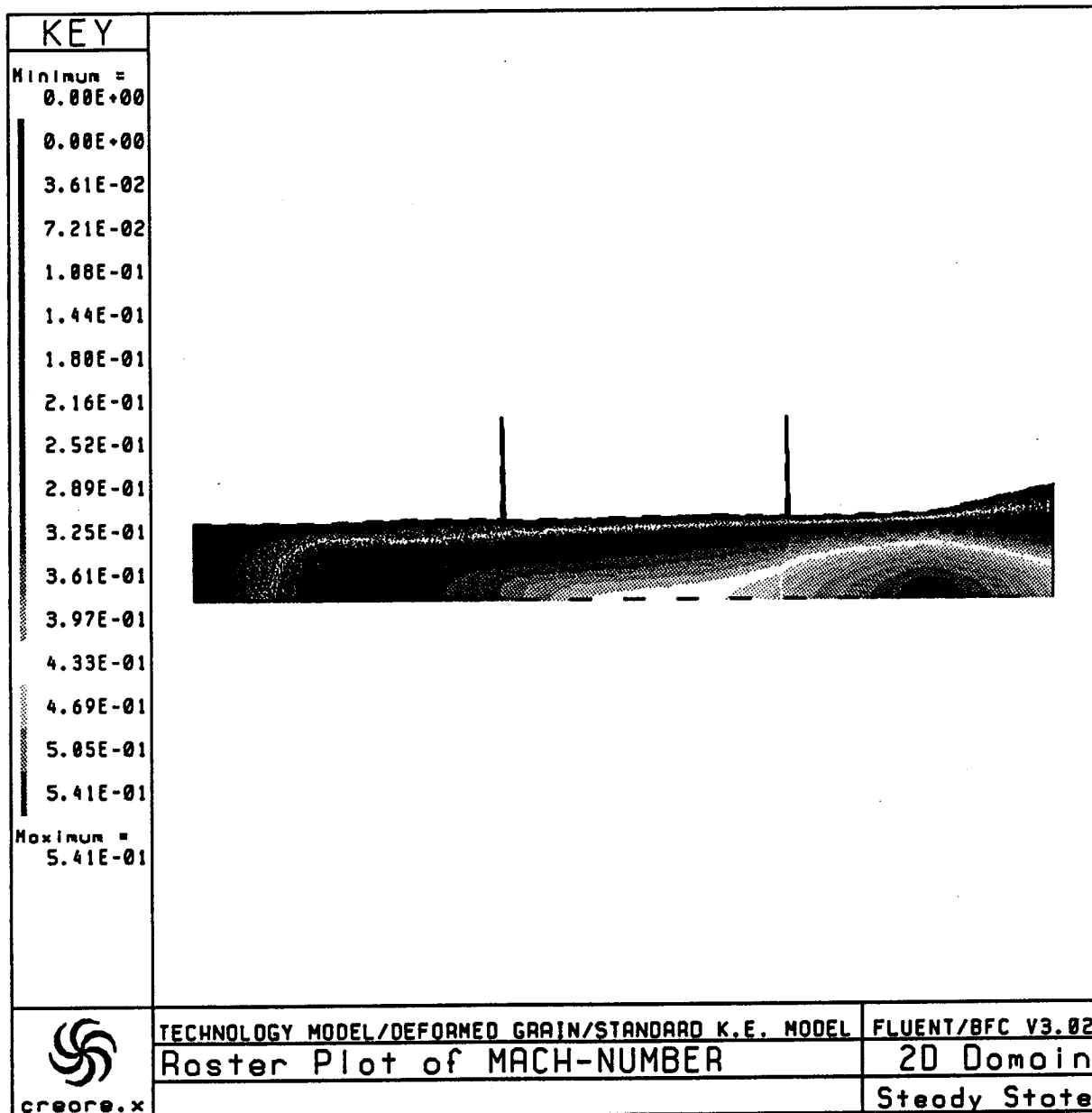
Figure 11. Raster Plot of the Mach Number for the SKE Model
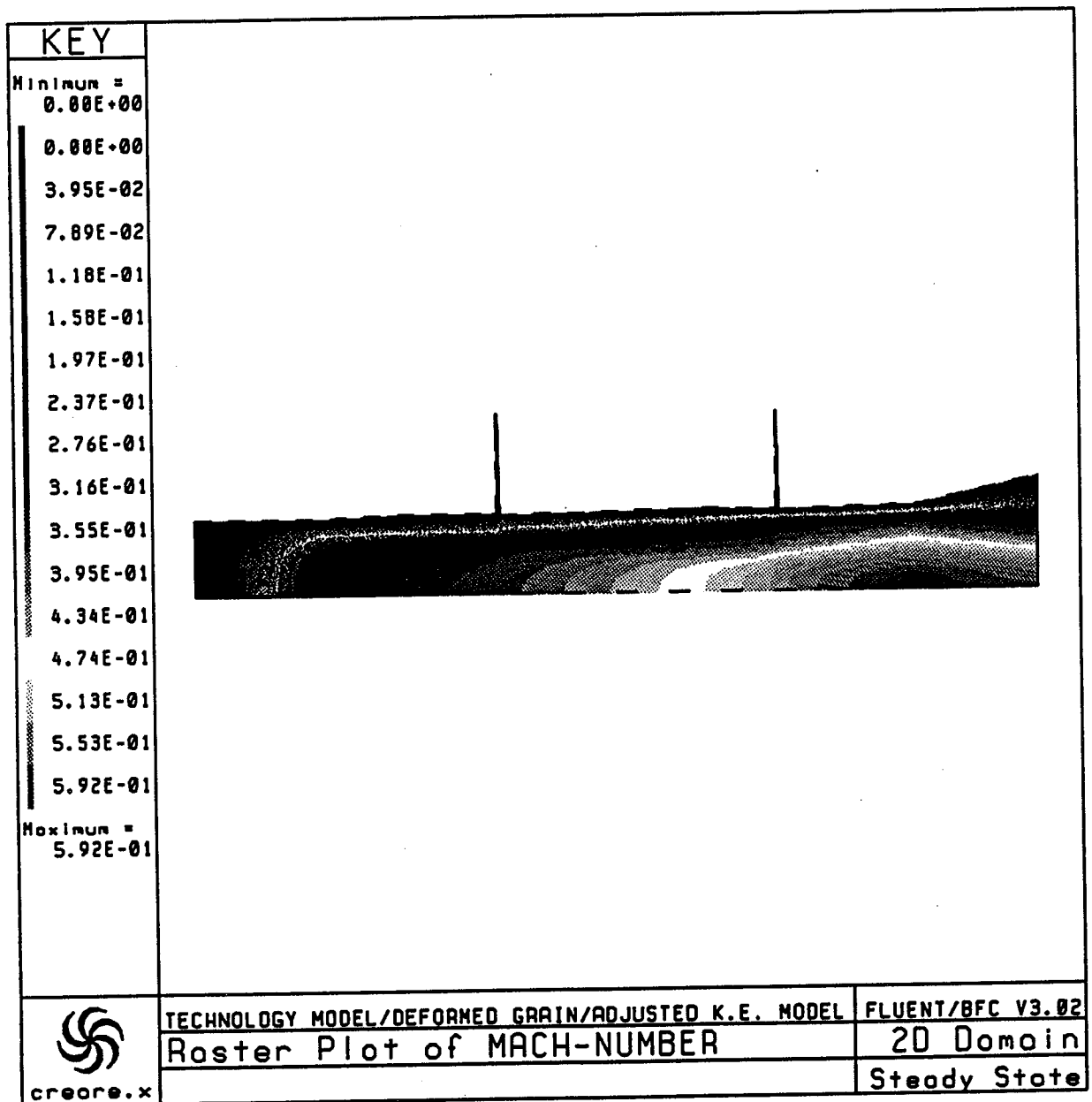
Figure 12. Raster Plot of the Mach Number for the AKE Model

KEY

Minimum =	2.84E+06
	2.84E+06
	2.91E+06
	2.98E+06
	3.06E+06
	3.13E+06
	3.20E+06
	3.27E+06
	3.34E+06
	3.41E+06
	3.49E+06
	3.56E+06
	3.63E+06
	3.70E+06
	3.77E+06
	3.84E+06
	3.92E+06
Maximum =	3.92E+06

TECHNOLOGY MODEL/DEFORMED GRAIN/STANDARD K.E. MODEL | FLUENT/BFC V3.02

Raster Plot of STAGNATION-PRESS. | 2D Domain

creare.x | | Steady State
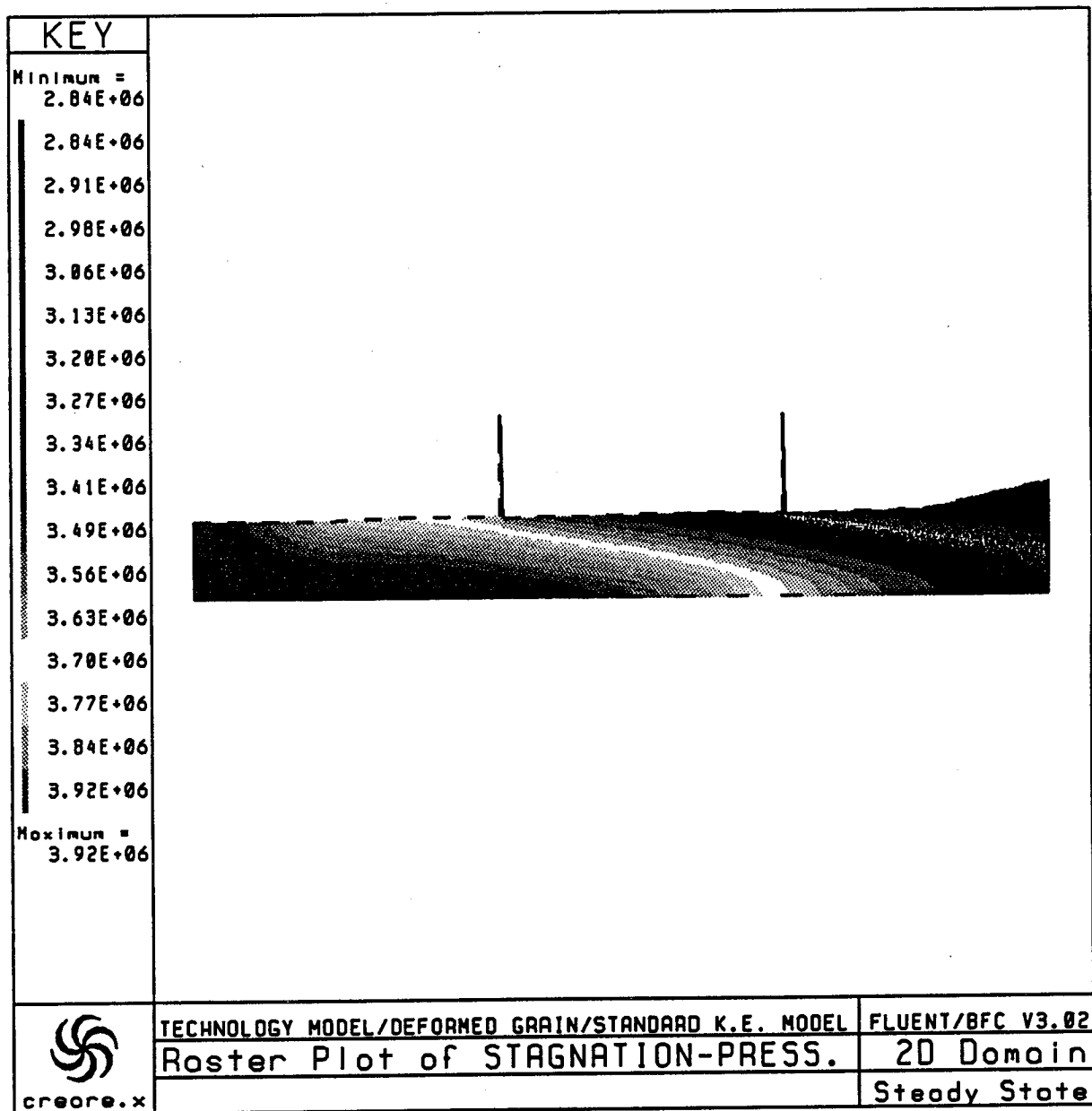
Figure 13. Raster Plot of the Total Pressure for the SKE Model

KEY	
Minimum =	2.80E+06
	2.80E+06
	2.85E+06
	2.91E+06
	2.96E+06
	3.01E+06
	3.06E+06
	3.11E+06
	3.16E+06
	3.22E+06
	3.27E+06
	3.32E+06
	3.37E+06
	3.42E+06
	3.47E+06
	3.53E+06
	3.58E+06
Maximum =	3.58E+06

TECHNOLOGY MODEL/DEFORMED GRAIN/ADJUSTED K.E. MODEL   FLUENT/BFC V3.02

Raster Plot of STAGNATION-PRESS.   2D Domain

Steady State

creare.x
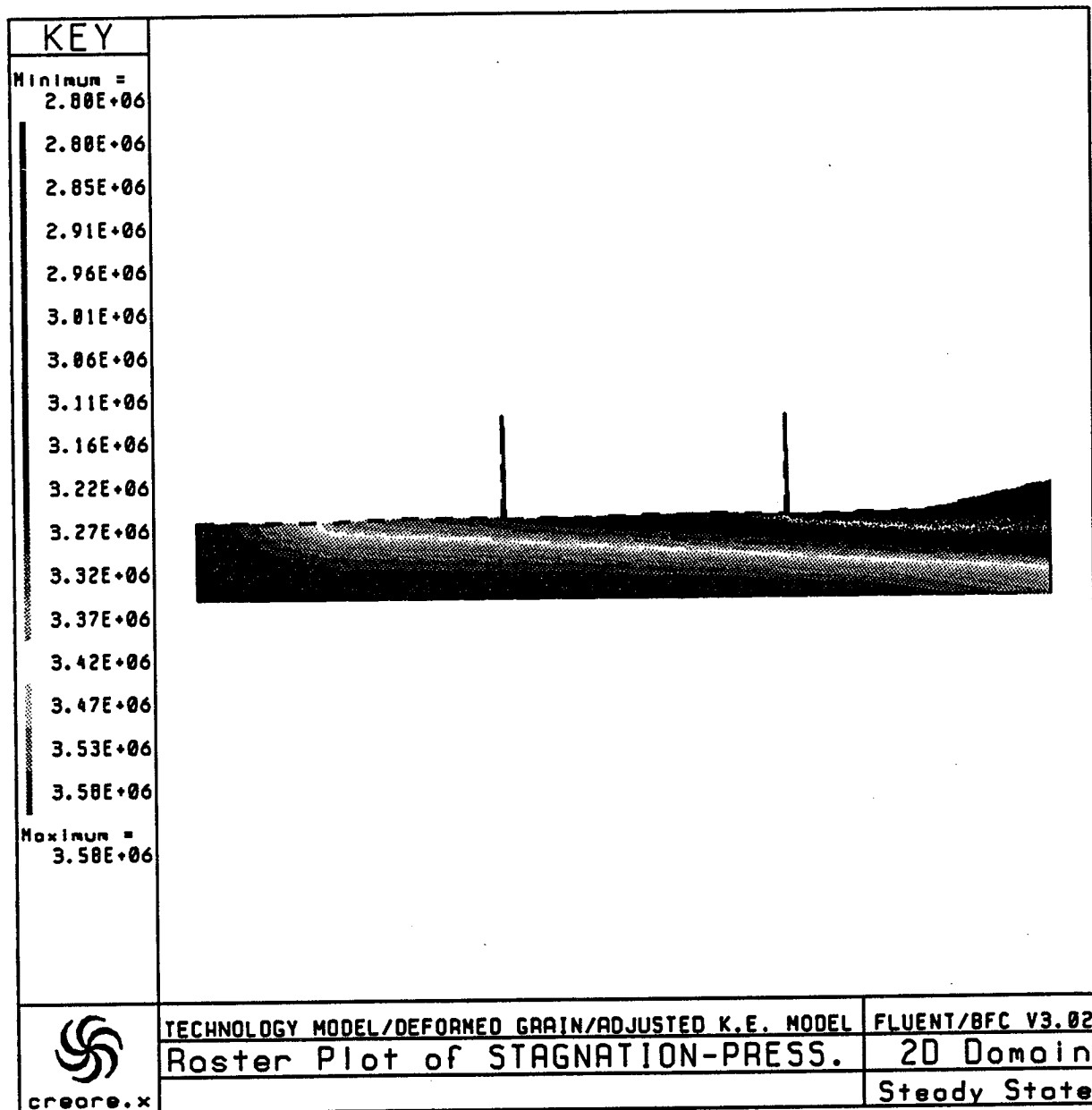
Figure 14. Raster Plot of the Total Pressure for the AKE Model

KEY

Minimum =
2.84E+06

3.57E+06

3.57E+06

3.58E+06

3.58E+06

3.58E+06

3.58E+06

3.59E+06

3.59E+06

3.59E+06

3.59E+06

3.60E+06

3.60E+06

3.60E+06

3.60E+06

3.61E+06

3.61E+06

Maximum =
3.91E+06

TECHNOLOGY MODEL/DEFORMED GRAIN/STANDARD K.E. MODEL | FLUENT/BFC V3.02

Raster Plot of PRESSURE | 2D Domain

| Steady State

creore.x
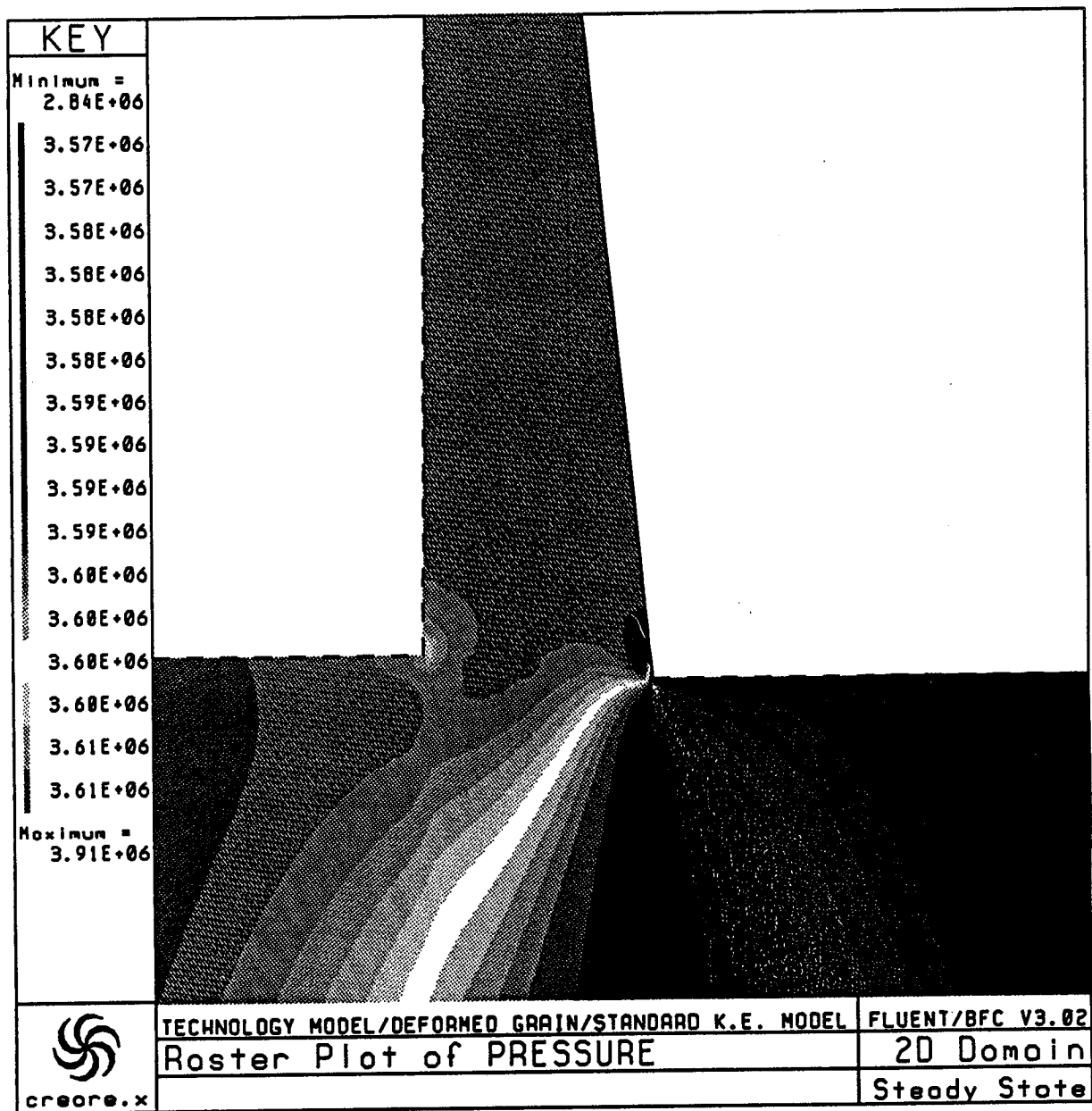
Figure 15. Raster Plot of the Static Pressure in the Forward Slot for the SKE Model

KEY	
Minimum =	2.84E+06
	3.14E+06
	3.14E+06
	3.15E+06
	3.15E+06
	3.16E+06
	3.16E+06
	3.16E+06
	3.17E+06
	3.17E+06
	3.18E+06
	3.18E+06
	3.18E+06
	3.19E+06
	3.19E+06
	3.20E+06
	3.20E+06
Maximum =	3.91E+06

creare.x

TECHNOLOGY MODEL/DEFORMED GRAIN/STANDARD K.E. MODEL FLUENT/BFC V3.02

Roster Plot of PRESSURE   2D Domain

Steady State
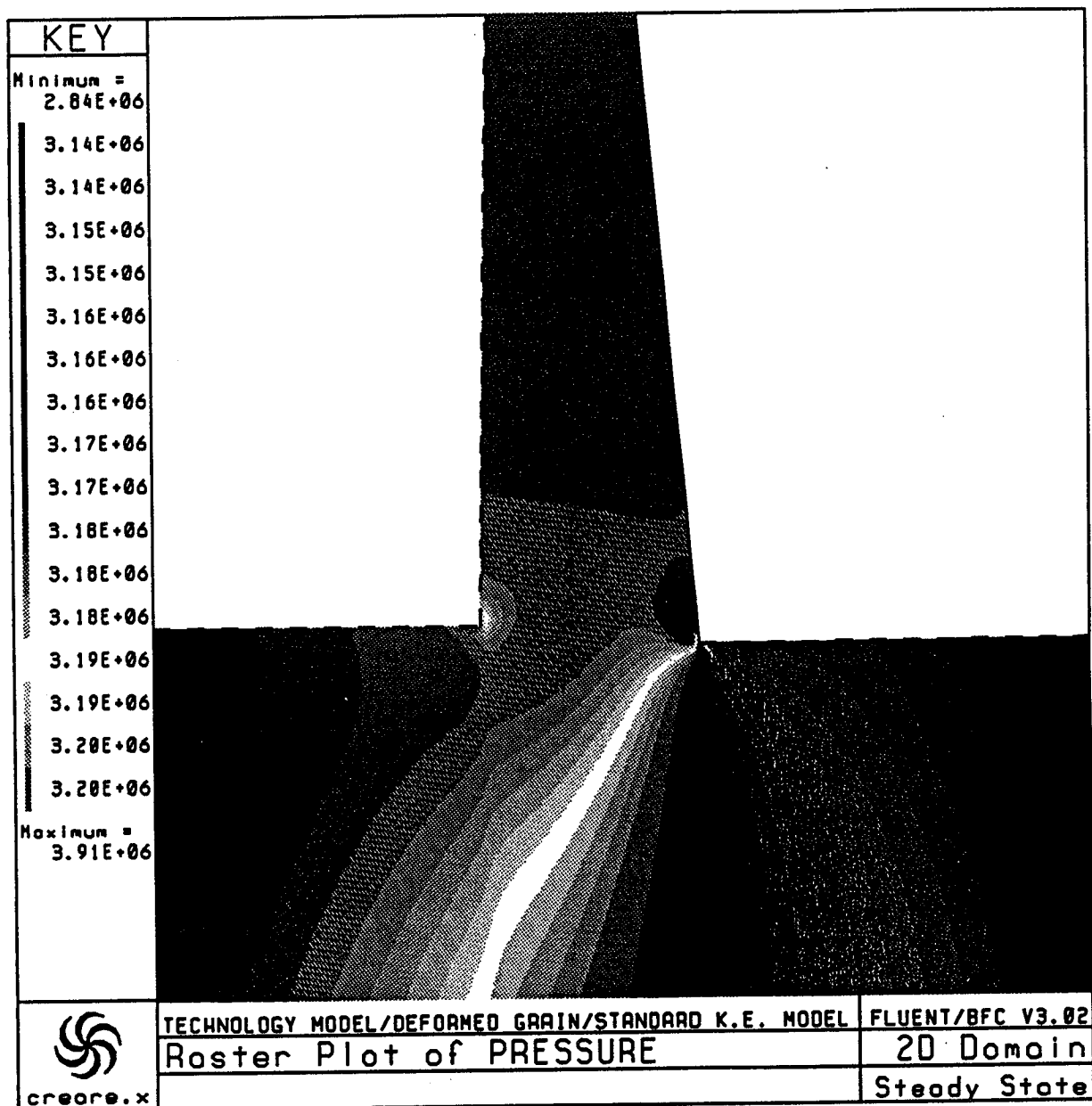
Figure 16. Raster Plot of the Static Pressure in the Aft Slot for the SKE Model

KEY

Minimum =
0.00E+00

0.00E+00
1.53E-02
3.07E-02
4.60E-02
6.13E-02
7.67E-02
9.20E-02
1.07E-01
1.23E-01
1.38E-01
1.53E-01
1.69E-01
1.84E-01
1.99E-01
2.15E-01
2.30E-01

Maximum =
5.41E-01

creare.x

TECHNOLOGY MODEL/DEFORMED GRAIN/STANDARD K.E. MODEL

Velocity Vectors colored by MACH-NUMBER

FLUENT/BFC V3.02

2D Domain

Steady State
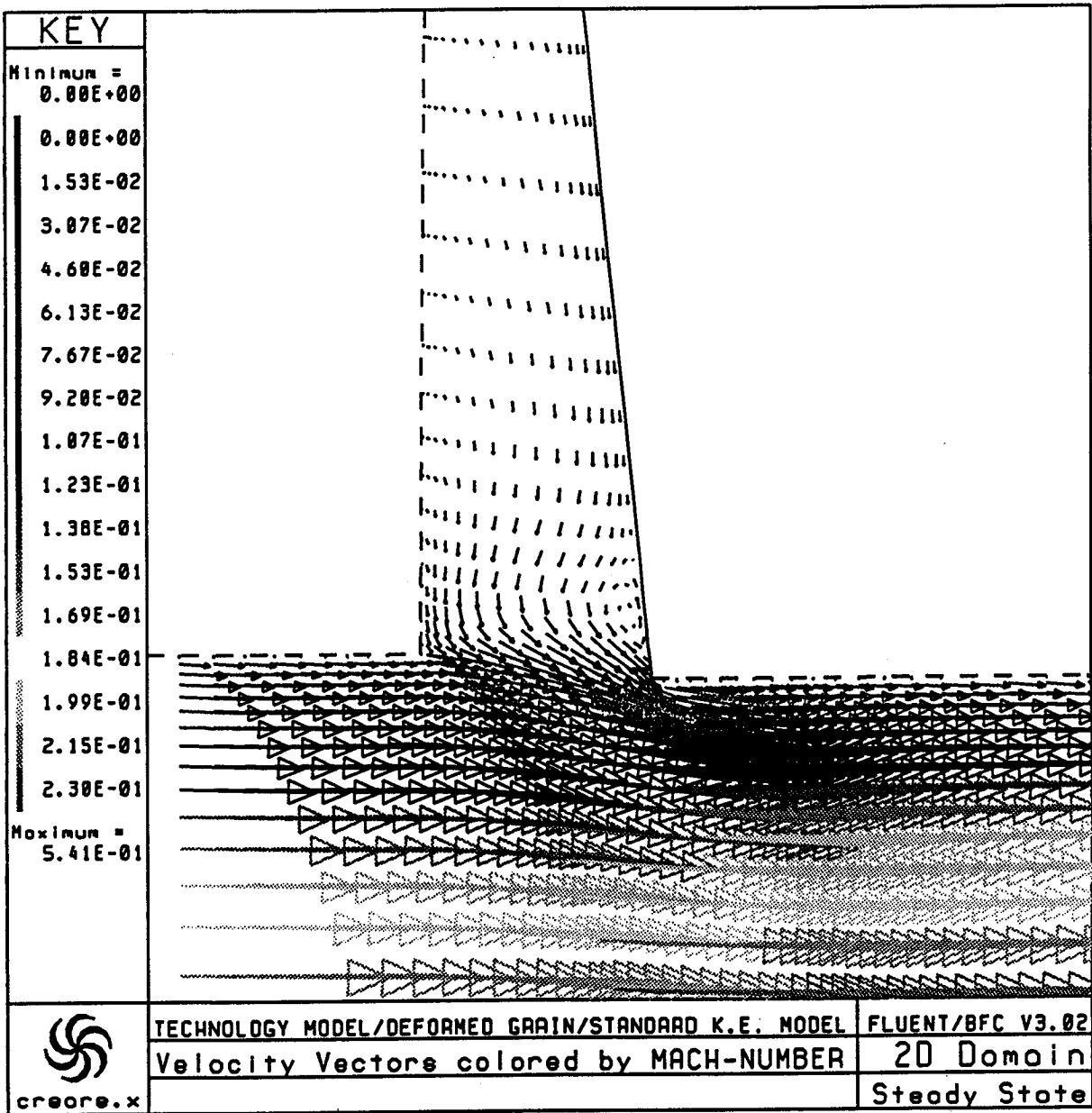
Figure 17. Velocity Field in the Forward Slot Region, SKE Model
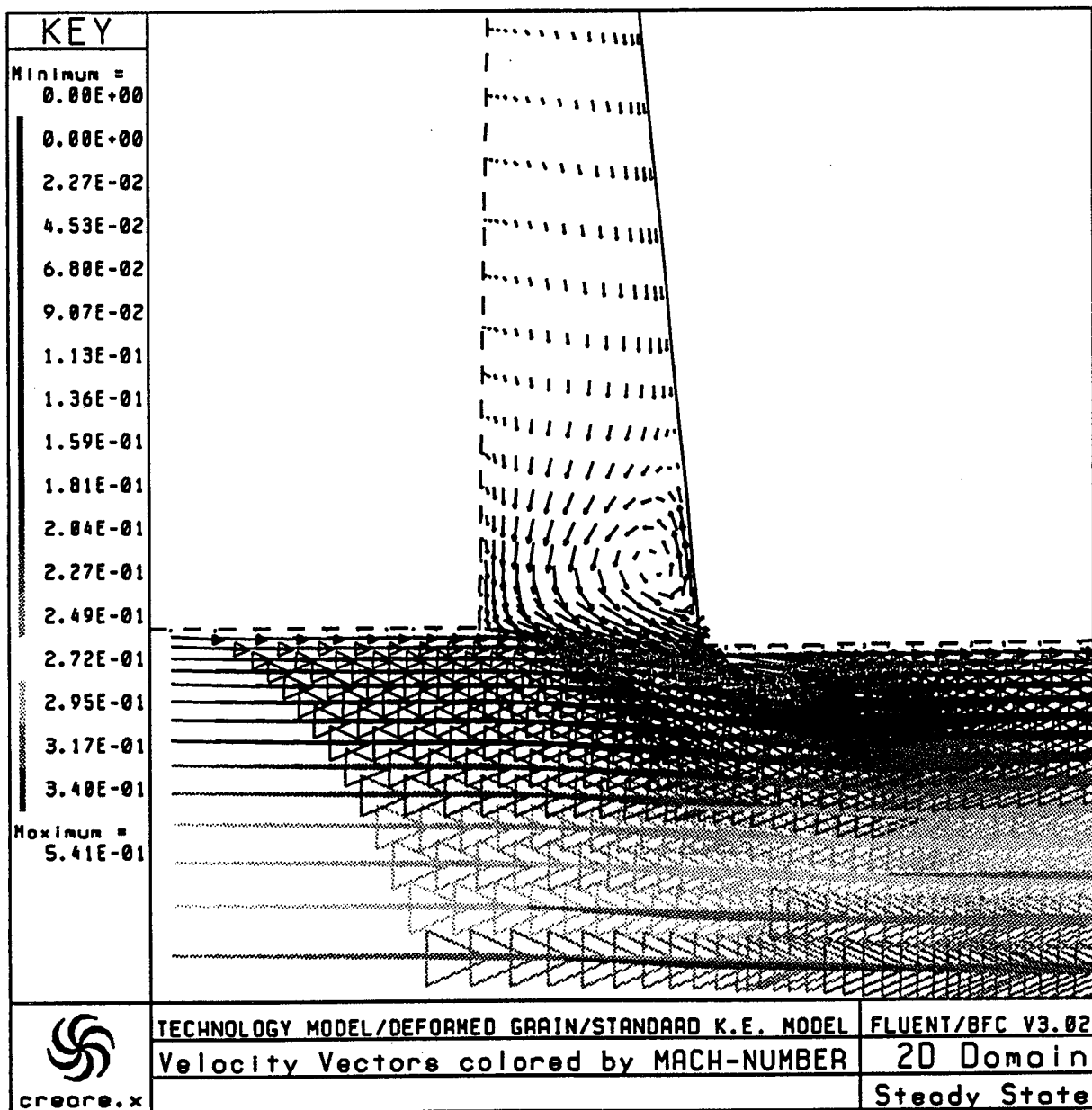
Figure 18. Velocity Field in the Aft Slot Region,
SKE Model
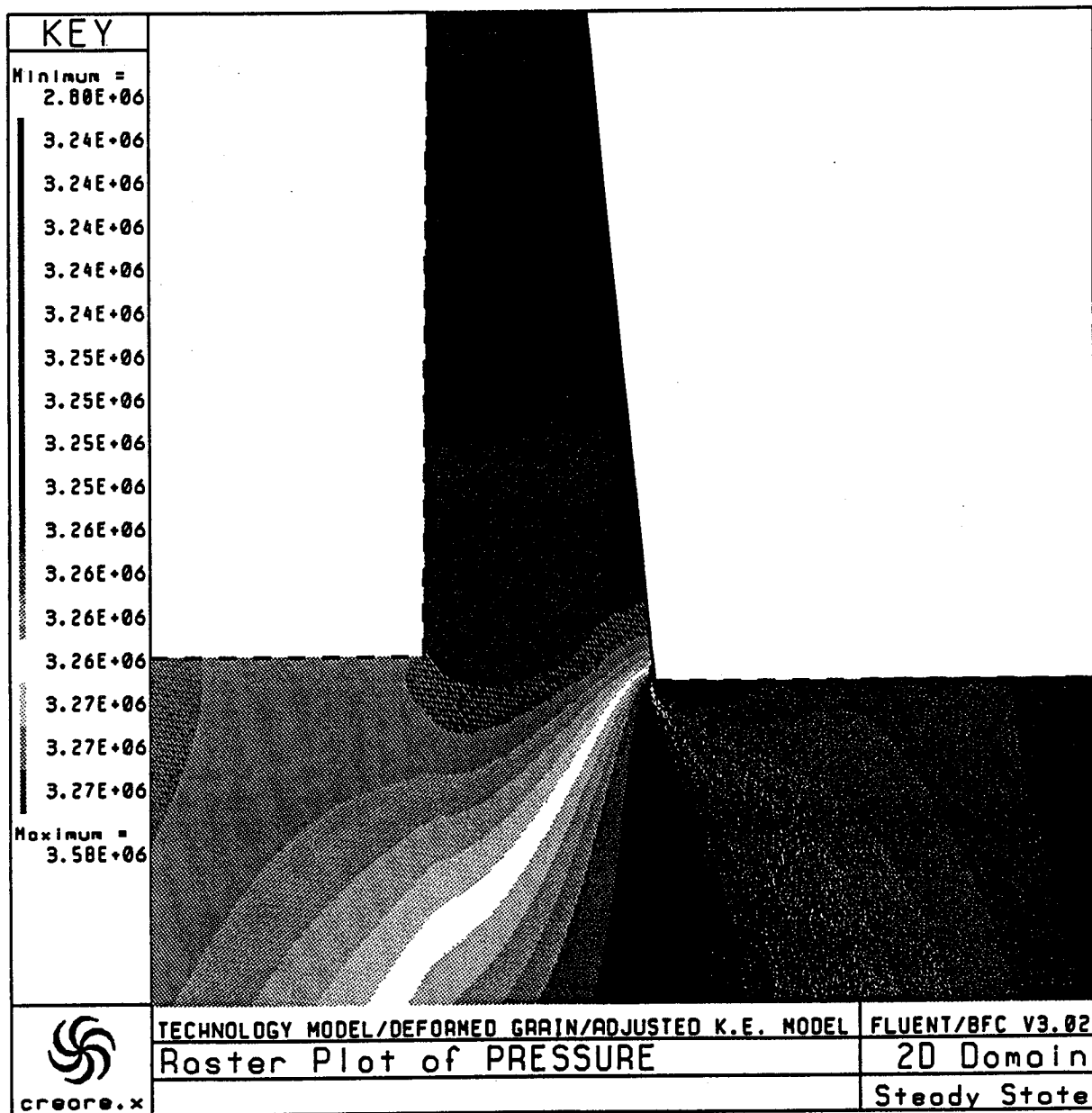
Figure 19. Raster Plot of the Static Pressure in the Forward Slot for the AKE Model

KEY

Minimum =	2.80E+06
	2.97E+06
	2.97E+06
	2.98E+06
	2.98E+06
	2.98E+06
	2.99E+06
	2.99E+06
	3.00E+06
	3.00E+06
	3.00E+06
	3.01E+06
	3.01E+06
	3.01E+06
	3.02E+06
	3.02E+06
	3.02E+06
Maximum =	3.58E+06

TECHNOLOGY MODEL/DEFORMED GRAIN/ADJUSTED K.E. MODEL | FLUENT/BFC V3.02

Roster Plot of PRESSURE | 2D Domain

creare.x | Steady State
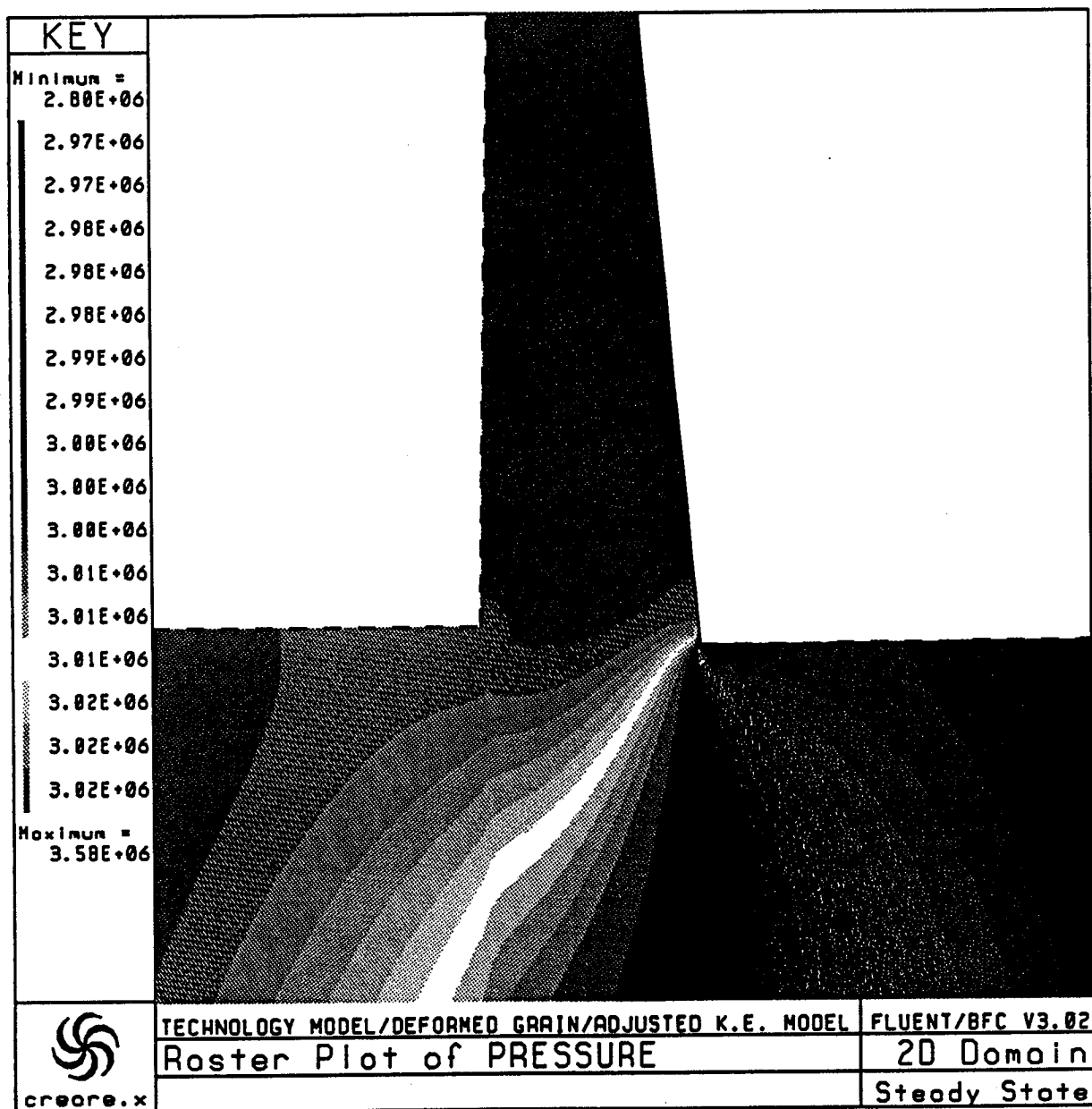
Figure 20. Raster Plot of the Static Pressure in the Aft Slot for the AKE Model

KEY

| Minimum = |
| 0.00E+00 |
| 0.00E+00 |
| 1.53E-02 |
| 3.07E-02 |
| 4.60E-02 |
| 6.13E-02 |
| 7.67E-02 |
| 9.20E-02 |
| 1.07E-01 |
| 1.23E-01 |
| 1.38E-01 |
| 1.53E-01 |
| 1.69E-01 |
| 1.84E-01 |
| 1.99E-01 |
| 2.15E-01 |
| 2.30E-01 |
| Maximum = |
| 5.92E-01 |

TECHNOLOGY MODEL/DEFORMED GRAIN/ADJUSTED K.E. MODEL | FLUENT/BFC V3.02
Velocity Vectors colored by MACH-NUMBER | 2D Domain
Steady State
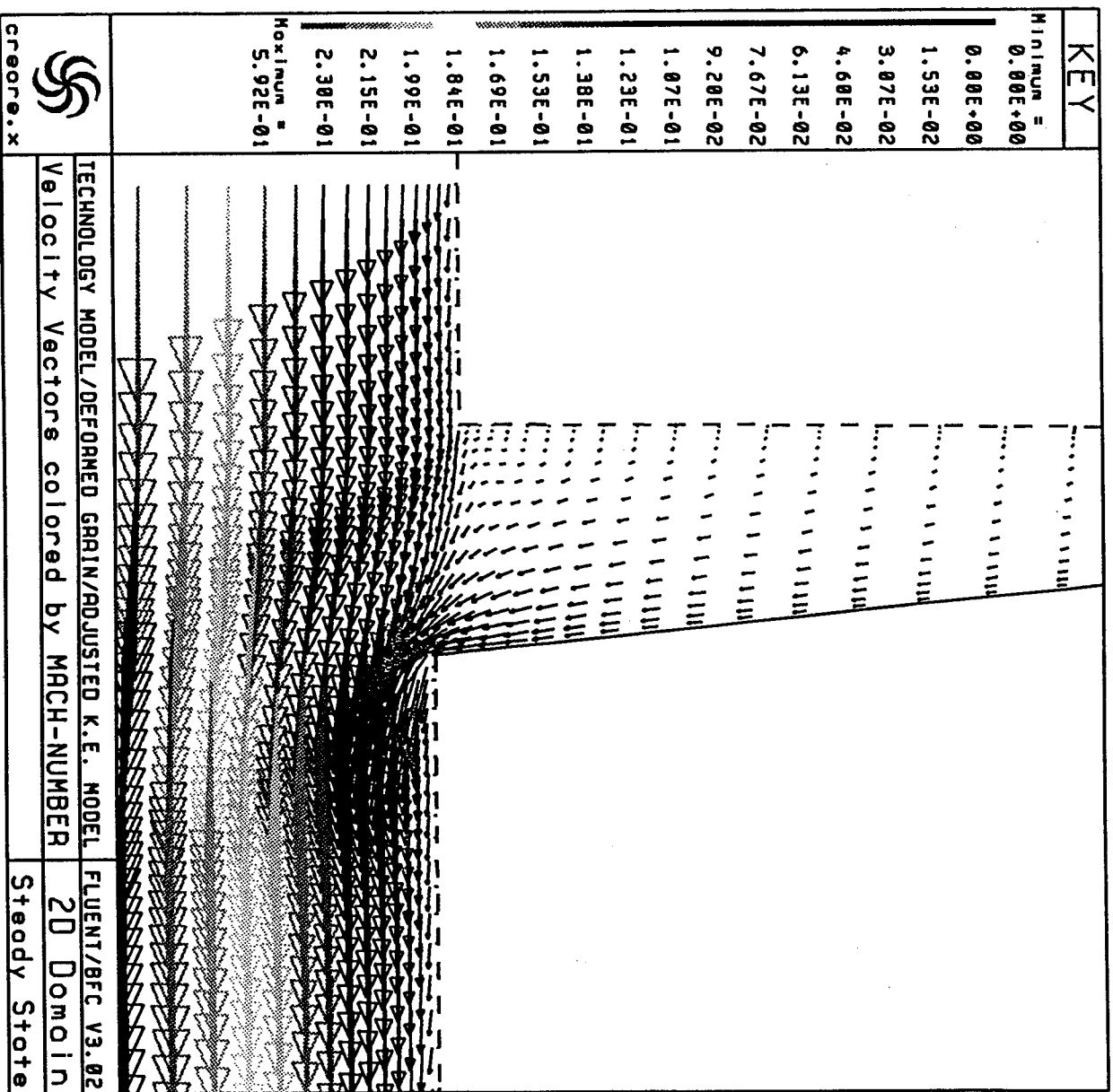
Figure 21. Velocity Field in the Forward Slot Region, AKE Model

KEY

Minimum =	0.00E+00
	0.00E+00
	2.27E-02
	4.53E-02
	6.80E-02
	9.07E-02
	1.13E-01
	1.36E-01
	1.59E-01
	1.81E-01
	2.04E-01
	2.27E-01
	2.49E-01
	2.72E-01
	2.95E-01
	3.17E-01
	3.40E-01
Maximum =	5.92E-01

creare.x

TECHNOLOGY MODEL/DEFORMED GRAIN/ADJUSTED K.E. MODEL — FLUENT/BFC V3.02

Velocity Vectors colored by MACH-NUMBER — 2D Domain

Steady State
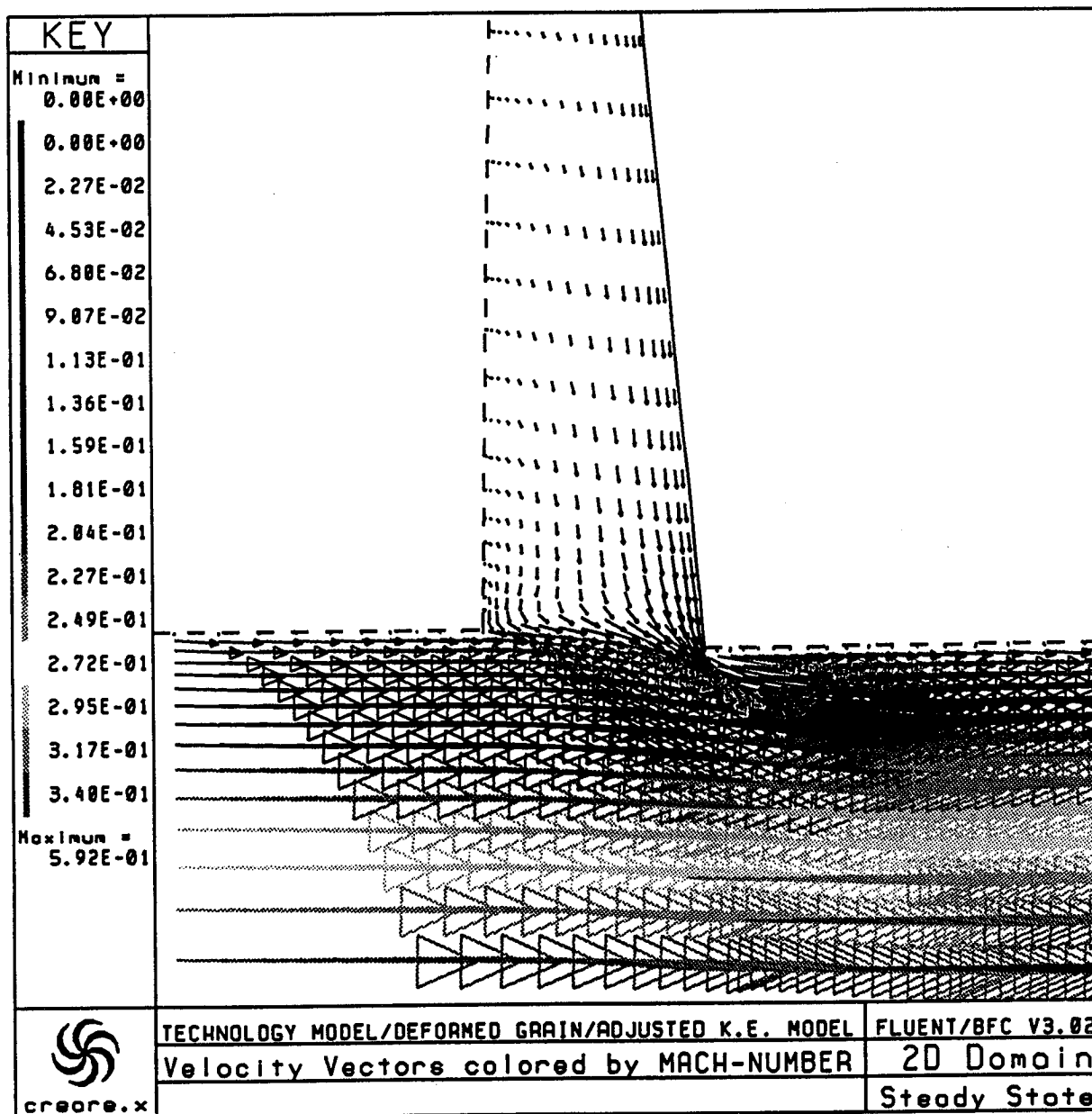
Figure 22. Velocity Field in the Aft Slot Region, AKE Model

Figure 23. Technology Model Mach Number
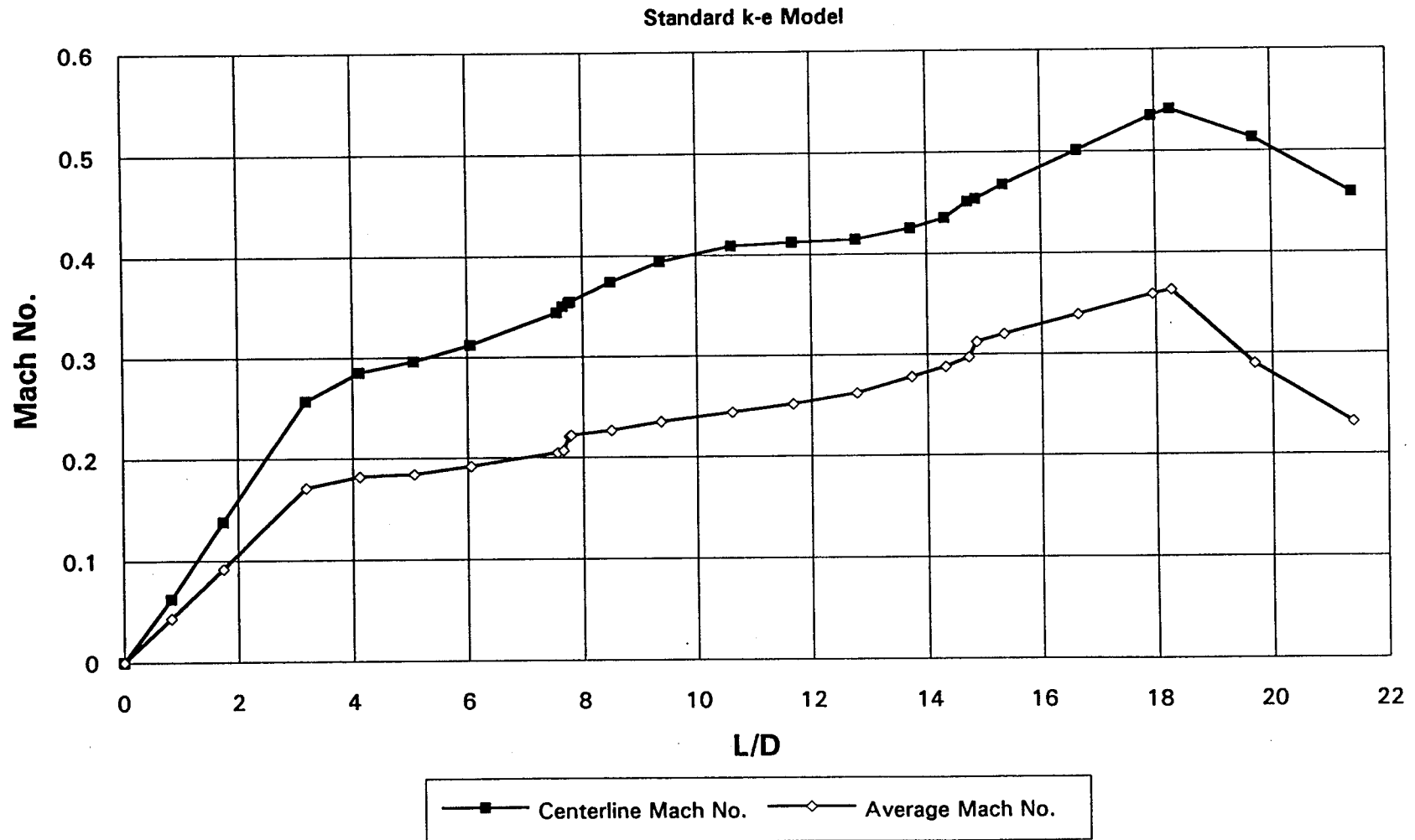
Standard k-e Model

Figure 24. Technology Model Mach Number

Adjusted k-e Model

Legend:
- ■ Centerline Mach No.
- ◇ Average Mach No.

X-axis: L/D
Y-axis: Mach No.

ERCI 07/17/92
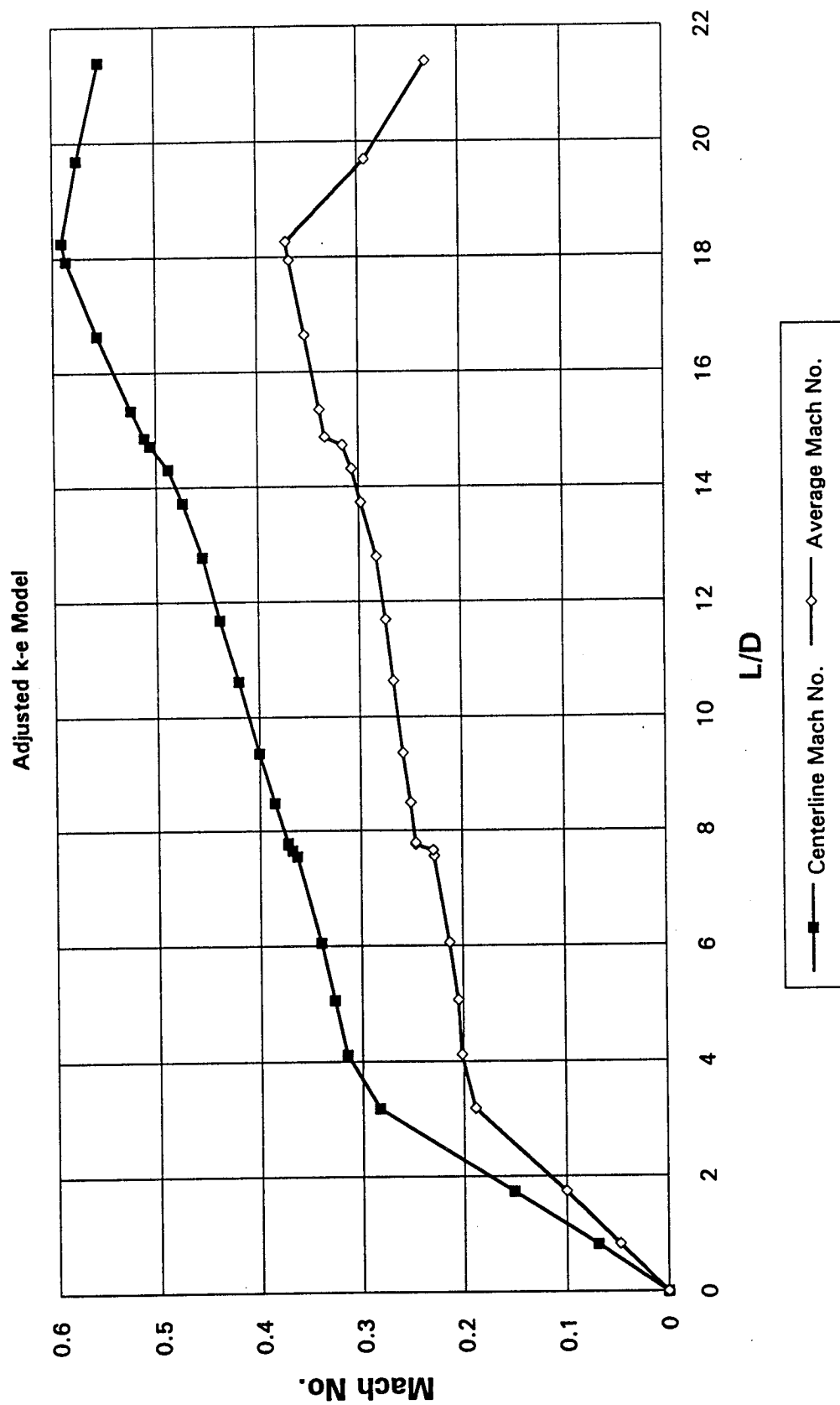
Figure 25. Technology Model Pressure

Analytic Culick Profile Model

ERC, Inc. 07/17/92
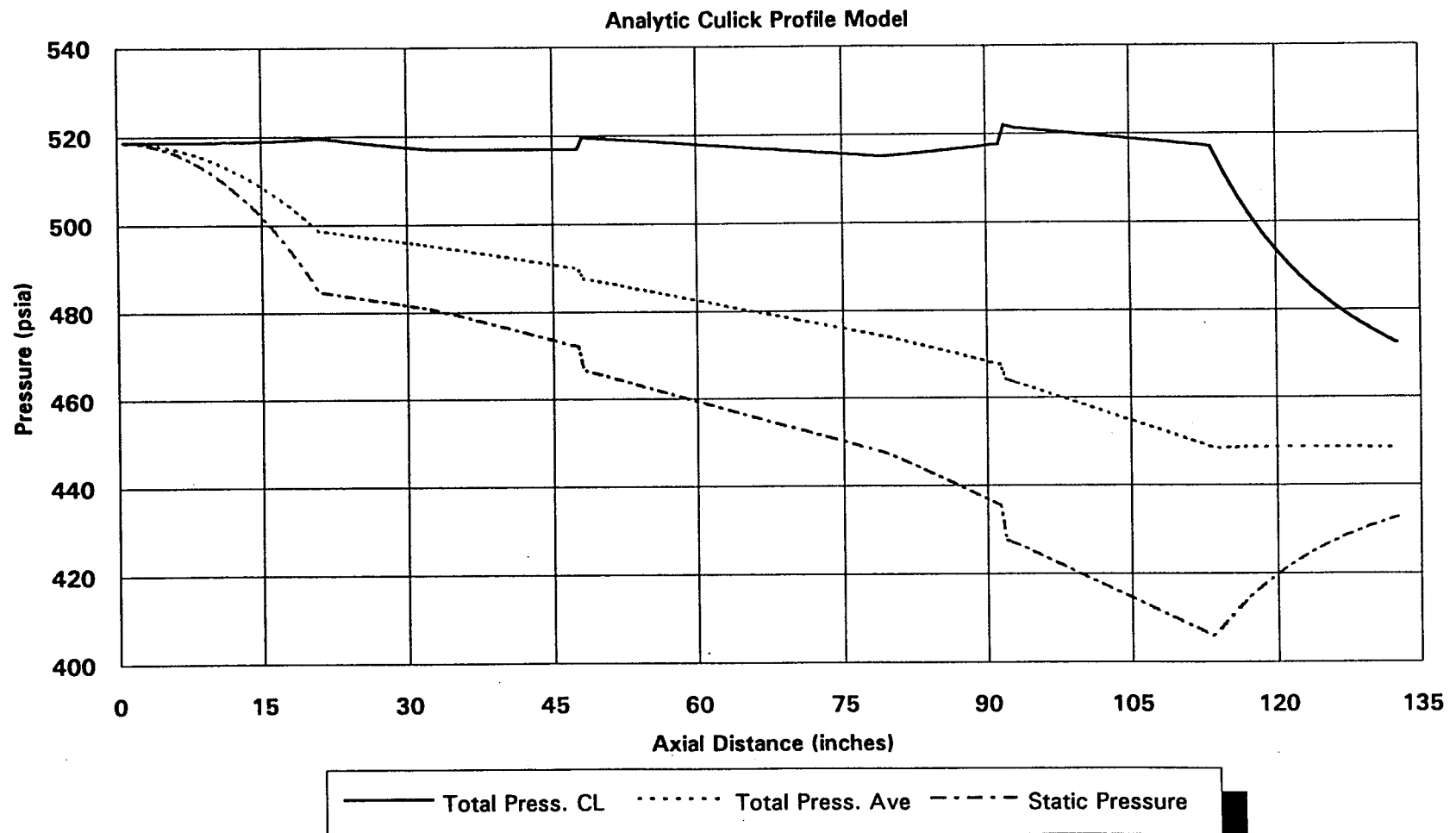
Figure 26. Technology Model Pressure

Analytic Bulk Profile Model

ERC, Inc. 07/17/92
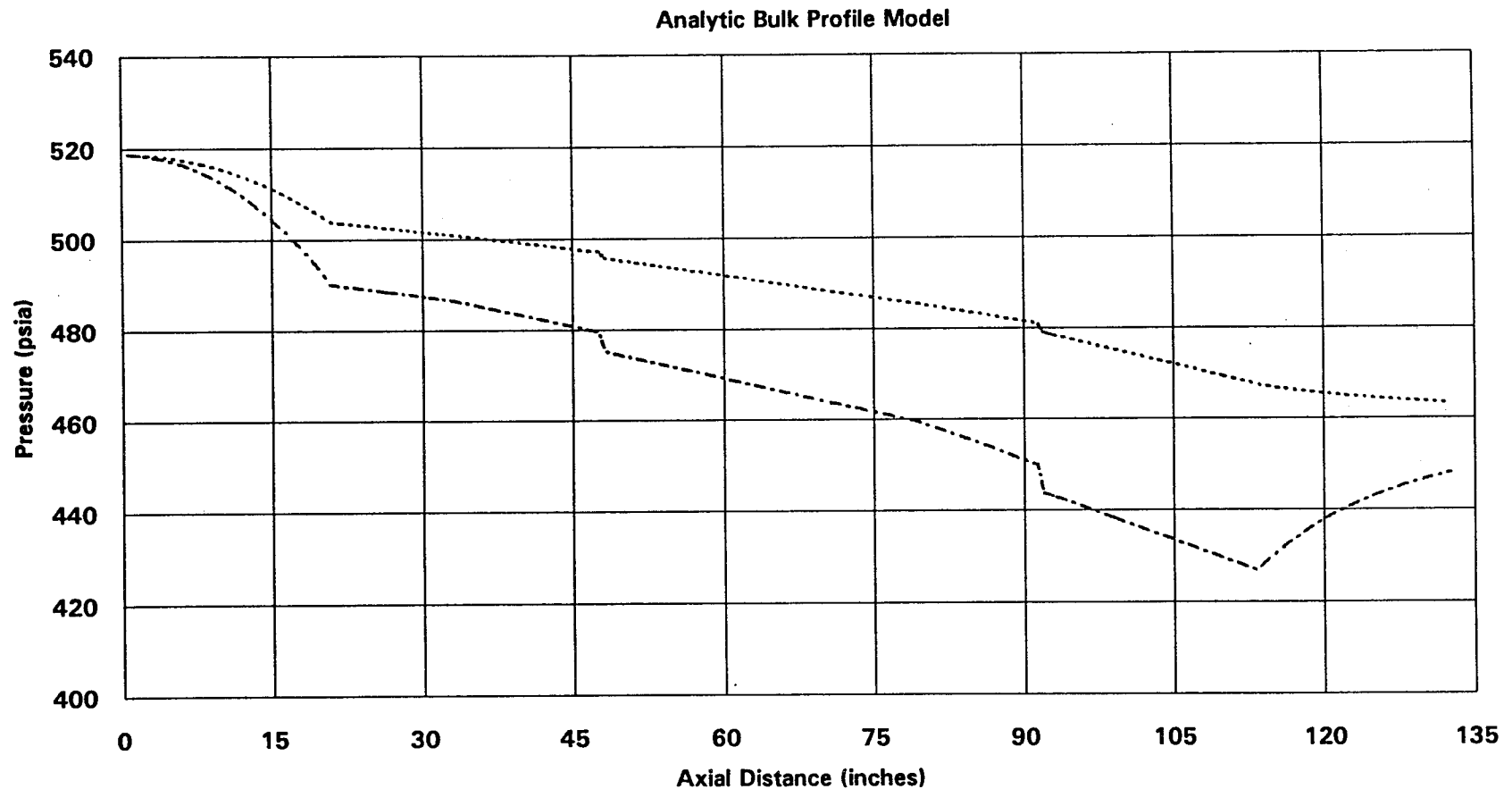
Figure 27. Technology Model Static Pressure

Standard k-e Model

ERC, Inc. 07/17/92
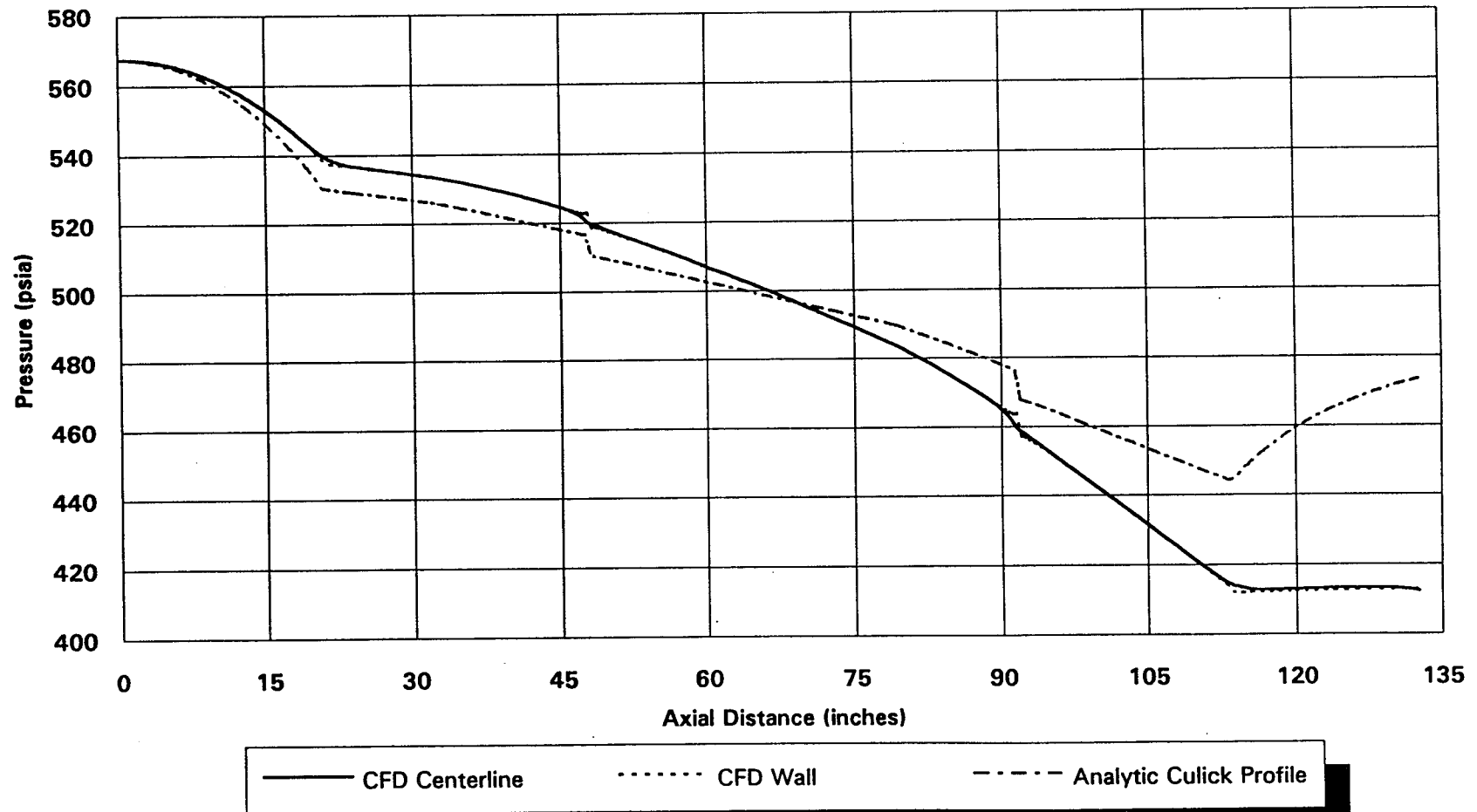
Figure 28. Technology Model Static Pressure

Adjusted k-e Model

Legend: CFD Centerline, CFD Wall, Analytic Culick Profile
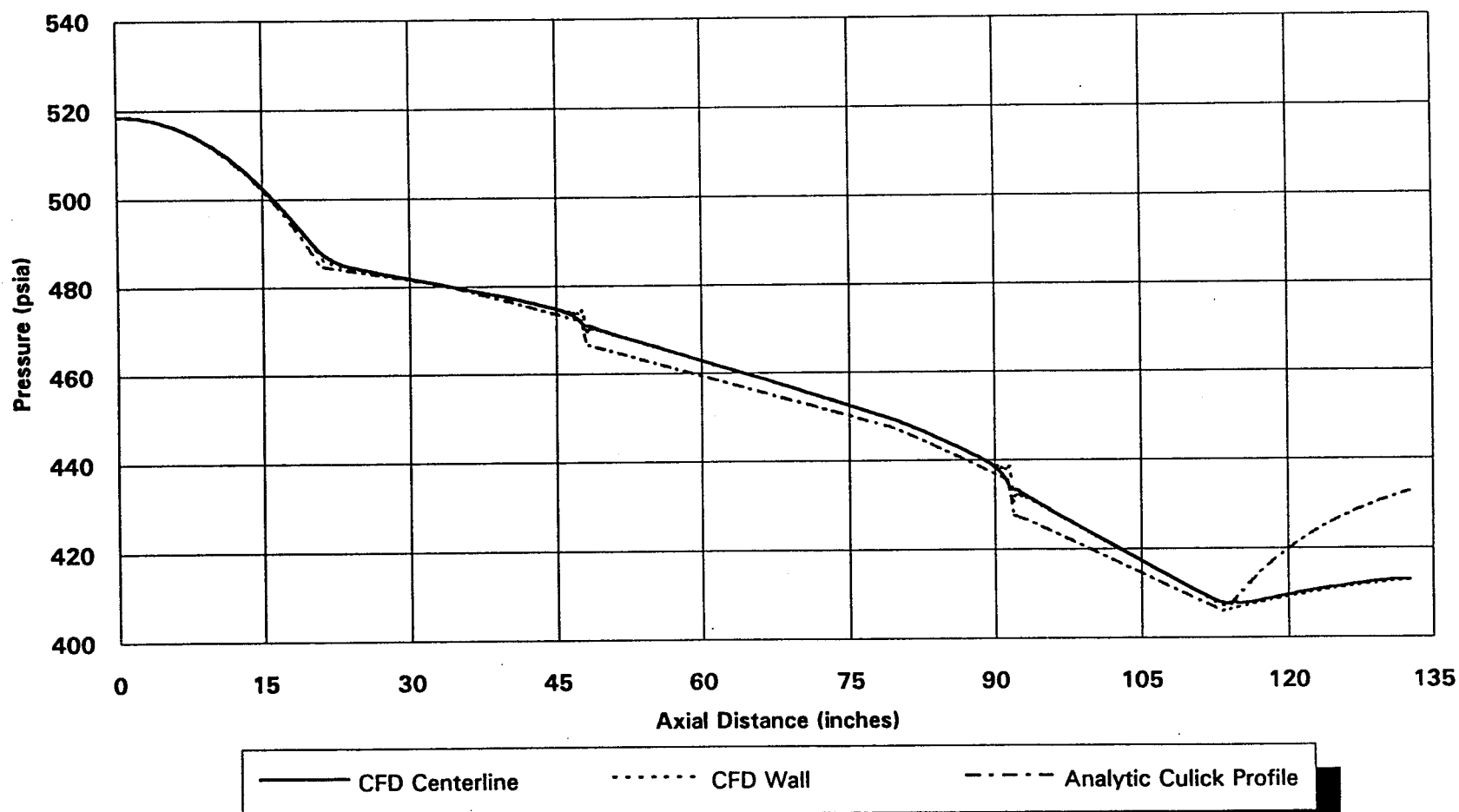
Figure 29. Technology Model Total Pressure

Standard k-e Model

Legend:
- – – – – CFD Centerline
- ⋯⋯⋯ CFD Wall
- ——— Culick Total Press. Centerline
- – ⋅ – ⋅ – Culick Total Press. Wall

Y-axis: Total Pressure (psia) — 400, 420, 440, 460, 480, 500, 520, 540, 560, 580

X-axis: Axial Distance (inches) — 0, 15, 30, 45, 60, 75, 90, 105, 120, 135

ERC, Inc. 07/17/92
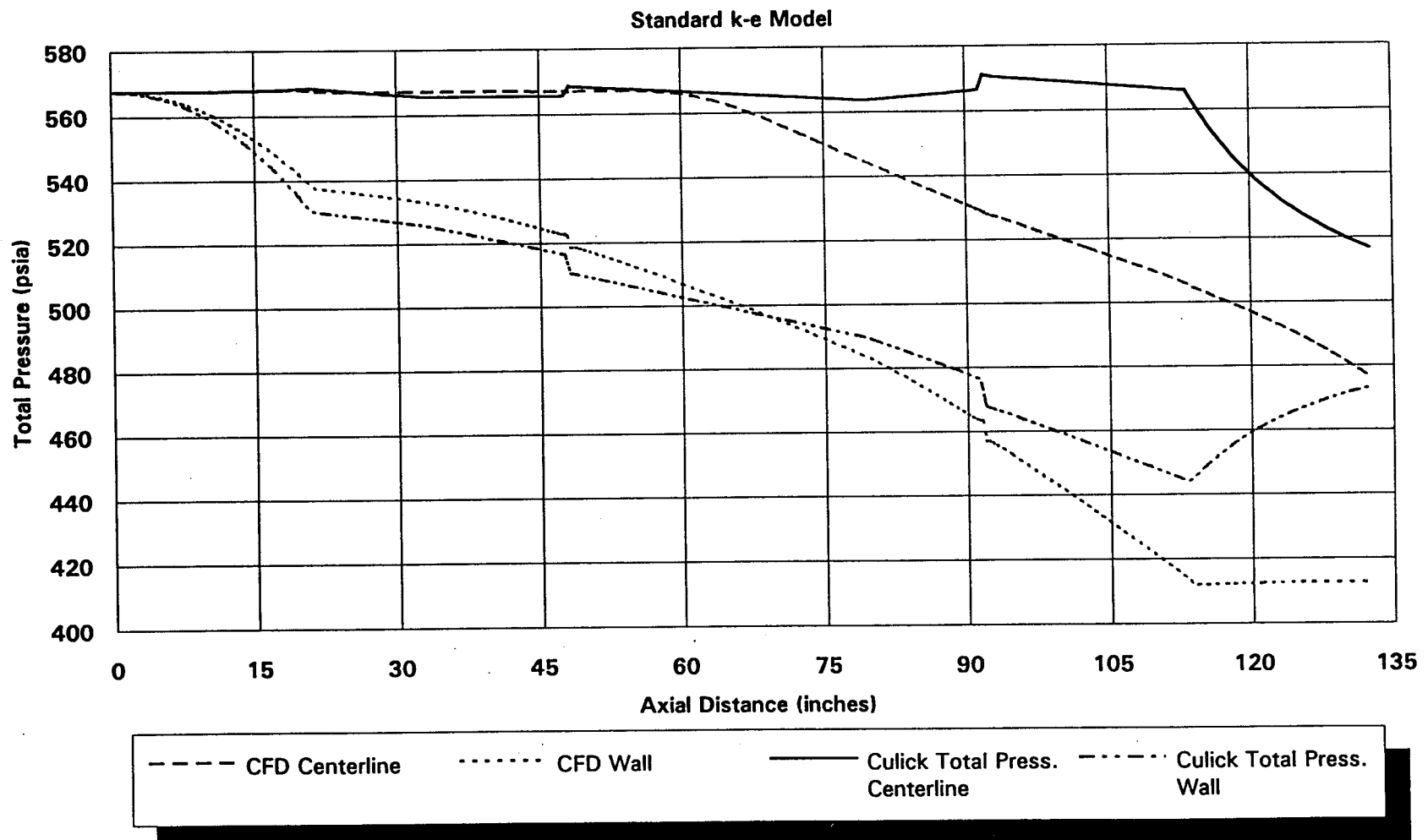
Figure 30. Technology Model Total Pressure

Adjusted k-e Model

Axial Distance (inches)

- - - - CFD Centerline   · · · · · · · CFD Wall   ——— Culick Total Press. Centerline   — · · — · · Culick Total PrRess. Wall

ERC, Inc. 07/17/92
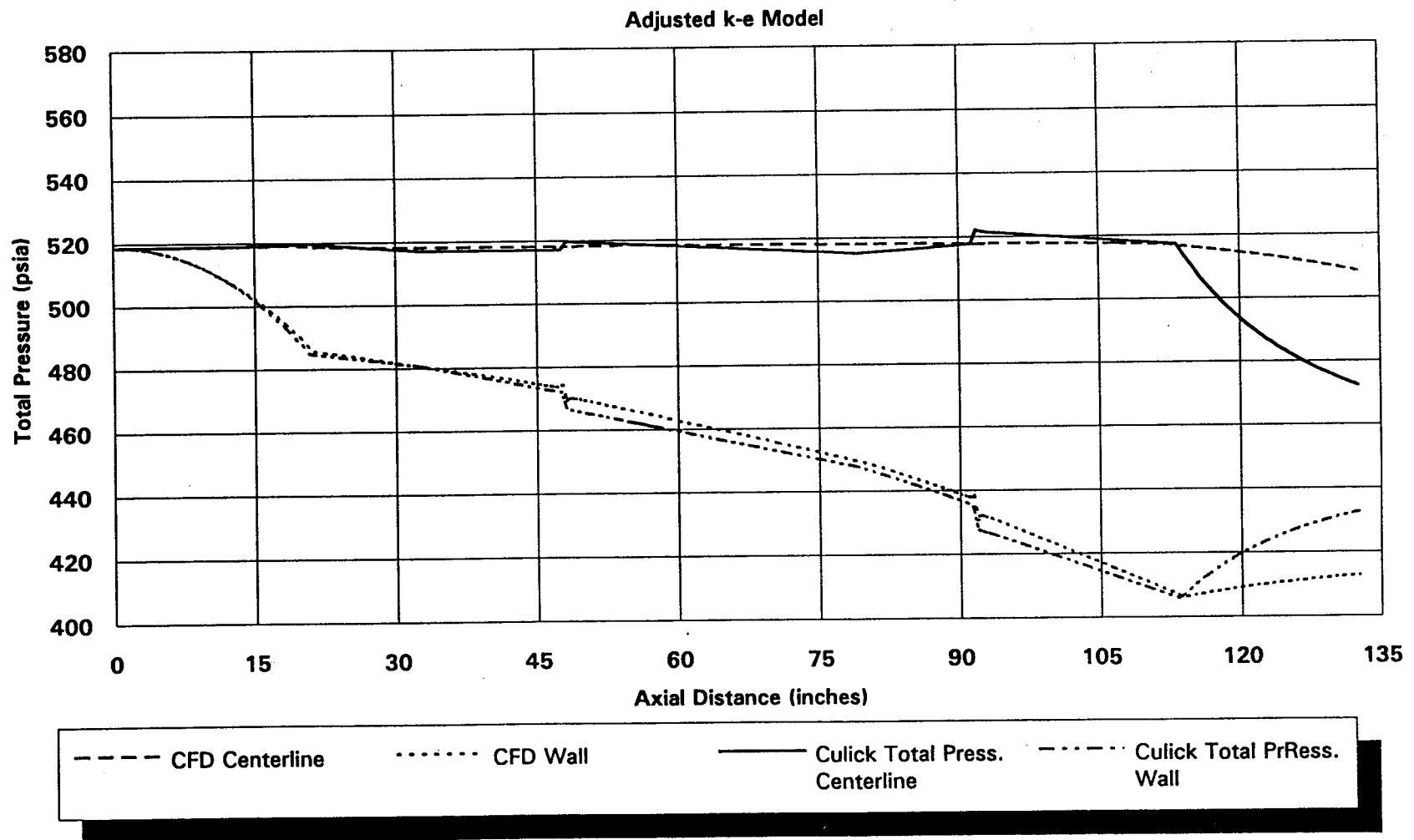
Figure 31. Technology Model Velocity Profiles

Head End to Aft Section

ERCI 07/17/92
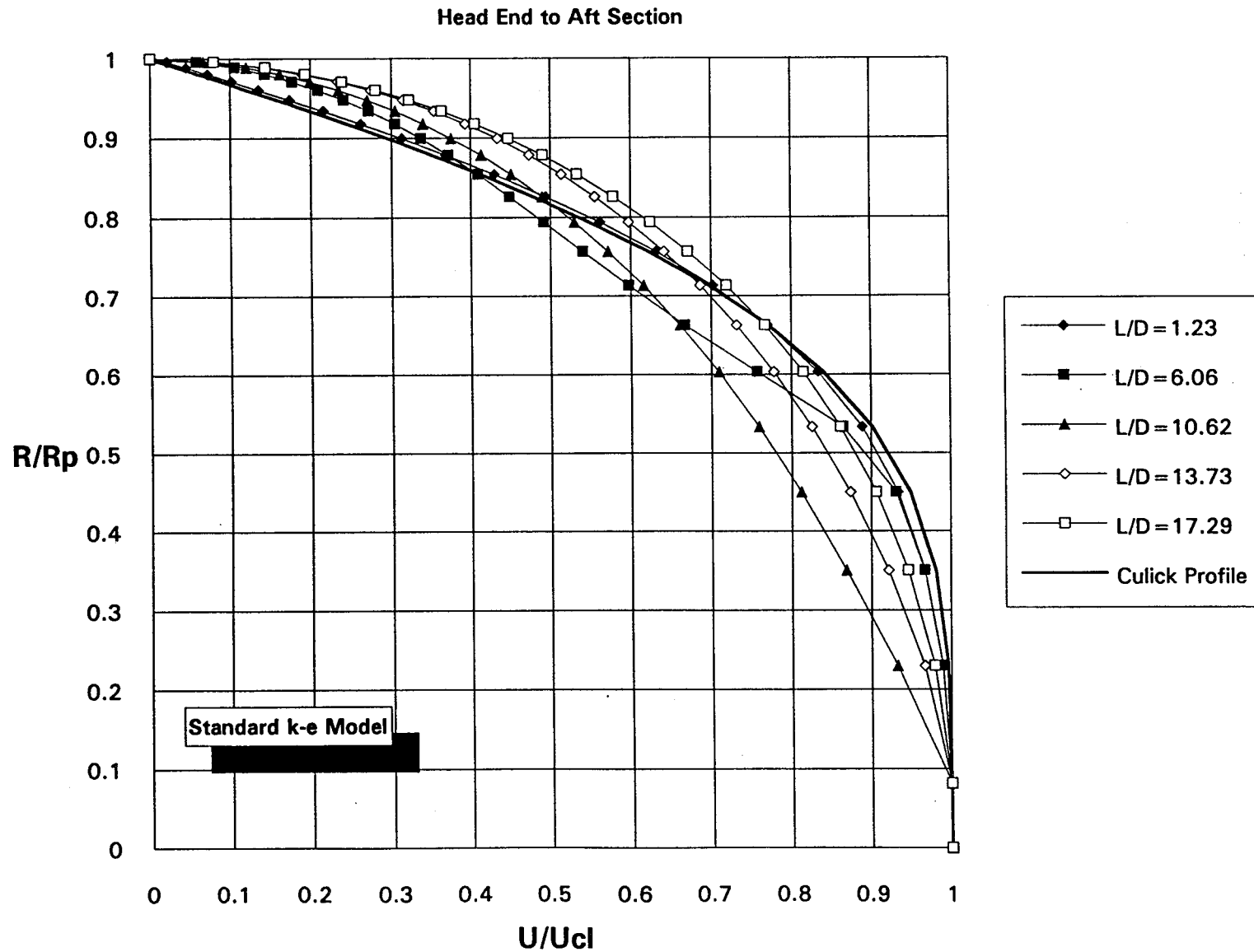
Figure 32. Technology Model Velocity Profiles

Head End Region

Legend:
- ▲——— L/D=0.24
- ○——— L/D=1.23
- ◆——— L/D=3.18
- □——— L/D=5.07
- ——— Culick Profile

Standard k-e Model

Axes: R/Rp (vertical), U/Ucl (horizontal)
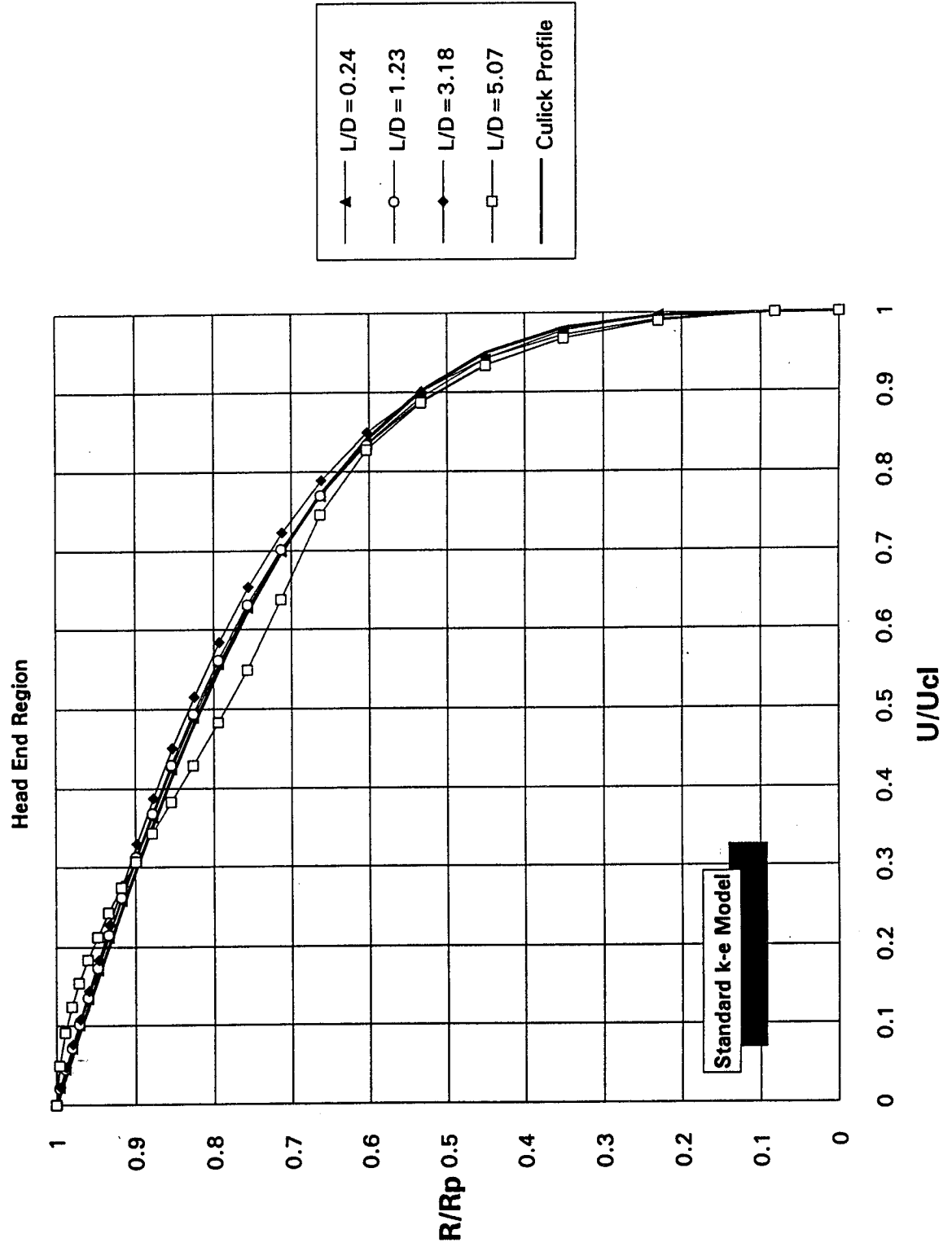
Figure 33. Technology Model Velocity Profiles

Forward Slot Region

Legend:
- L/D = 6.06
- L/D = 7.56
- L/D = 7.76
- L/D = 8.06
- L/D = 10.62
- Culick Profile

Standard k-e Model

R/Rp

U/Ucl

ERCI 07/17/92
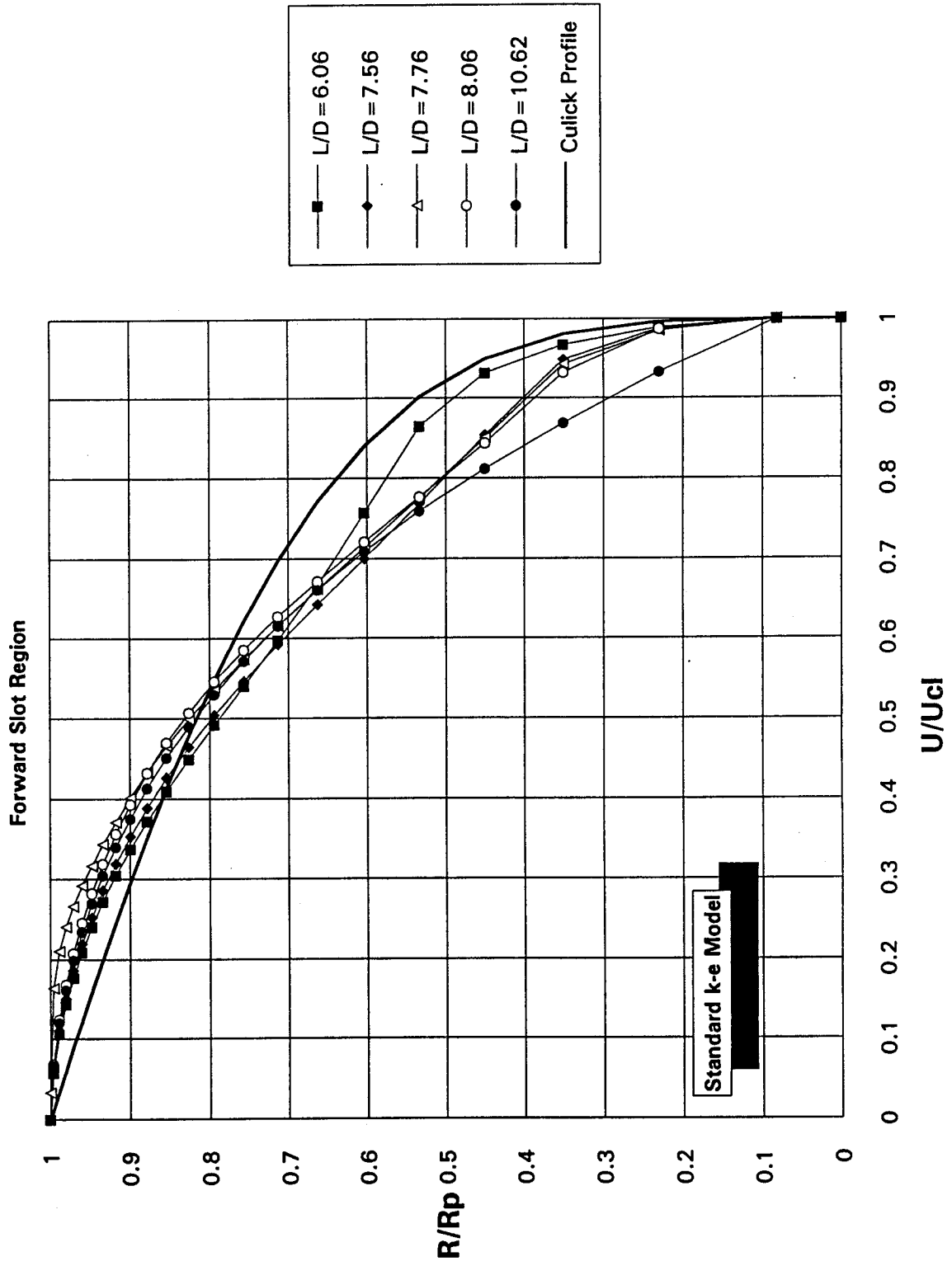
Figure 34. Technology Model Velocity Profiles
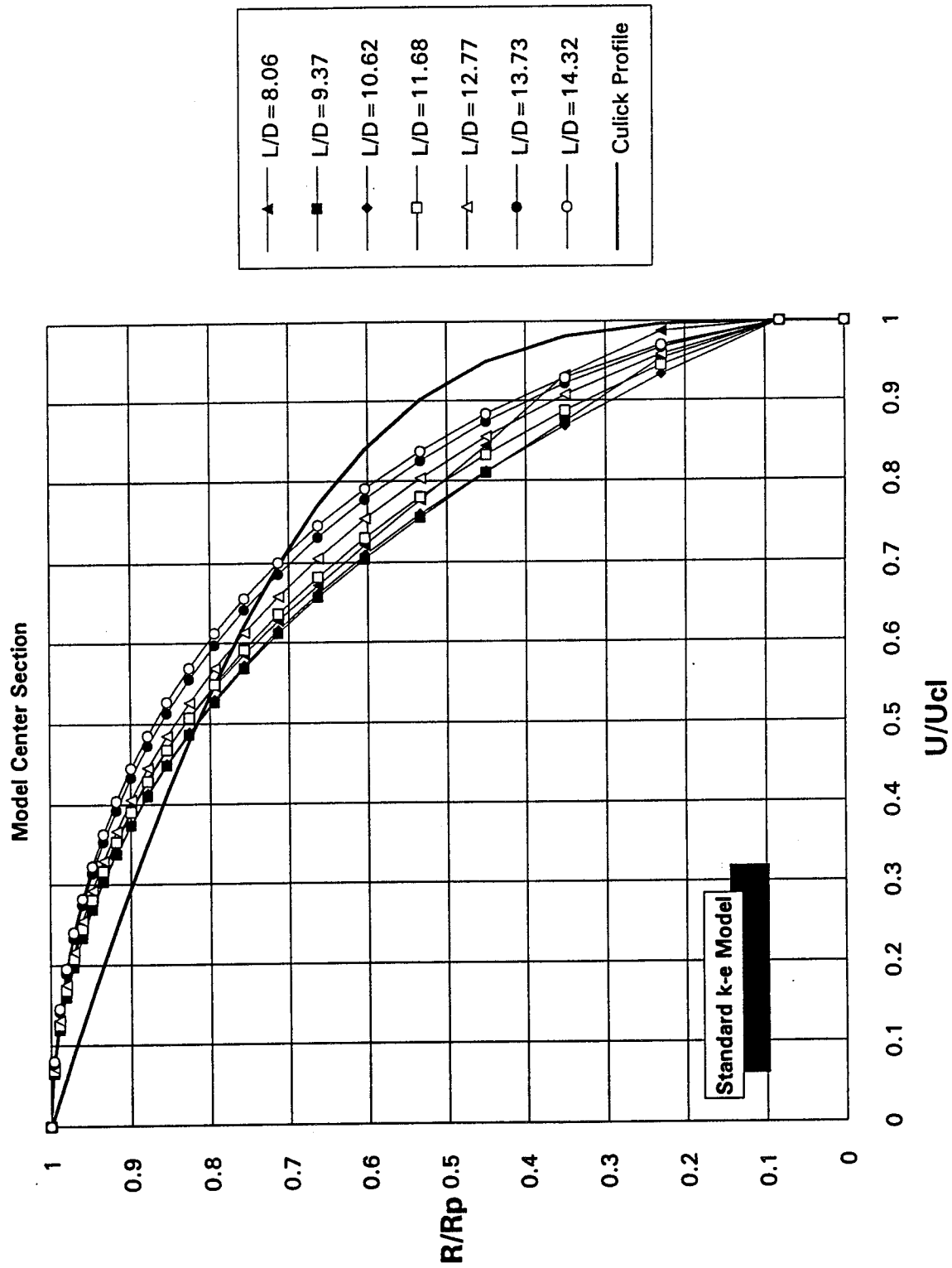
Figure 35. Technology Model Velocity Profiles

Aft Slot Region

Legend:
- L/D = 14.60
- L/D = 14.73
- L/D = 15.34
- L/D = 16.63
- Culick Profile

Standard k-e Model

U/Ucl

R/Rp
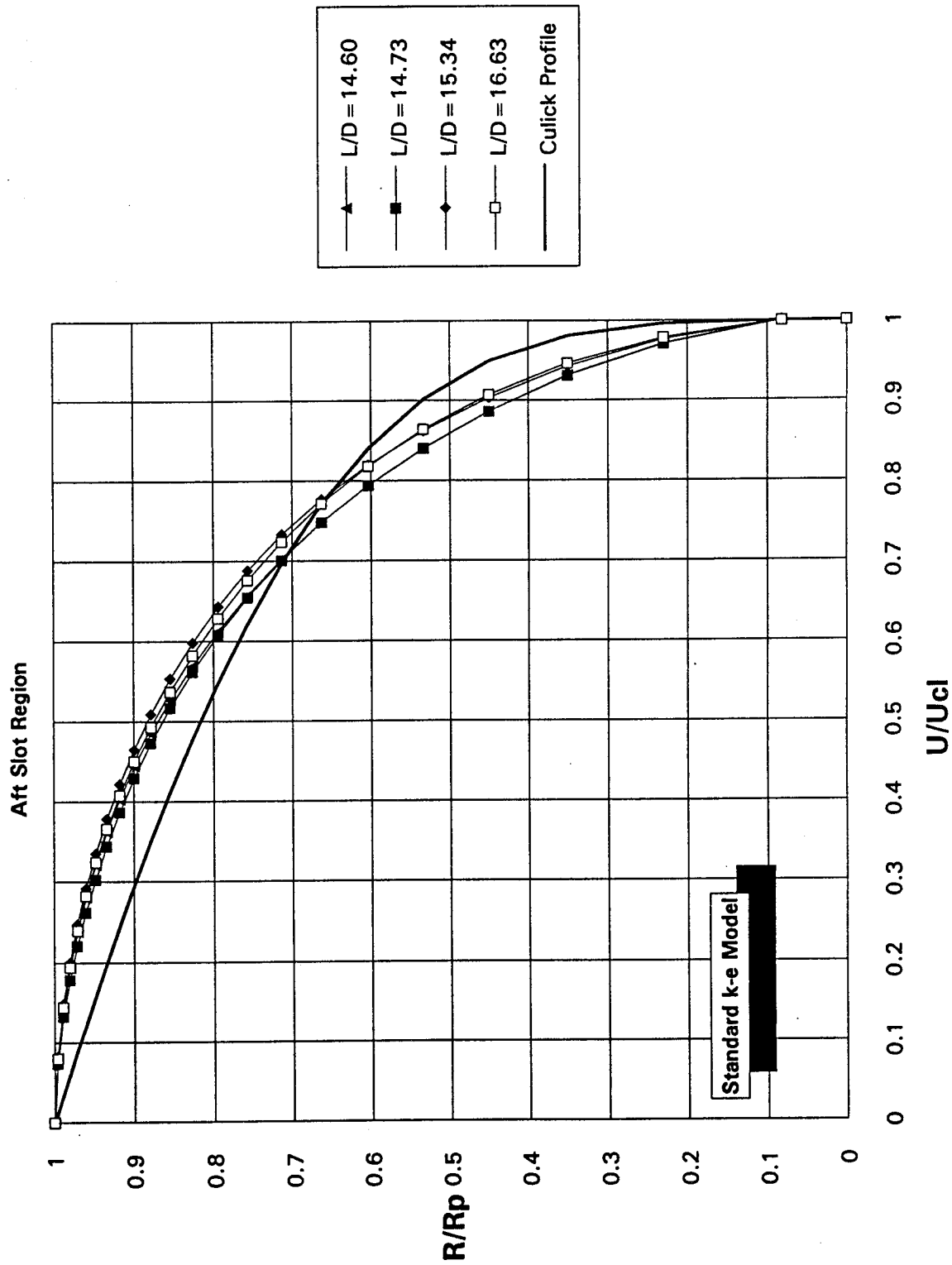
Figure 36. Technology Model Velocity Profiles

Aft Section

Legend:
- L/D = 17.29
- L/D = 18.55
- L/D = 19.69
- L/D = 20.82
- Culick Profile

Standard k-e Model

U/Ucl

R/Rp
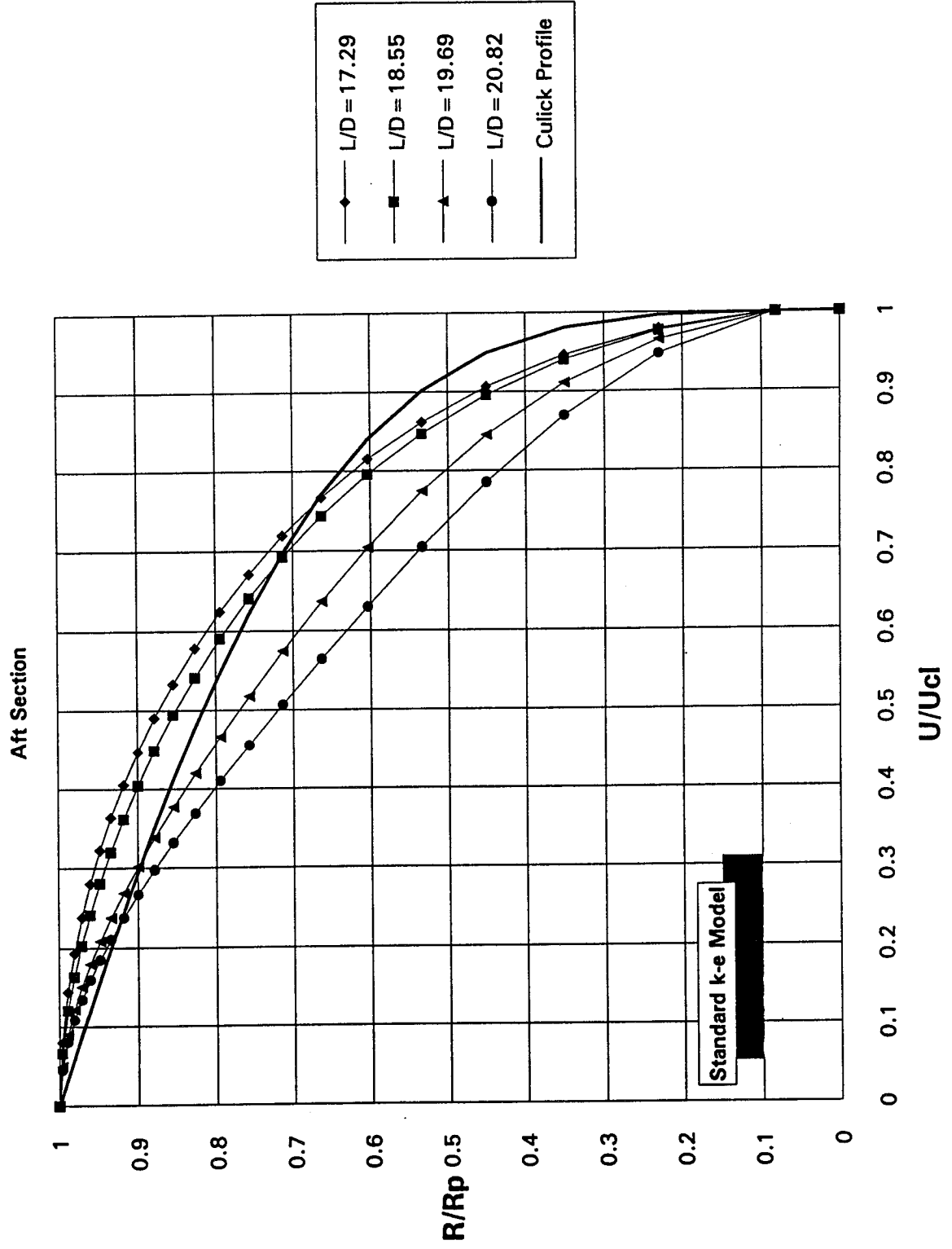
Figure 37. Normalized Kinetic Energy

2K/Ucl^2

| 0 | 0.01 | 0.02 | 0.03 | 0.04 | 0.05 | 0.06 | 0.07 | 0.08 | 0.09 | 0.1 |

Standard k-e Model

R/Rp

| 0 | 0.1 | 0.2 | 0.3 | 0.4 | 0.5 | 0.6 | 0.7 | 0.8 | 0.9 | 1 |

Technology Model at L/D = 0.24
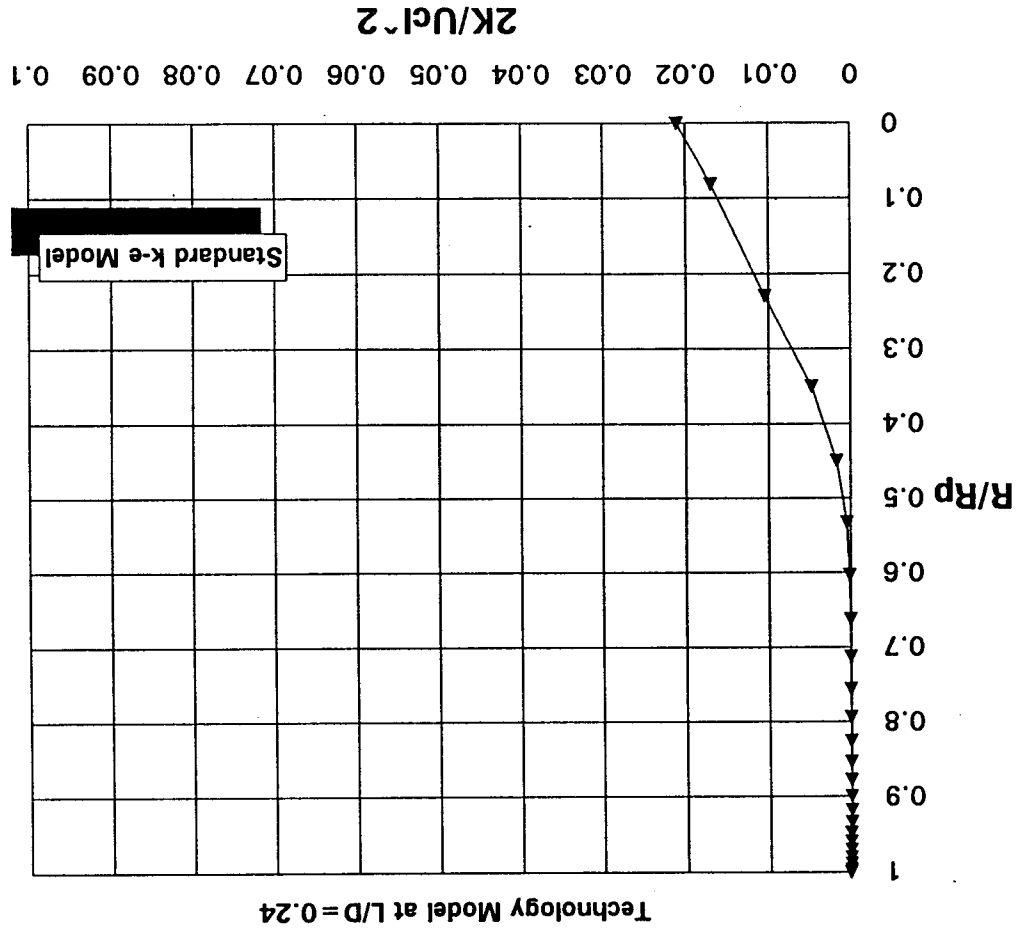
Figure 38. Normalized Kinetic Energy

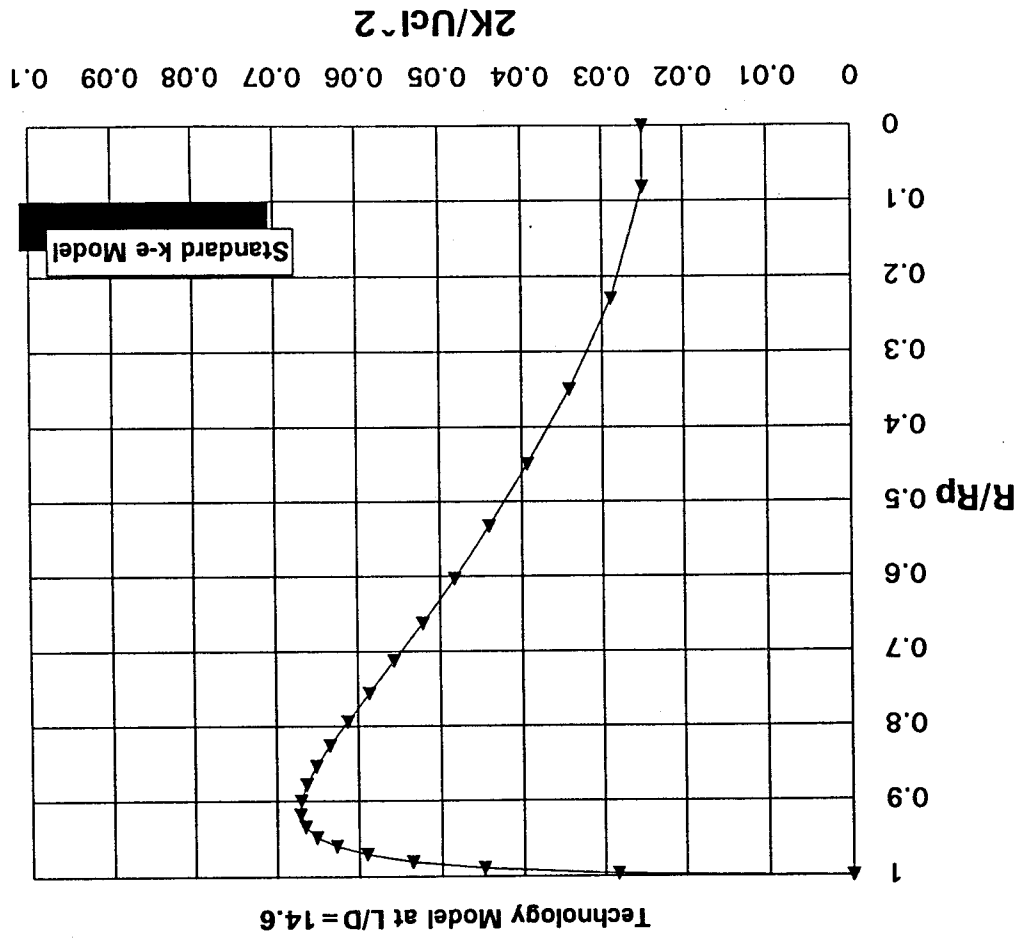Technology Model at L/D = 1.23

Standard k-e Model

2K/Ucl^2

R/Rp
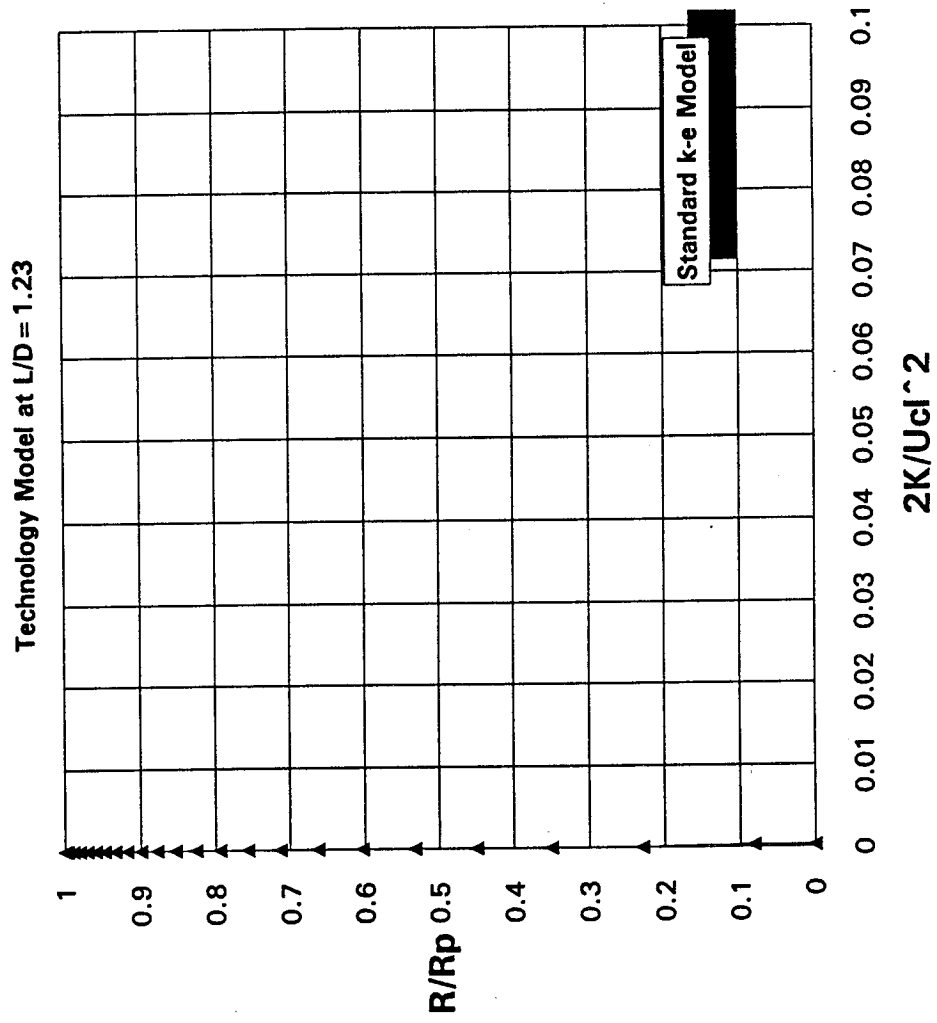
Figure 39. Normalized Kinetic Energy
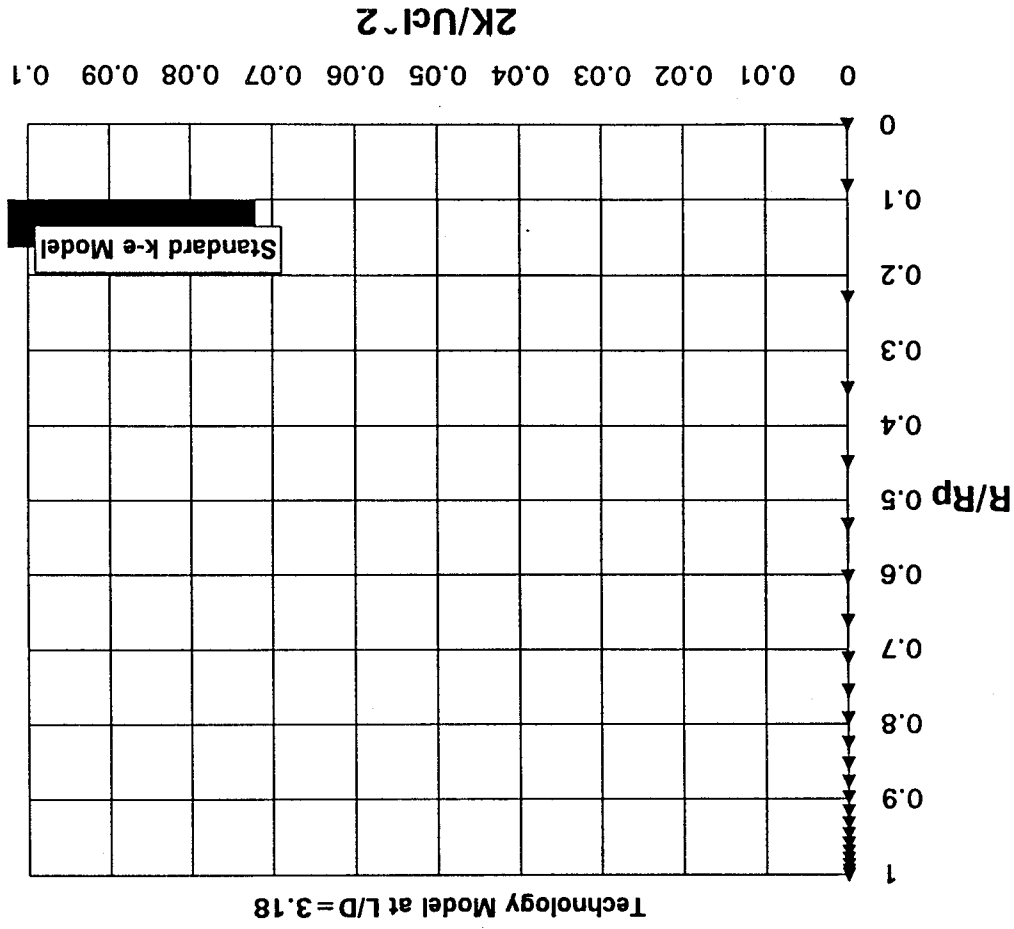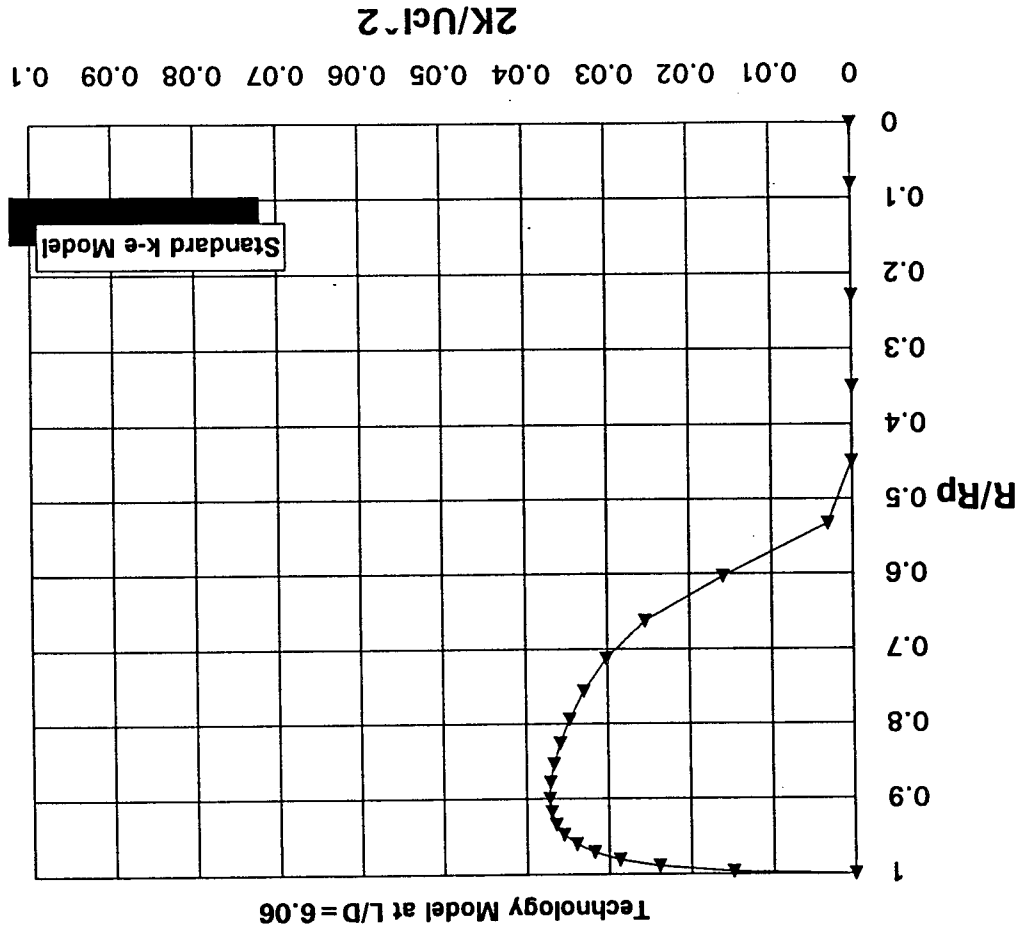
Figure 41. Normalized Kinetic Energy
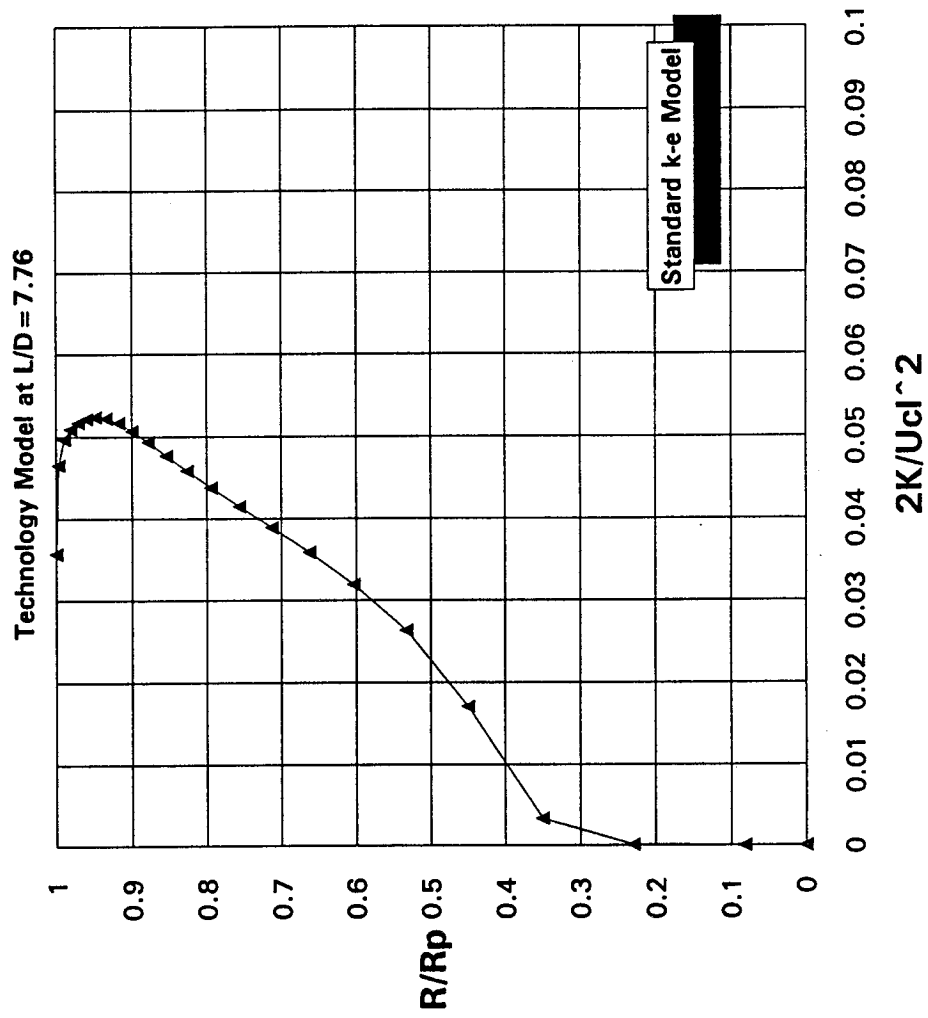
Figure 42. Normalized Kinetic Energy

Standard k-e Model

Technology Model at L/D = 8.06

2K/Ucl^2

R/Rp

2K/Uci^2

0   0.01 0.02 0.03 0.04 0.05 0.06 0.07 0.08 0.09 0.1

Standard k-e Model

R/Rp

Technology Model at L/D = 11.68
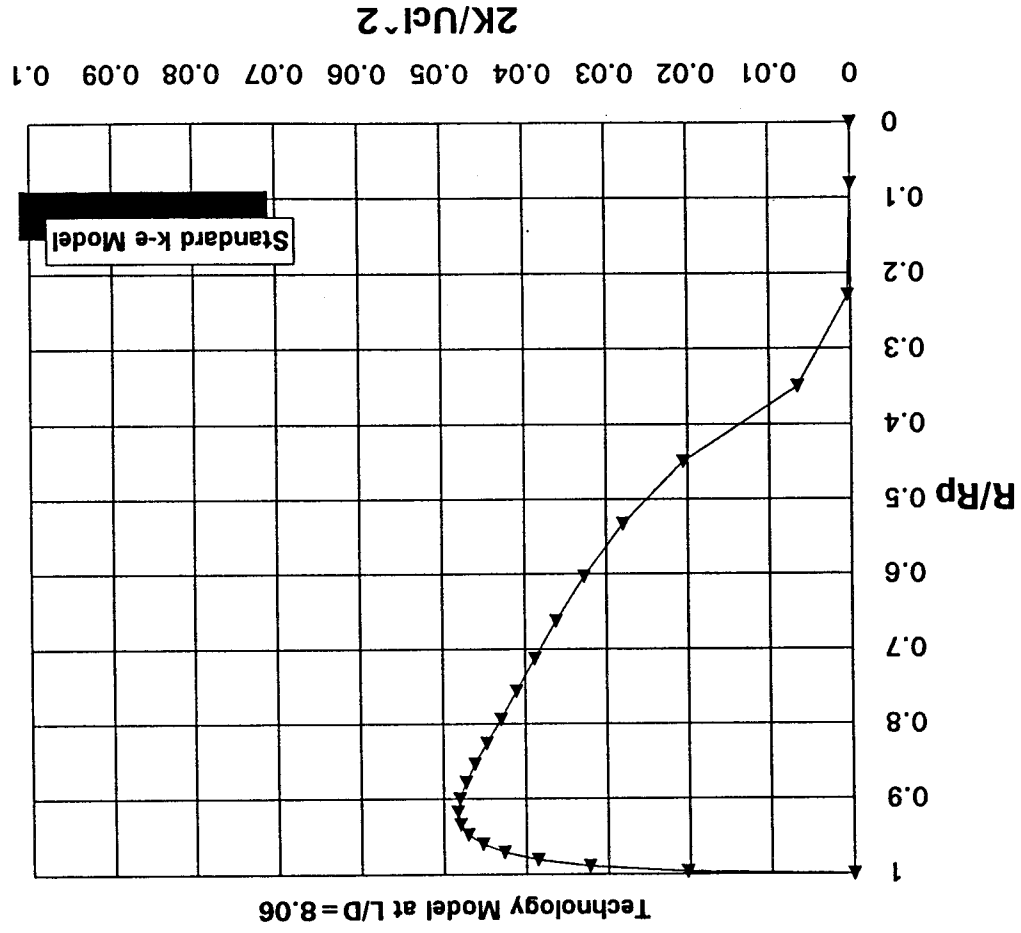
Figure 43. Normalized Kinetic Energy
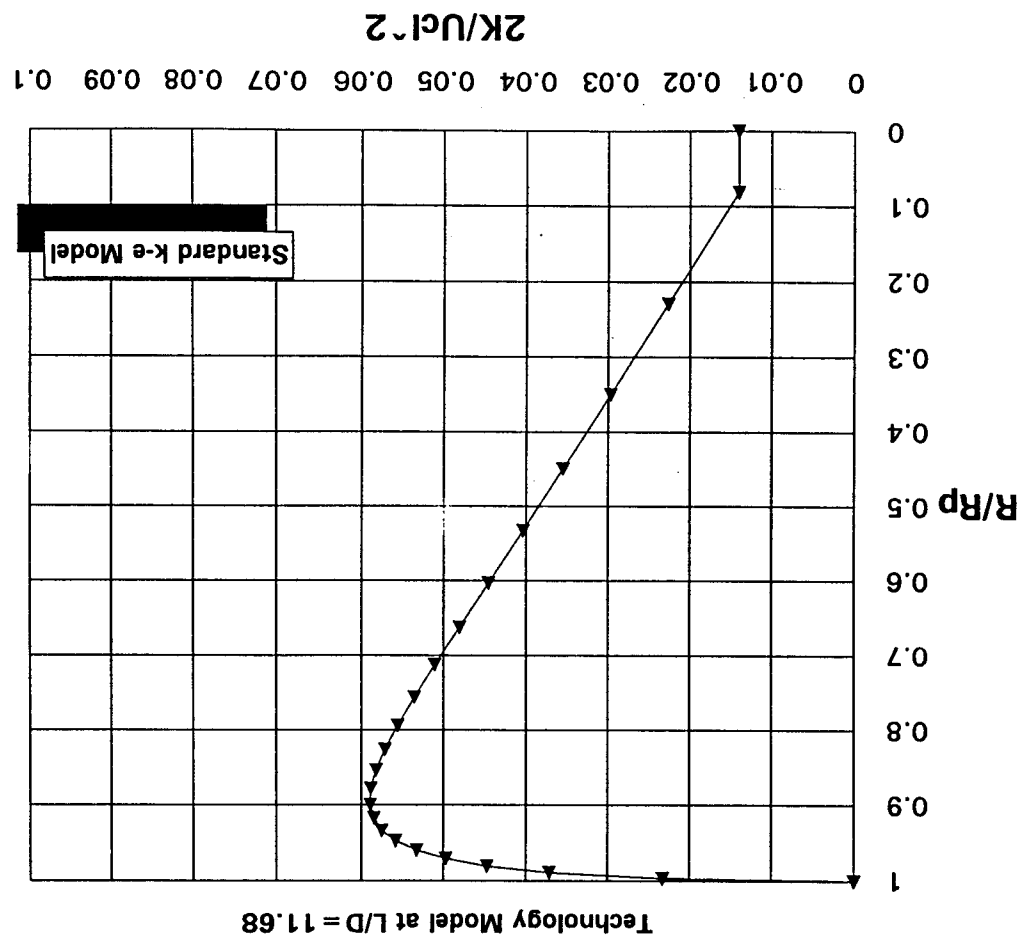
Figure 44. Normalized Kinetic Energy

Technology Model at L/D = 13.73

Standard k-e Model

R/Rp

2K/Ucl^2

2K/Ucl^2

0   0.01 0.02 0.03 0.04 0.05 0.06 0.07 0.08 0.09 0.1

Standard k-e Model

R/Rp
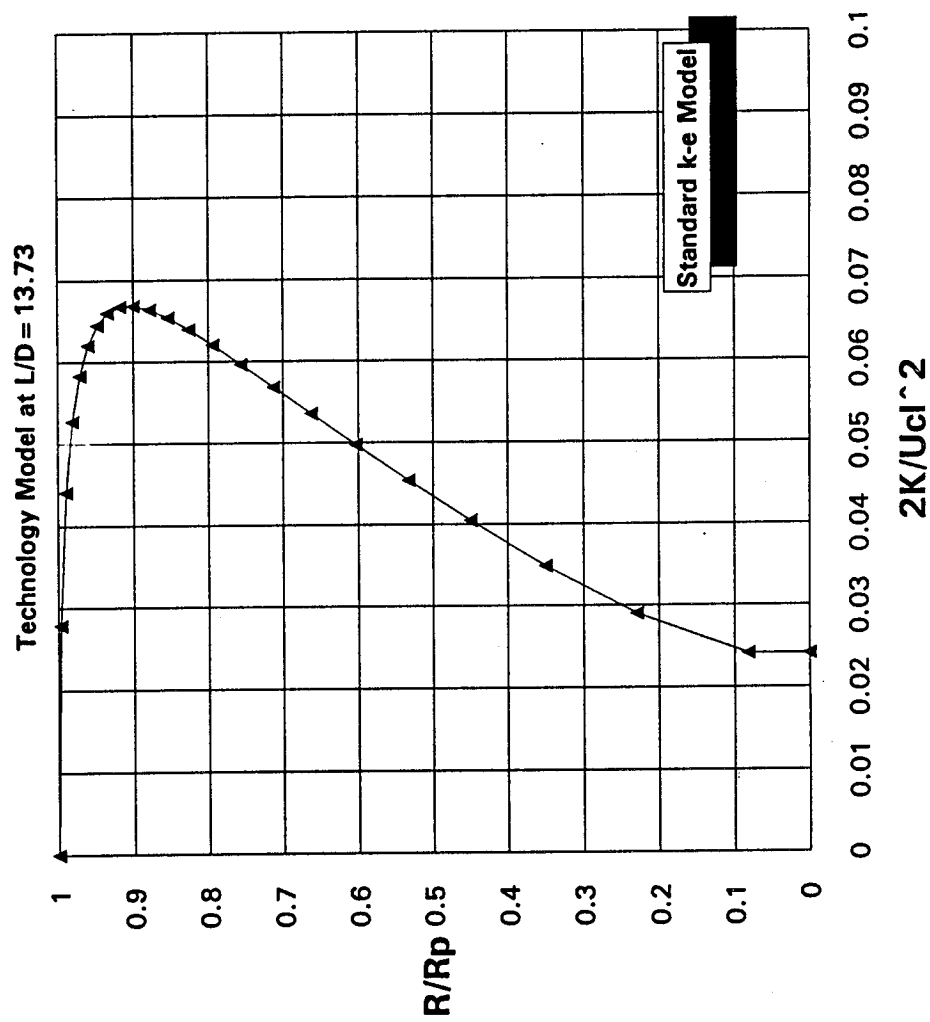
Technology Model at L/D = 15.34

Figure 46. Normalized Kinetic Energy
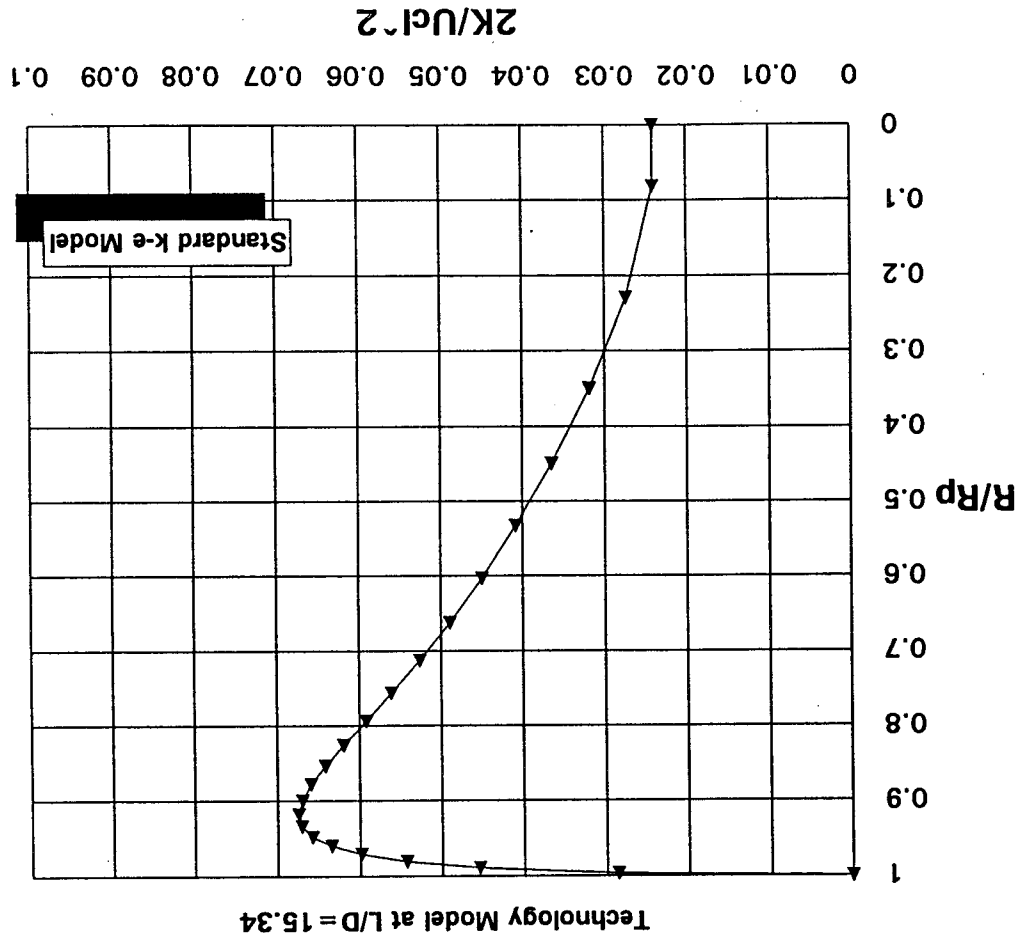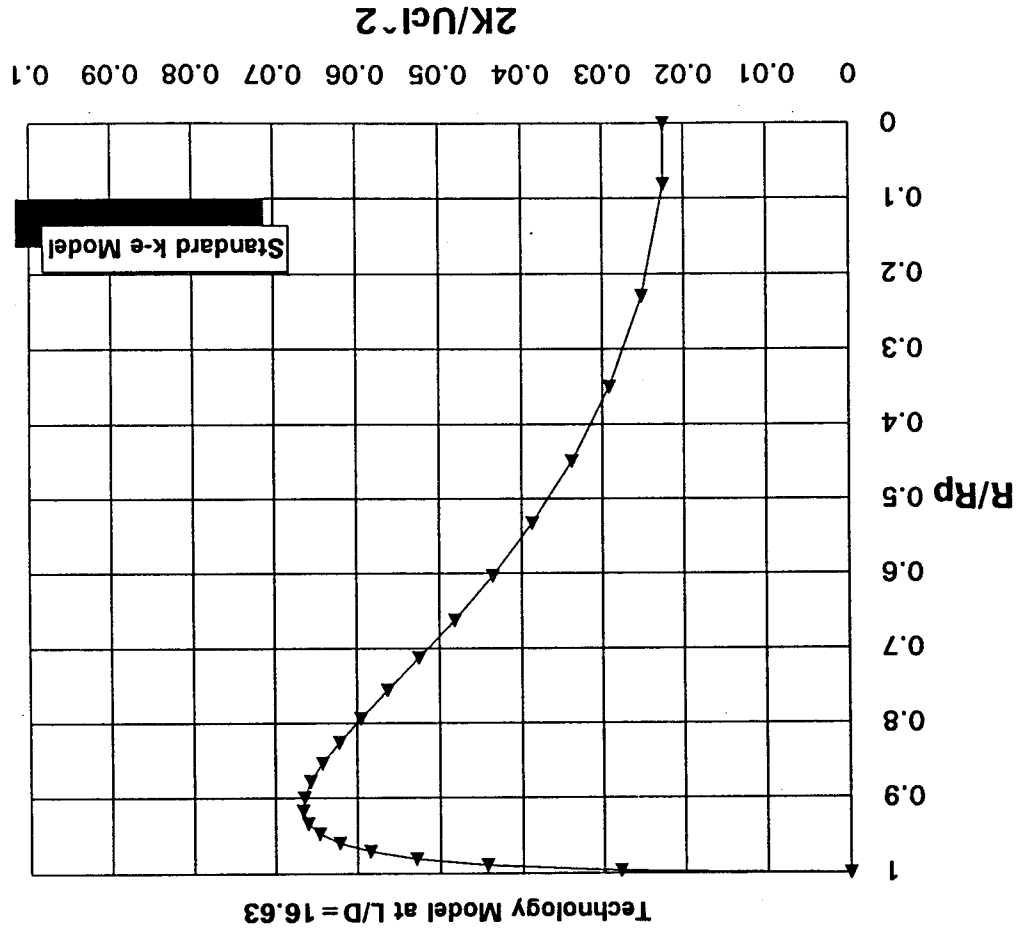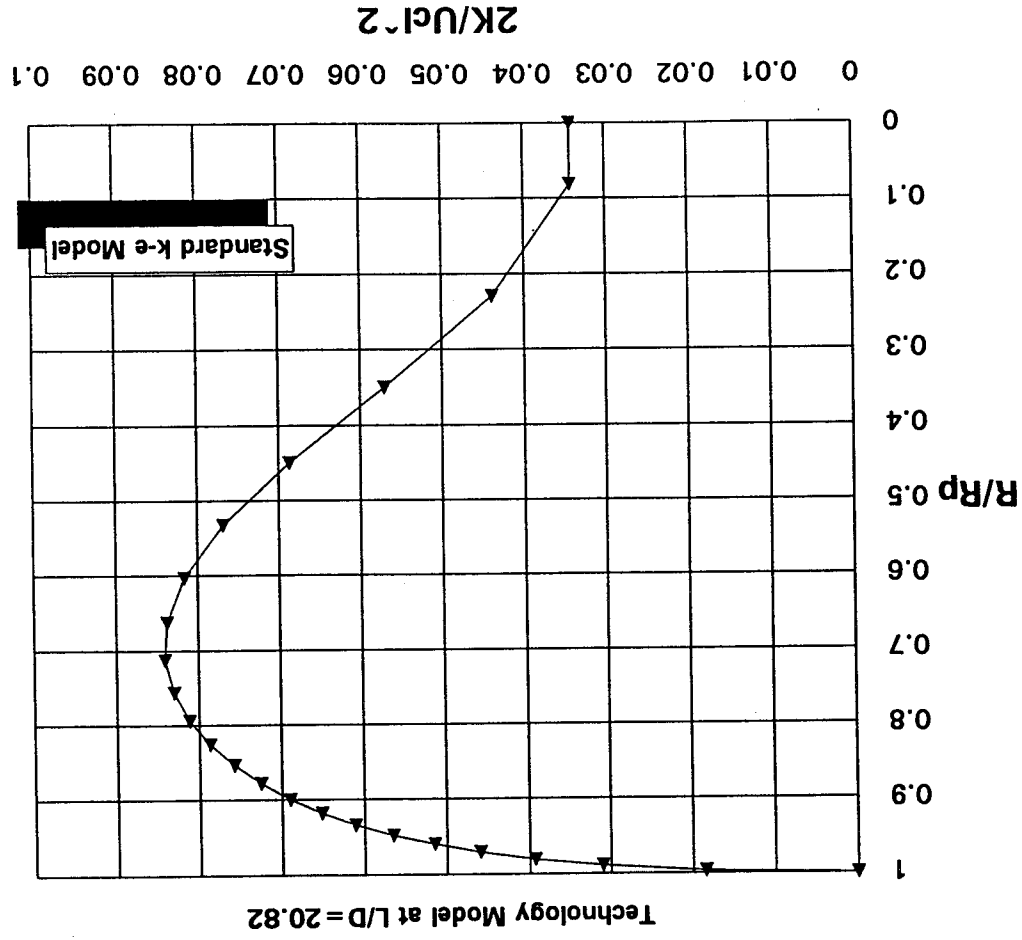
Figure 49. Technology Model Velocity Profiles

Head End to Aft Section

ERCI 07/17/92

Legend:
- L/D = 1.23
- L/D = 6.06
- L/D = 10.62
- L/D = 13.73
- L/D = 17.29
- Culick Profile

Adjusted k-e Model

R/Rp

U/Ucl
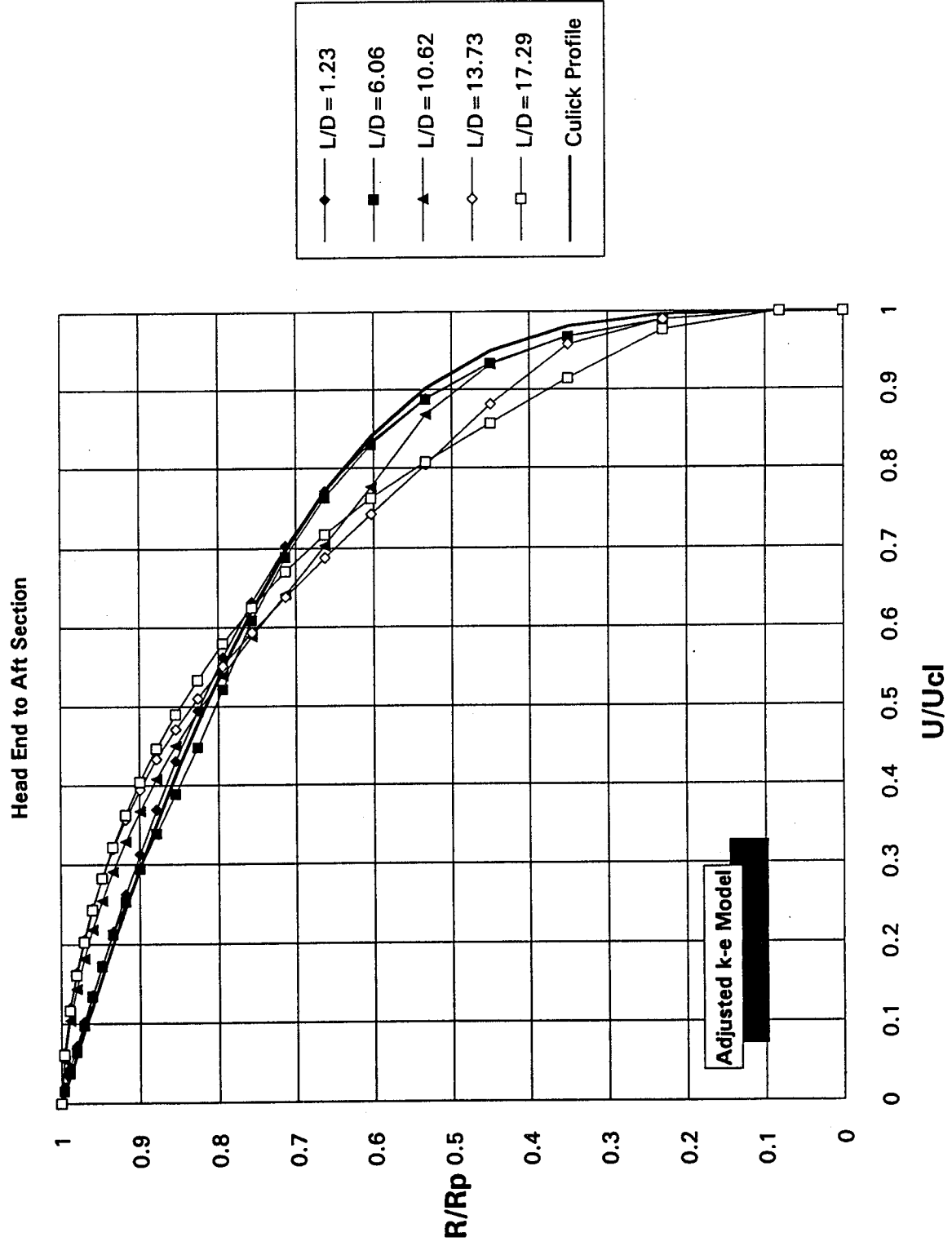
Figure 50. Technology Model Velocity Profiles

Head End Region

Legend:
- L/D = 0.24
- L/D = 1.23
- L/D = 3.18
- L/D = 5.07
- Culick Profile

Axes: R/Rp (vertical), U/Ucl (horizontal)

Adjusted k-e Model
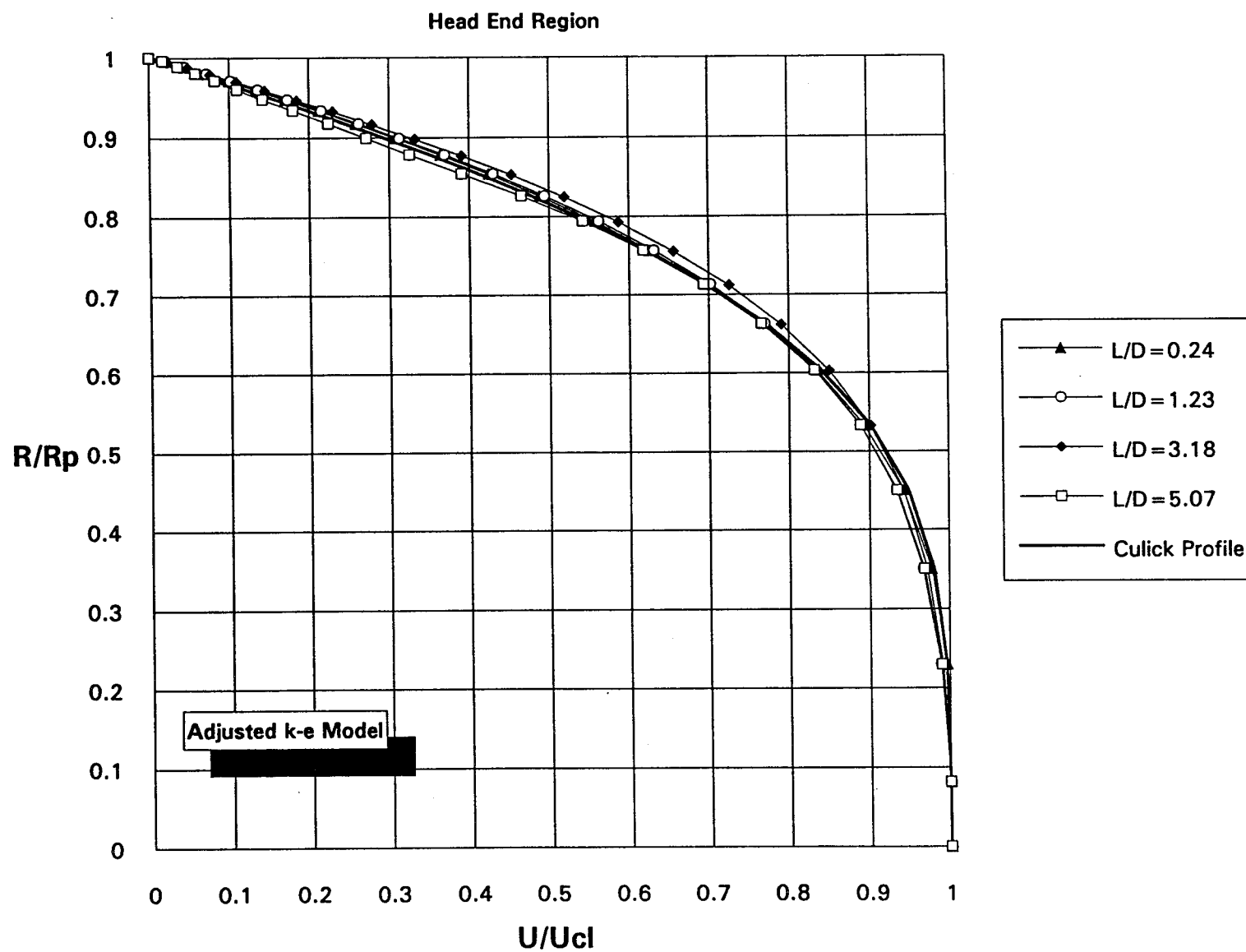
Figure 51. Technology Model Velocity Profiles

Forward Slot Region

Legend:
- ■ L/D = 6.06
- ♦ L/D = 7.56
- △ L/D = 7.76
- ○ L/D = 8.06
- ● L/D = 10.62
- —— Culick Profile

Adjusted k-e Model

U/Ucl

R/Rp
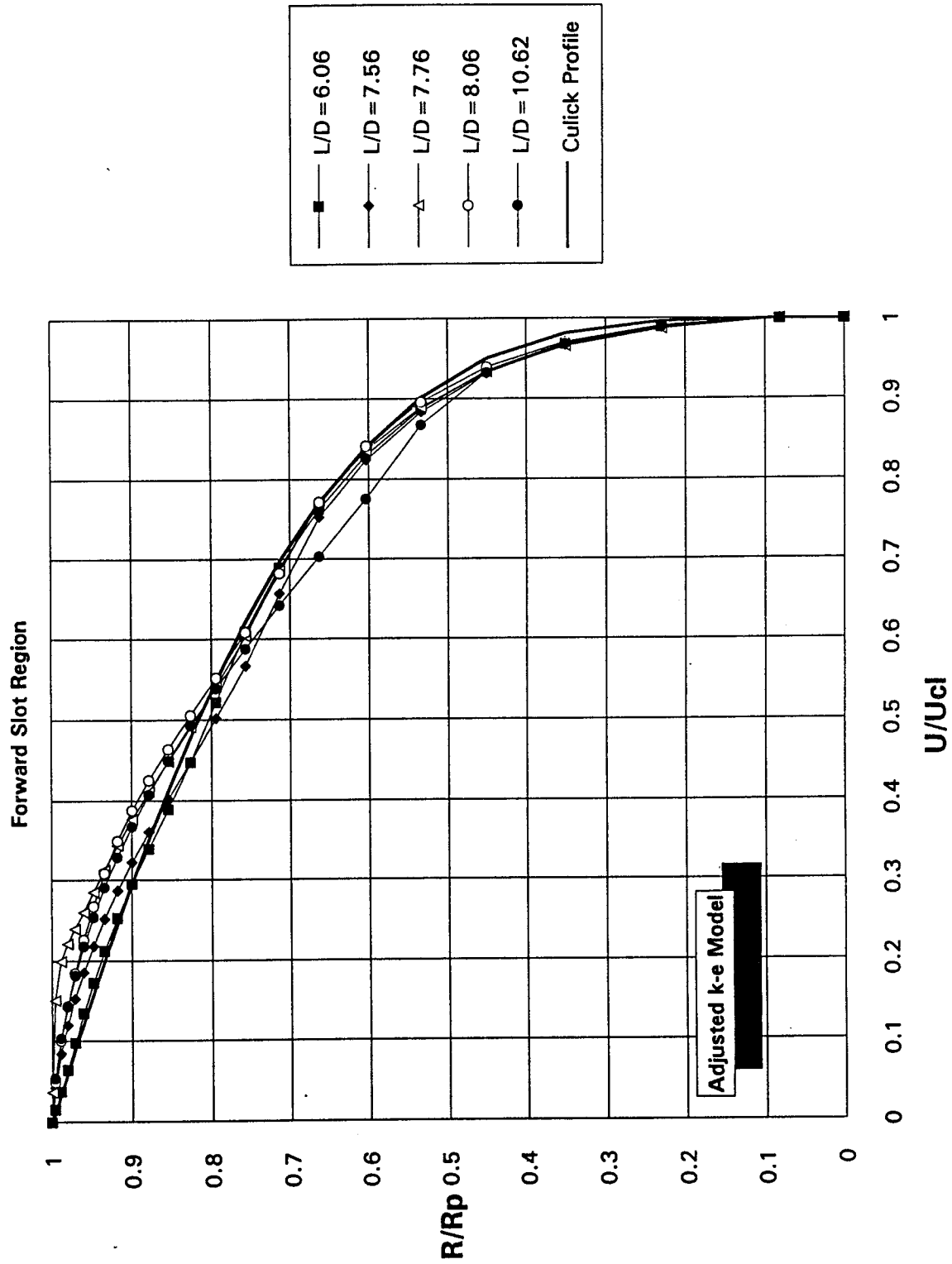
Figure 52. Technology Model Velocity Profiles

Model Center Section

Legend:
- ▲ L/D = 8.06
- ■ L/D = 9.37
- ◆ L/D = 10.62
- □ L/D = 11.68
- △ L/D = 12.77
- ● L/D = 13.73
- ○ L/D = 14.32
- —— Culick Profile

Adjusted k-e Model

Axes: R/Rp (vertical), U/Ucl (horizontal)
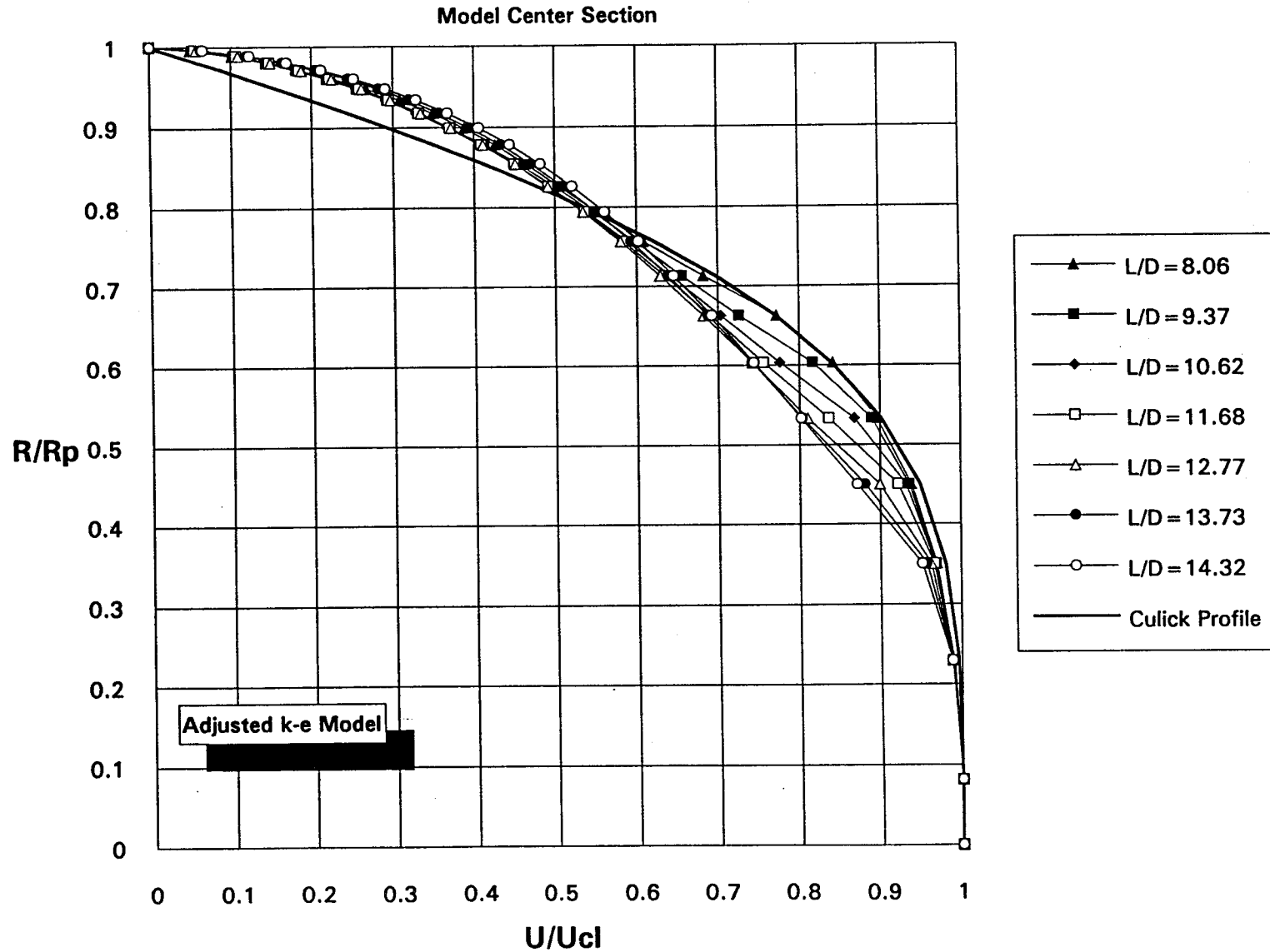
Figure 53. Technology Model Velocity Profiles

Aft Slot Region

ERCI 07/17/92
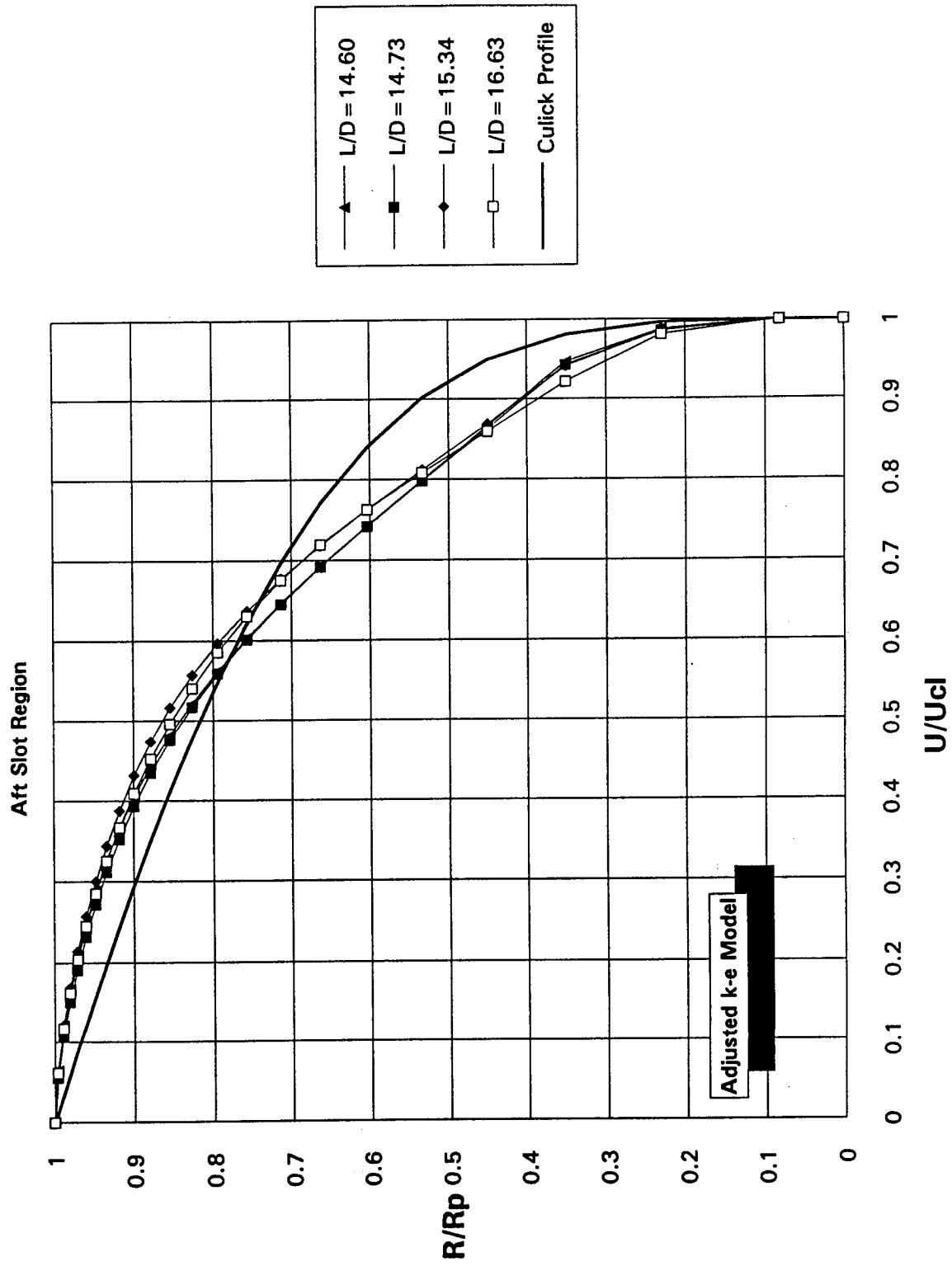
Figure 54. Technology Model Velocity Profiles

Aft Section

Legend:
- L/D = 17.29
- L/D = 18.55
- L/D = 19.69
- L/D = 20.82
- Culick Profile

Adjusted k-e Model

Axes: R/Rp (vertical), U/Ucl (horizontal)
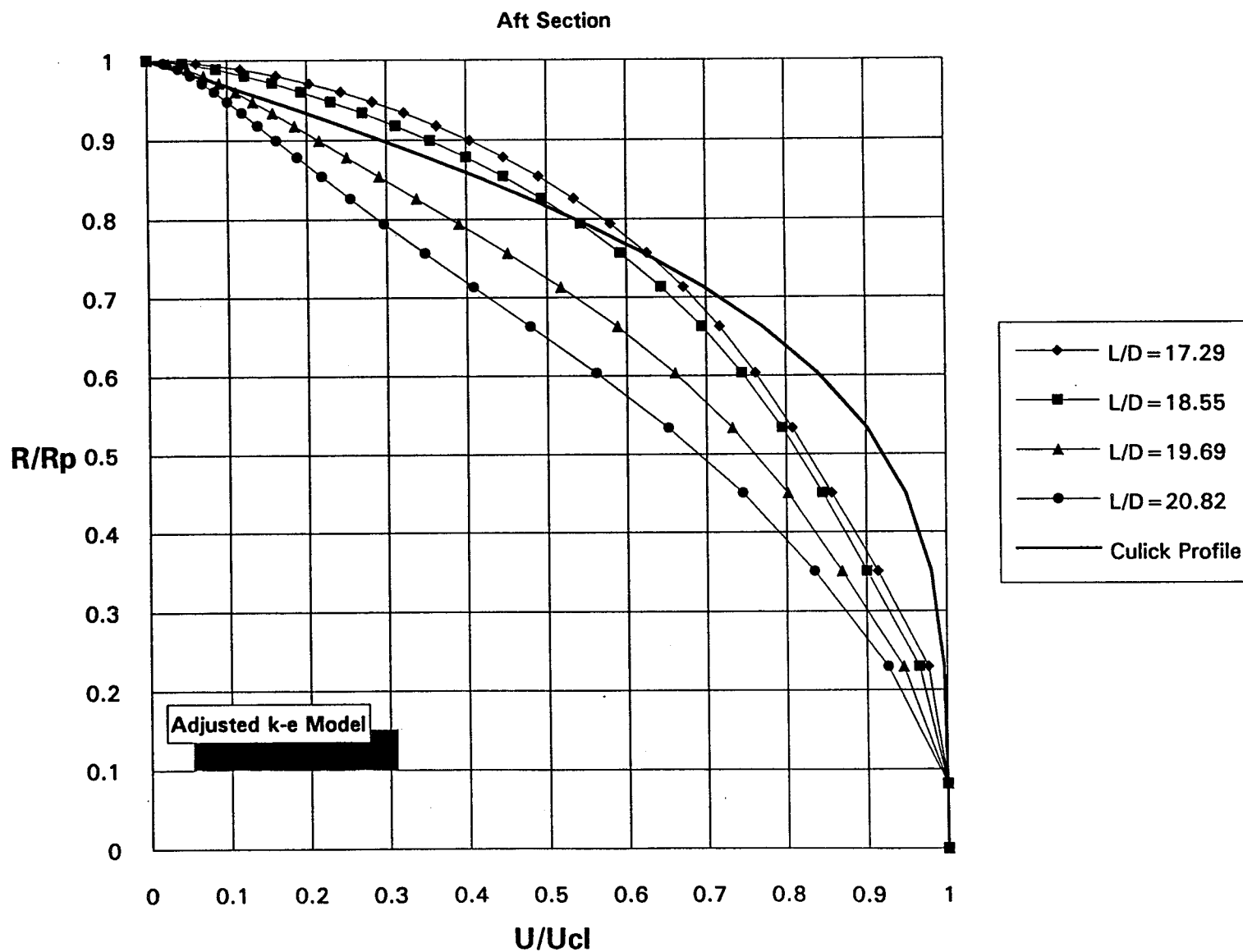
Figure 55. Normalized Kinetic Energy

Technology Model at L/D = 0.24

ERC, Inc. 07/17/92
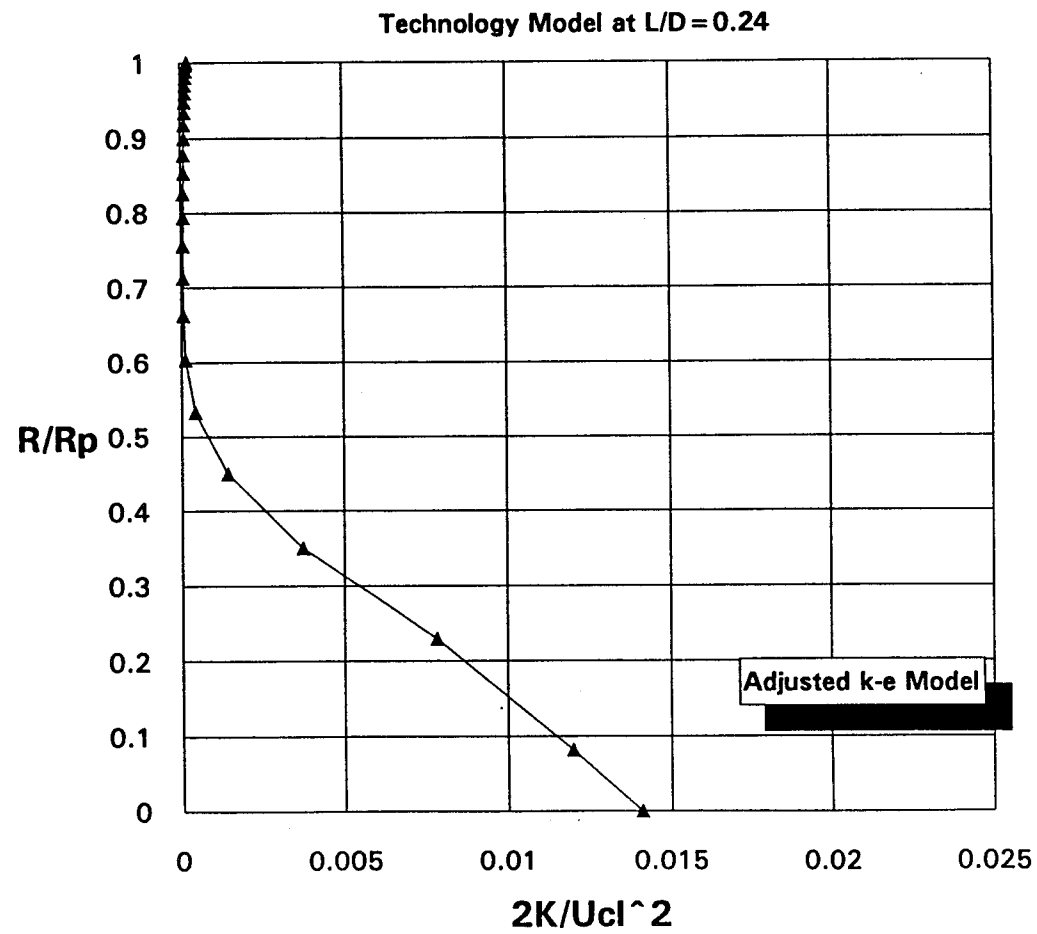
Figure 56. Normalized Kinetic Energy

Technology Model at L/D = 1.23

X-axis: 2K/Ucl^2

Y-axis: R/Rp

Adjusted k-e Model
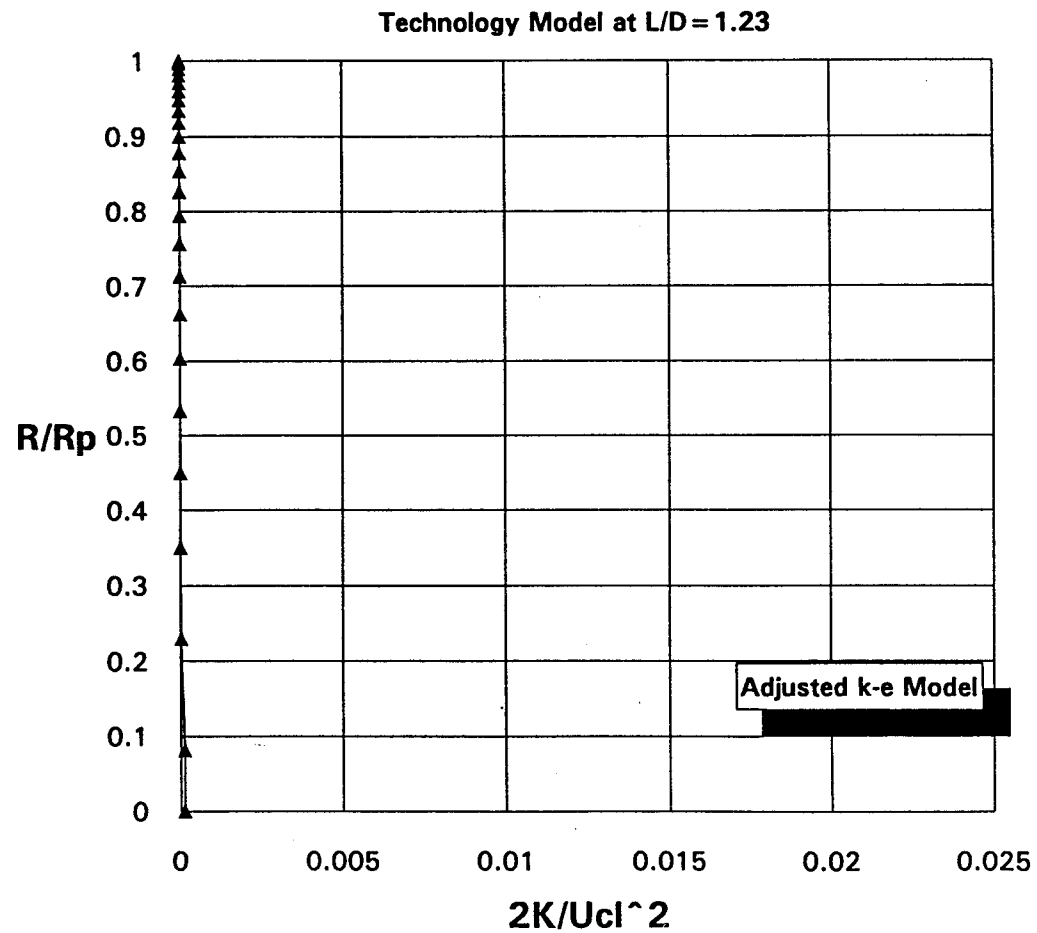
Figure 57. Normalized Kinetic Energy

Technology Model at L/D=3.18
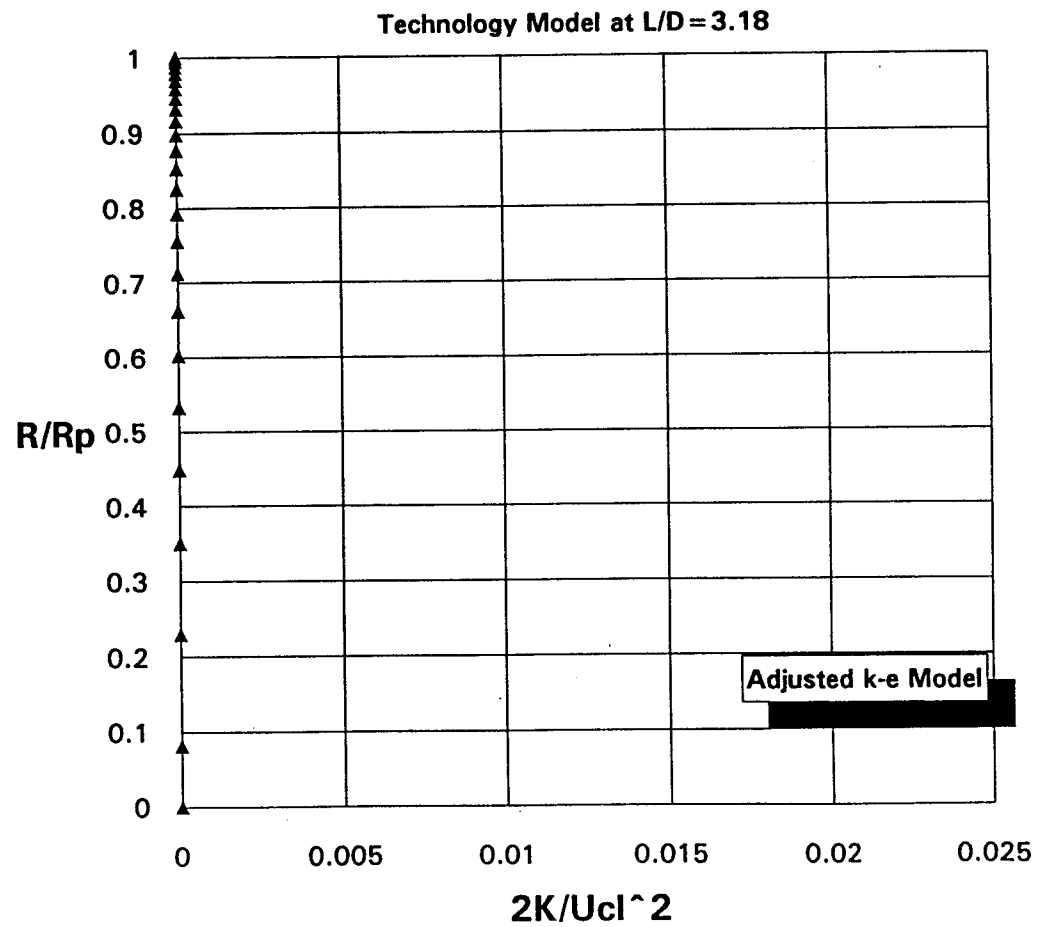
Figure 58. Normalized Kinetic Energy

Technology Model at L/D = 6.06

Legend: Adjusted k-e Model

Y-axis: R/Rp (0 to 1)

X-axis: 2K/Ucl^2 (0 to 0.025)
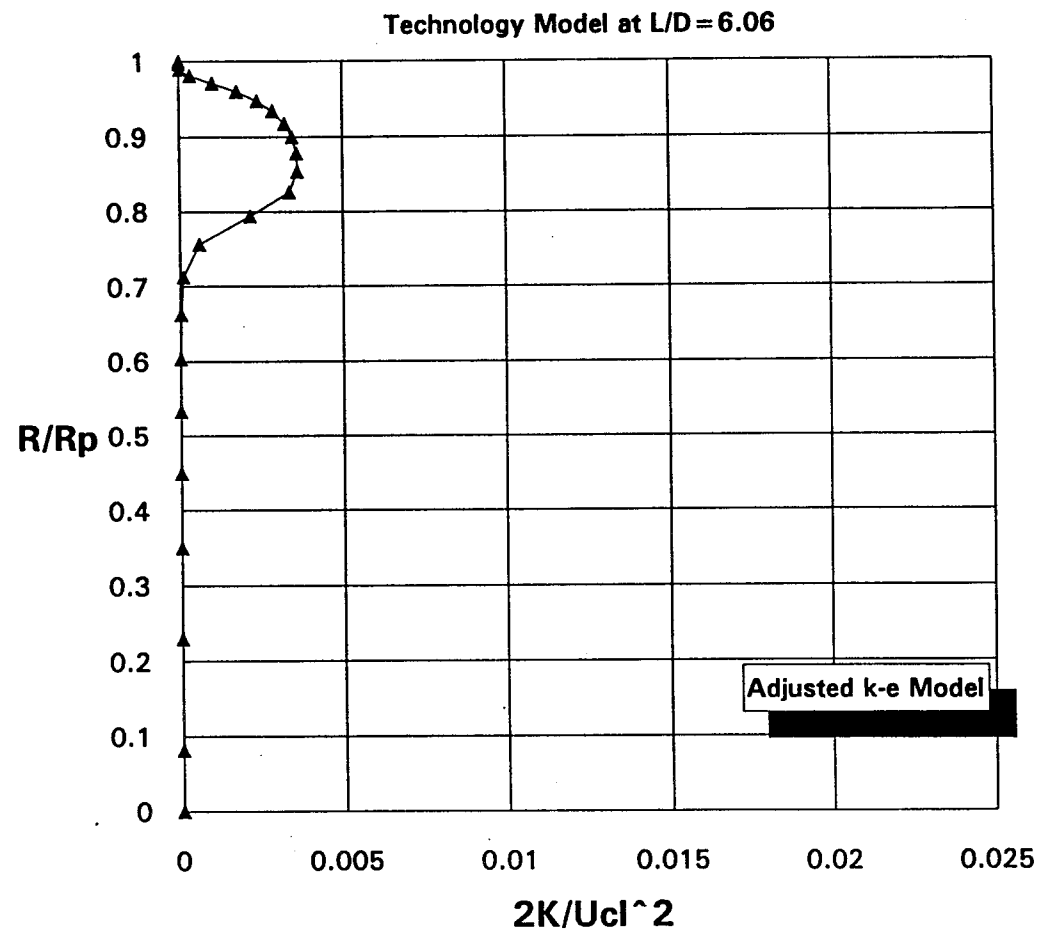
Figure 59. Normalized Kinetic Energy

Technology Model at L/D = 7.76

2K/Ucl^2

R/Rp
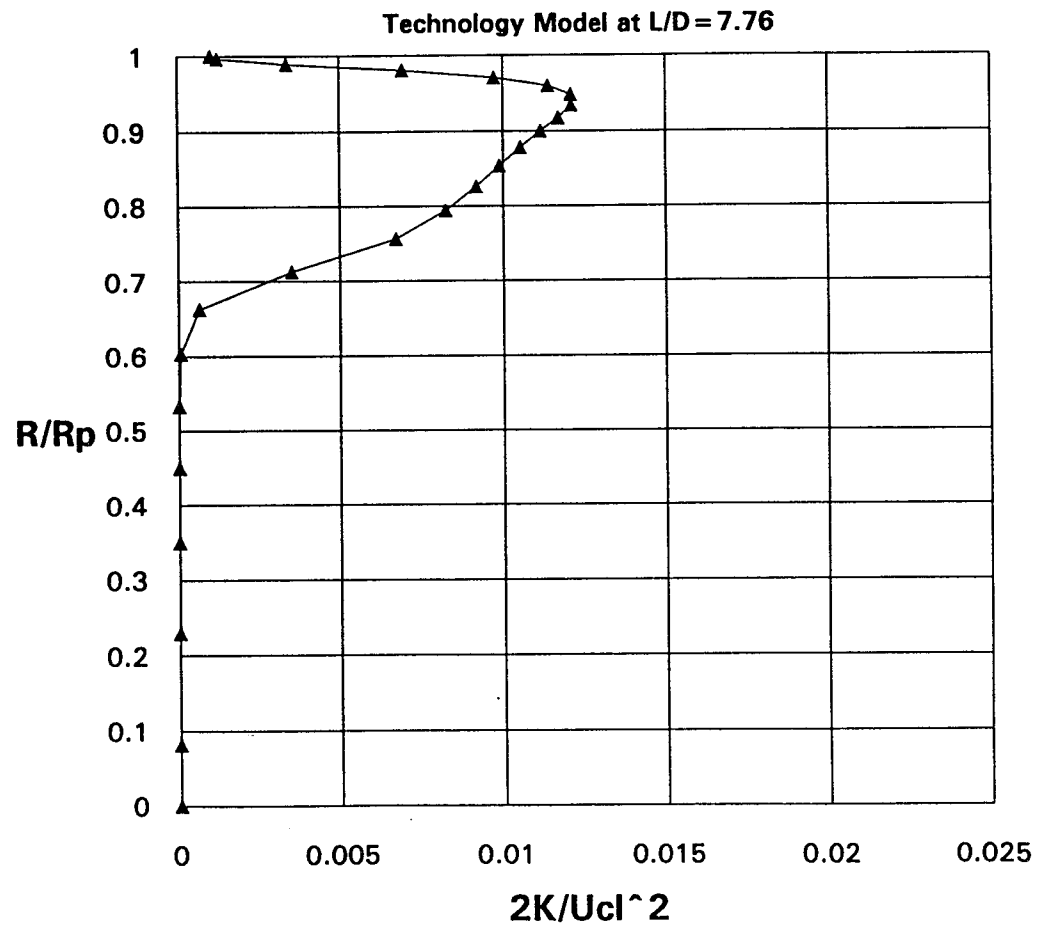
Figure 60. Normalized Kinetic Energy

Technology Model at L/D = 8.06

Axis labels: R/Rp (vertical), 2K/Ucl^2 (horizontal)

Legend: Adjusted k-e Model
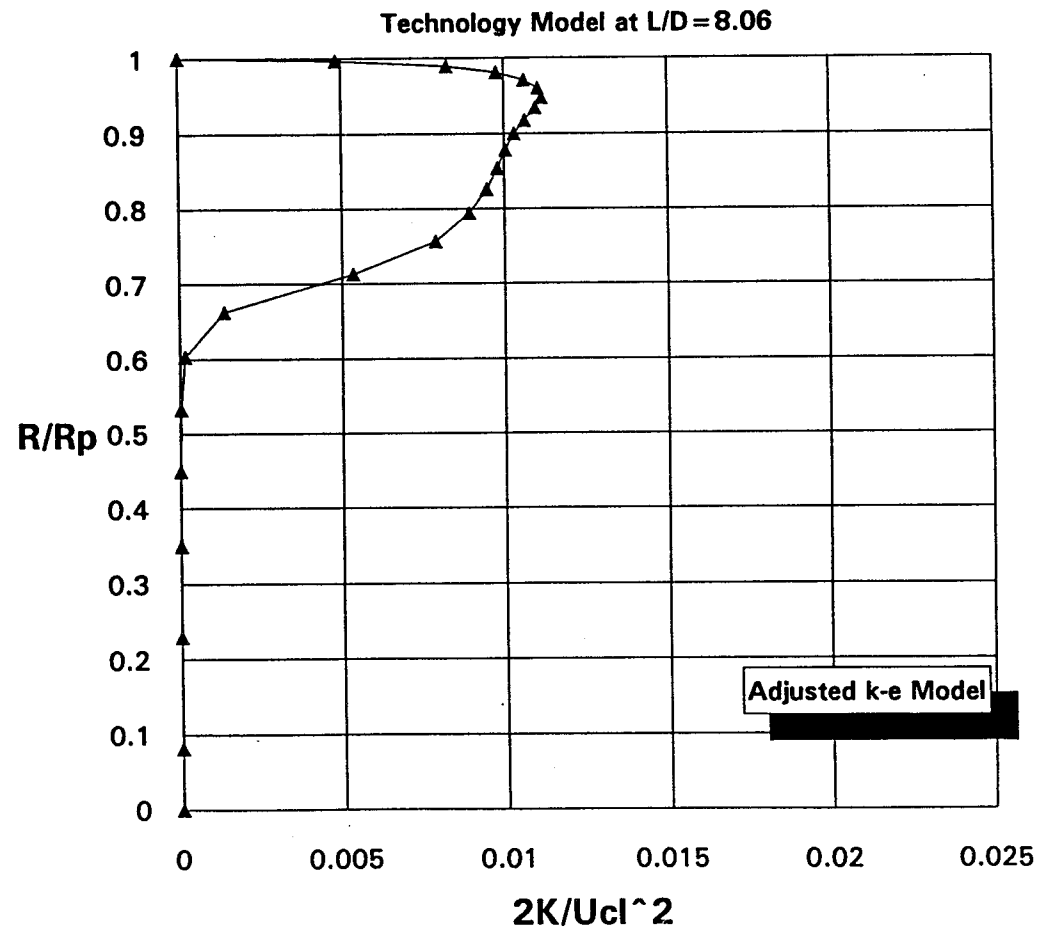
Figure 61. Normalized Kinetic Energy

Technology Model at L/D = 11.68

Adjusted k-e Model

R/Rp

2K/Ucl^2
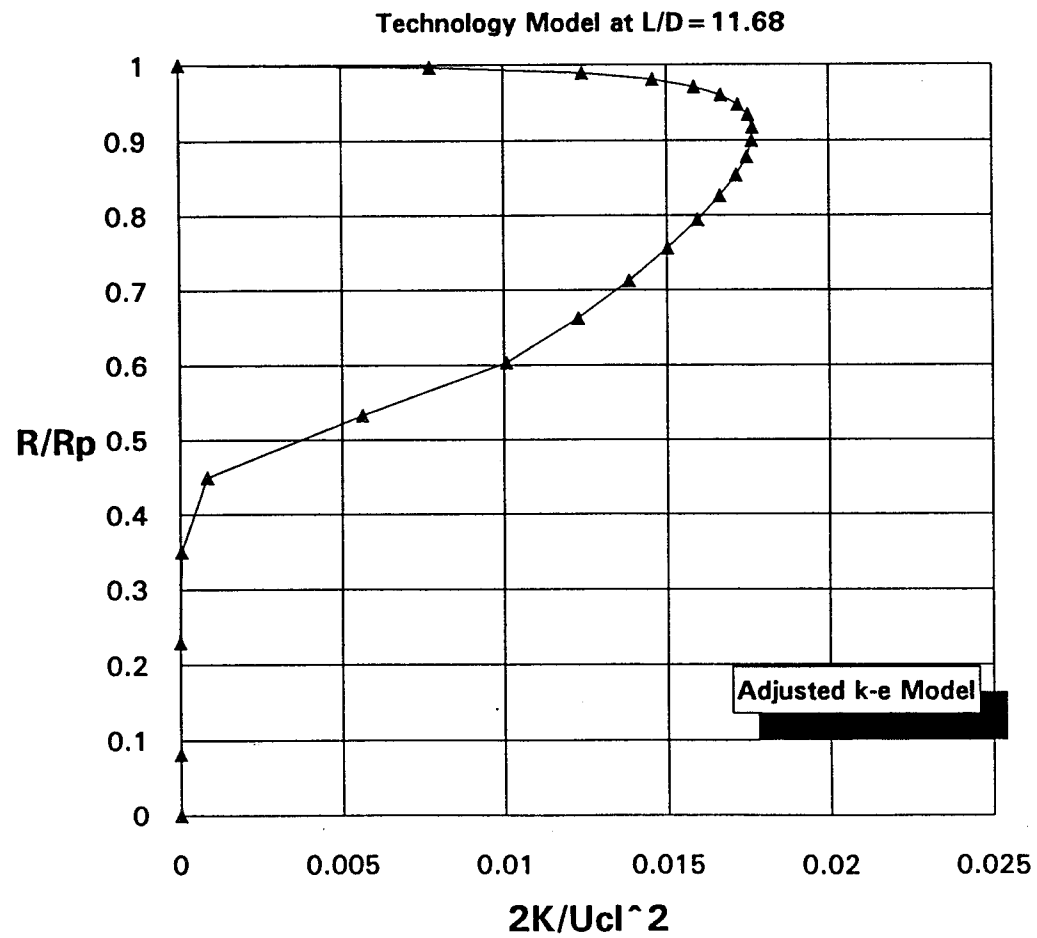
Figure 62. Normalized Kinetic Energy

Technology Model at L/D = 13.73

Legend: Adjusted k-e Model

Y-axis: R/Rp (0 to 1)
X-axis: 2K/Ucl^2 (0 to 0.025)
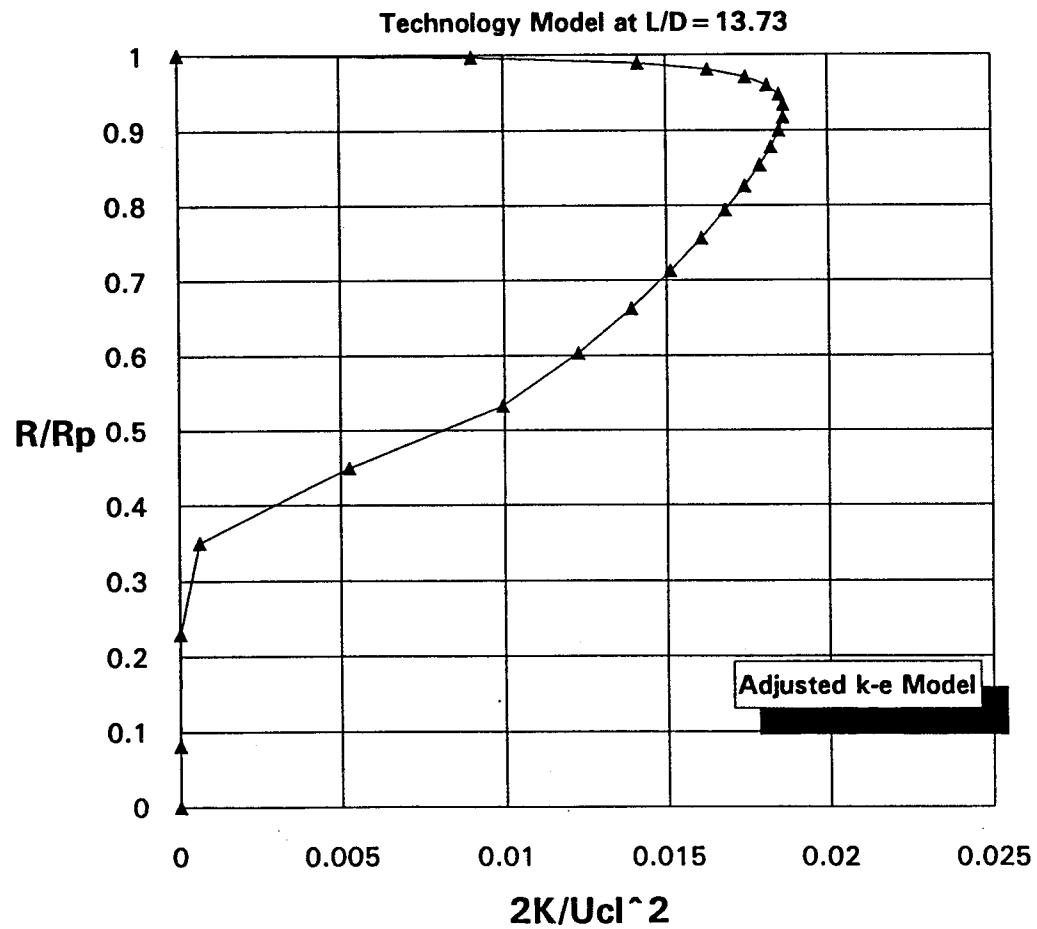
Figure 63. Normalized Kinetic Energy

Technology Model at L/D = 14.6
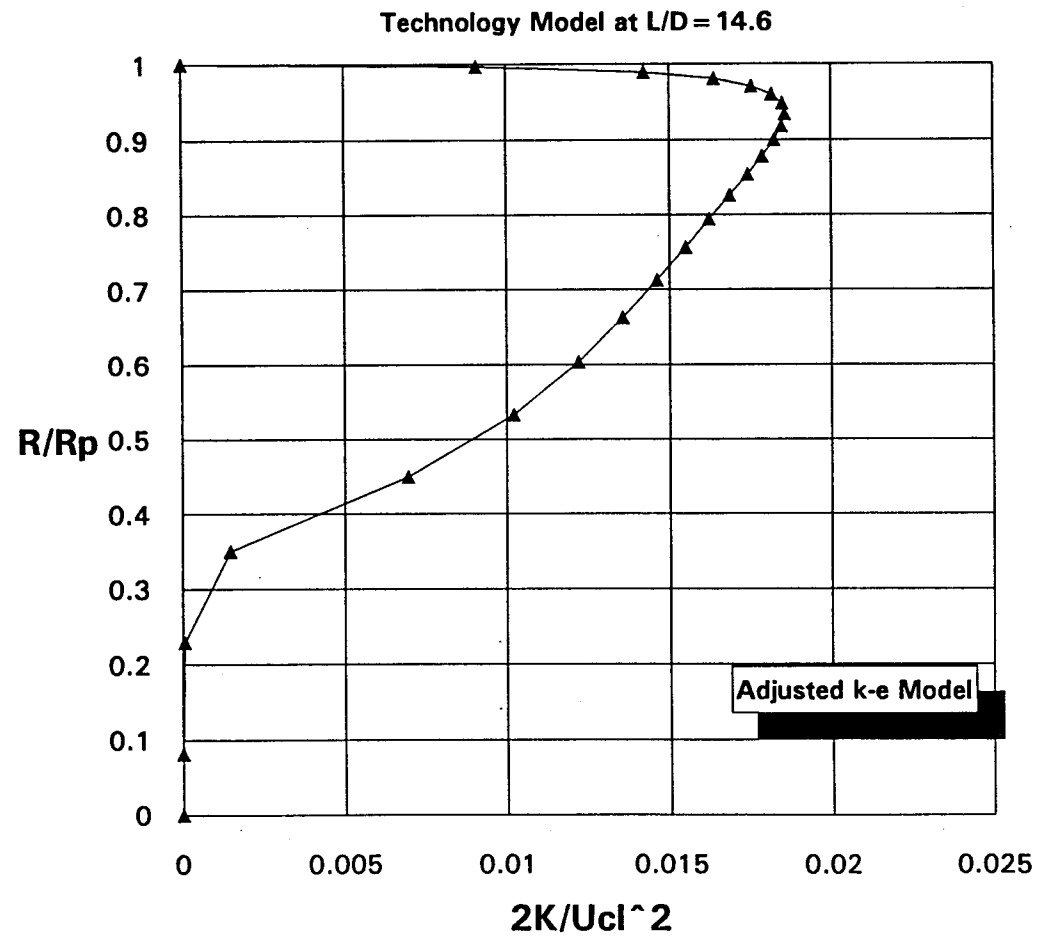
Figure 64. Normalized Kinetic Energy

Technology Model at L/D = 15.34

Axis labels: R/Rp (vertical), 2K/Ucl^2 (horizontal)

Legend: Adjusted k-e Model
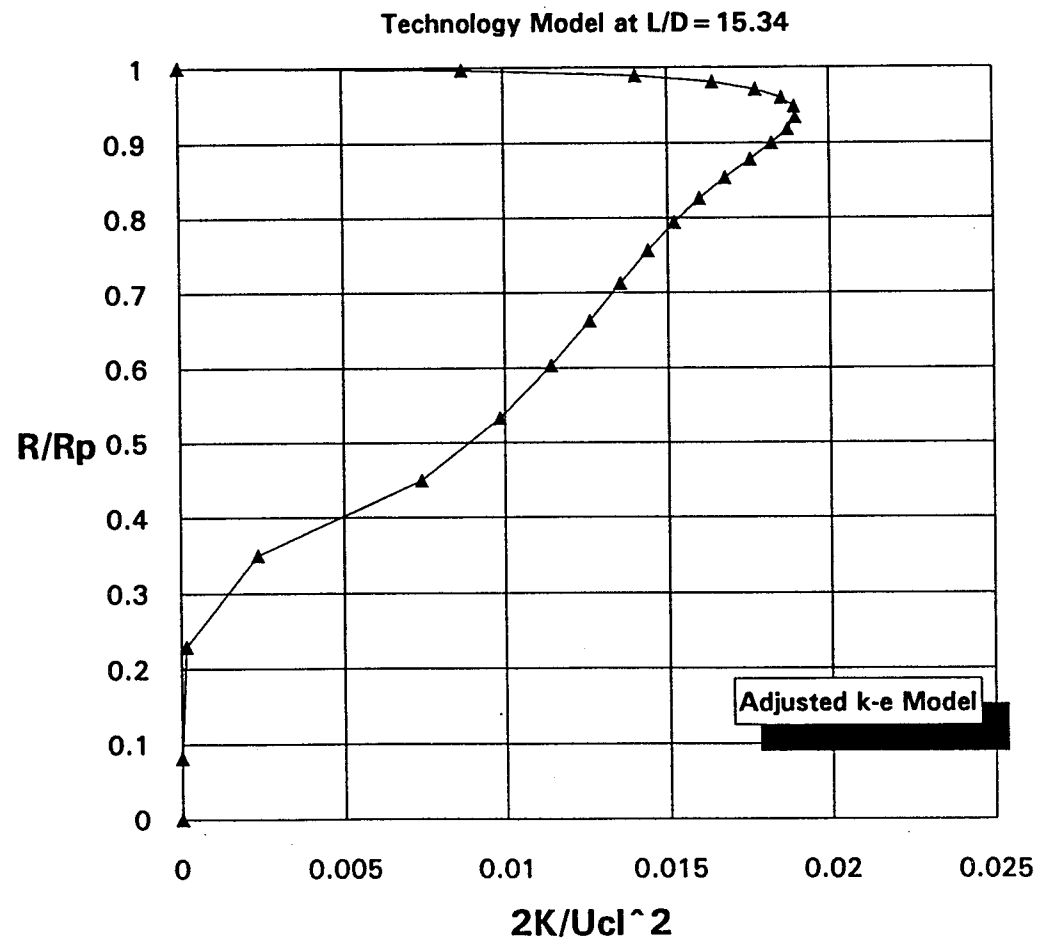
Figure 65. Normalized Kinetic Energy

Technology Model at L/D = 16.63

ERC, Inc. 07/17/92
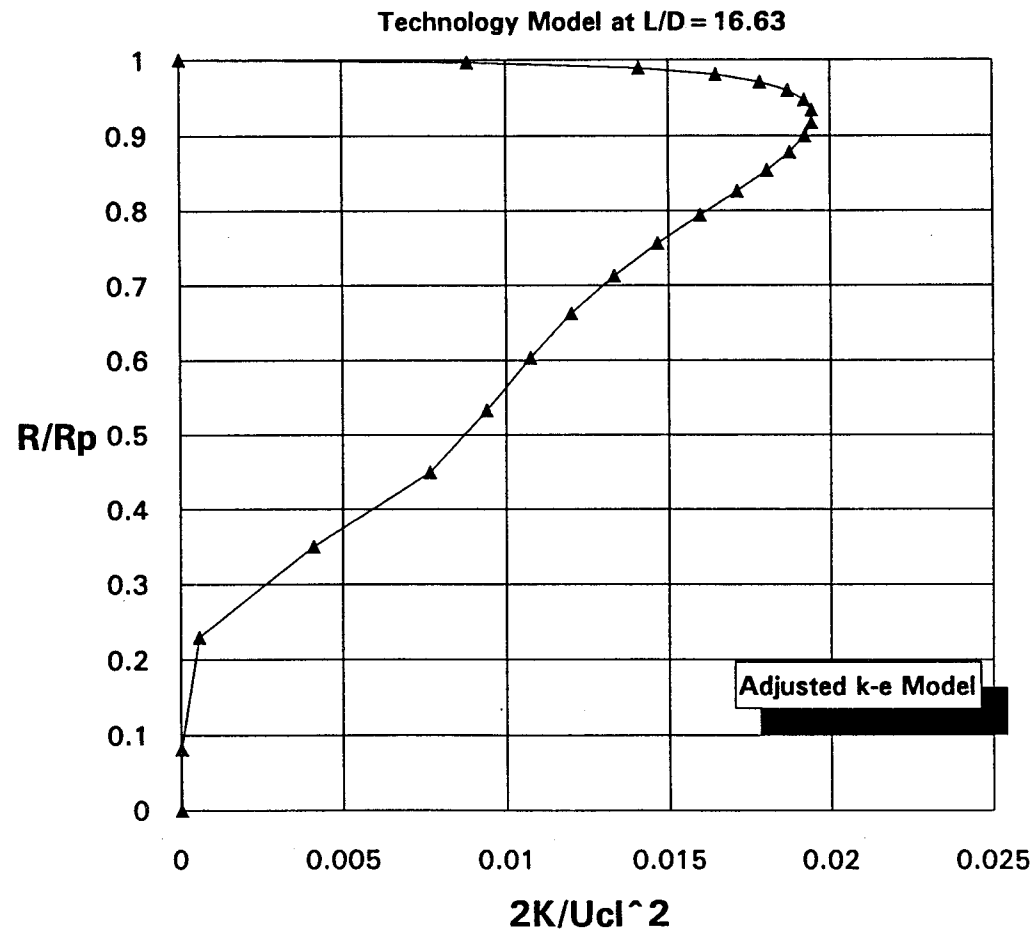
Figure 66. Normalized Kinetic Energy

Technology Model at L/D = 20.82

Adjusted k-e Model

R/Rp

2K/Ucl^2
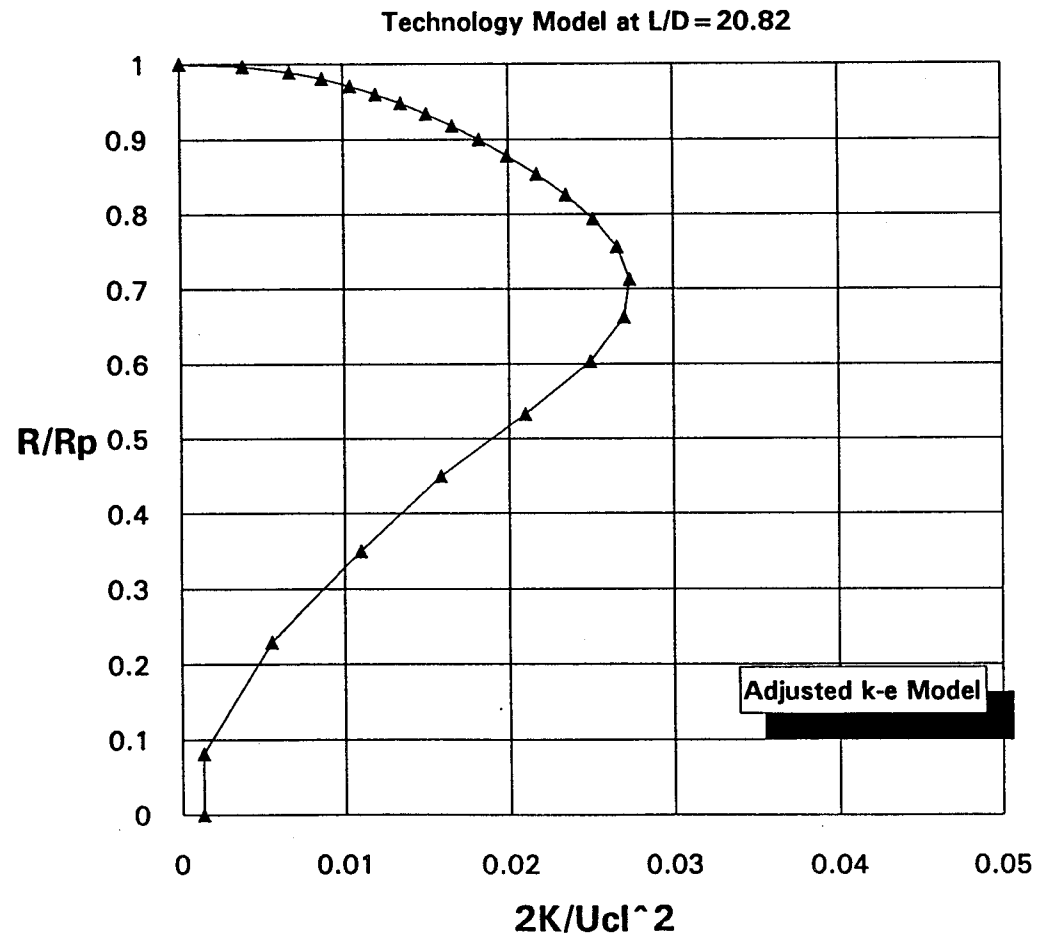
AIAA 94-3292

The Determination of Forces and Moments on a Gimballed SRM Nozzle Using a Cold Flow Model

R. Harold Whitesides
ERC, Incorporated
Huntsville, AL

David L. Bacchus and John E. Hengel
NASA/Marshall Space Flight Center
Huntsville, AL

30th AIAA/ASME/SAE/ASEE Joint Propulsion Conference
June 27-29, 1994 / Indianapolis, IN

THE DETERMINATION OF FORCES AND MOMENTS ON A
GIMBALLED SRM NOZZLE USING A COLD FLOW MODEL

R. Harold Whitesides*
ERC, Inc.
Huntsville, Alabama

David L. Bacchus** and John E. Hengel***
NASA Marshall Space Flight Center
Huntsville Alabama

Abstract

The Solid Rocket Motor Air Flow Facility (SAF) at NASA Marshall Space Flight Center was used to characterize the flow in the critical aft end and nozzle of a solid propellant rocket motor (SRM) as part of the design phase of development. The SAF is a high pressure, blow-down facility which supplies a controlled flow of air to a subscale model of the internal port and nozzle of a SRM to enable measurement and evaluation of the flow field and surface pressure distributions. The ASRM Aft Section/Nozzle Model is an 8 percent scale model of the 19 second burn time aft port geometry and nozzle of the Advanced Solid Rocket Motor, the now canceled new generation space Shuttle Booster. It has the capability to simulate fixed nozzle gimbal angles of 0, 4, and 8 degrees. The model was tested at full scale motor Reynolds Numbers with extensive surface pressure instrumentation to enable detailed mapping of the surface pressure distributions over the nozzle interior surface, the exterior surface of the nozzle nose and the surface of the simulated propellant grain in the aft motor port. A mathematical analysis and associated numerical procedure were developed to integrate the measured surface pressure distributions to determine the lateral and axial forces on the moveable section of the nozzle, the effective model thrust and the

* Manager, Propulsion Group; AIAA Associate
   Fellow
** Deputy, Experimental Fluid Dynamics
   Branch; AIAA Member
*** Aerospace Engineer

effective aerodynamic thrust vector (as opposed to the geometric nozzle gimbal angle). The nozzle lateral and axial aerodynamic loads and moments about the pivot point are required for design purposes and require complex, three-dimensional flow analyses. The alignment of the thrust vector with the nozzle geometric centerline is also a design requirement requiring three-dimensional analyses which were supported by this experimental program. The model was tested with all three gimbal angles at three pressure levels to determine Reynolds number effects and reproducibility.

This program was successful in demonstrating that a measured surface pressure distribution could be integrated to determine the lateral and axial loads, moments and thrust vector alignment for the scaled model of a large space booster nozzle. Numerical results were provided which are scaleable to the full scale rocket motor and can be used as benchmark data for 3-D CFD analyses.

Introduction

Background

The Advanced Solid Rocket Motor (ASRM) program provided the first opportunity to employ the Solid Rocket Motor Air Flow Facility[1] (SAF) at NASA Marshall Space Flight Center to characterize the flow in the critical aft end and nozzle of a solid rocket motor as part of the design phase of development. The SAF shown in Figure 1 is a high pressure, blow-down facility which supplies a controlled flow rate of air to a subscale model of the internal port and nozzle of a solid propellant rocket motor (SRM) to enable measurement and evaluation of the internal flow field. The ASRM Aft Section/Nozzle Model was conceived and developed as a means of

providing the ASRM program with some early flow field data in severe flow environment areas of the motor around the case/nozzle joint underneath the submerged nozzle nose and in the nozzle itself. The ASRM program has since been canceled but the effort was continued in order to develop and demonstrate the value of solid rocket motor (SRM) cold flow model testing to provide experimentally-based definition of aft motor and nozzle entrance flow fields, particularly, three-dimensional, separated flow associated with gimballed nozzle design. This paper will deal primarily with a particular test series designed to measure the surface pressure distribution over the model aft port and nozzle interior surfaces with the nozzle at varying gimbal angles to determine the efficiency and degree of flow turning in the nozzle and the associated nozzle loads and thrust vector alignment. A mathematical analysis was developed to integrate the three-dimensional forces and moments resulting from the surface pressure distribution associated with various nozzle gimbal angles.

Objectives

Past experience on numerous SRM development programs[2,3] has proven that failure to understand and control the flow field environment in motor port and nozzle entrance regions can result in decreased performance and even motor failure. The complex, three-dimensional, recirculating flow field in the aft chamber of a motor with a submerged nose, gimballed nozzle is difficult to accurately predict with CFD analyses. A number of previous experimental programs[4-10] have shown that cold flow studies with subscale models are effective in studying the mean flow field characteristics of full scale rocket motors. More specific test objectives are listed as follows:

1) Characterize the flow field in the aft chamber region.

   a) Measure the circumferential flow velocities around the submerged nozzle nose at gimbal angles of 4 and 8 degrees.

   b) Measure the convective heating environment on the nozzle and aft dome surfaces and at the nozzle/case joint.

2) Characterize the flow field through the entire nozzle.

   a) Measure the nozzle flow performance parameters.

   b) Determine the aerodynamic thrust vector alignment for nozzle gimbal angles of 0, 4, and 8 degrees.

   c) Determine the aerodynamic moment component of nozzle gimbal torque.

3) Evaluate the ASRM baseline nozzle nose design.

4) Provide data for the validation of CFD computer models of the flow in the aft end and nozzle of the ASRM.

Several series of tests are planned to accomplish the above stated objectives. This paper will cover the testing accomplished to achieve the objectives as stated in items 2) and 3) and to acquire the experimental data to accomplish the CFD analysis objectives as stated in item 4).

Experimental Approach

The stated objectives were met through an experimental program which included the design and modification of an existing checkout model to operate an 8 percent scale model of the aft port and nozzle geometry of the ASRM at a burn time of 19 seconds. The model was instrumented with numerous wall static pressure taps and tested in the SAF with ambient air as the medium while operating at full scale motor Reynolds number. The model wall pressure data was obtained over a range of nozzle gimbal angles and model flow rates. A mathematical analysis was developed to integrate the surface pressure distribution to obtain the forces, moments and effective thrust vector alignment. The model and facility are described in further detail below.

Model

The ASRM Aft Section/Nozzle Model, shown in Figure 2, is an 8 percent scale model of the aft portion of the aft segment of the ASRM including the nozzle. The ASRM Aft Section/Nozzle model was conceived as a modification of the SAF Checkout Model which

2

was designed solely for the purpose of evaluating the facility and control system performance over its entire range of operational pressures and flow rates. The checkout model consisted simply of a cylindrical chamber made in three axial "spool" sections and a converging/diverging nozzle. The ASRM Aft Section/Nozzle model uses Checkout Model chamber sections with internal sleeve inserts designed to match the motor propellant geometry and an ASRM scaled submerged nose nozzle. Thus the ASRM Aft Section/Nozzle Model uses solid walls at the propellant bore surface and all of the flow enters through the upstream model port. A simulated burn time of 19 seconds was selected since it matches the time of the roll recovery maneuver of the Space Shuttle. This maneuver requires a relatively large nozzle gimbal angle of approximately 4 degrees at an early burn time which results in the generation of the maximum circumferential pressure and flow gradients. At this burn time, the forward axial velocity from the propellant underneath the nose is small compared to the axial motor port velocity approaching the nozzle and therefore, the effects of not having wall mass injection underneath the submerged nozzle nose region are mitigated. Since this model has solid walls, and therefore no mass addition, a washout screen and a profile screen with a radially varying porosity was used to generate a Culick[11] cosine velocity profile in the aft port to simulate the wall injection driven profile in an actual solid propellant rocket motor.[12]

The Checkout Model nozzle was replaced by an 8 percent scaled ASRM nozzle complete with submerged nose and contoured expansion section. A model scale factor of 8 percent was selected to allow a nozzle gimbal angle of 8 degrees in the existing Checkout Model diffuser and to make the model port diameter requirements compatible with the Checkout Model chamber spool pieces. Fixed nozzle gimbal angles of 0, 4, and 8 degrees may be tested through the use of wedge shaped adapter flanges between the nozzle and the model chamber as shown in Figure 2. Figure 3 shows a close-up of the aft port and nozzle at a gimbal angle of 8 degrees.

The ASRM Aft Section/Nozzle Model makes use of the existing diffuser pipe by adding an adapter section to connect the diffuser pipe to the model aft chamber flange. The current diffuser diameter allows the 8 percent model nozzle to gimbal up to 8 degrees without nozzle contact with the diffuser wall. The diffuser is required to achieve nozzle exit plane pressures down to approximately 4 psia which result from the required test conditions.

Facility

The Marshall Space Flight Center has developed a national cold flow test facility which provides a broad range of capabilities to investigate the flow field in SRM's to meet both current and projected needs utilizing state of the art test techniques and instrumentation. The Solid Rocket Motor Air Flow Facility, depicted in Figure 1, is a high pressure, blow-down system discharging to atmosphere through the solid rocket model. The air storage is comprised of eight storage tanks having a combined capacity of 9100 ft^3. The storage tanks are charged up to a maximum pressure of approximately 1900 psig from a 3500 psig dry air supply system. The inlet air is filtered through a bonded fiberglass filter with cylindrical canisters that has a 0.3μ filter rating. The remotely operated isolation valve is downstream of the filter and is rated for a maximum pressure of 1960 psig. This valve can be shut down at maximum speed in case of emergency. The actual test model inlet pressure is controlled by a quiet trim control valve. The valve uses a hydraulic operator for actuation and will hold the test model stagnation pressure constant at a set-point value as the supply tank pressure decays. Downstream of the quiet valve, a pilot operated safety relief valve is located to discharge 100% of the flow operating at 1320 psia. The nominal air weight flow range for system design is 20 to 320 lbm/sec which will be precisely metered by a sub-critical venturi located at a minimum of 10 L/D's downstream of the control valve. Mass flow through the system is limited by choked metering nozzles upstream of the model and/or by sonic flow through the SRM model nozzle. A diffuser shown downstream of the model in Figure 1 enables the full scale booster nozzle expansion ratios to be modeled without inducing flow separation.

The addition of thermal conditioning for the inlet air flow as well as plenum chamber

3

conditioning of the inlet flow will be added as special model needs develop.

Instrumentation

The model provides the capability to install approximately 350 gages located axially and circumferentially at stations throughout the model and facility. These measurements include total, static, differential, dynamic and velocity pressures as well as total temperatures and heat flux in the aft chamber region of the model.

A profile rake to verify the velocity profile is located just downstream of the flow conditioning screens. The velocity profile rake was used to measure ten total pressures across the model inlet diameter as well as the wall static pressure. A boundary layer rake was also available to measure the near wall velocity profile.

Five-hole prism probes will be used to measure the magnitude and direction of the three-dimensional flow in the submerged nose cavity around the nozzle. The prism probes are located in ports 26, 27, and 28 as shown in Figure 4. A maximum of three probes can be used simultaneously and distributed about the available locations to minimize disruptions of the flow.

Static pressure taps are located in the aft chamber wall, underneath the submerged nozzle and throughout the entire nozzle. In addition, static taps replace the rake and the probes when these instruments are not in use at particular locations, since there are a number of circumferential locations at each measurement station. Figure 4 also shows the static tap planes in the nozzle.

Locations for future heat flux gages are also shown in Figure 4.

Data Acquisition

The data acquisition system includes an electronic scanning system and a millivolt level digital system for thermocouple or other low level voltage inputs. The millivolt level digital system is configured for 80 thermocouple channels, 40 of which are type K thermocouples. The system is also configured for 40 strain gauges or other

low level voltage inputs. All pressure measurements are recorded by an electronic pressure scanning system. This system is a 256 channel unit which has modules that can record ranges of differential and absolute pressures. Each data scan or frame of data will average up to 10 measurements of model pressures. A data scan completes a frame in about 3 seconds. The system has a measurement capability to record up to 20,000 pressures per second. Internal calibration is completed for the system before each test run.

A data reduction program reduces the data to engineering units and calculates the flow rate. A performance program averages the frames of data, statistically analyzes the data and calculates local Mach numbers, velocities and flow rate. This program was developed using a Microsoft spreadsheet program, EXCEL 4.0 operating in the "Windows" environment.

Data Analysis

A companion FORTRAN program was also developed to calculate the nozzle forces and moments from the measured surface pressures in the aft chamber and nozzle of the model. A single averaged value of surface pressure for each static pressure tap was passed to the Nozzle Performance Program (NPP) from the EXCEL Model Analysis Program (MAP) along with the model chamber pressure and flow rate. The surface pressures over the gimballed portion of the nozzle were then integrated to calculate the two components of force and the moment about the effective nozzle pivot point. These calculations determined the lateral and blowoff loads transmitted to the flex seal bearing as well as the hinge moment due to internal aerodynamic forces. The static pressures in both the nozzle and aft motor chamber along with the measured model total pressure were used to calculate the thrust vector magnitude and direction relative to the nozzle axis. These calculations also enabled the determination of the nozzle discharge and thrust coefficients.

Nozzle Performance Test Plan

As previously mentioned, this paper will deal only with the test series designed to evaluate nozzle performance. These tests

4

primarily measure the alignment of the flow field in the nozzle relative to the nozzle centerline at various gimbal angles and are a measure of the performance of the nozzle design in turning and discharging the flow in an efficient manner. The pressure distributions over the nozzle and aft case surfaces were integrated to determine the orientation of the actual aerodynamic thrust vector with respect to the motor centerline. The difference between the aerodynamic thrust vector and the nozzle centerline was then determined and compared to the ASRM design specification limit value of 1 degree. Other calculated parameters included the internal aerodynamic moment about the nozzle pivot point and the nozzle lateral and axial force loads which are transmitted to the nozzle flex bearing, and the nozzle mass discharge and thrust coefficients. The active instrumentation for these nozzle performance tests included all static pressure taps in the model with no requirements for velocity probes.

The facility and also this model were designed to enable testing at the full scale motor Reynolds number. The nominal model operating pressure was determined by matching the ASRM aft port Reynolds number of 31.E06 at a burn time of 19 seconds. The sensitivity of the test results to Reynolds number was checked by also conducting tests at 87 and 50 percent of nominal operating pressure. The model flow rates directly follow from the model throat diameter and the model chamber pressure. The general test matrix is listed in Table I below.

Table I
General Test Matrix

Gimbal Angle (degrees)	Model Pressure (psia)	Model Flow Rate (lbm/sec)
0,4,8	609	210
0,4,8	528	182
0,4,8	304	105

Analysis Equations

The momentum equation in general integral form is typically used as shown in Equation 1 to calculate the thrust of a rocket motor.

$$F_T = -\int_{A_e} \rho \underline{V} \cdot \underline{V} \cdot \underline{n} \cdot dA - \int_{A_e} (P - P_\infty) \cdot \underline{n} \cdot dA \quad (1)$$

The diagram of Figure 5 shows that the net thrust may also be calculated by considering the internal and external pressure distributions around the rocket motor and nozzle walls. The resulting equation is:

$$F_T = \int_{SRM} P \cdot \underline{n} \cdot dA + \int_{A_e} P \cdot \underline{n} \cdot dA$$
$$= \int_{SRM} (P - P_\infty) \underline{n} \cdot dA \quad (2)$$

where $\underline{n}$ is the unit vector normal to the control surface given by:

$$\underline{n} = -\sin\varphi' \underline{e}_z + \cos\theta \cdot \cos\varphi' \underline{e}_x + \sin\theta \cdot \cos\varphi' \underline{e}_y \quad (3)$$

For a rocket motor with a nozzle gimballed in the y-z plane, as shown in Figure 3, Equation 2 gives:

$$F_y = \int_{Z=0}^{Z=L} \int_{\theta=0}^{\theta=2\pi} P(\theta,z) \cdot \sin\theta \cdot \cos\varphi' \cdot dA + P_\infty A_e \sin\alpha \quad (4)$$

and,

$$F_z = -\int_{Z=0}^{Z=L} \int_{\theta=0}^{\theta=2\pi} P(\theta,z) \cdot \sin\varphi' \cdot dA + P_\infty A_e \cos\alpha \quad (5)$$

Therefore the effective aerodynamic nozzle vector angle may be determined by:

$$\alpha_{eff} = \tan^{-1} \frac{F_y}{F_z} \quad (6)$$

Model Forces

The basic approach of this paper will be to use forms of Equation 2 to determine the resultant thrust components of a cold flow model with a nozzle at various fixed gimbal angles. The specific parameters of interest include the lateral and axial forces on the nozzle, the moment about the pivot point and the effective thrust vector alignment as compared with the geometric nozzle gimbal angle.

A schematic of the cold flow model with nomenclature is shown in Figure 3. The model does not have a closed end like the rocket motor therefore Equation 2 must be modified to include a term for the momentum flux and pressure force at the inlet plane, A_i. The resulting equation for the total thrust is:

$$F_T = \int_{A_i} (\rho \underline{V} \cdot \underline{V} + P) \underline{n} \cdot dA$$
$$+ \int_{Model} P \, \underline{n} \cdot dA + \int_{A_e} P_\infty \, \underline{n} \cdot dA \qquad (7)$$

The first term on the right hand side of Equation 7 accounts for the momentum flux and pressure of the model inlet plane flow. This term is calculated for the model from measured flow rate and static pressure at this particular plane. The velocity profile is axisymmetric at this plane and thus a two-dimensional profile may be used to calculate the momentum flux.

The second term on the right hand side of Equation 7 is the integral of the measured pressure distribution over the entire model aft chamber and nozzle surfaces. This term is calculated by Equation 8:

$$P \cdot \underline{n} \cdot dA = dF_{x'} \cdot \underline{e}_{x'} + dF_{y'} \cdot \underline{e}_{y'} + dF_{z'} \cdot \underline{e}_{z'}$$

where:

$$dF_{x'} = P \cdot \cos\theta' \cdot \cos\varphi' \cdot dA$$
$$dF_{y'} = P \cdot \sin\theta' \cdot \cos\varphi' \cdot dA \qquad (8)$$
$$dF_{z'} = P \cdot (-\sin\varphi') \cdot dA$$

and,

$$dA = \left(r_s + \frac{1}{2} \cdot \Delta r_s\right) \cdot \frac{1}{\cos\varphi'} \cdot d\theta' \cdot dZ'$$

Note that the prime coordinates denote the coordinates referenced to the gimballed nozzle centerline. The forces referenced to the normal coordinate system based on the model chamber centerline are calculated as below:

$$F_y = F_{y'} \cdot \cos\alpha + F_{z'} \cdot \sin\alpha \qquad (9)$$
$$F_z = -F_{y'} \cdot \sin\alpha + F_{z'} \cdot \cos\alpha \qquad (10)$$

Equations 8, 9, and 10 are used for all axisymetric geometry sections. The geometry section underneath the nozzle nose that includes the edges of the stacked shims in the nozzle

bearing distorts during nozzle gimballing and thus is not axisymetric. This distorted bearing surface is expressed in the three-dimensional Cartesian coordinates rather than cylindrical coordinates. The axial and circumferential grid for this surface is structured and the projected area in each of three directions is subjected to a pressure determined from an average of the pressure at each of the four corners of each elemental surface. The pressure forces in all three directions for all elemental surfaces of the bearing are integrated to get the force components for the entire bearing surface.

Model Moments

In addition to the nozzle forces and thrust vector alignment, calculation of the aerodynamic moment about the nozzle pivot point is also of interest to nozzle designers. The moment about the point or x-axis in the y-z plane (see Figure 8) is calculated for each element as follows:

$$M_{x'} = \int r_s \cdot \sin\theta' \cdot P \cdot (-\sin\varphi') \cdot dA$$
$$- \int z' \cdot P \cdot (\sin\theta' \cdot \cos\varphi') \cdot dA \qquad (11)$$

and,

$$M_x = M_{x'} \qquad (12)$$

The angle θ is defined as being 0 degrees on the x-axis and goes from 90 degrees on the nozzle upper wall to -90 degrees on the nozzle lower wall in the x-y gimbal plane.

Experimental Results

The initial model checkout testing included an evaluation of the velocity profile screen located upstream in the model port as shown in Figure 2. The velocity profile "screen" is actually a plate with a radially varying hole density pattern designed to provide a Culick cosine velocity profile for the flow as it approaches the aft model and nozzle entrance region. This profile, as described in Equation 13 below, more nearly represents the velocity profile in the full scale motor where the flow field is entirely wall mass injection driven. Of course, the actual velocity profile in the aft end of the full scale motor is altered somewhat due to partial

6

turbulent transition[13] as well as the small divergent wall angle.

$$\frac{U_x}{U_{CL}} = \cos\left(\frac{\pi}{2}\frac{r^2}{R^2}\right) \qquad (13)$$

The velocity profile was measured at the rake station shown in Figure 2 for all three gimbal angles of 0, 4, and 8 degrees. The results for gimbal angles of 0 and 8 degrees are shown in Figures 6 and 7 with comparisons to the theoretical Culick cosine profile. These profiles are reasonably close to the reference Culick profile and are symmetric in both the horizontal and vertical planes. A comparison of Figure 6 with Figure 7 also confirms that the rake station is far enough upstream such that the flow is unaffected by the nozzle gimbal angle. The rake station is the forward most station at which pressures are measured and used in the calculation of model forces and moments. The assumption of axisymmetric flow must be made at this station and it appears from Figure 7 that this assumption is justified.

The basic test program consisted of running the 9 combinations of three pressures, 609, 528, and 304 psia, and three gimbal angles, 0, 4, and 8 degrees. The base test condition was 609 psia for a model chamber pressure with the lower pressures used to determine Reynold's number effect and reproducibility. Table II is a summary of the calculated parameters at all three gimbal angles for the baseline pressure of 609 psia. The calculated effective thrust vector angle is plotted versus geometric nozzle gimbal angle in Figure 8. The design limit allows a 1 degree variance between the "dynamic thrust vector" and the geometric nozzle centerline. Of course, lateral offsets in the bearing also contribute to the thrust vector misalignment in the full scale motor. The experimental results indicate effective angles more than the geometric angles. While this is theoretically possible, it probably indicates an experimental resolution error on the order of 0.1 to 0.2 degrees.

A summary plot of the nozzle moment about the pivot point is shown in Figure 9 versus nozzle gimbal angle for the three test pressures. The moment is calculated for the moveable section of the nozzle and thus has significance for TVC actuator load calculations. The moment

on the entrance nose of the nozzle is a large non-restoring moment and the moment in the exit expansion section is a smaller restoring moment. Thus, the net moment on the gimballed nozzle is non-restoring. The flow is not aligned completely with the nozzle by the time it reaches the throat plane and thus the exit expansion section is subjected to asymmetric pressure distributions and a restoring moment is generated since the center of pressure is aft of the pivot point. On the entrance nose the center of pressure is forward of the pivot point, thus, an unstable non-restoring moment is generated. In Figure 9, as the gimbal angle is increased from 4 to 8 degrees, the gains in the positive vectoring moment approximately balance the increase in the negative non-restoring moment on the entrance nose section. These results can be applied directly to the full scale motor by using the geometric scale factor and pressure ratio between the model and the motor.

The actual pressure distribution for the model at various gimbal angles is shown in Figures 10, 11, and 12. The data is non-dimensionalized by the upstream model total pressure and plotted versus model axial station for Figures 10 and 11. The throat plane is located at 28.19 inches and the nose tip is at 26.222 inches. A plot of the model geometry with station numbers is shown in Figure 13. All lines in these graphs are at the 180 degree circumferential station which is at the bottom of the nozzle. The nozzle is gimballed counterclockwise which lowers the nose and raises the exit cone. Thus, the flow turns against the nose on the lower half of the nozzle and generates higher wall pressures. The pressure at 180 degrees is shown to increase with gimbal angle as expected. The effect of continued flow turning in the nozzle exit expansion section is clear in Figure 11.

The nozzle pressure ratios are plotted versus circumferential position in Figure 12 for several stations on the nozzle nose at gimbal angles of 0, 4, and 8 degrees. The locations of the pressure taps are shown in Figure 4. Figure 12 shows that as the gimbal angle is increased, the pressure on the lower half of the nozzle increases while the pressure on the upper half of the nozzle decreases. At a gimbal angle of 0 degrees the circumferential distribution is relatively flat.

Table II

Experimental Forces and Moments

$$\frac{P = 609 \text{ psia}}{R_e = 33 \times 10^6}$$

Parameter	Gimbal Angle, deg		
	0	4	8
F_y, Nozzle Nose to Throat, lbf	-2.81	766	1,585
F_y, Nozzle Throat to Exit, lbf	0.14	-308	-634
F_y, Model Total, lbf	11.19	-1,115	-2,195
F_z, Nozzle Nose to Throat, lbf	12,678	12,663	12,555
F_z, Nozzle Throat to Exit, lbf	-3,308	-3,292	-3,241
F_z, Model Total Thrust, lbf	-15,567	-15,479	-15,450
M_x, Nozzle Nose to Throat, in-lbf	-50.94	-586	-748
M_x, Nozzle Throat to Exit, in-lbf	-41.11	62.9	211
M_x, Model Total Moment, in-lbf	-92.05	-4,636	-8,730
Effective Thrust Vector Angle, deg	-0.0412	4.12	8.09

Contour plots of the surface pressure distribution on the nozzle nose and forward portion of the exit cone are shown in Figures 14, 15, and 16 for gimbal angles of 0, 4, and 8 degrees, respectively. The pressure contour values are pressure differences referenced to the pressure at the 90 degree position at each axial station. The pressure difference contours from 90 degrees to 180 degrees are positive and from 90 degrees to 0 degrees they are negative due to the effects of the flow turning against the lower half of the nozzle nose. The effects of flow turning are seen to exist downstream past the throat to station 29.0. The presence of non-zero pressure contours at the zero gimbal angle are believed to be due to some asymmetries in the approach flow field.

Conclusions

(1) The 8% scale model of the ASRM was successfully tested over a range of flow conditions to provide definition of the complex three-dimensional surface pressure distributions in the aft chamber and nozzle entrance regions for gimbal angles of 0, 4, and 8 degrees.

(2) The aerodynamic thrust vector alignment and nozzle moments about the bearing pivot point were successfully determined from the measured surface pressure distribution. The lateral and axial nozzle design loads were likewise determined.

(3) The moments about the nozzle pivot point were non-restoring on the nozzle nose and restoring in the expansion section with the net moment being non-restoring.

Acknowledgments

References

1. Bacchus, D. L., O. E. Hill and R. H. Whitesides, "Facility For Cold Flow Testing of Solid Rocket Motor Models," 1992 JANNAF Propulsion Meeting, Indianapolis, Indiana, 24-27 Feb. 1992.

2. Wilson, W. G., et al, "Titan IV SRMU PQM-1 Overview," AIAA 28th Joint Propulsion Meeting, Nashville, TN, AIAA 92-3819, July 6-8, 1992.

3. Johnson, David H. and Daniel D. Lauterbach, "Coupled Flow/Structural Analysis of the Redesigned Titan IV SRMU," AIAA 28th Joint Propulsion Conference, Nashville, TN, AIAA 92-3825, July 6-8, 1992.

4. Dunlap, R., A. M. Blackner, R. C. Waugh, R. S. Brown, and P. G. Willoughby, "Internal Flow Field Studies in a Simulated Cylindrical Port Rocket Chamber," United Technologies Chemical Division, San Jose, California, Journal of Propulsion and Power, Vol. 6, 1990.

5. Waesche, R. H. W., W. H. Sargent, and J. F. Marchman, "Space Shuttle Solid Rocket Motor Aft-End Internal Flows," Journal of Propulsion and Power, Vol. 4, 1989.

6. Whitesides, R. H., A. Gosh, S. L. Jenkins, and D. L. Bacchus, "Cold Flow Determination of the Internal Flow Environment Around the Submerged TVC Nozzle for the Space Shuttle SRM," 1989 JANNAF Propulsion Meeting , Cleveland Convention Center, Cleveland, Ohio, May 23-25, 1989.

7. Whitesides, R. H., A. Majumdar, S. Jenkins, and D. L. Bacchus, "Experimental Determination of Convective Heat Transfer Coefficients in the Separated Flow Region of the Space Shuttle Solid Rocket Motor," 28th Aerospace Sciences Meeting, Reno, Nevada, AIAA 90-0043, January, 1990.

8. Majumdar, A. K., R. H. Whitesides, S. L. Jenkins, and D. L. Bacchus, "Effect of Idealized Asymmetric Inhibitor Stubs on Circumferential Flow in the Space Shuttle SRM," Journal of Propulsion and Power, Vol. 6, No. 1, January - February 1990.

9. Waesche, R. H. W., J. F. Marchman, and S. Kuppa, "Effects of Grain Slots on Flow in a Solid Rocket Motor," Journal of Propulsion and Power, Vol. 7, 1991.

10. Waesche, R. H. W., J. F. Marchman, and S. Kuppa, "Effects of Grain and Aft-Dome Configuration on Aft-End SRB Internal Flows," Journal of Propulsion and Power, Vol. 7, 1991.

11. Culick, F. E. C., "Rotational Axisymmetric Mean Flow and Damping of Acoustic Waves in Solid Propellant Rocket Motors," AIAA Journal, Vol. 4, No. 8, 1966, 1462-1464.

12. Dunlap, R., P. G. Willoughby, and R. W. Hermsen, "Flowfield in the Combustion Chamber of a Solid Propellant Rocket Motor," AIAA Journal, Vol. 12, No. 10, 1974, 1440-1442.

13. Beddini, R. A., "Injection Induced Flows in Porous-Walled Ducts," AIAA Journal, Vol. 24, No. 11, Nov. 1986, 1766-1773.
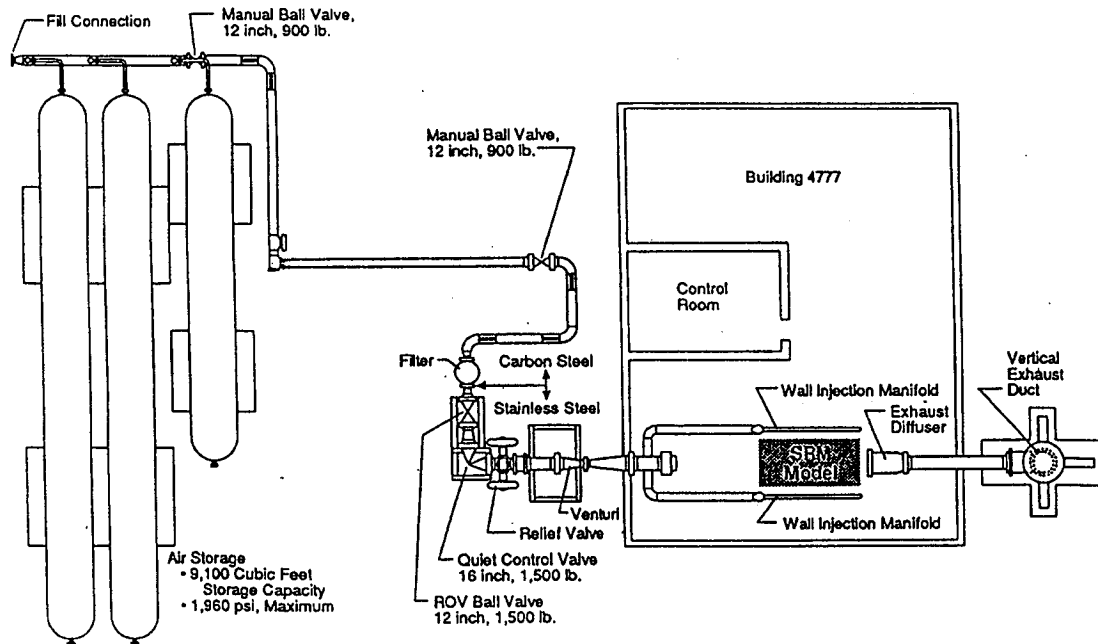
Figure 1. Solid Rocket Motor Air Flow Facility
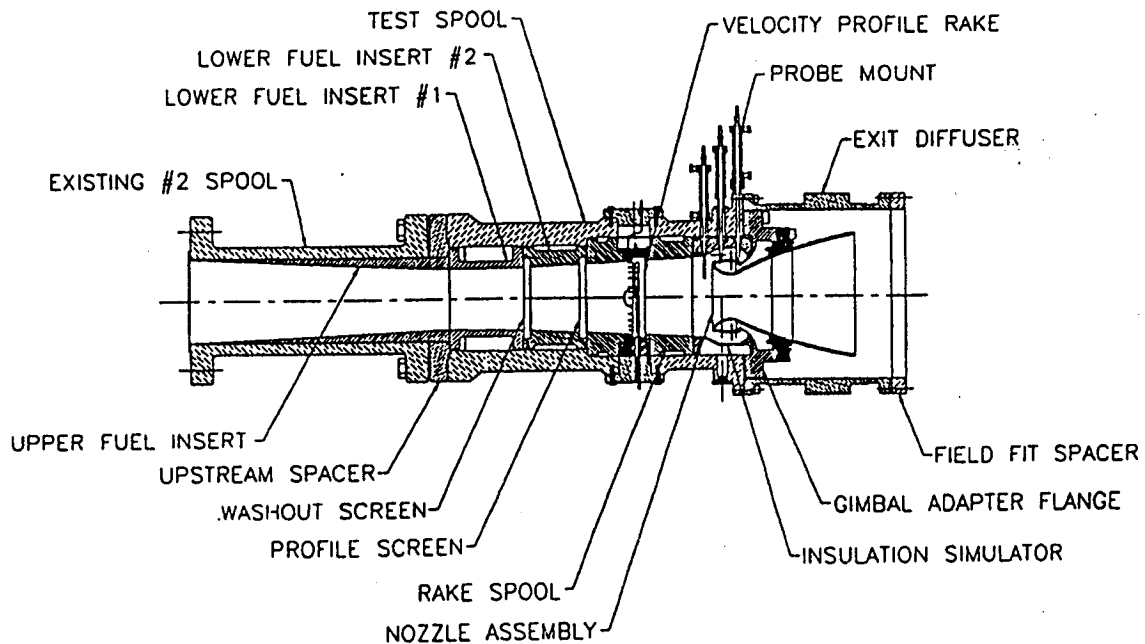
Figure 2. ASRM Aft Section/Nozzle Model at 19 Second Burn Time
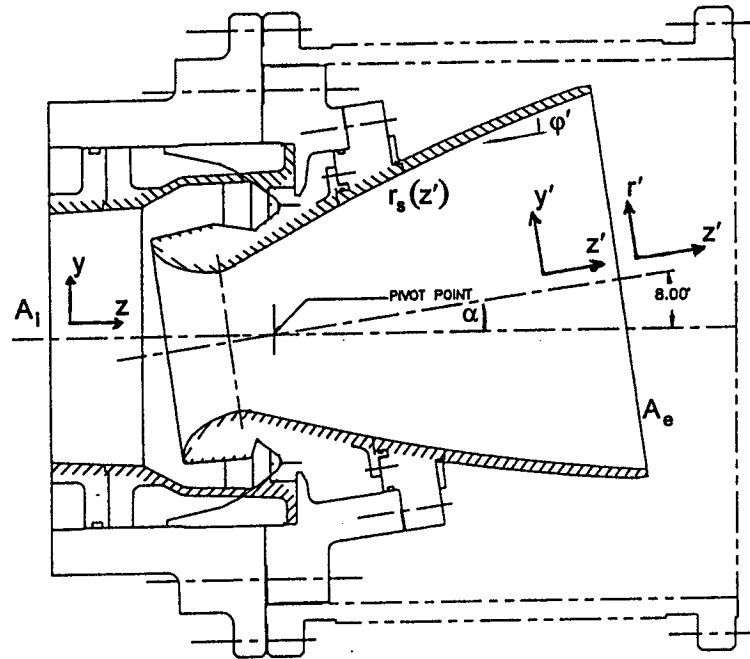
Figure 3. Nozzle Nomenclature Sketch
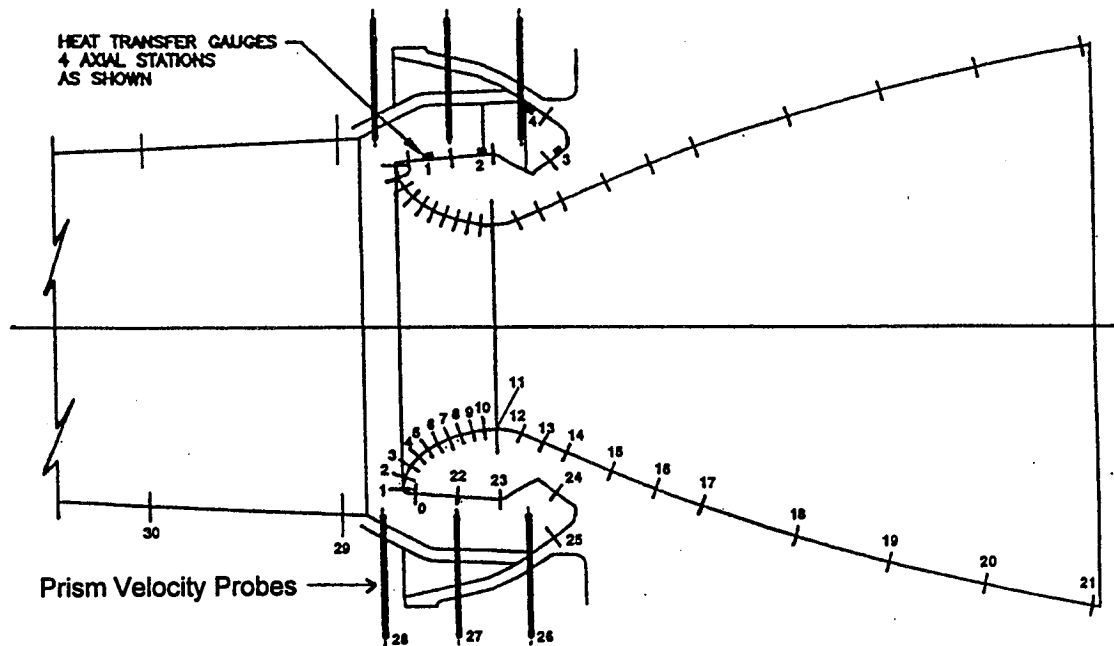
Figure 4. Measurement Plane Number Layout

11

Figure 5. Rocket Motor Momentum and Pressure Thrust

Figure 6. Velocity Profile, 0 Degree Gimbal Angle
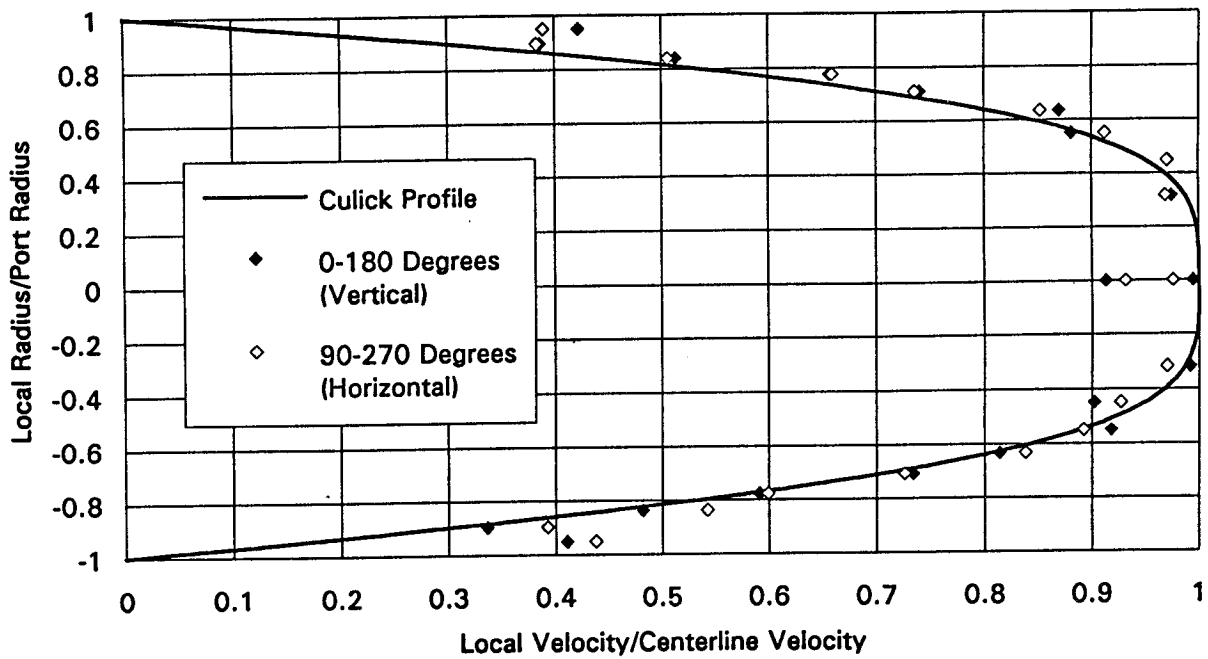
Figure 7. Velocity Profile, 8 Degree Gimbal Angle
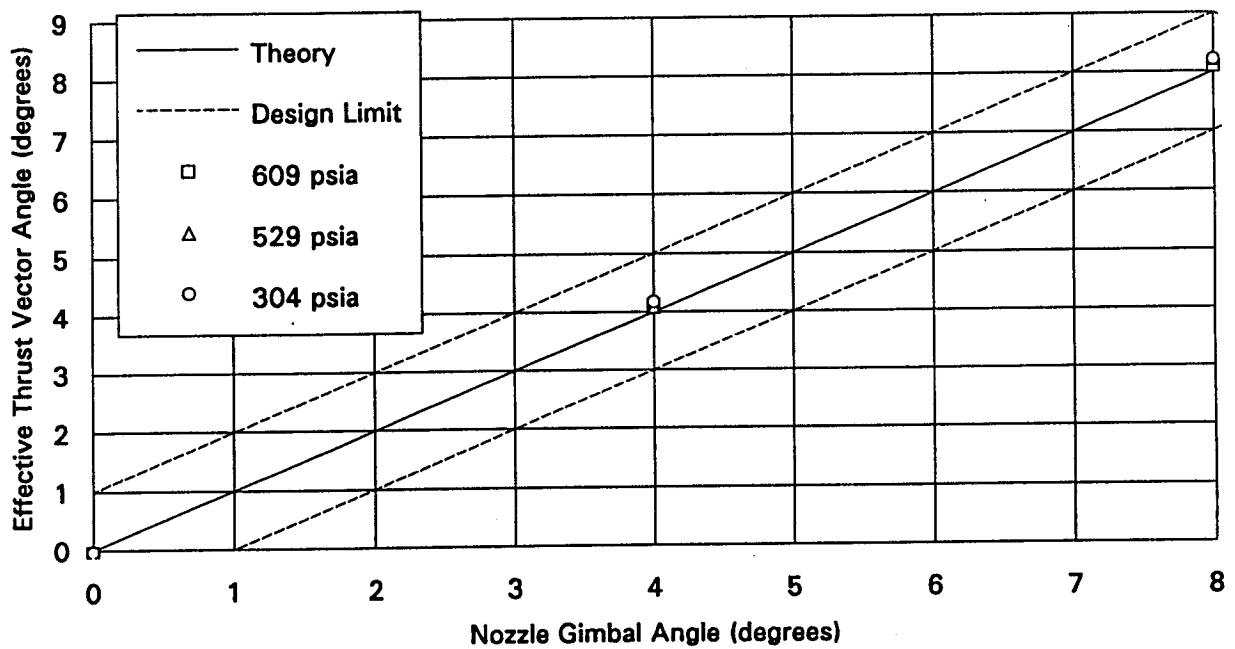
Figure 8. Effective Thrust Vector Angle Correlation
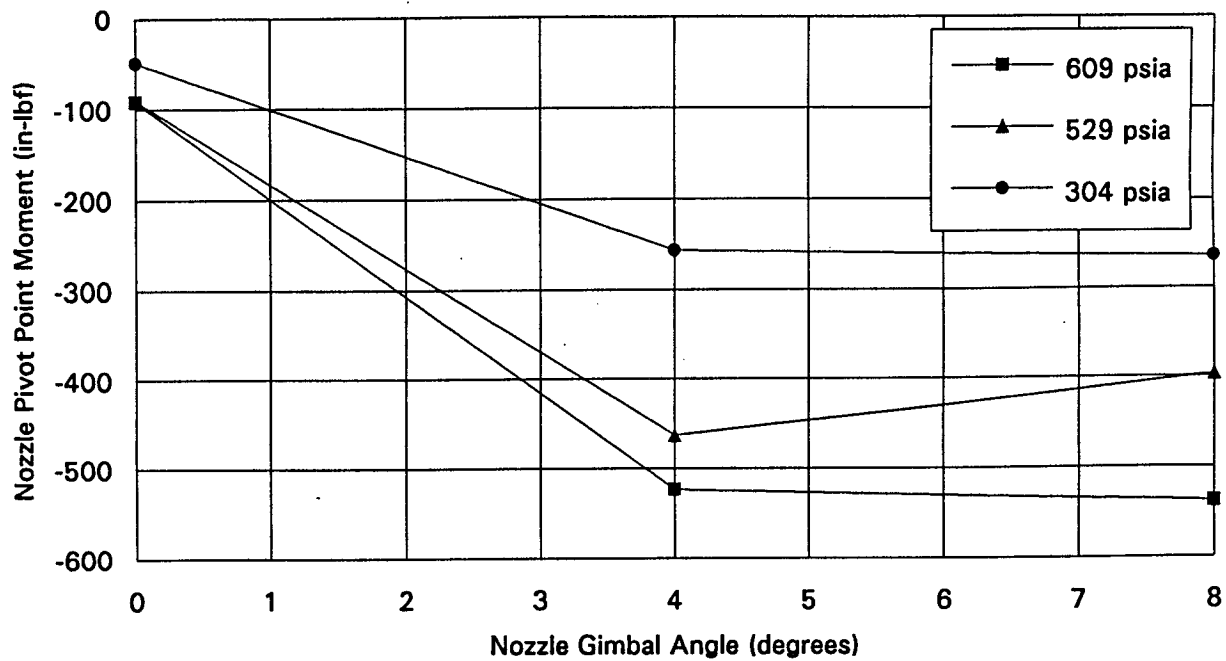
Figure 9. Pivot Point Moment Versus Gimbal Angle
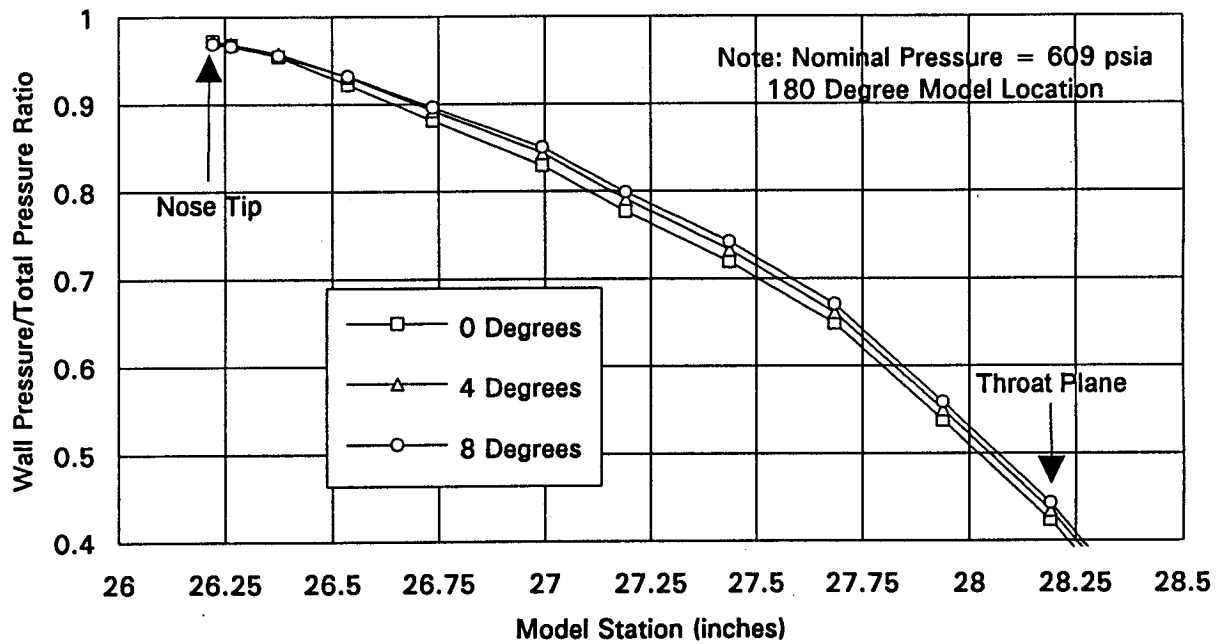
Figure 10. Nozzle Pressure Ratios, Upstream of Throat

14
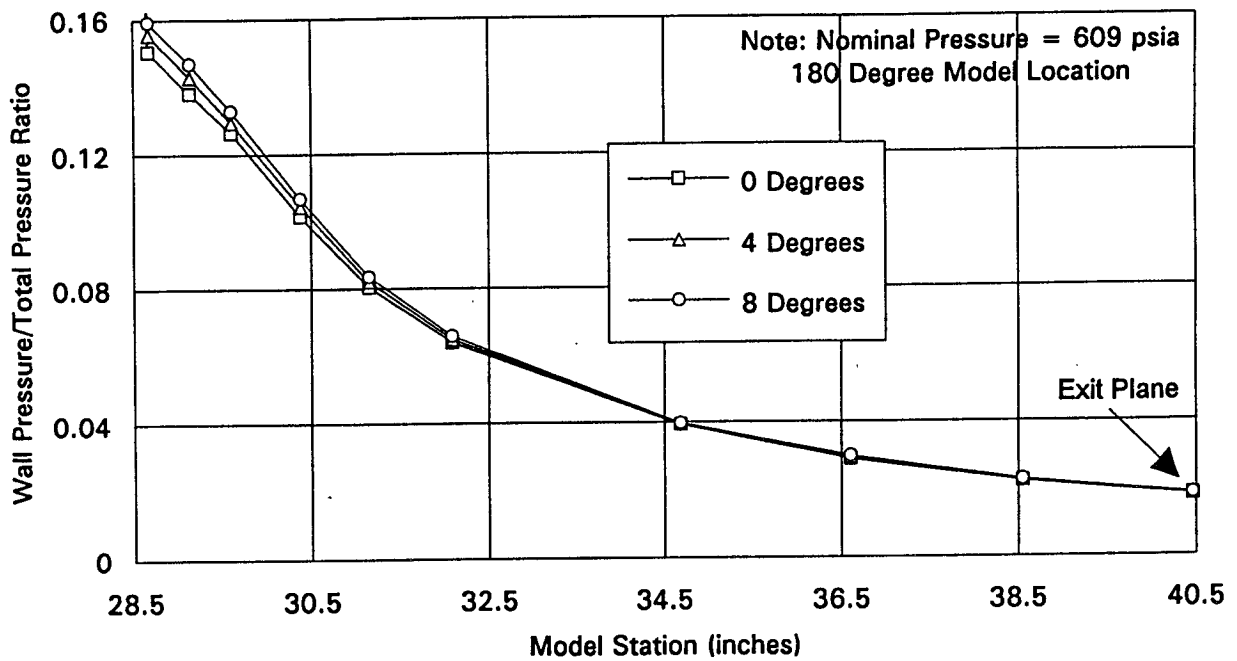
Figure 11. Nozzle Pressure Ratios, Downstream of Throat
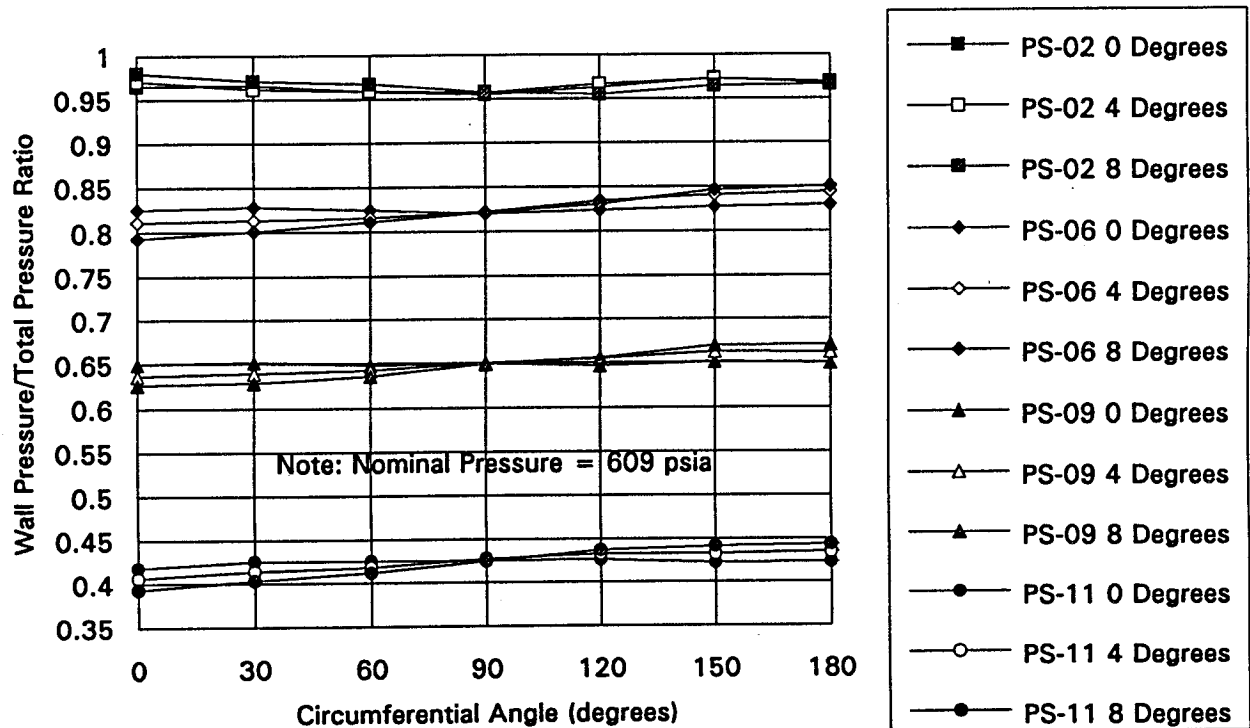
Figure 12. Circumferential Nozzle Pressure Ratios, Upstream of Throat

15
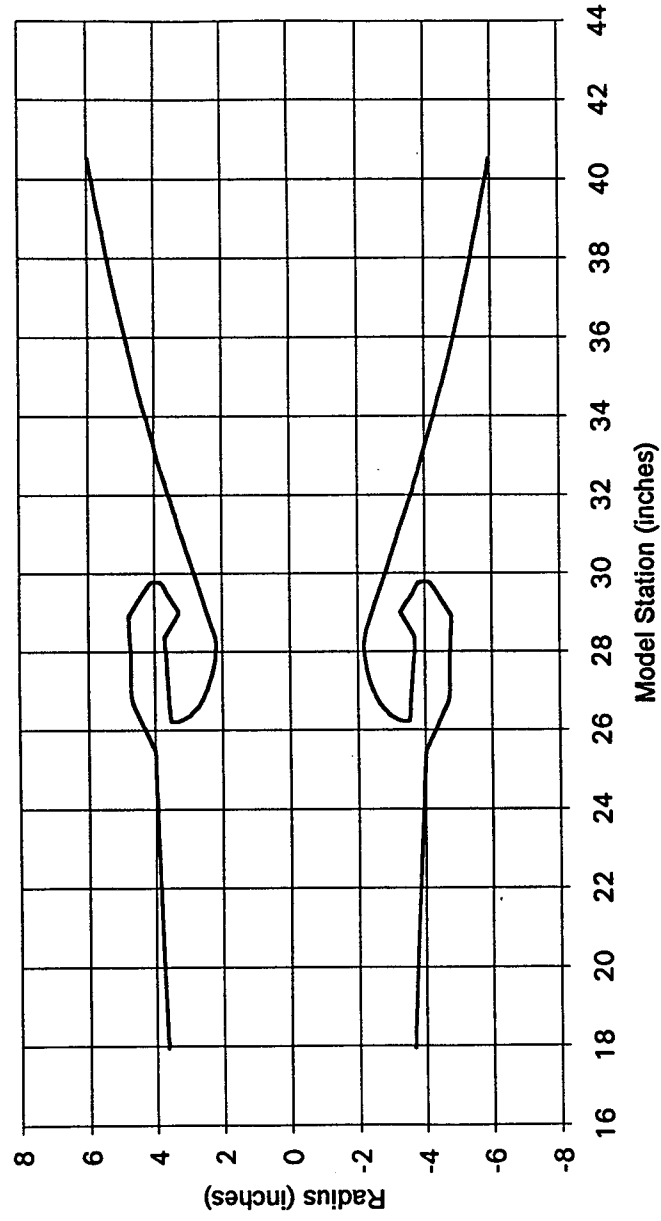
Figure 13. Model Geometry
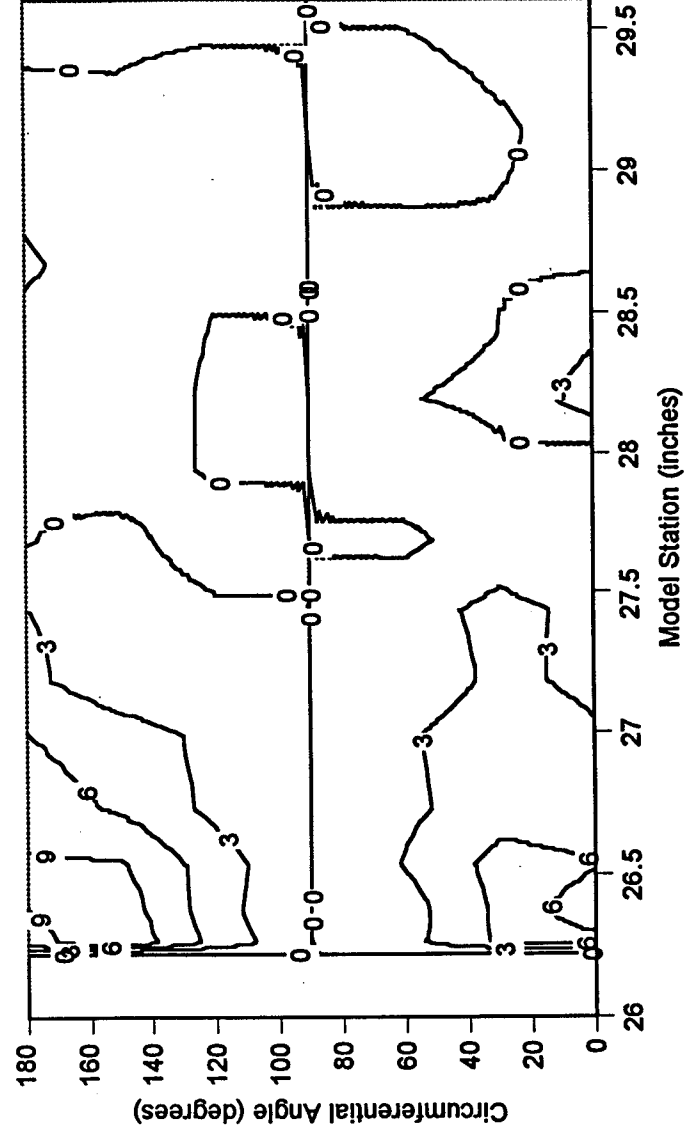
Figure 14. Nozzle Pressure Contours, 0 Degree Gimbal Angle

16
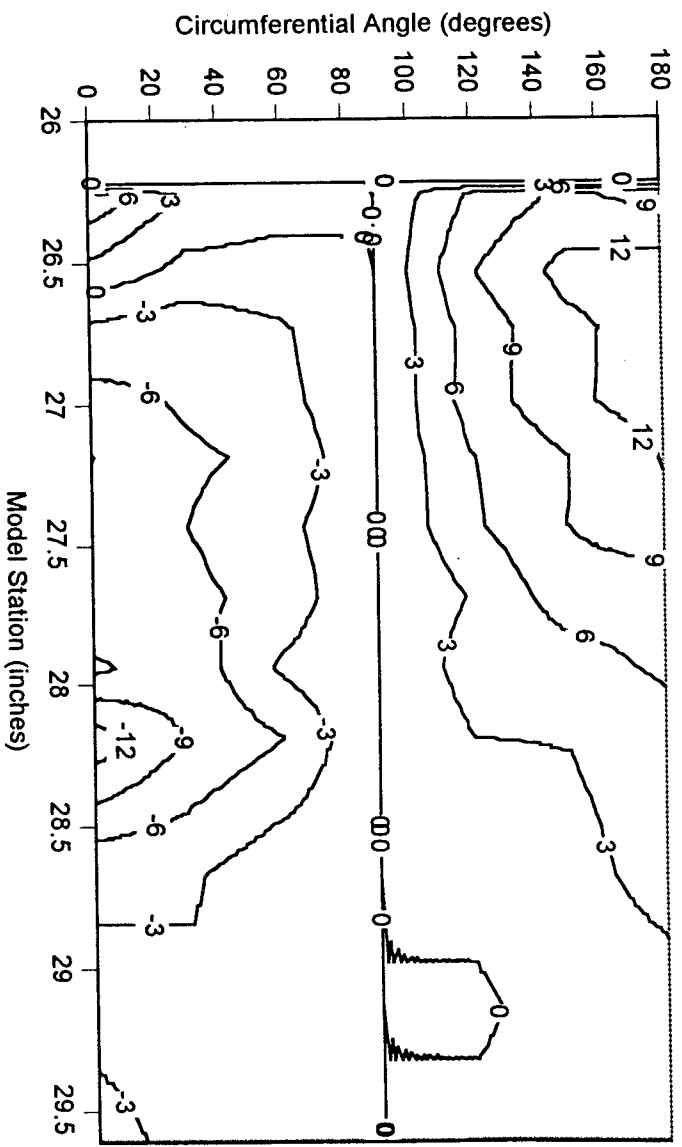
Figure 15. Nozzle Pressure Contours, 4 Degree Gimbal Angle
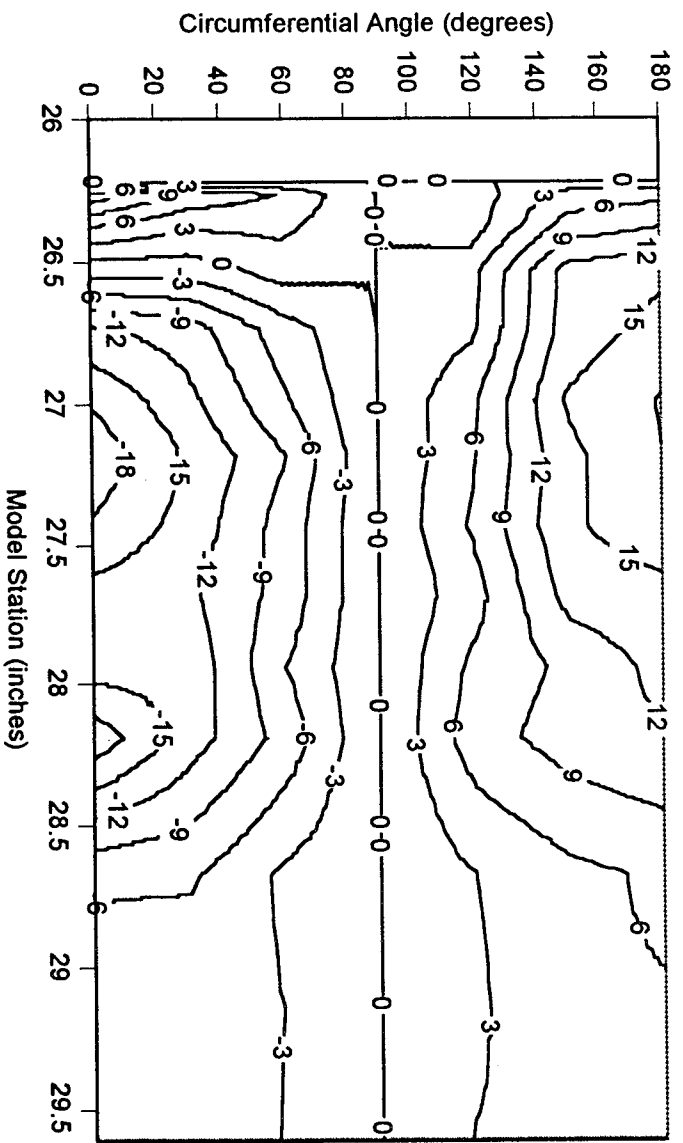
Figure 16. Nozzle Pressure Contours, 8 Degree Gimbal Angle

17

ASRM Aft Section/Nozzle Model Analysis

A computational flow field analysis of the ASRM Aft-Segment/Nozzle Model which will be tested in the SAF was performed during the month of February, 1992. The flow field for this model was computed several months ago using Fluent β-version 4.0. However, since several bugs existed in the Fluent β-version 4.0 code, Fluent/BFC was recently utilized to obtained a flow field solution using a code which has been verified against a specific set of test problems.

The geometry for this model comes from ERCI drawing H2002-1, rev. C. The model is an 8% representation of the full-scale motor aft-section, nozzle and nozzle exit cone. Figure 9 shows the ASRM Aft Section/Nozzle Model 552. The inlet boundary for the computational flow field problem is shown in the figure. The computational solution was computed through the full nozzle exit cone in order to obtain pressure estimates at the static pressure tap locations used in the coldflow test.

A full view of the computational grid is shown in Figure 10. The grid is spaced in the radial directional such that the grid lines are close enough to the wall to provide good shear stress estimates in the near wall region. The axial grid lines are spaced so that the grid lines are closer in regions of higher axial gradients such as near the nozzle nose. Since it is difficult to discern any detail in the nozzle nose region in Figure 10, Figure 11 provides a close-up view of the grid in this region. The full grid incorporates 230 axial grid lines. There are 30 radial grid lines upstream of the nozzle nose grid change position shown in Figure 11. There are 20 radial grid lines downstream of this grid change position. The region behind the submerged nose is resolved by 16 axial grid lines and 40 radial grid lines. The grid lines are clustered closer together near the boundary between the port flow and the submerged region as shown in Figure 11. This is done to better resolve the dividing streamline between the port flow and the submerged region which will be shown with the solution data.

The boundary conditions for this analysis are summarized in Table 5. The inlet for this problem was set as a stagnation pressure boundary. A value of 600 psia was assigned as the stagnation pressure at this inlet. This value was chosen as a reasonable estimate of the stagnation pressure at this location in the SRMAFTE facility test of the ASRM Aft Section/Nozzle Model test. The value of the inlet turbulence kinetic energy will be further parameterized as time allows.

Figure 12 shows a raster plot of the Mach number throughout the ASRM Aft Section/Nozzle Model. The maximum Mach number reached at the end of the nozzle exit cone was 3.64. A radial velocity gradient is evident at the model throat with the flow first approaching supersonic conditions near the wall. This gradient reverses itself as flow continues through the nozzles so that the centerline velocity is higher.

Figure 13 shows a raster plot of the static pressure in the model. There is no radial pressure gradient until the flow approaches the nozzle nose. The figure shows a

definite affect on the flow field just upstream of the nose. A radial pressure gradient is observed upstream of the nose and continuing through the nozzle throat region of the nozzle. The strong radial pressure gradient observed in the nozzle throat region precludes the use of one-dimensional predictions of the wall pressures or mass flow rates in this region. This has been observed in the checkout model facility test and good comparisons between the CFD predicted pressure ratio at the throat wall and the experimental measurements have been observed. Figure 14 illustrates this radial pressure gradient by showing contours of constant pressure in the throat region. This figure also illustrates the two-dimensional character of the flow in the nozzle.

The experimental static pressure tap locations as called out in ERCI drawing H2003-1, rev. A are shown in Table 6. These locations are illustrated in Figure 15. The actual static pressure tap locations as measured from the ASRM Aft Section/Nozzle Model itself are not available at this time. However, the tap locations given in Table 6 should be close enough to provide a good estimate of the pressure profile along the nozzle nose and through the nozzle exit cone. The numerically calculated static pressures are reported at these locations in order to provide a computational estimate for comparison with the measured data. These estimates should be updated when the actual measured tap locations become available since strong axial pressure gradients could impact the computational estimates if the tap locations are significantly different from the design drawing. The calculated static pressures at the various gauge positions have been obtained by linearly interpolating between computational nodes. A higher order interpolation will be used if the observed test measurements do not adequately match the numerical predictions.

The raster plot of stagnation pressure shown in Figure 16 illustrates a previously observed phenomena about the total pressure behind the submerged nozzle. The total pressure is controlled by the inherent total pressure in the flow near the wall just upstream of the submerged region. This is well illustrated by Figure 16 which shows that the total pressure behind the submerged nose is less than that at the centerline in this region. Instead the total pressure is being controlled the slightly less energetic stream of flow passing down the port near the wall.

Figure 17 shows the velocity field in the immediate region of the nozzle nose. The maximum velocity shown in the figure is 45 m/s. The stagnation point and dividing streamline between the port flow and the recirculation in the region behind the nozzle nose is clearly shown. Recirculating flow from the cavity behind the submerged nose causes a good bit of curvature to the dividing streamline.

Figure 9. ASRM Aft Section/Nozzle Model 552
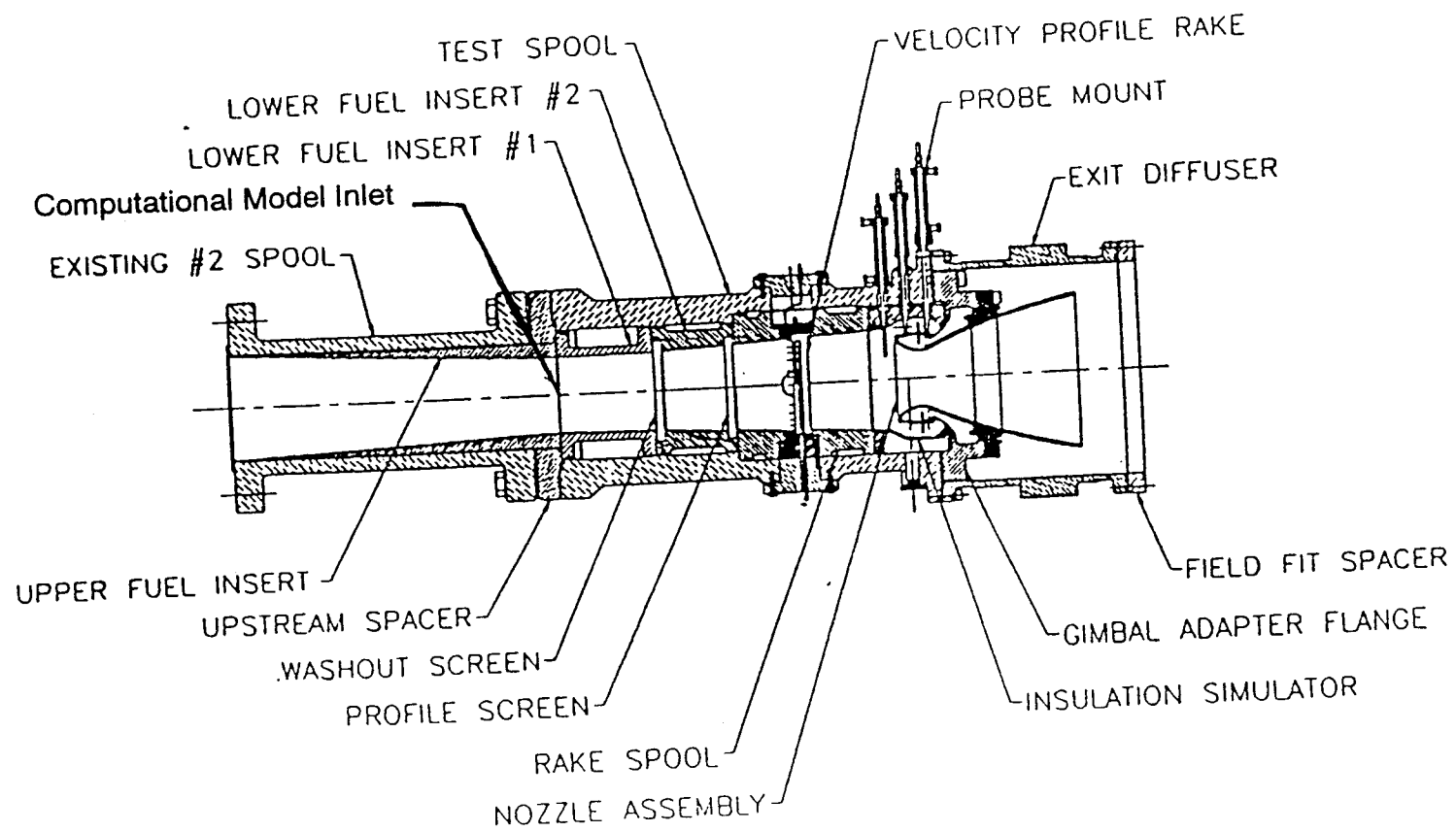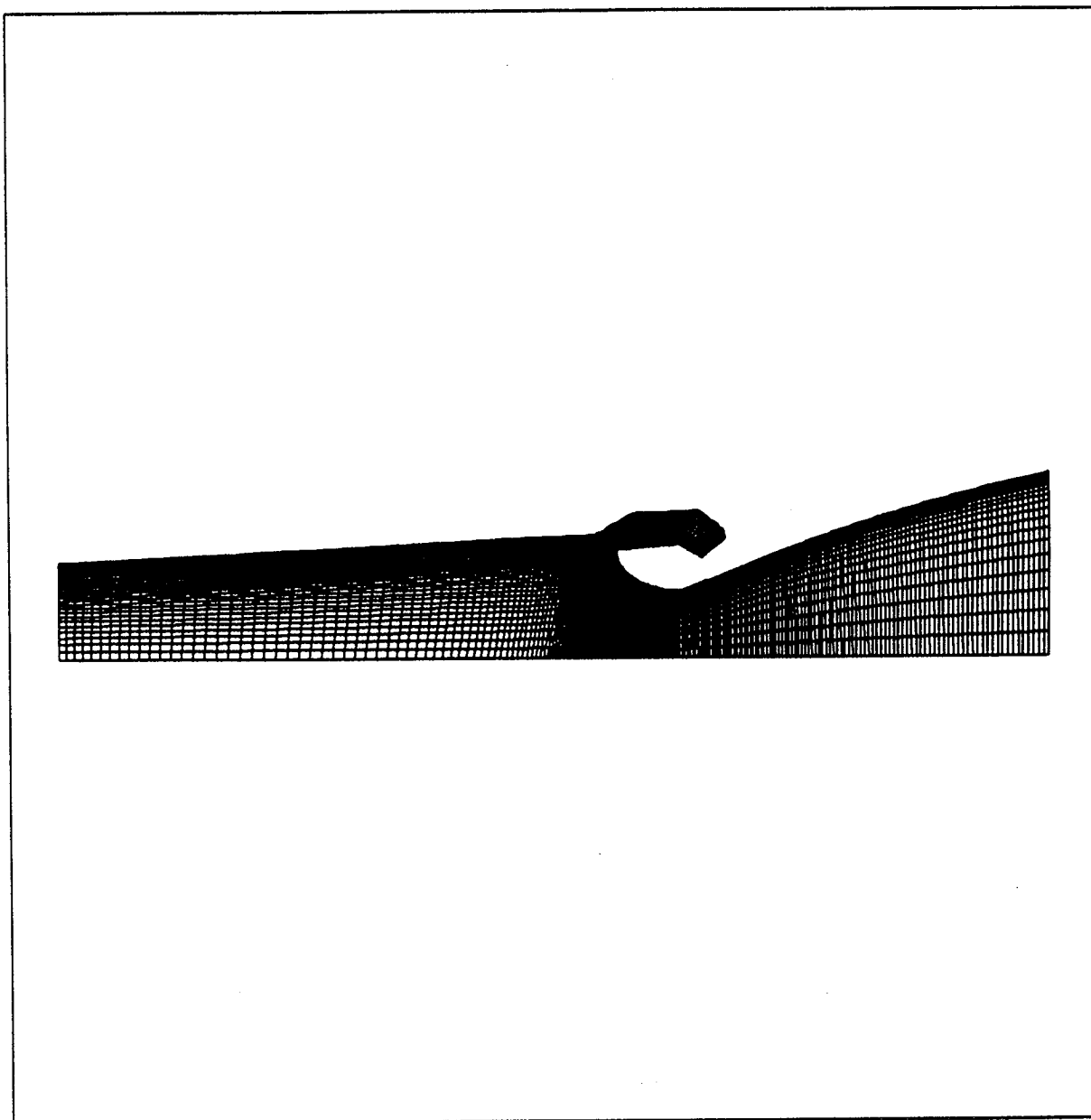
Figure 10. Full View of the ASRM Aft Section/Nozzle
Model Computational Grid
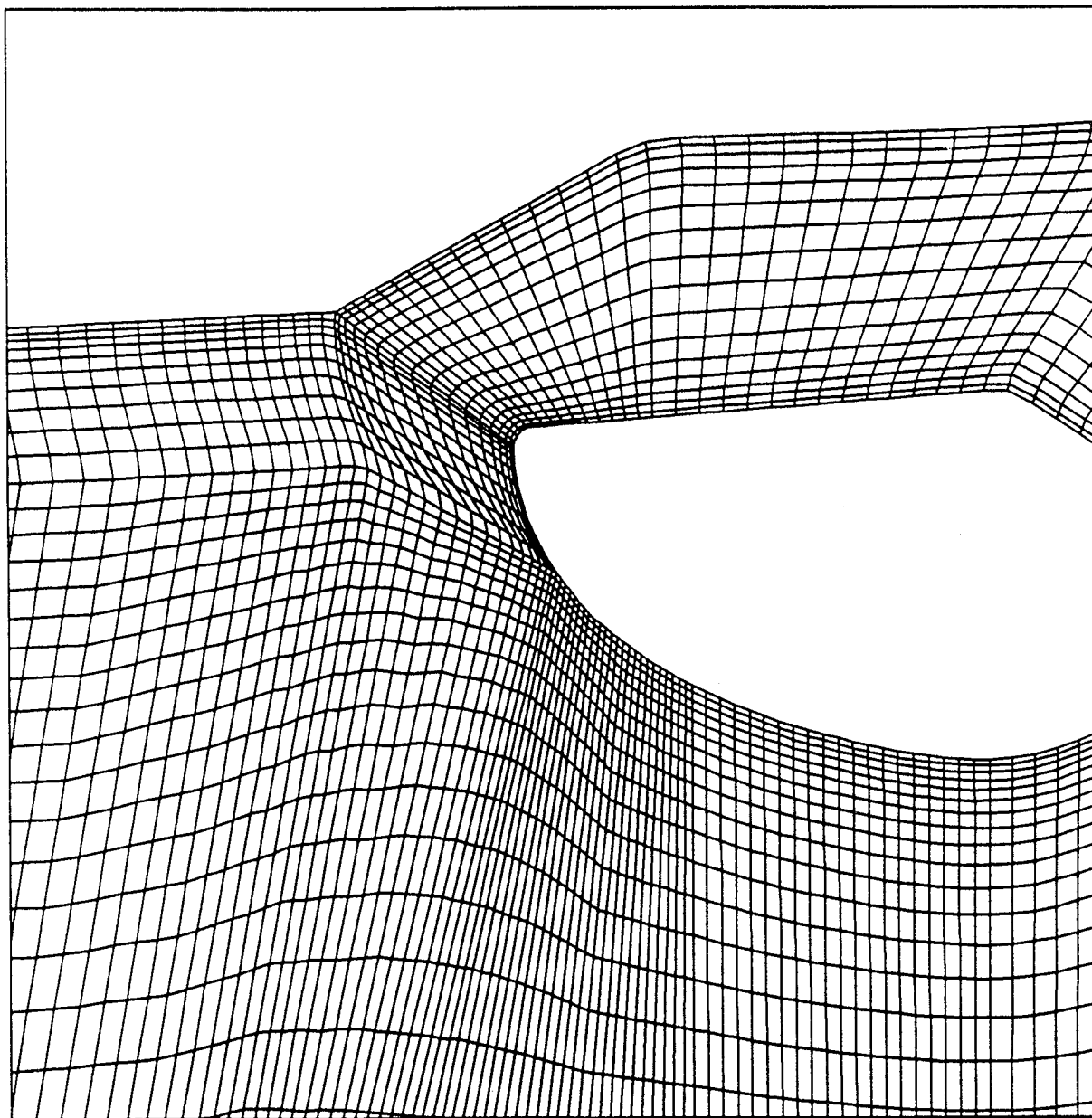
Figure 11. Close-up View of the ASRM Aft Section/Nozzle Model Computational Grid in the Nose Region
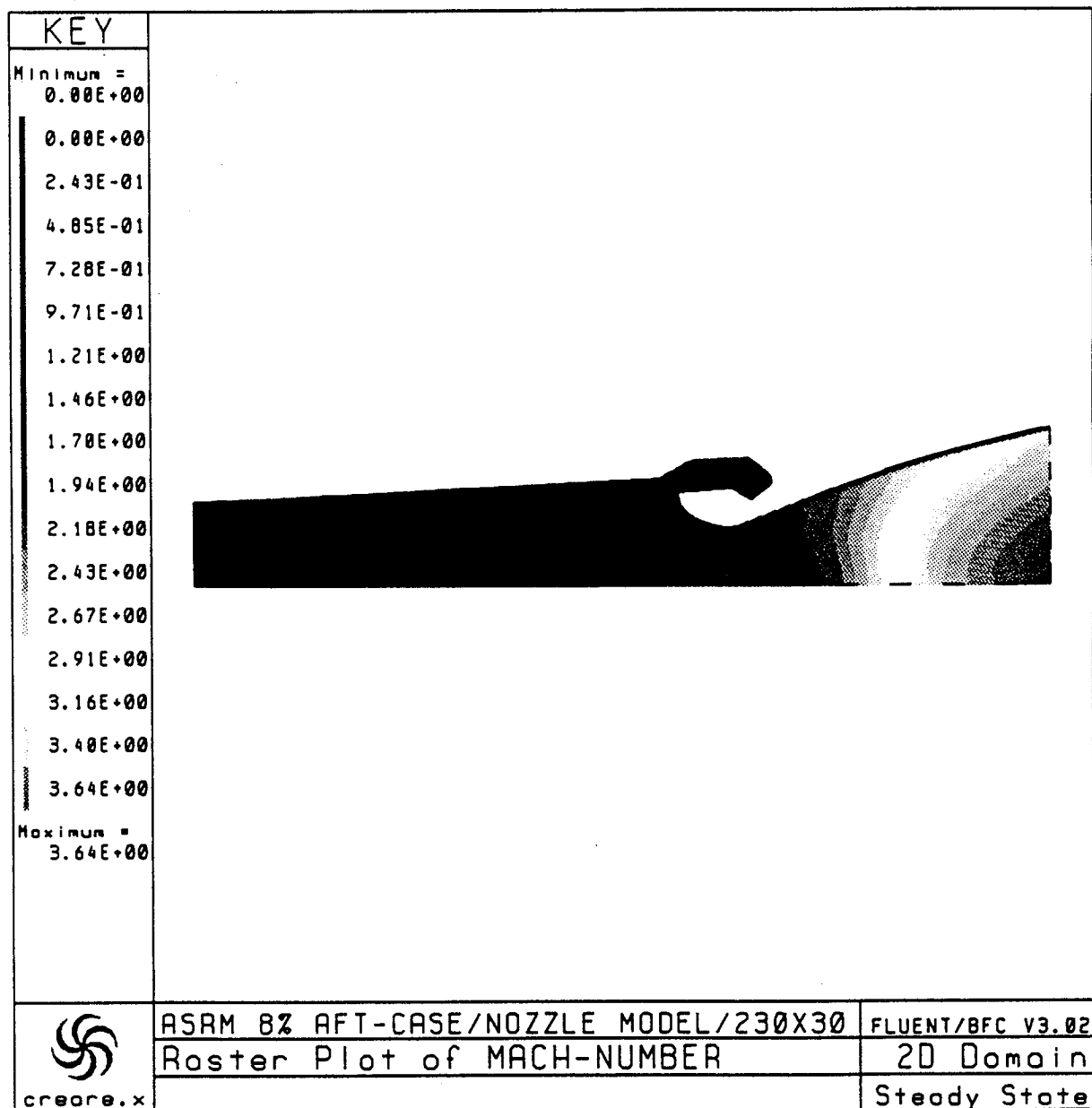
Figure 12. Mach Number Raster Plot for the ASRM Aft
Section/Nozzle Model
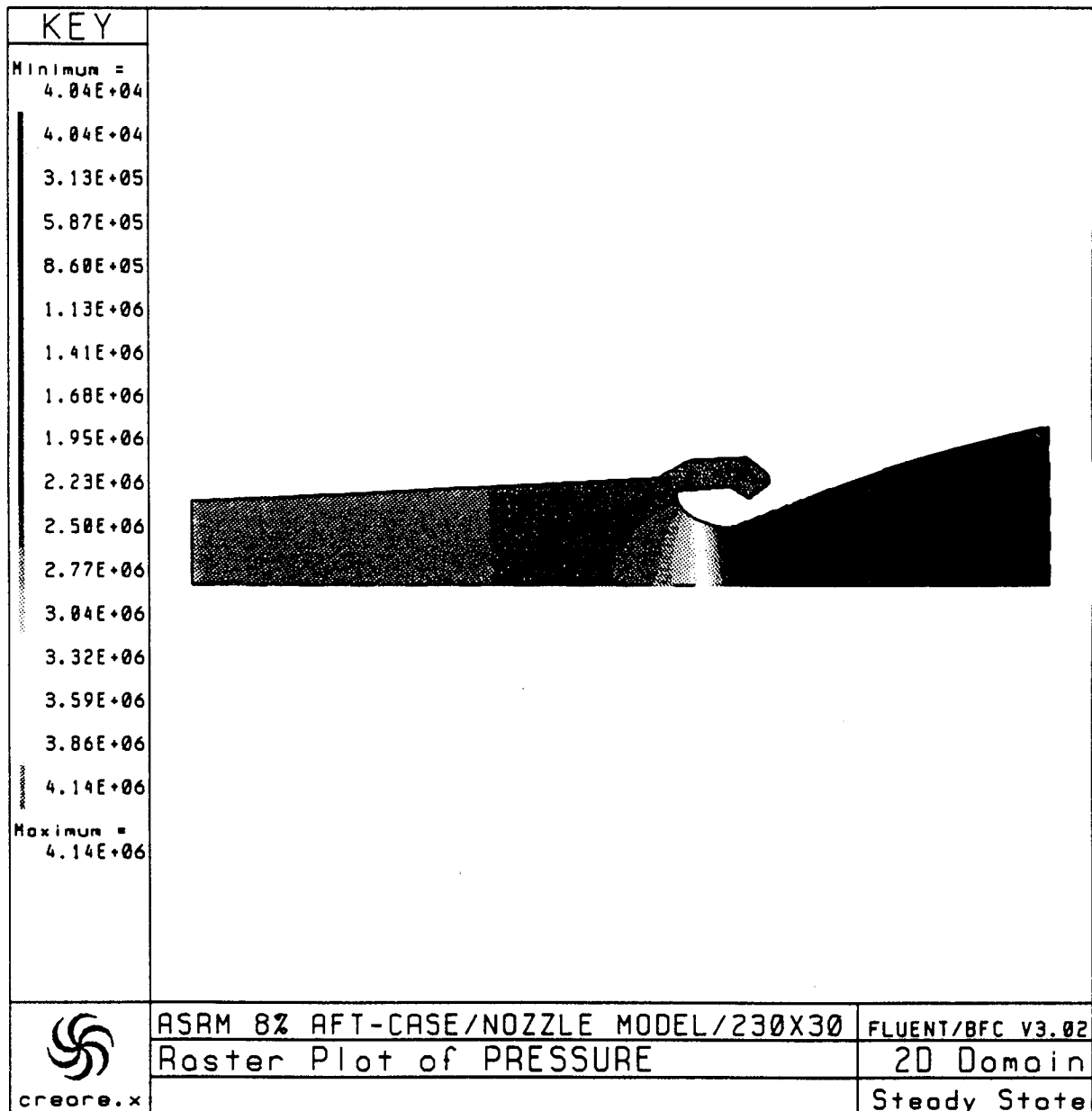
Figure 13. Raster Plot of Static Pressure in the ASRM Aft Section/Nozzle Model
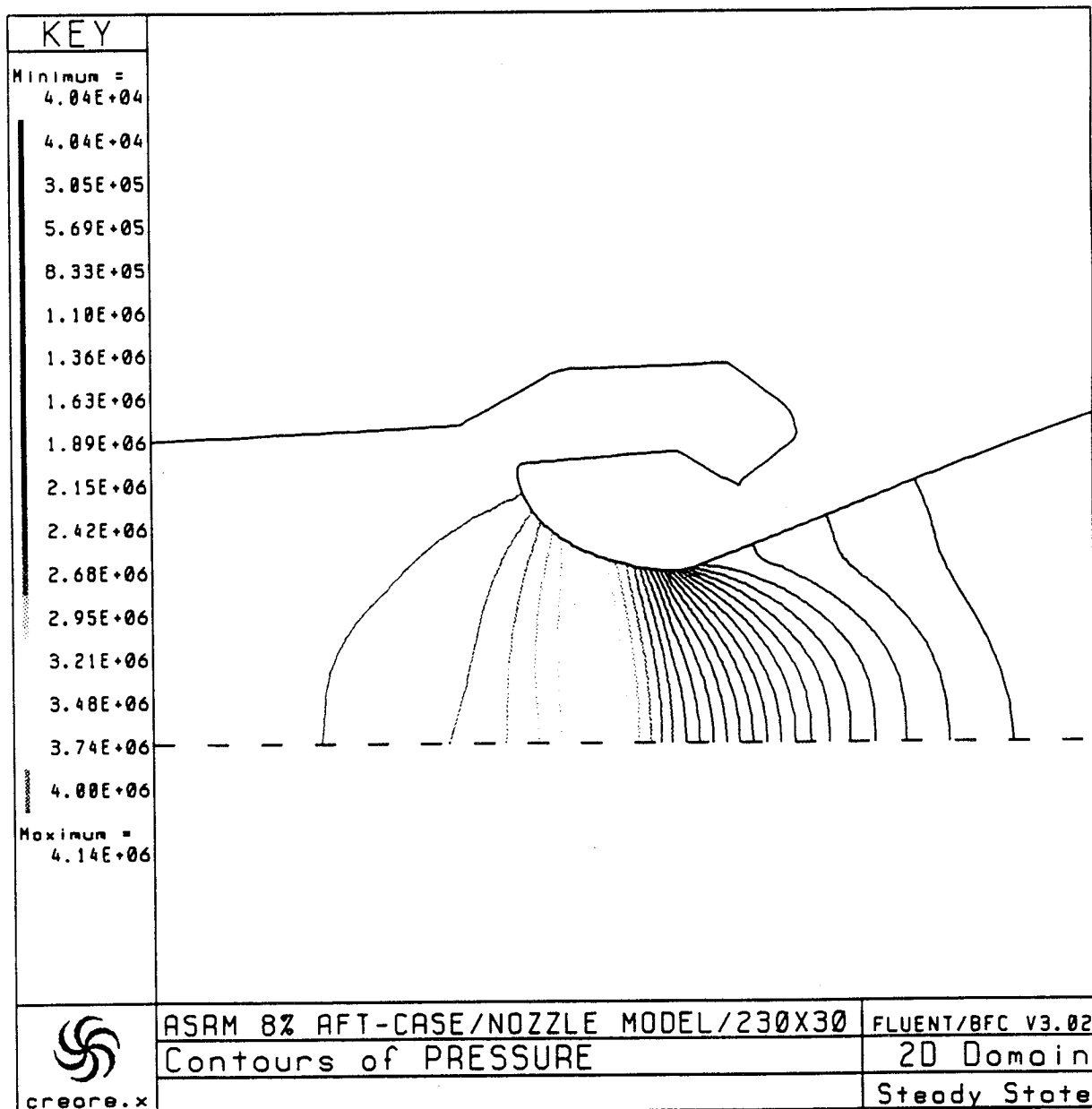
Figure 14. Radial Static Pressure Contours in the Nozzle Region of the ASRM Aft Section/Nozzle Model

Figure 15. Static Pressure Tap Locations in the ASRM Aft Section/Nozzle Model

ANGULAR LOCATION OF
STATIC PRESSURE TAPS

STATIC PRESSURE TAPS
NORMAL TO SURFACE
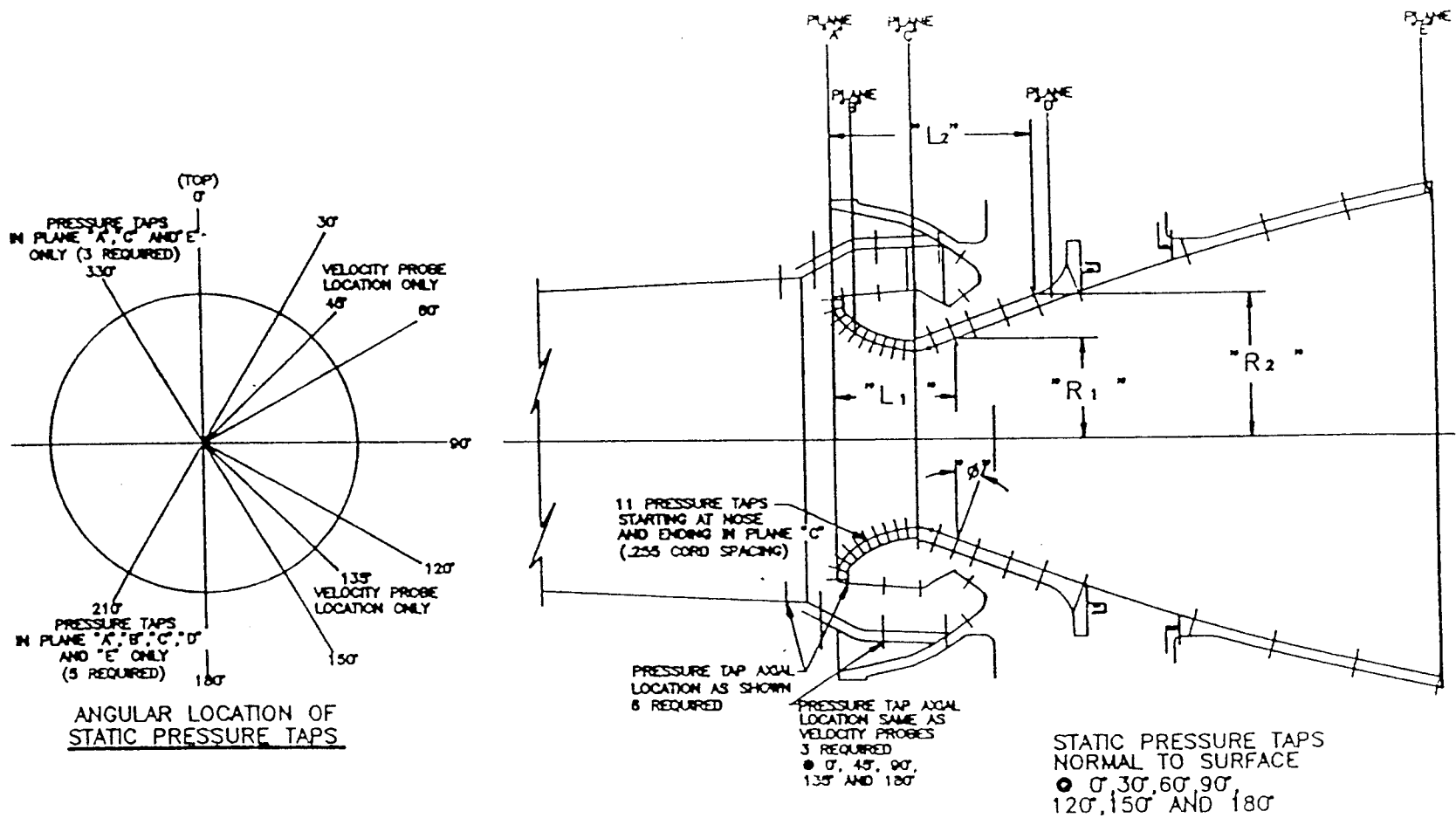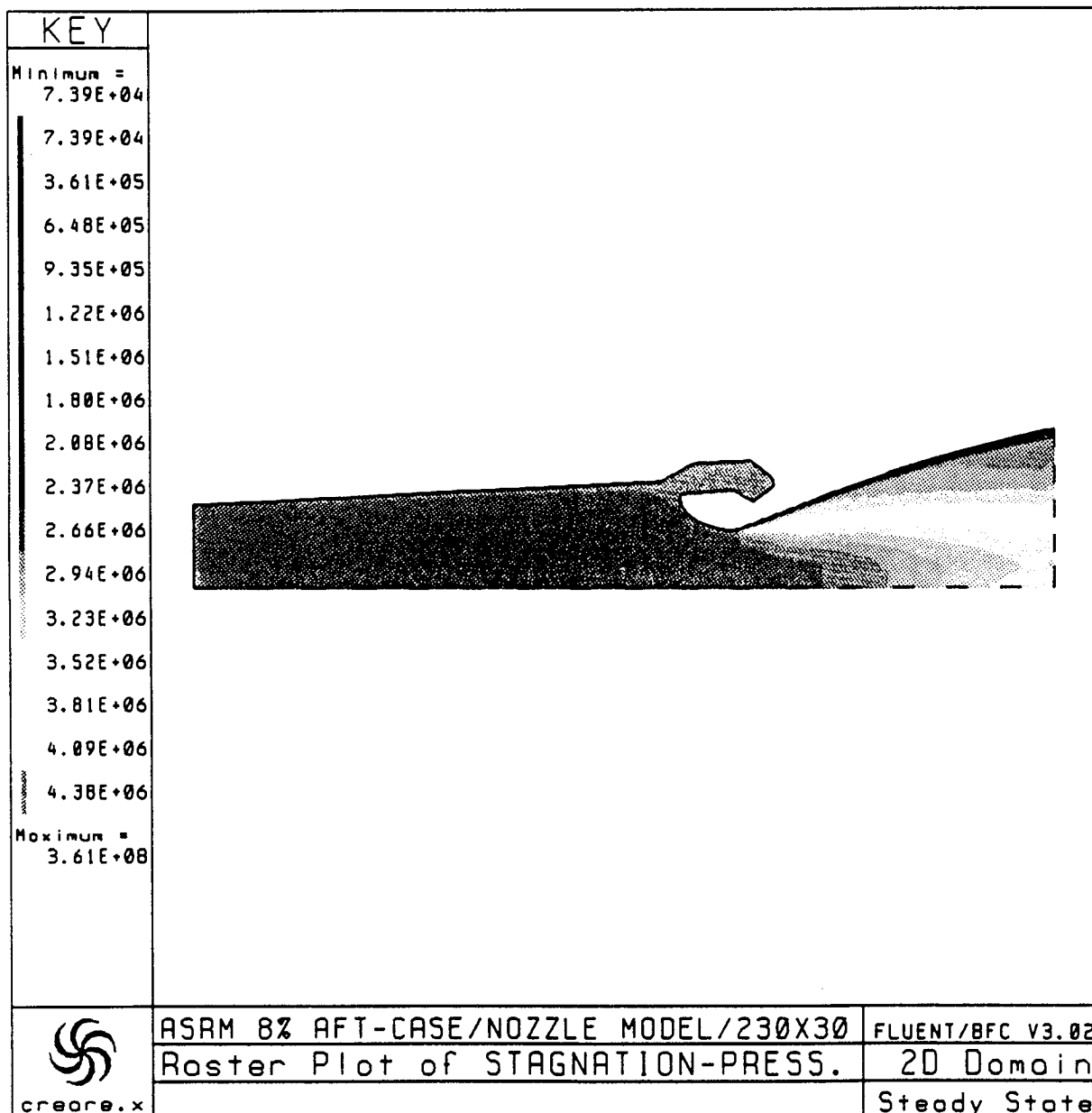
Figure 16. Total Pressure Raster Plot in the ASRM Aft Section/Nozzle Model

KEY

Minimum =	0.00E+00
	0.00E+00
	3.00E+00
	6.00E+00
	9.00E+00
	1.20E+01
	1.50E+01
	1.80E+01
	2.10E+01
	2.40E+01
	2.70E+01
	3.00E+01
	3.30E+01
	3.60E+01
	3.90E+01
	4.20E+01
	4.50E+01
Maximum =	6.55E+02

ASRM 8% AFT-CASE/NOZZLE MODEL/230X30   FLUENT/BFC V3.02

Velocity Vectors   2D Domain

creare.x   Steady State
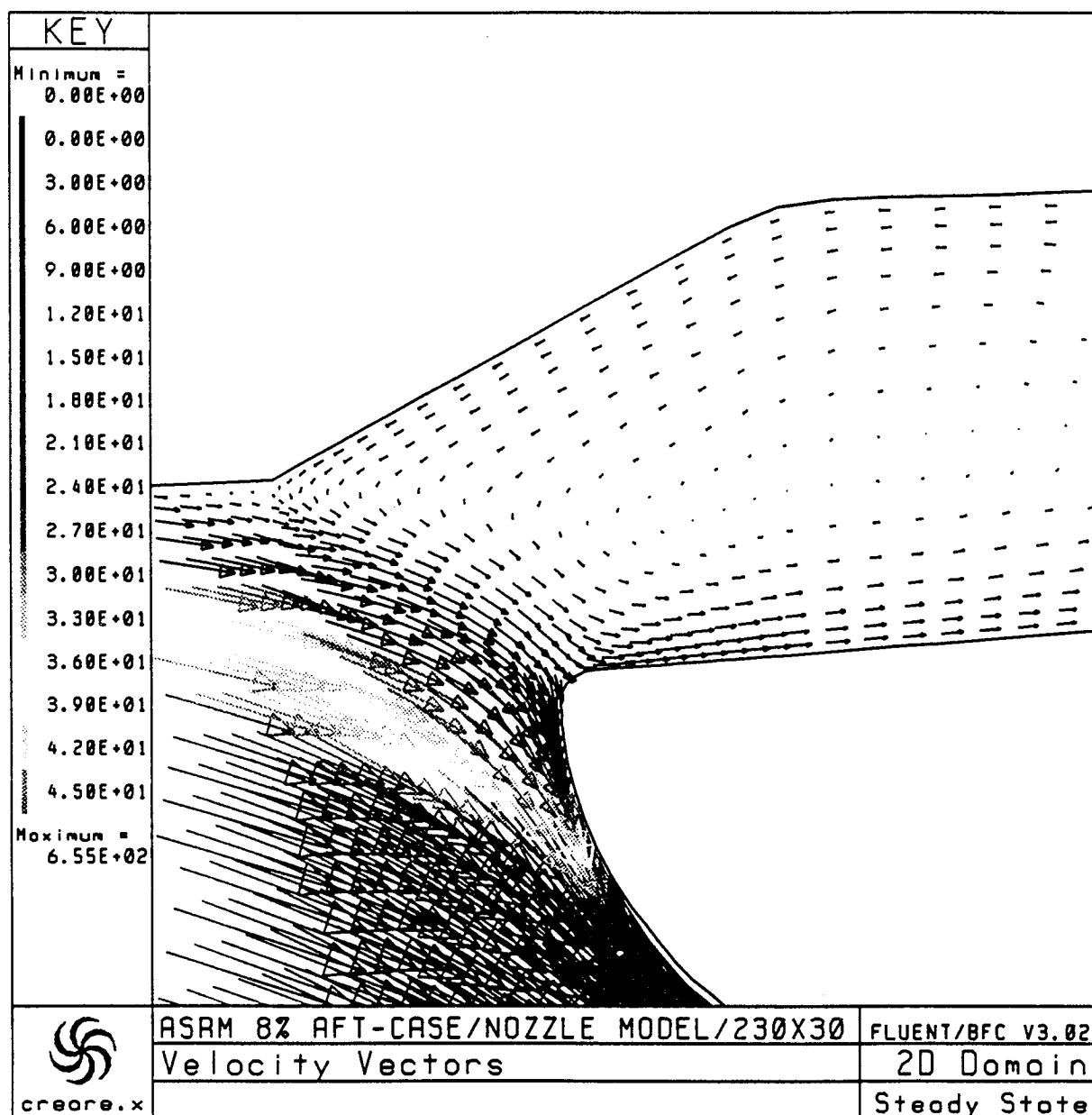
Figure 17. Velocity Field in the Submerged Nozzle Nose Region of the ASRM Aft Section/Nozzle Model

ASRM Aft Segment/Nozzle Water Flow Model Analysis

A drilled-hole velocity profile plate was constructed for the 8 % scale water flow aft segment/nozzle model. The purpose of the plate was to produce a Culick velocity profile in the model port downstream of the plate. A Culick velocity profile was needed in the model port so that experimental data could be gathered in the region of the nozzle nose for a model port velocity profile which was more representative of full-scale motor conditions near the nozzle nose. However, the initial experimental data collected from the water flow facility using the velocity profile plate showed that an irregular Culick velocity profile was produced by the drilled-hole plate. Figure 20 shows a schematic of where the plate and measuring devices are located in the aft segment/nozzle model. The first measurements were taken just downstream of the plate at station 34. The other measurements discussed in this section were taken in front of the nozzle nose at station 29. Figure 21 shows the measured velocity profile for the 1500 gpm water flow run using a Kiel probe measurement device. The results show a dip in the velocity profile between a radius of 1.25 and 1.75 inches from the centerline compared to a nominal Culick velocity profile. This irregularity in the velocity profile still exist at the downstream measurement station 29. A CFD investigation of the water flow model was initiated to determine if these results could be duplicated for a computational solution.

Measurement station 34 was chosen as the inlet plane for the CFD analysis since this location was the nearest experimental measurement to the drilled-hole plate and an experimentally measured velocity profile at this position would be input to the CFD code as the inlet velocity boundary condition. A grid was constructed for the water flow model geometry and is shown in Figure 22. The water flow model geometry was constructed from MicroCraft drawings 80M45060 80M45080, 80M52597, 80M53698, and 80M5321. The grid resolution was 35 radial grid lines in the model port and 20 radial grid lines through the nozzle. A total of 160 axial grid lines were used to resolve the axial flow. Figure 23 shows an enlarged view of the grid in the region of the nozzle nose. The thermochemical properties for water were used to describe the fluid properties and the analysis was assumed incompressible. These properties are shown in Table 1.

Table 1. Thermochemical Properties for Water Model

Density (lbm/ft^3)	62.253
Molecular Weight	18.0153
Viscosity (lbm/ft-sec)	6.7867x10^{-4}
Specific Heat Ratio	1.4
Total Temperature (°R)	530

The general boundary conditions used to solve this problem are as follows. An inlet velocity boundary condition was specified at the port model inlet. All solid walls were modeled using a non-slip wall boundary condition. A symmetry boundary condition was

used along the model centerline and the downstream nozzle exit boundary condition was modeled as a subsonic outlet.

Two inlet velocity profiles were used in the analysis at the inlet velocity boundary discussed in the previous paragraph. The first was a nominal Culick velocity profile and the second was an experimentally based velocity profile constructed from the Kiel probe experimental data taken at measurement station 34. Figure 24 shows the velocity profiles utilized in this analysis along with the experimental measurement data interpolated to the CFD grid locations. The centerline data point was added by using a least squares linear fit through the previous two measurement points. The velocity at the wall was assumed to be zero. The experimental Kiel probe data was used to construct the inlet velocity profile by linearly interpolating between the experimental data points and the two calculated points at the wall and centerline. The resultant experimental velocity profile was then integrated to determine the average velocity and mass flow rate associated with the profile. This information was then used to construct a Culick velocity profile with the same mass flow rate using the equation shown below:

$$U = \frac{\pi}{2} U_{AVG} \cos\left[\frac{\pi}{2} \cdot \frac{r^2}{R^2}\right]$$

Where U is the velocity at any radial location, r is the radial distance from the centerline, R is the port radius at the inlet, and U_{AVG} is the average inlet velocity. Figure 24 and the remaining plots showing velocity profiles at station 29 are plotted using a normalized velocity The normalization has been performed by integrating the profile to determine the average velocity and then dividing the absolute velocity by the average velocity. All the normalized velocity profile plots shown for the water flow analysis exhibit the same mass flow rate.

The kinetic energy of turbulence and dissipation rate must also be specified at the inlet boundary. The turbulent kinetic energy intensity on the downstream side of the velocity profile plate would vary experimentally from the wall to the centerline. However, since no good experimental data which would accurately specify the turbulence intensity level is currently available, a simplification of the analysis has been made. A constant turbulence intensity value of 10% across the model port has been chosen. This value of the turbulence intensity is derived from the turbulence intensity levels observed in the motor aft end as computed in the ASRM full-length motor port analysis. The turbulence kinetic energy specified at each inlet radial location was computed from the equation:

$$\kappa = 1.5^*(uI)^2$$

where I, is the turbulence intensity, u, is the steady state velocity component at a particular radial location across the model port, and κ is the turbulence kinetic energy.

This equation can be used along with the input velocity profile to determine the kinetic energy of turbulence at each grid point across the model port inlet. The dissipation rate profile across the port is determined by the equation:

$$\varepsilon = C_\mu^{.75}(\kappa^{1.5}/\lambda)$$

where ε, is the dissipation rate, κ is the turbulent kinetic energy, C_μ is a constant equal to 0.09, and λ is the length scale. The length scale, λ, is determined from mixing length theory to be: $\lambda = 0.07L$, where L is a characteristic upstream flow dimension which in this analysis was assumed to be directly related to the size of the drilled holes in the velocity profile plate. The velocity profile plate is divided into six porosity levels. A different hole size is used for each of the six porosity levels. There was also a small interface region between the two most inner porosity sections which contained several different hole sizes due to the methodology used to design the plate. No attempt was made to take this into account in the CFD analysis. Six different regions of hole sizes are considered and these along with the corresponding computed length scale are shown in Table 2.

Table 2. Drilled Hole Size, Distribution and Associated Length Scale.

Radial distance from the centerline (inches)	Hole Radius (inches)	Length Scale (inches)
0 - 1.654	.117	8.19×10^{-3}
1.654 - 2.131	.09375	6.56×10^{-3}
2.131 - 2.558	.0703	4.921×10^{-3}
2.558 - 2.847	.04685	3.2795×10^{-3}
2.847 - 3.000	.03125	2.1875×10^{-3}
3.000 - 3.457	.02345	1.6415×10^{-3}

Values of the kinetic turbulent energy and the dissipation rate were computed for the two velocity profiles used in this analysis.

As stated previously, a CFD solution was obtained for two inlet velocity profiles, the Kiel probe experimental data profile and a nominal Culick profile. Figure 25 shows a plot of the CFD generated velocity profiles plotted at measurement station 29. The figure shows that there is a significant downstream dependency of the flow on the inlet velocity profile. The CFD velocity profile computed for station 29 has a significant dip between a radial distance from the centerline of from 1.0 to 2.0 inches. This dip is not present at station 29 when the Culick inlet profile is used in the CFD analysis. Figure 26 shows a plot of the CFD results for the experimentally based profile along with the measurement data taken from the Kiel probe and the hot film probe. As previously stated, the CFD curve and the experimental data are normalized to the same mass flow rate.
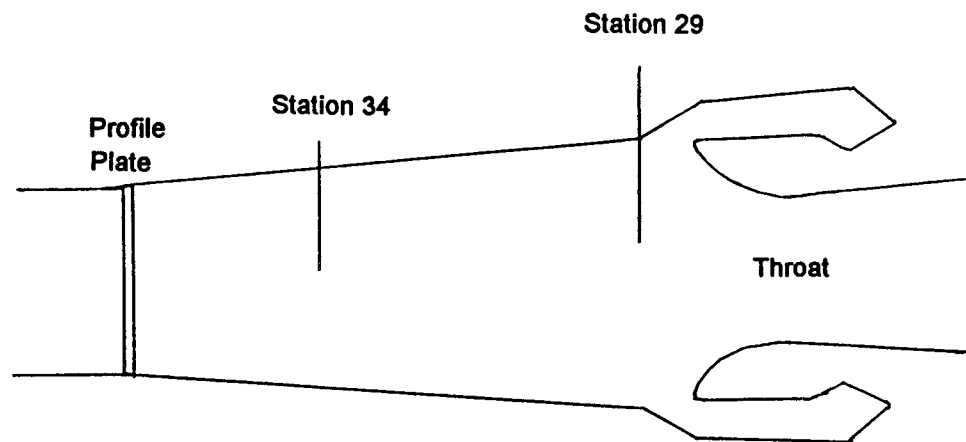
Location	Distance from Nozzle Throat	Radius
Plate	14.513"	3.410"
Station 34	10.227"	3.646"
Station 29	2.705"	4.012"

Figure 20. ASRM 8% Scale Water Flow Aft Segment/Nozzle Model Geometry and Measurement Locations

Figure 21. Experimental Kiel Probe Velocity Profile Data at Station 34.

ERC, Inc 12/11/92
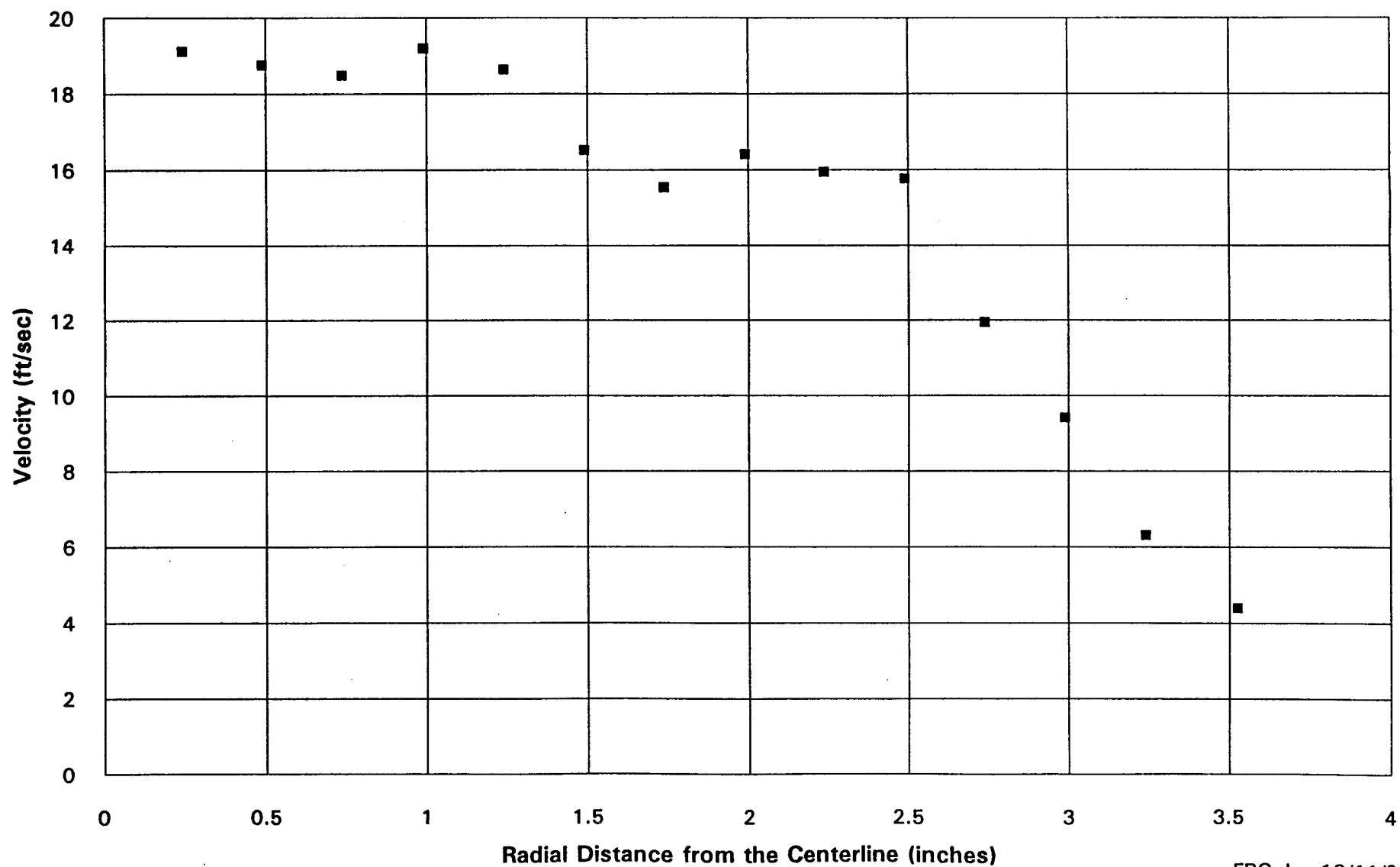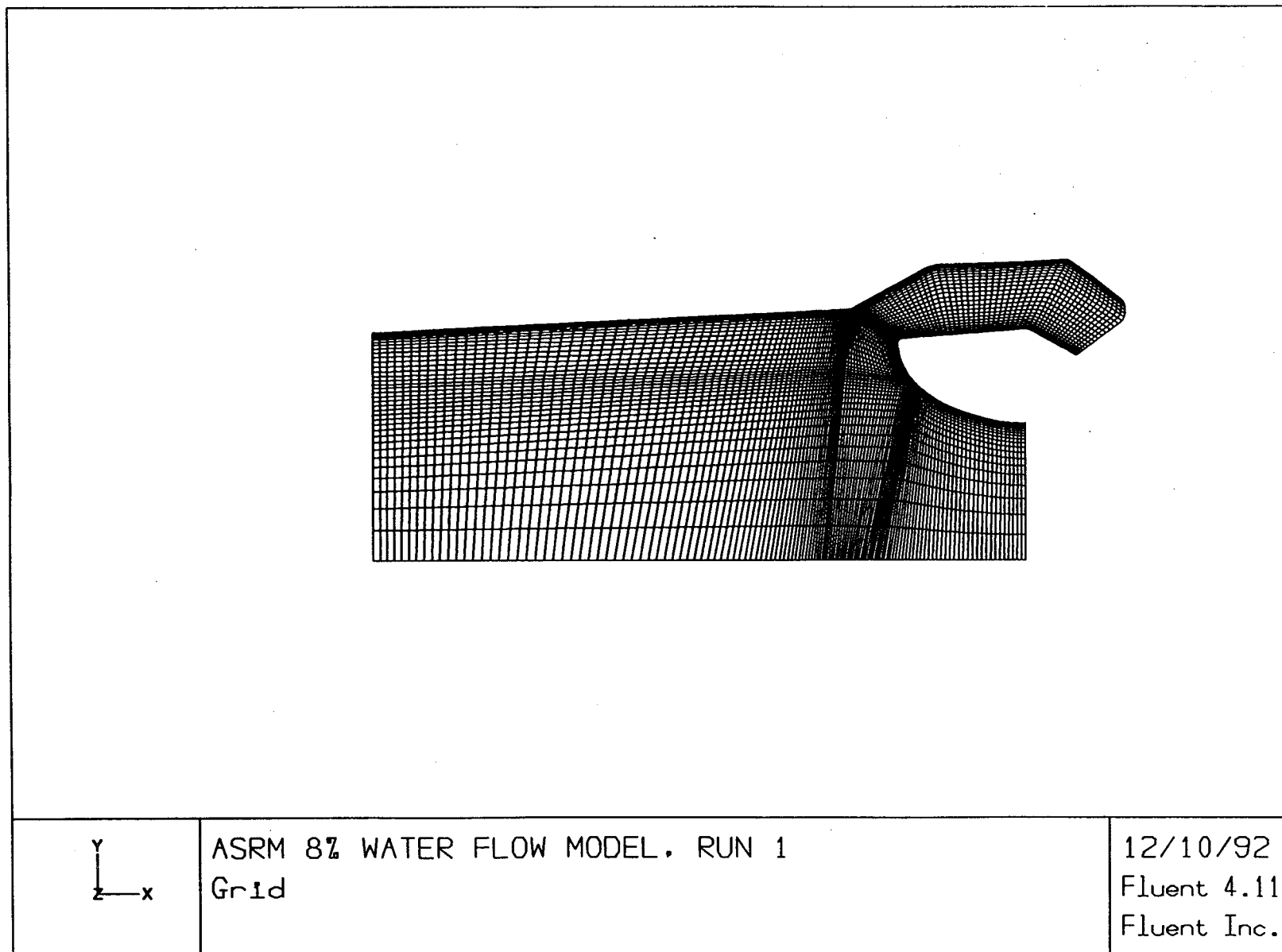
Figure 22. Computational Grid for the ASRM Water Flow Aft Segment/Nozzle Model

```
 Y
 |
 |___ x
 Z
```

ASRM 8% WATER FLOW MODEL. RUN 1	12/10/92
Grid	Fluent 4.11
	Fluent Inc.
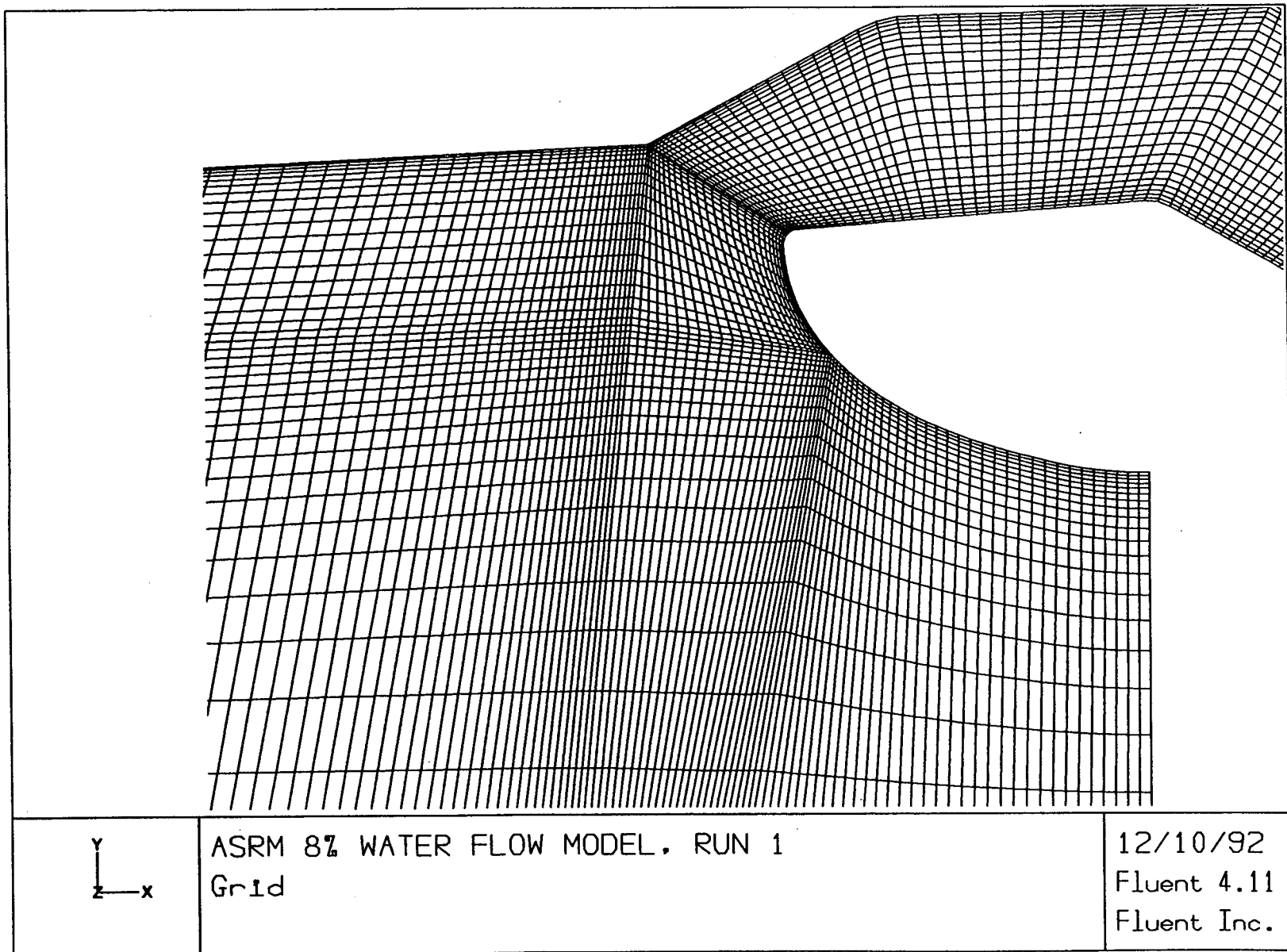
**Figure 23. Computational Grid for the Nose Region of the ASRM
Water Flow Aft Segment/Nozzle Model**

Figure 24. Inlet Boundary Velocity Profiles Used in the Water Flow Analysis.

ERC, Inc. 12/11/92
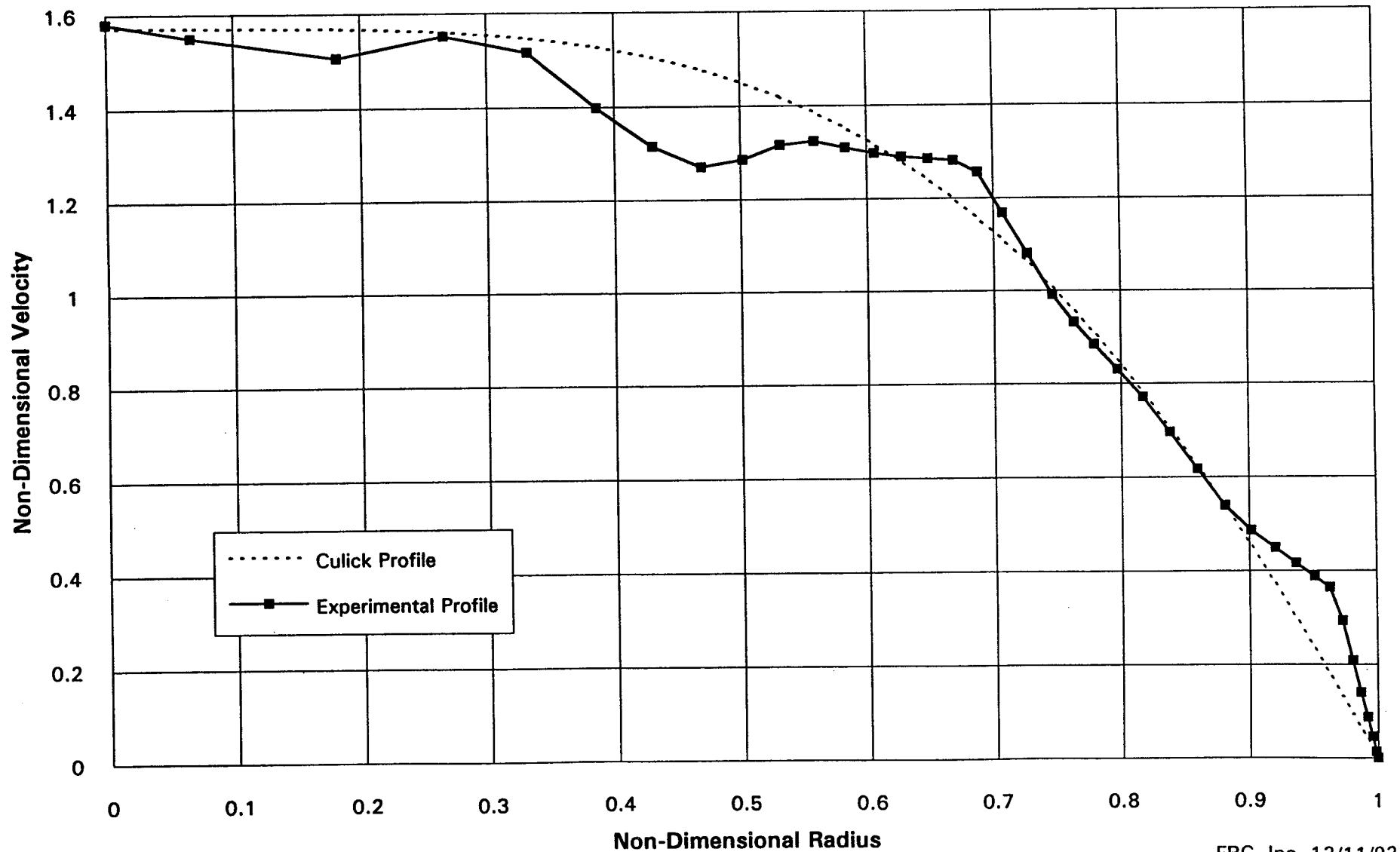
Figure 25. CFD Computed Velocity Profiles at Station 29.

Normalized Velocity (vertical axis): 0.00, 0.25, 0.50, 0.75, 1.00, 1.25, 1.50, 1.75, 2.00, 2.25, 2.50

Radial Distance from Centerline (in.) (horizontal axis): 0.00, 0.25, 0.50, 0.75, 1.00, 1.25, 1.50, 1.75, 2.00, 2.25, 2.50, 2.75, 3.00, 3.25, 3.50, 3.75, 4.00, 4.25

Legend:
CFD - Exper
CFD - Culick
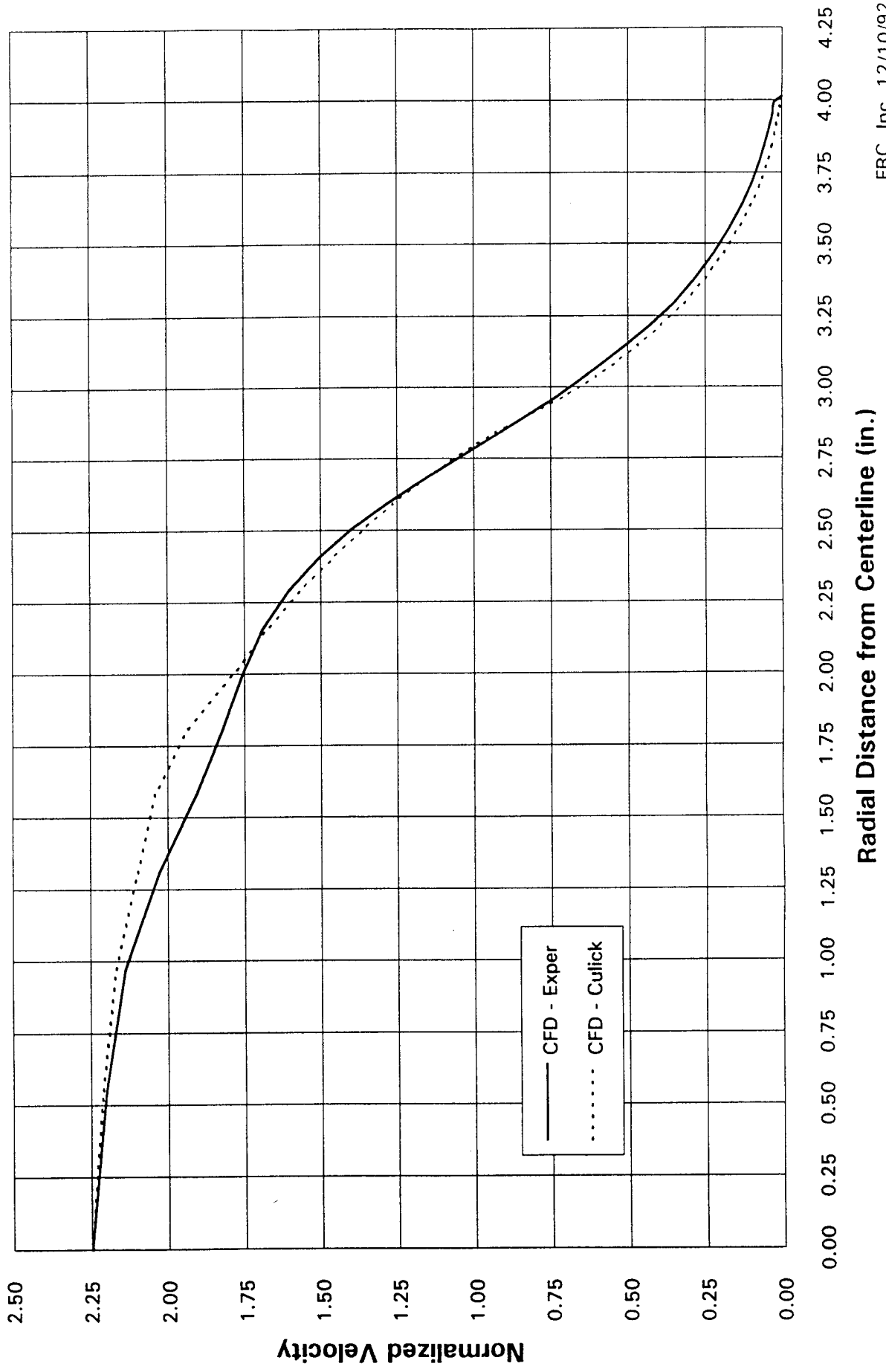
Figure 26. Experimental Data and CFD Predicted Velocity Profiles at Station 29.

ERC, Inc. 12/10/92
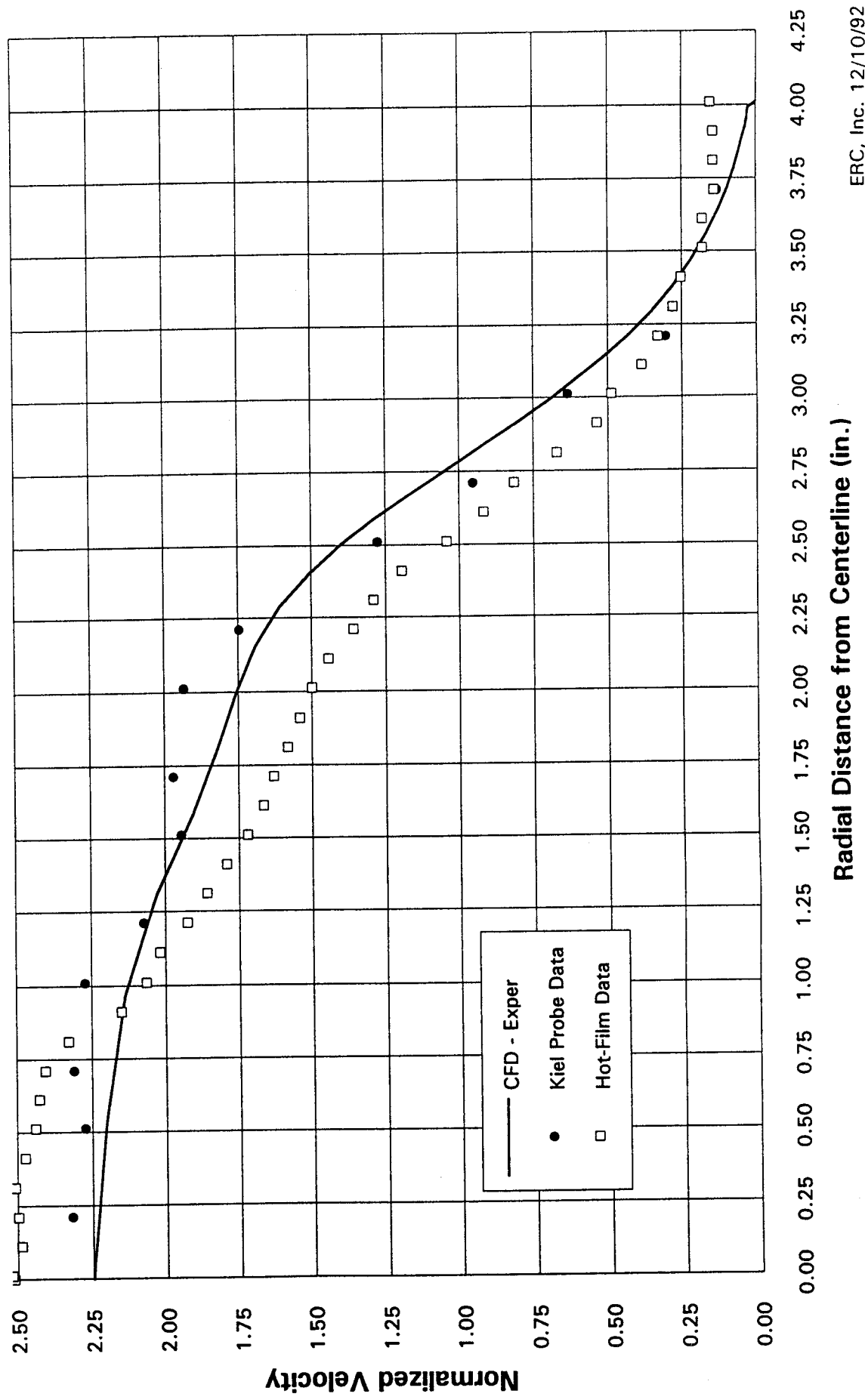
2 February 1994

To: John E. Hengel, ED34

From: R. Harold Whitesides
           David C. Purinton
           ERC, Incorporated

Subject: Effect of tank loss on SAF performance.

This memorandum addresses the effect of losing one of the large, 60 foot long (1250 cubic feet) tanks on the performance capabilities of the Solid Rocket Motor Air Flow Facility (SAF). The tank is assumed to be permanently removed from the location to fill another project need.

Presently the storage tanks and associated capacity are listed in Table I. The effect of losing one large tank would be a reduction in total volume from 9100 cubic feet to 7850 cubic feet.

The most obvious effect of a reduction in tank storage capacity is the effect on available test duration for a given model and test conditions. The initial facility requirement was for a thirty second minimum usable test duration. The basic approach taken here was to determine the impact on the test duration for each of the currently active models as well as potential future models from which the facility maximum flow and thrust design loads were derived.

This analysis computes the pressure in the facility storage tanks as a function of time. It takes into account the mass discharged from the tanks during the run time as well as the temperature drop of the air. The analysis inputs include the initial tank pressure and temperature, the gas constant, specific heat ratio, tank volume, and flowrate.

The program uses the two following equations to solve the problem under investigation. Equation (1) is derived by differentiating the equation of state with respect to time. Equation (2) yields the relationship between pressure and temperature for an adiabatic expansion of tank gases.

$$P_2 = \left[-RT_1\dot{m} + M_1 R \frac{(T_2 - T_1)}{\Delta t} \right] \frac{\Delta t}{V} + P_1 \qquad (1)$$

$$T_2 = T_1 \left(\frac{P_2}{P_1} \right)^{\frac{\gamma-1}{\gamma}} \qquad\qquad (2)$$

In the above equations R is the gas constant, γ is the specific heat ratio, V is the tank volume, M is the mass in the tank, T is the temperature, P is the pressure, $\dot{m}$ is the mass flowrate, and Δt is the time step. Thus, the values at time 1 and time 2 as denoted by the subscripts on the variables are separated by time Δt. It should also be noted that these two equations need to be solved simultaneously. Excel 4.0 was used to solve these equations by using the iterative solving capability of the software. It should be noted that these runs do not take into account the time it takes the model to stabilize at the required run conditions. Also, pressure differences between the tank and upstream of the valve are not included. These effects should be small except for the large throat models.

Table II gives a summary of the results and will be discussed shortly. The attached plots show the pressure bleed down history for each run performed. The conditions for each run can be seen in Table II. For each model there are three runs made. The three runs for the Checkout Model are the highest, lowest and an intermediate pressure level run for this model. The runs for the SRM Aft Section/Nozzle Model represent a run to match the full scale Reynolds Number, and a plus and minus 25% Reynolds Number scan. The runs for the SRM Technology Model include a run to match the full scale Reynolds Number, a run at the facility maximum flow conditions, and a lower pressure and flowrate run. The runs for the 6.5% Scaled Slag Ejection Model represent a run to match the full scale Reynolds Number and two additional runs at 75% and 50% of the full scale Reynolds Number. There is only one run each for the 12 inch, 8 inch, and 6 inch throat models, but these runs are the maximum possible for each of these models, respectively.

Table II shows that most of the models will be unaffected by the loss of the single 1250 cubic foot air storage tank. The are, however, some notable exceptions. The Checkout Model high pressure run would require a shortening of the test duration to 27.2 seconds. The SRM Aft Section/Nozzle Model run at the plus 25% Reynolds Number would have to shortened to 4.8 seconds. However, even with the full 9100 cubic foot air storage capacity this run could only last 5.6 seconds. This fact has been realized and the current test program for this model has lowered the level of the upper Reynolds Number scan.

The run times for the SRM Technology Model would be unaffected by the loss of a single 1250 cubic foot air storage tank. Likewise, the 6.5% Scaled Slag

Ejection Model would not require any modification as far as run times are concerned. The last three models represent potential future models that could be tested in the SAF facility. The 12 inch throat model operating with the conditions shown could be run for a 30 second test. The 8 inch throat model would require a 4 second shorter run time with the loss of a single air storage tank. The 6 inch throat model would need the run time to be shortened by 4.2 seconds, but even with the full 9100 cubic foot storage capacity now present, this model could only be run for a 16.5 second test duration. When using the numbers in Table II it should be remembered that the start up time was not taken into account in this study.

The effects of shortened test times can be offset by optimizing facility operation and data system recording. There are several ideas which have been mutually exchanged with testing personnel. The goal of these ideas would be to enable test durations of five to ten seconds to be acceptable. The ideas which relate to facility operation include: 1) Optimization of control valve parameters for a particular model flow rate to minimize start-up time and enhance steadiness of control at a specific flow condition. 2) Preset valve opening and rate of opening during test to enable disconnecting feedback commands to enhance steadiness of flow and decrease start-up times. Valve settings for a particular flow rate would be determined by trial and error. The ideas relating to data system recording include: 1) acquisition of a faster data recording system and 2) acquire only one frame of data with 11-21 samples of each channel per frame using the highest possible sampling rate. 3) Minimize number of channels of data per test, possibly using multiple tests to acquire data for all desired measurement stations.

cc: ED31/Andrews
      ED34/Bacchus
      ED34/Dill
      ED35/Aaron
      ED35/Gwin
      ED35/Pepper

Table I. SAF Storage Tank Capacity

Tank Cylindrical Length	Volume (cu. ft.)	Number	Total Volume (cu. ft.)
60 feet	1250	6	7500
45 feet	800	2	1600
		Total	9100
		Less one 60 ft tank	-1250
		Revised Total Tank Volume	7850

Table II. SAF Tank and Model Parameters

Model	Flow rate	Initial Tank Press.	Manifold Press.	Model Press.	Final Tank Press.	Lower Tank Limit	Margin	Minimum Run Time
Checkout	320	1800	1200	610	1515/1469	1500	+15/-31	30/27.2
	160	1200	600	305	1058/1035	750	+308/+285	30/30
	20	200	75	38	182/179	94	+88/+85	30/30
Aft Section/ Nozzle	246	1800	1407	715	1581/1546	1759	-178/-213	5.6/4.8
	197	1800	1125	572	1625/1597	1406	+219/+191	30/30
	148	1700	844	429	1568/1547	1055	+513/+492	30/30
Technology Model	278	1800	1200	516	1553/1513	1500	+53/+13	30/30
	232	1800	1000	430	1594/1561	1250	+344/+311	30/30
	54	500	233	100	452/444	291	+161/+153	30/30
Slag Model	138	1800	1035	623	1677/1658	1294	+383/+364	30/30
	103.5	1600	776	467	1508/1493	970	+538/+523	30/30
	69	1100	517.5	311.5	1039/1028	647	+392/+381	30/30
12 in Throat	1083	1800	416	416	806/614	520	+286/+94	30/30
8 in Throat	918	1800	793	793	968/824	991	-23/-167	29.2/25.2
6 in Throat	746	1800	1146	1146	1129/1018	1433	-304/-415	16.5/14.3

Notes:

(1.) All of the above models are run in Mode A except for the last three models listed in the table which are run in Mode B.

(2.) In columns with two numbers, the first refers to the facility with 9100 cubic feet of storage and the second refers to the facility with 7850 cubic feet of storage.

(3.) The lower tank limit is found by multiplying the manifold pressure by a factor of 1.25 (estimated minimum control valve pressure ratio).

(4.) A positive margin means that a 30 second test condition is attainable where as a negative margin means the run time will be less than 30 seconds.

(5.) Units are psia, seconds, and pounds per second.

SAF Tank Pressure Drop for Checkout Model

Legend:
- 9100 cu. ft. 320 lbm/sec
- 7850 cu. ft. 320 lbm/sec
- 9100 cu. ft. 160 lbm/sec
- 7850 cu. ft. 160 lbm/sec
- 9100 cu. ft. 20 lbm/sec
- 7850 cu. ft. 20 lbm/sec

X-axis: Time (seconds)
Y-axis: Tank Pressure (psia)

ERC, Inc. 02/02/1994
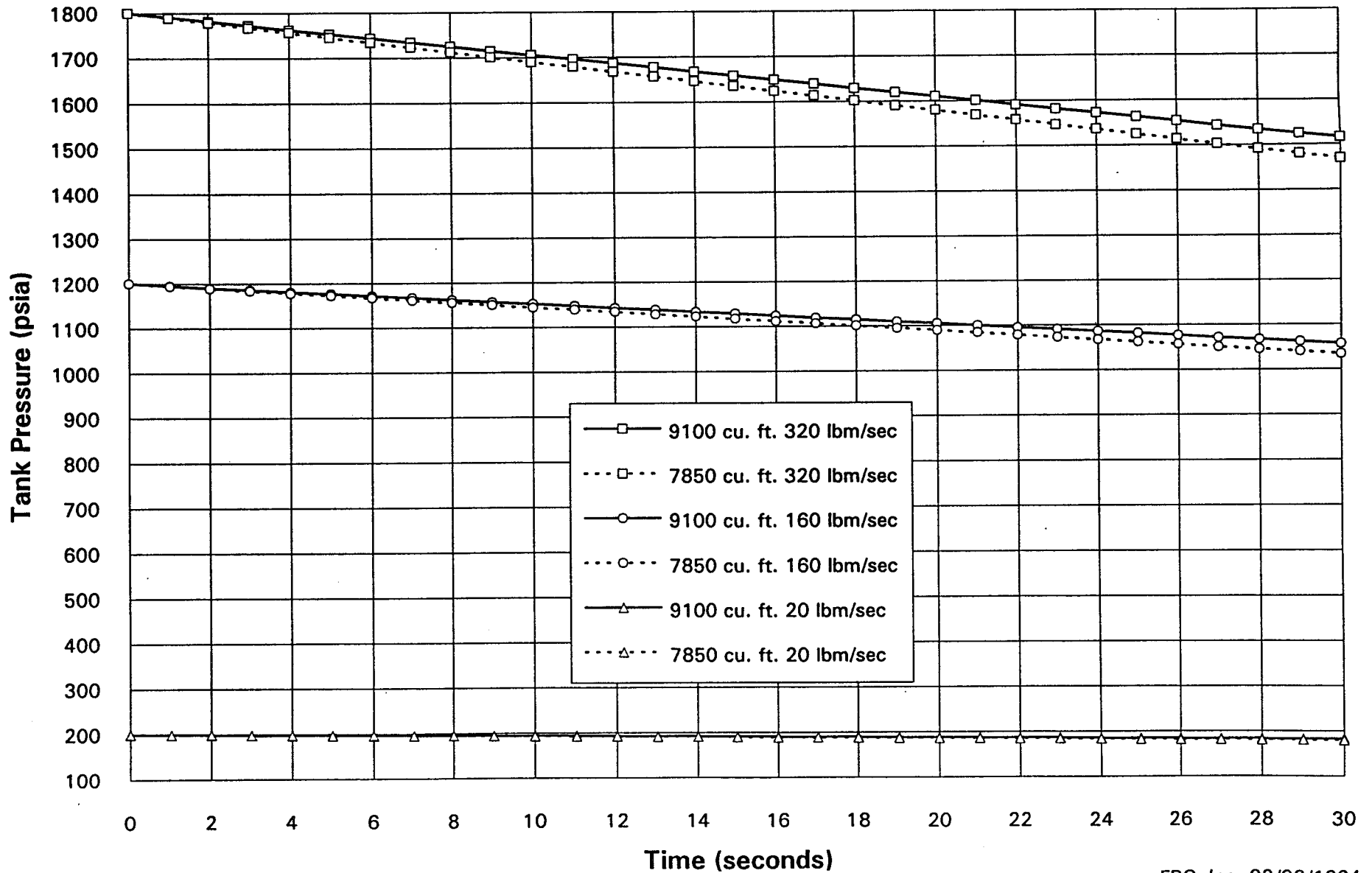
SAF Tank Pressure Drop for 8% SRM Aft Section/Nozzle Model

Tank Pressure (psia)

Time (seconds)

Legend:
- 9100 cu. ft. 246 lbm/sec
- 7850 cu. ft. 246 lbm/sec
- 9100 cu. ft. 197 lbm/sec
- 7850 cu. ft. 197 lbm/sec
- 9100 cu. ft. 148 lbm/sec
- 7850 cu. ft. 148 lbm/sec

ERC, Inc. 02/02/1994
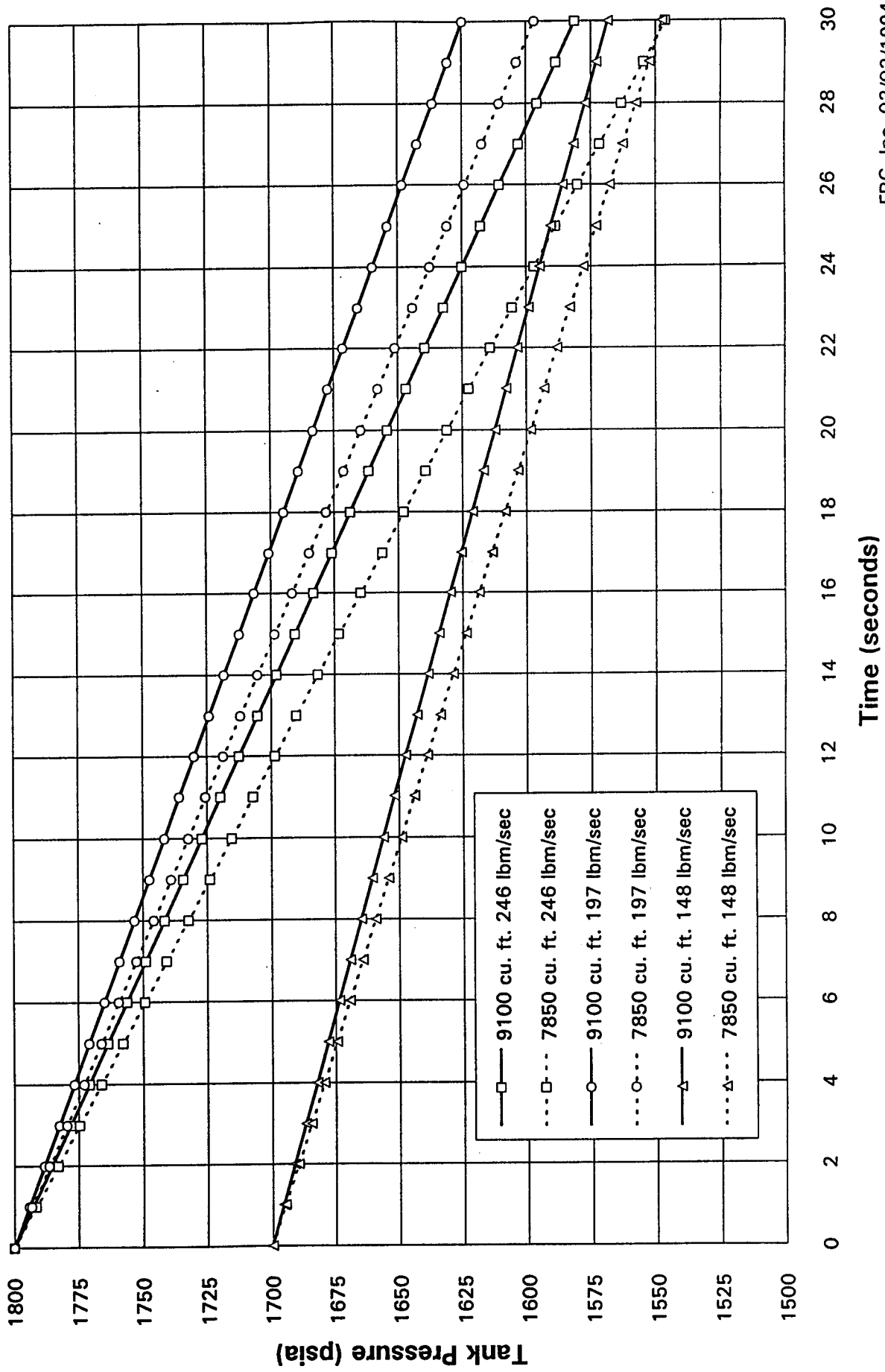
SAF Tank Pressure Drop for Technology Model

Legend:
- 9100 cu. ft. 278 lbm/sec
- 7850 cu. ft. 278 lbm/sec
- 9100 cu. ft. 232 lbm/sec
- 7850 cu. ft. 232 lbm/sec
- 9100 cu. ft. 54 lbm/sec
- 7850 cu. ft. 54 lbm/sec

X-axis: Time (seconds)
Y-axis: Tank Pressure (psia)

ERC, Inc. 02/02/1994
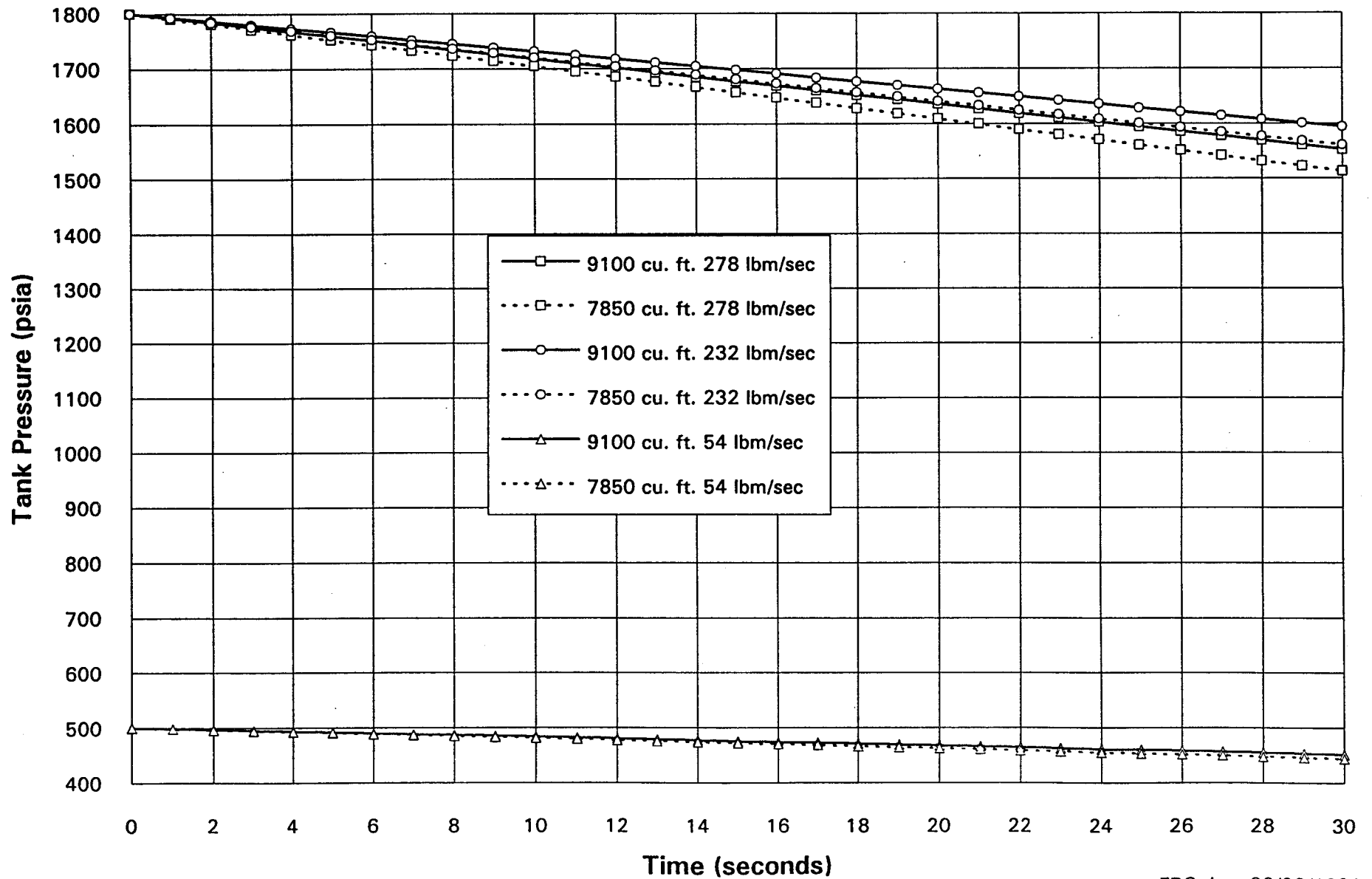
SAF Tank Pressure Drop for 6.5% Scaled Slag Ejection Model

Tank Pressure (psia)

Time (seconds)

Legend:
- 7850 cu. ft. 69 lbm/sec
- 9100 cu. ft. 69 lbm/sec
- 7850 cu. ft. 103.5 lbm/sec
- 9100 cu. ft. 103.5 lbm/sec
- 7850 cu. ft. 138 lbm/sec
- 9100 cu. ft. 138 lbm/sec

Time axis: 0, 2, 4, 6, 8, 10, 12, 14, 16, 18, 20, 22, 24, 26, 28, 30

Pressure axis: 1000, 1050, 1100, 1150, 1200, 1250, 1300, 1350, 1400, 1450, 1500, 1550, 1600, 1650, 1700, 1750, 1800
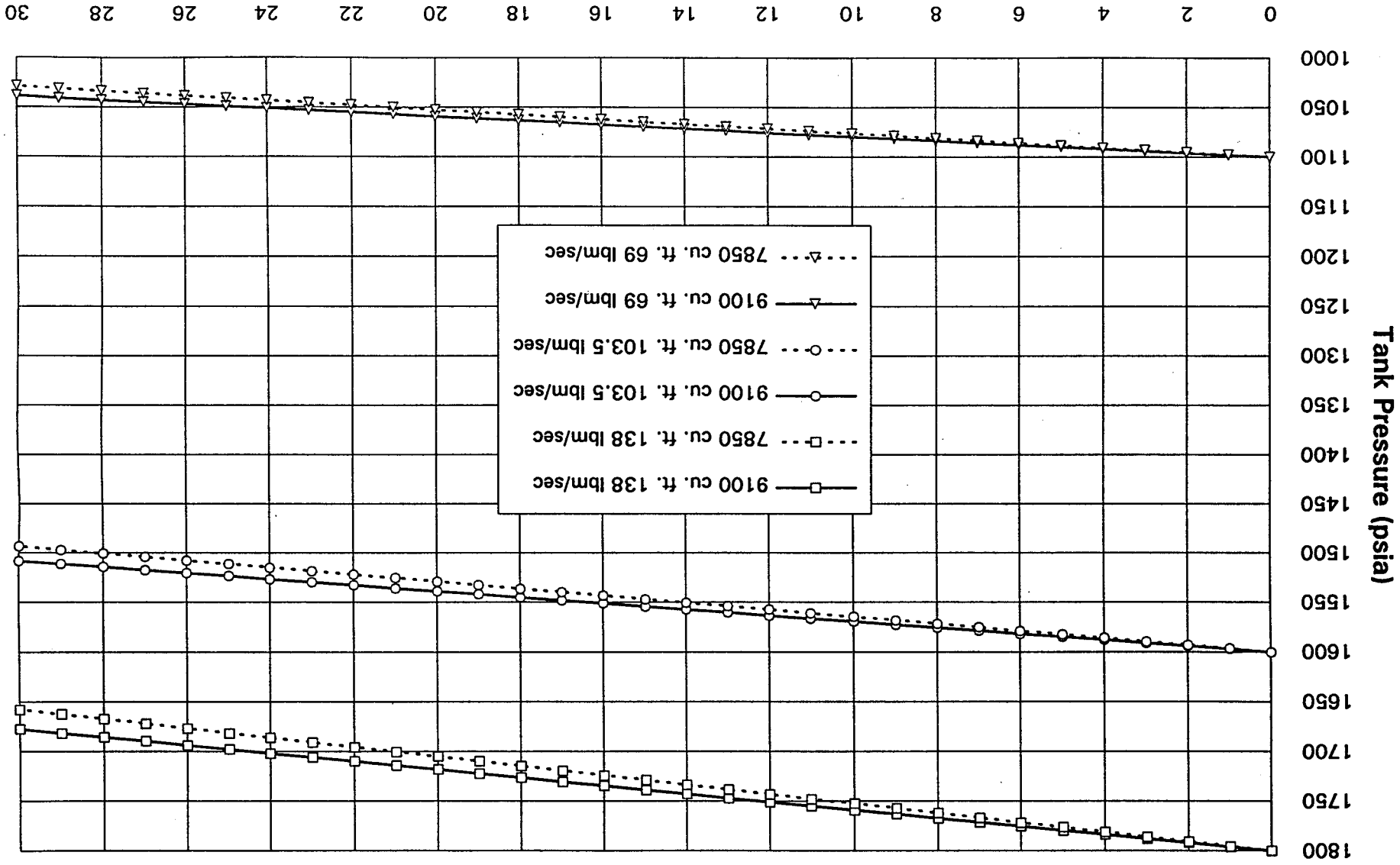
SAF Tank Pressure Drop for Potential Future SRM Models

Legend:
- —□— 9100 cu. ft. 1083 lbm/sec 12 in throat
- ···□··· 7850 cu. ft. 1083 lbm/sec 12 in throat
- —○— 9100 cu. ft. 918 lbm/sec 8 in throat
- ···○··· 7850 cu. ft. 918 lbm/sec 8 in throat
- —△— 9100 cu. ft. 746 lbm/sec 6 in throat
- ···△··· 7850 cu. ft. 746 lbm/sec 6 in throat

Tank Pressure (psia)

Time (seconds)

ERC, Inc. 02/02/1994
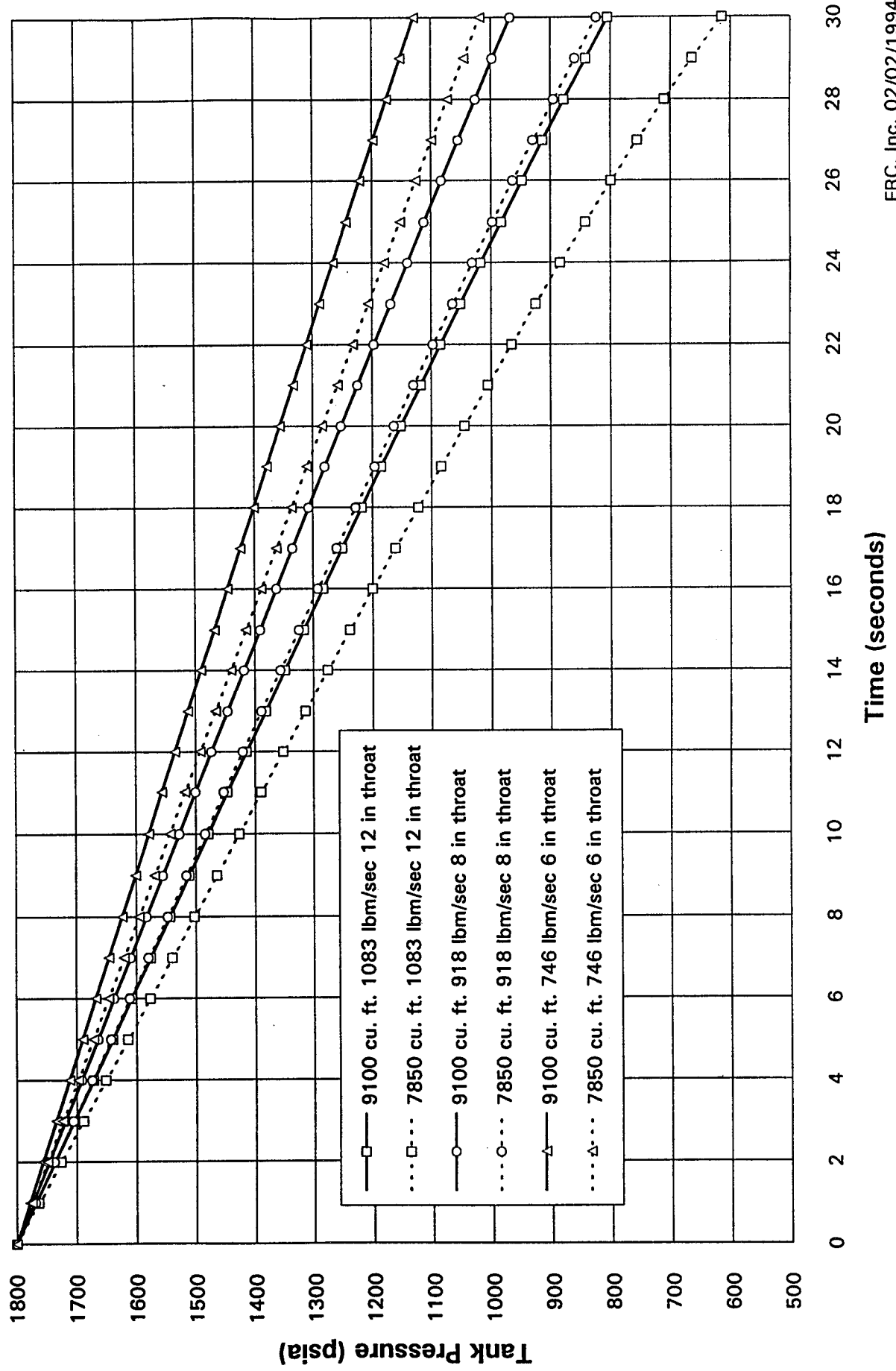
SAF Model Testing Plan 1995-1996

General. - This plan outlines SAF Model testing needs for the immediate next few weeks, the intermediate next few months and longer range for late 1995 and 1996. The plan outline is developed considering the current status and results of testing achieved in the last half of 1994. Past results are not reviewed here. Recommendations for future testing are based on current model testing status and envisioned SRM program needs and funding possibilities.

Near Term Plan - 1st Quarter 1995.

RSRM Nozzle Slag Ejection Model - There is still interest in investigating the triggering mechanism for slag ejection. Spin testing of 5 inch motors is currently in progress at Thiokol to determine propellant ingredient characteristics responsible for increases in slag production. Unsteady gas dynamics around the nozzle nose separated flow region may be involved as evidenced by very low frequency oscillations associated with the flow entrainment and ejection of slag pooled underneath the nozzle nose. Also, the possible role of periodic vortex shedding from the aft NBR inhibitor must be investigated and was a part of the original model test plan. An AIAA paper on this topic has recently been accepted for the Propulsion Meeting in July. Immediate test objectives for the remaining tests are :

1) Determine if unsteady vortex phenomena around the submerged nozzle nose is the source and cause of the very low frequency pressure oscillations observed during slag ejection in both the model and the motor.

2) Determine if there is an oscillating flow rate component for the ejected slag (water) that relates to the oscillating component of the model chamber pressure.

3) Determine if resonance between the inhibitor hole tone and the model acoustic frequencies has any effect on flow ingestion and discharge of the model slag underneath the nozzle nose.

Specific remaining tasks required to accomplish these objectives include:

1) Develop and implement instrumentation required to determine if there is a periodicity to water ingestion and ejection and measure only the frequency.

2) Implement boroscope viewing and recording of the activity of the simulated slag pool underneath the nozzle nose.

3) Conduct test program over previously established ranges of water flow rates and model pressures with and without water flow.

Intermediate Term Plan - 2nd & 3rd Quarter, 1995.

RSRM NBR Inhibitor Dynamics Model - There has been an expressed interest by the RSRM Chief Engineer's Office in continuing the inhibitor dynamics testing with cold flow models. It is well established that there are significant interactions between inhibitor hole tone frequencies and RSRM acoustic modes which increase the amplitude of dynamic pressure oscillations. Other investigators have analyzed the problem and some cold flow testing has been done, but not with models that are properly scaled to RSRM such that application of results to RSRM is straight forward. The development of cold flow models and correlating analytical models will give MSFC the capability to evaluate in a timely manner the effect of material property and design changes on the potentially critical issue of thrust oscillation.

Specific test objectives for the proposed near term tests of interest include:

1) Demonstrate ability to achieve tuning condition between inhibitor edge tone frequency and model longitudinal modes through the use of empirical models to design inhibitors and set test conditions.

2) Determine effect of inhibitor geometry, inhibitor material modulus and model dynamic pressure on the amplitude of the oscillating pressure component using both single and double joints and inhibitors.

3) Develop and implement instrumentation to measure the frequency (and amplitude if possible) of the NBR inhibitor vibration.

4) Develop analytical model based on measured critical Strouhal numbers for scaled model geometry that is applicable to full scale RSRM and can be used to gage inhibitor height, thickness and material modulus changes on the amplitude of the pressure oscillations.

    Specific tasks to be accomplished include:

1) Conduct inhibitor tuning tests with thick and/or aluminum inhibitors to determine Strouhal numbers and develop empirical models capable of predicting hole tone and acoustic mode resonance. Modify cold flow model to enable testing to simulate both center and aft RSRM joints and inhibitors.

2) Determine effect of inhibitor geometry, material modular and dynamic pressure on the amplitude of the oscillating chamber pressure for deformed flexible inhibitors scaled to RSRM. Develop instrumentation to enable measurement of the frequency of flexible inhibitor dynamic motions.

<u>Longer Term Plan - Late 1995, 1996.</u>

<u>RSRM 10% Scale Full Length Porous Wall Model</u> - A 10% scale model of the RSRM including all segments with wall mass addition and the nozzle can be readily adapted from an existing model configured to ASRM zero burn time geometry. The porous liners could be changed to represent any RSRM burn time. The porous wall RSRM model could then be used to evaluate the static and dynamic environments of interest as related to specific motor upgrades involving both design and material changes. Also, the model would enable the evaluation of specific unanticipated concern issues as they arise on a short schedule response basis.

1) <u>Inhibitor Dynamics</u> -- The coupling between unsteady flow phenomena at the NBR inhibitors and chamber acoustics would be evaluated at all field joints at various burn times. Frequency coupling and dynamic pressure amplitude enhancement would be investigated with inhibitor geometry and stiffness variations. Results could be scaled directly to RSRM and used to evaluate inhibitor design and/or material changes and improvements under consideration.

2) <u>Insulation Environments</u> -- The change to asbestos-free insulation will warrant the development of higher confidence levels in the thermal and erosion environments for all areas in the motor. Zones of separated flow in the motor at various burn times create uncertainties in the environment which can be measured with heat flux gages in the simulated insulation surface. This data in terms of heat transfer coefficients can be scaled directly to the full scale motor.

3) <u>Nozzle Extension Performance</u> -- The model nozzle can be configured to represent the proposed nozzle extension and various extension geometries (conical and contoured) can be evaluated on the basis of maximum thrust coefficient; including comparison of thrust coefficients for both the extended nozzle and the existing nozzle.

Specific tasks to be accomplished would include:

1) Install 10% SRM Model, as is, and verify basic design approach, operation and instrumentation of the large scale porous wall model.

2) Design and manufacture new porous liners and nozzle for RSRM geometry and joint locations for selected burn time(s). Conduct basic checkout testing including instrumentation.

3) Conduct inhibitor dynamics tests with all three joints at selected burn times. Test instrumentation would be comprehensive to include evaluation of local internal environments (heat flux gages) as well as nozzle performance (pressure taps).

<u>References:</u>

1) RSRM 6.5% Scaled Slag Ejection Tests, Pretest Report, ERCI/HSV-TR94-01, February 1994.

2) Thermal/Flow Modeling Developed in Support of the RSRM, AIAA Large Solid Rockets: Advances Through Experience, Thiokol & ERC, Inc., October 4-6, 1994.

3) RSRM NBR Inhibitor Dynamics Model, Objectives/Requirements, ED31, ERC, December 2, 1994.

4)   RSRM NBR Inhibitor Dynamics Model, Extended Test Plan, ERC, Inc., January 18, 1995.

ASRM Igniter Exhaust Port Model Analysis

Plans were made to use the Checkout Model 538 in a special test series to evaluate the discharge coefficients of the ASRM Igniter Exhaust Ports. A special test plate was to be mounted between spool pieces that would contain various hole configurations to duplicate both the circular and the oval port holes in the aft dome closure of the igniter case. Information on the geometry of the aft closure and port holes was obtained from Aerojet and used to revise ERC drawing H5203 which includes the forward ASRM segment and igniter geometry. This information was used to design the test plates for the cold flow model.

A pretest report for the ASRM Igniter Exhaust Port Tests was written by ERC and is included in this appendix. The scope of this work included calculations of pressure drop across the test plates which had ASRM full scale igniter ports. The flow conditions necessary to match the full scale Reynolds Number were also calculated. From these it was possible to calculate the flow conditions to be run in the Checkout Model to match the full scale Reynolds Number. These calculations were included in the pretest report. An initial version of the pretest report was given to NASA/MSFC personnel for review and comment received back were incorporated into the final version of the report which were distributed to NASA/MSFC personnel.

Experimental data for the ASRM Igniter Exhaust Port Model was transferred via modem from the NASA/MSFC VAX to the 486 computer at ERC. This data was examined for outlying data points and was then analyzed. The data was used to determine a discharge coefficient for both the circular and elliptical sharp edged holes as well as the chamfered circular and elliptical holes. The discharge coefficient for each hole was plotted as a function of Reynolds Number. A number of curve fits were tried on the data with the most usable being a log-log fit. This log-log curve fit was used to determine the discharge coefficient at the full-scale Reynolds Number for the square edged circular and elliptical holes. An area weighted average was then determined for the full scale igniter with one circular hole and eleven elliptical holes. The value of this average was 0.9042. The plots of the data, included here as Figures 12 and 13, and the area weighted discharge coefficient were given to D. Bacchus, ED34.

Figure 12. ASRM Ignitor Discharge Port Tests
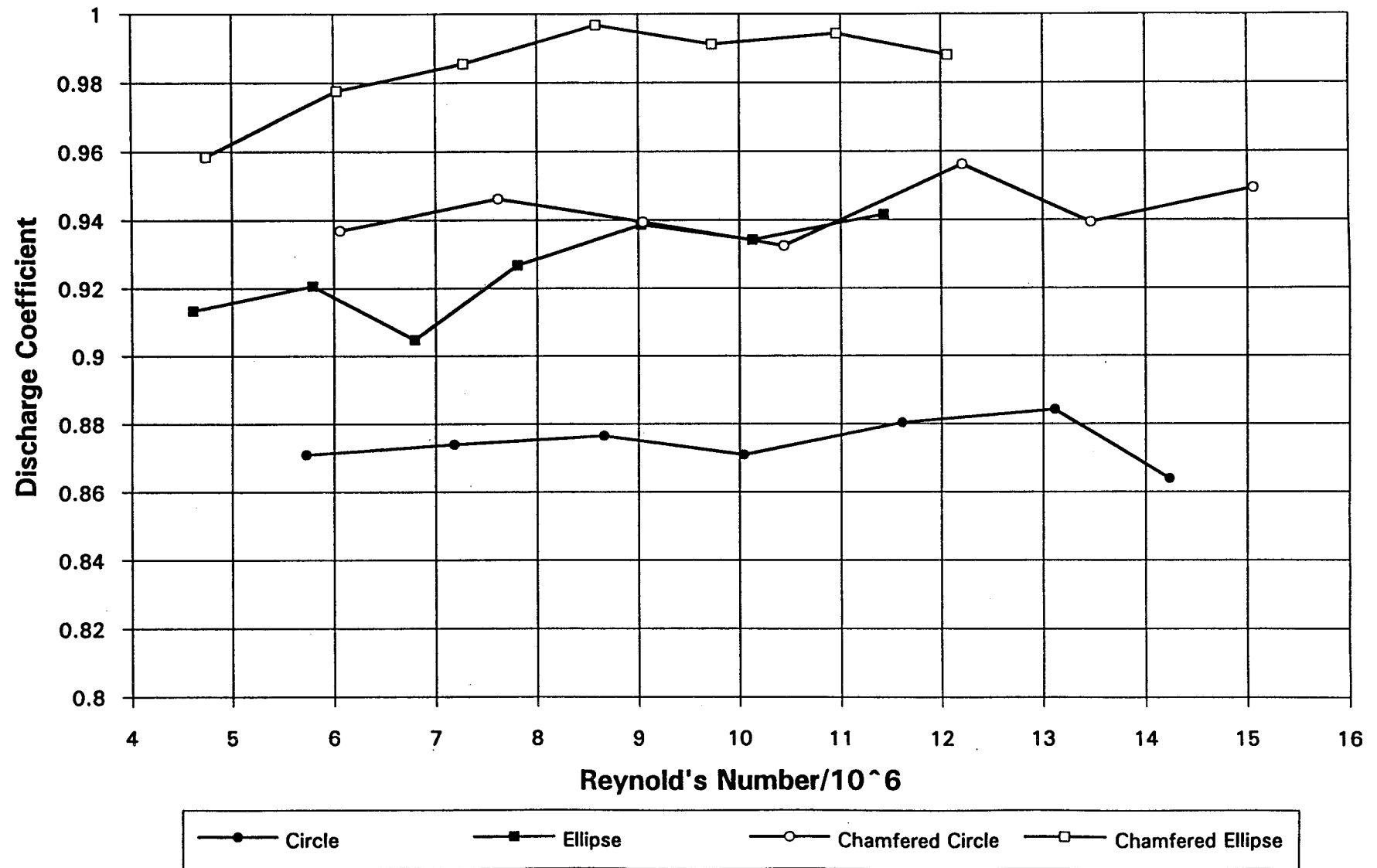
Figure 13. ASRM Ignitor Discharge Port Tests
Log-Log Curve Fit

Discharge Coefficient vs. Reynold's Number/10^6
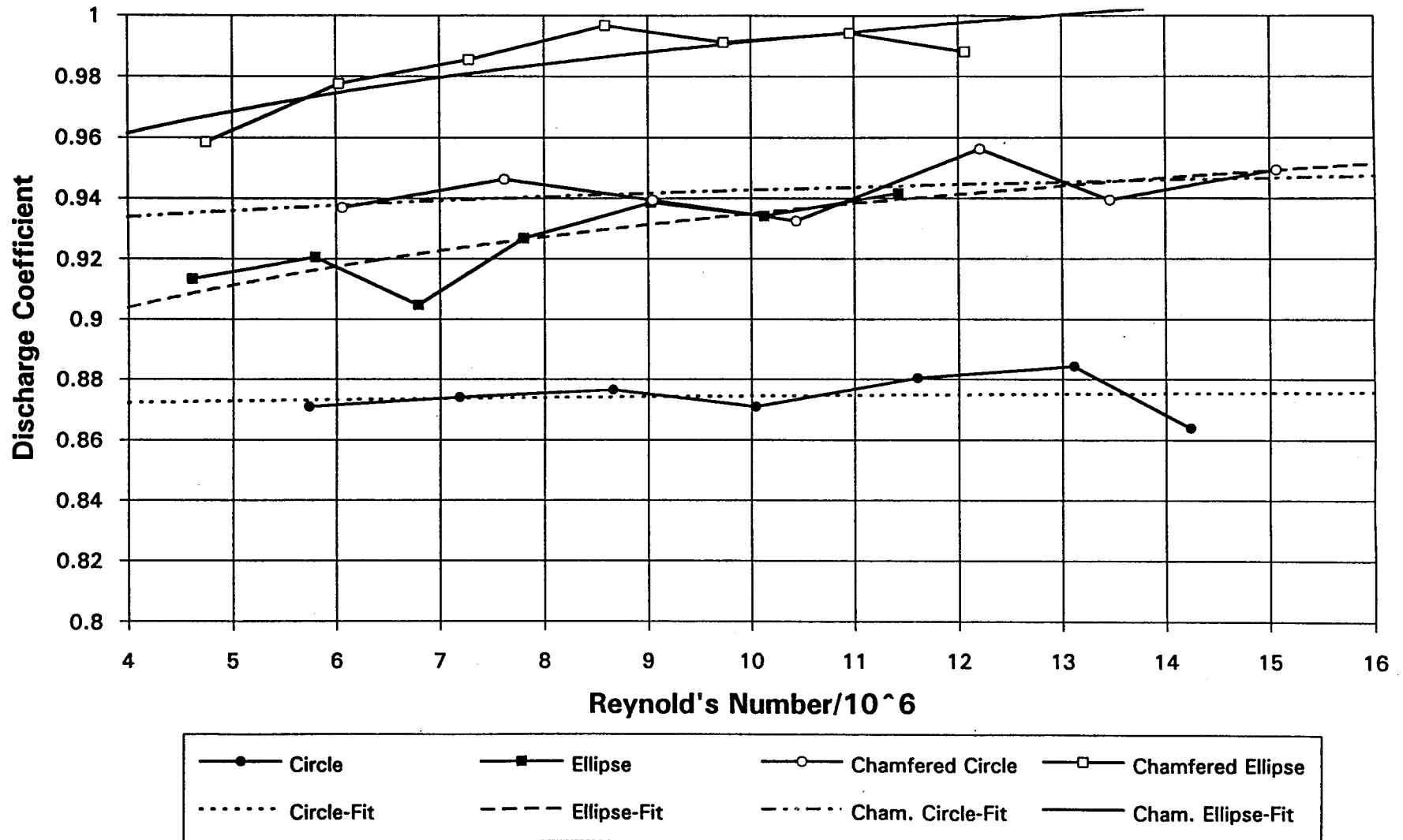
PRELIMINARY

PRETEST REPORT

ASRM IGNITER DISCHARGE PORT FLOW TESTS

17 June 1993

Prepared for:
National Aeronautics and Space Administration
George C. Marshall Space Flight Center
Marshall Space Flight Center, AL 35812

Contract NAS8-39095

Prepared by:
ERC, Incorporated
Huntsville Operation
555 Sparkman Drive, Suite 1622
Huntsville, AL 35816

PREFACE

This report was prepared by the Huntsville Operation of ERC, Incorporated for the Fluid Dynamics Division of the Science and Engineering Directorate, George C. Marshall Space Flight Center, National Aeronautics and Space Administration. This effort was performed under Contract NAS8-39095 with David L. Bacchus serving as the Contracting Officer's Technical Representative.

The ERCI contributors to this report are David C. Purinton, who will serve as Performance Data Analyst, and R. Harold Whitesides, who serves as Project Engineer. The NASA/MSFC Test Engineer will be Jack Hengel.

TABLE OF CONTENTS

LIST OF TABLES

LIST OF FIGURES

1.0 INTRODUCTION

In past test firings of the ASRM Igniter the internal pressure of the igniter was higher than what had previously been predicted. It has been suggested that the higher pressure is a result of the discharge coefficient of the sharp edged, oval discharge ports being lower than the value used in the prediction calculations. In order to have a more accurate value of the discharge coefficient to use in the pressure predictions a series of tests have been proposed to measure the discharge coefficient experimentally.

These tests will utilize the Solid Rocket Motor Air Flow Test Equipment (SRMAFTE). This facility is capable of testing various solid rocket motor model configurations over a wide range of chamber pressures and flowrates and is capable of full scale RSRM Reynolds Number simulation of a 10% scale model. This test will use Checkout Model 538 which is a 10% scale RSRM model. Test plates incorporating both circular and oval holes will be placed between spool pieces in the model and the pressure drop and flowrate through the plates will be measured in order to determine the discharge coefficient of the igniter discharge ports.

2.0 OBJECTIVES

The primary objective of the ASRM Igniter Discharge Port Flow Tests is to measure the discharge coefficient of the ASRM full scale igniter discharge ports. This will be accomplished by measuring the pressure drop across a test plate with either a circular or an elliptical orifice like those present in the ASRM igniter. The mass flow rate through the orifices will also be measured so that the discharge coefficient can be determined.

A secondary objective of the tests will be to evaluate the effect of possible improvements to the design of the circular and elliptical holes in order to improve the discharge coefficient. These improvements could be such things as chamfering or rounding the upstream edges of the discharge ports.

Objective 1: Determine the discharge coefficient of the full scale ASRM Igniter discharge ports.

By measuring the pressure drop and the mass flow through full scale discharge ports of the ASRM igniter it will be possible to determine the discharge coefficient of both the circular and the elliptical ports. A Reynolds number scan

can also be done in order to determine the variance of the discharge coefficients with Reynolds number.

Objective 2: Evaluate the effect of possible improvements to the discharge ports such as chamfering or rounding.

By placing various discharge port configurations in the model for testing, it will be possible to determine possible improvements to the discharge coefficients of the igniter ports. Test plates can be made with discharge ports which have chamfered or rounded ports. By measuring the pressure drop and mass flow rate through these ports it will be possible to evaluate any improvements.

3.0 TEST REQUIREMENTS

The test requirements for the ASRM Igniter Discharge Port Flow Tests were developed using Reynolds number similarity between the full scale motor and the cold flow model. The test prediction calculations are shown in Table 1 and Table 2 gives a detailed test matrix. A chamber pressure and mass flow rate were determined for both the circular and elliptical discharge ports in order to match the full scale Reynolds number of the ASRM igniter. In order to apply the results to a wider range of cases, tests will also be run over a range which goes from slightly below full scale Reynolds Number to over 200% of the full scale Reynolds Number.

It should be noted that the minimum mass flow rate for the Checkout Model 538 was 20 lbm/sec during the checkout testing of the facility. The mass flow rates to match the full scale Reynolds Number are less than this value. For this reason the calculations in Table 1 go well beyond the conditions needed to match the full scale Reynolds Number.

These tests can be run in either Mode "A" or Mode "B". Mode A refers to the mode of operation in which the four metering nozzles are located in the manifold arms. These metering nozzles are absent in Mode B. These tests can be run in either Mode A or Mode B because the flowrates and pressures are such that the metering nozzles will not be choked.

The spool piece order of 3-2-1 will allow the test plate to be placed between spool pieces #2 and #1. This will allow both the pressure upstream and downstream of the test plate to be measured relatively closely to the plate and minimize test assembly time.

4.0 FACILITY and MODEL DESCRIPTION

The Solid Rocket Motor Air Flow Test Equipment (SRMAFTE) Phase II configuration is shown in Figure 1. The air storage for the SRMAFTE consists of eight storage tanks having 9100 cubic feet of storage capacity. This air supply is a pressure blowdown system which is valved through the test model to the atmosphere. The inlet air is filtered through a bonded fiberglass cylindrical canisters filter that is designed for a maximum pressure of 1960 psig and a maximum flowrate of 320 lbm/s. The ROV isolation valve is downstream of the filter and is rated for a maximum pressure of 1960 psig. This valve can be shut down at maximum speed in case of emergency. The actual test model inlet pressure is controlled by a quiet trim control valve. The valve uses a hydraulic operator for actuation and will hold the test model stagnation pressure constant for each test run. Downstream of the quiet valve, a pilot operated relief valve is located to discharge 100% of the flow operating at 1320 psia. The flowrate will be metered by a venturi, which is stationed downstream of the quiet valve. The mass flow through the system is ducted through the test model diffuser. Before the air reaches the atmosphere, it is ducted through an 85db Silencer which is located outside of building 4777.

The Checkout Model 538 consists of three model chamber spool pieces with a converging/diverging nozzle. The nozzle throat and exit diameters are scaled to 10% RSRM/ASRM size at motor ignition. The spool pieces numbered 1 and 3 are interchangeable. Figure 2 describes the test names of specific model components and their axial stations. All Test Requirements will use this model terminology to describe various calculations at different axial stations along the flow of the Checkout Model 538. It should be noted that Figure 2 shows the test equipment set-up for Mode A although the tests can be run in either Mode A or Mode B. Figure 2 also shows the location of the test plate between spool pieces #2 and #1. This test plate represents full scale discharge orifices and thickness as shown on ERC, Inc. drawing H5203-1C. The circular hole is the one present at the center of the igniter where as the oval holes are spaced around the aft dome of the igniter.

5.0 INSTRUMENTATION

The ASRM Igniter Discharge Port Flow Tests will have approximately 12 model measurements, which are located axially and circumferentially throughout the model at key locations (or stations) in the model. These measurements include total and static pressures as well as bulk temperatures. A detailed listing

of Instrumentation is shown in Tables 4 - 6. Figure 3 shows the model instrumentation location by station location and circumferential location both of which are used in the instrumentation labeling scheme to quantify the measurement.

A total of 12 test measurements will be taken for each test and are broken down into individual measurements in the following list:

7   Static Pressure Taps
1   Total Pressure Probes
4   Temperature Probes
_____
12   Total

This listing provides the number of measurements required to complete the test objectives. Ranges of all of the measurements are provided in Tables 4 - 6.

Pressure data will be measured using absolute pressure transducers with appropriate ranges connected to an electronic scanning system. This system is a 256 channel unit which has modules that can record ranges of differential and absolute pressures. These measurements will be recorded as digital test data on a Hewlett Packard recorder and will be translated into engineering units. The recording method will use frames of averaged data per test, at steady state, which is in turn read into the Aero Fluids Analysis System (AFAS) VAX. The AFAS database measurement label standard indicates specific formats by which an instrumentation label can be determined. Table 7 shows the instrumentation label format that will be used for ASRM Igniter Discharge Port Flow testing.

6.0 PERFORMANCE REDUCTION PROGRAM

The model performance data will be transferred from the NASA AFAS VAX to ERCI's Tri-Star 486 computer via a Hayes modem. This data, in turn, will be "read" into EXCEL 4.0, which is a spreadsheet program. The data will then be statistically analyzed for outlying points, averaged and used for calculations to evaluate the system performance.

A performance program will be developed specifically for the ASRM Igniter Discharge Port Flow testing. The input data will be in terms of averaged frames of data over a period of time at steady state conditions. Ten to twenty frames of data per measurement, per test, is expected. Sometimes the framed data has a value that is inconsistent with the other values in a particular steady state frame. This anomaly could be caused by a number of reasons, however, in order to have

an averaged frame that represents steady state, all anomalies or "outliers" will have to be deleted before an averaged value can be determined from one set of values in a frame. Therefore, the performance program will include a statistical algorithm to delete any extreme points from the steady state data. Extreme points are defined as a point that does not fall in the range of ω/σ or range divided by the population. The algorithm compares each observation with the nearest point in a small sample of data. If one observation is not statistically close to the rest of the sample data, the point is removed. This method is described to be a valid method for a small population of data.[1] The data will then be averaged and used in the 1-D equations in Table 3 to describe characteristics of the flow through the required pressure ranges.

The program will use one-dimensional equations as shown in Table 3. Specific calculations that will be made include local Mach numbers, total pressures, static pressures, total temperatures, and local velocities. In addition, for the ASRM Igniter Discharge Port Tests, Reynolds Number and discharge coefficient will be calculated. Excel 4.0 will be utilized to manipulate the test data. EXCEL 4.0 operates in a windows environment and utilizes a spreadsheet to manipulate data. This software has proven to be powerful in program customization and graphical results. The EXCEL 4.0 graphics package will provide excellent graphical displays of the results.

Computational Fluid Dynamic (CFD) calculations will also accompany the 1-Dimensional performance calculations, since 3-Dimensional effects are present around the oval discharge ports.

---

[1]Dixon, Wilfred J. and F. J. Massey, Jr. Introduction to Statistical Analysis, McGraw-Hill, Inc., New York: 1969.

Table 1. ASRM IGNITER DISCHARGE PORT TESTS - MODE A or B

Constants:	
Temperature (Deg. R):	530
Gamma:	1.4
Viscosity (lbm/ft sec):	1.24E-05
Gas Const. (lbf ft/lbm R):	53.353

Reynold's Number Match

P1:	119.47	psia
Mass Flow (circle):	12.68	lbm/sec
Mass Flow (ellipse):	8.60	lbm/sec

Note: P1 is upstream of plate in Spool Piece #3
P2 is downstream of the plate in Spool Piece #1.

Hole Type:	**Circle**	Area (sq. in.):	5.11
Diameter (in.):	2.55	Char. Len. (in.):	2.55
		Cd:	0.9

Hole Type:	**Ellipse**	Area (sq. in.):	3.46
Length (in.):	2.786	Char. Len. (in.):	1.93
Width (in.):	1.393	Cd:	0.9

Pman	P1	P2	Mass Flow	Delta P	Re#
psia	psia	psia	lbm/sec	psid	***
100	100	14.70	10.616	85.30	5.14E+06
125	125	14.70	13.270	110.30	6.43E+06
150	150	30.15	15.924	119.85	7.71E+06
175	175	35.17	18.578	139.83	9.00E+06
200	200	40.20	21.232	159.80	1.03E+07
225	225	45.22	23.886	179.78	1.16E+07
250	250	50.25	26.540	199.75	1.29E+07
275	275	55.27	29.194	219.73	1.41E+07
300	300	60.30	31.849	239.70	1.54E+07
325	325	65.32	34.503	259.68	1.67E+07
350	350	70.35	37.157	279.65	1.80E+07

Pman	P1	P2	Mass Flow	Delta P	Re#
psia	psia	psia	lbm/sec	psid	***
100	100	14.70	7.202	85.30	3.90E+06
125	125	14.70	9.002	110.30	4.88E+06
150	150	14.70	10.803	135.30	5.85E+06
175	175	14.70	12.603	160.30	6.83E+06
200	200	14.70	14.403	185.30	7.80E+06
225	225	14.70	16.204	210.30	8.78E+06
250	250	34.09	18.004	215.91	9.75E+06
275	275	37.49	19.805	237.51	1.07E+07
300	300	40.90	21.605	259.10	1.17E+07
325	325	44.31	23.406	280.69	1.27E+07
350	350	47.72	25.206	302.28	1.37E+07

Full Scale Ignitor Properties	
Chamber Pressure (psia)	2000
Chamber Temp. (Deg R):	6100
Gamma:	1.14
Molec. Wt.:	28
Viscosity (lbm/ft. sec.):	6.20E-05
Throat Velocity (ft./sec.):	3397.11
Density (lbm/cu. ft.):	0.527613

Full Scale Reynold's Numbers

Circular Hole
Re#: 6.14E+06

Elliptical Hole
Re#: 4.66E+06

Table 2. ASRM Igniter Discharge Port Test Matrix

Note: Spool Piece Order will be 3-2-1 in the direction of flow.
Test Plate between spool pieces 2 and 1.
Test to be run in Mode A or Mode B
$Cd = 0.9$

Test Condition	Manifold Press. (psia)	Chamber Press. (psia)	Mass Flow (lbm/sec)	Discharge Port Orifice
1	100.00	100.00	10.62	Circle
2	125.00	125.00	13.27	Circle
3	150.00	150.00	15.92	Circle
4	175.00	175.00	18.58	Circle
5	200.00	200.00	21.23	Circle
6	225.00	225.00	23.89	Circle
7	250.00	250.00	26.54	Circle
8	100.00	100.00	7.20	Ellipse
9	125.00	125.00	9.00	Ellipse
10	150.00	150.00	10.80	Ellipse
11	175.00	175.00	12.60	Ellipse
12	200.00	200.00	14.40	Ellipse
13	225.00	225.00	16.20	Ellipse
14	250.00	250.00	18.01	Ellipse
15	100.00	100.00	10.62	Chamfer. Circle
16	125.00	125.00	13.27	Chamfer. Circle
17	150.00	150.00	15.92	Chamfer. Circle
18	175.00	175.00	18.58	Chamfer. Circle
19	200.00	200.00	21.23	Chamfer. Circle
20	225.00	225.00	23.89	Chamfer. Circle
21	250.00	250.00	26.54	Chamfer. Circle
22	100.00	100.00	7.20	Chamfer. Ellipse
23	125.00	125.00	9.00	Chamfer. Ellipse
24	150.00	150.00	10.80	Chamfer. Ellipse
25	175.00	175.00	12.60	Chamfer. Ellipse
26	200.00	200.00	14.40	Chamfer. Ellipse
27	225.00	225.00	16.20	Chamfer. Ellipse
28	250.00	250.00	18.01	Chamfer. Ellipse

Table 3. Formulas Used in Performance Calculations

Mach Number	$$\frac{A}{A*} = \frac{1}{M}\left[\left(\frac{2}{\gamma+1}\right)\left(1+\frac{\gamma-1}{2}M^2\right)\right]^{\frac{\gamma+1}{2(\gamma-1)}}$$
Total Pressure (psia)	$$\frac{P_o}{P} = \left(1+\frac{\gamma-1}{2}M^2\right)^{\frac{\gamma}{\gamma-1}}$$
Total Temperature (Deg R)	$$\frac{T_o}{T} = 1+\frac{\gamma-1}{2}M^2$$
Discharge Coefficient	$$C_D = \frac{\text{Measured Flow Rate}}{0.53175 P_o A* \Big/ \sqrt{T_o}}$$
Reynolds Number (port)	$$Re = \frac{\rho V d_{port}}{\mu}$$

Table 4. STATIC PRESSURES

Note: Spool pieces arranged in 3-2-1 order in the direction of flow.

No.	Parameter	Location	Station	Range/Units
1	PS-LS0G	Manifold Pipe (South Leg of 8" Pipe) at 90 deg	-23.0	15 to 800 psia
2	PS-LN0U	Manifold Pipe (North Leg of 8" Pipe) at 270 deg	-23.0	15 to 800 psia
3	PS-C00A	Adapter (Aft End of 16" Dia. Section) at 0 deg	28.7	15 to 405 psia
4	PS-S10G	Model Aft (Spool Piece #1) at 90 deg	80.5	15 to 405 psia
5	PS-S10U	Model Aft (Spool Piece #1) at 270 deg	80.5	15 to 405 psia
6	PS-S30G	Model Forward (Spool Piece #3) at 90 deg	44.6	15 to 405 psia
7	PS-S30U	Model Forward (Spool Piece #3) at 270 deg	44.6	15 to 405 psia

Table 5. TOTAL PRESSURES

Note: Spool pieces arranged in 3-2-1 order in the direction of flow.

No.	Parameter	Location	Station	Range/Units
1	PT-C00N	Adapter (Aft End of 16" Dia. Section) at 180 deg	28.7	15 to 405 psia

Table 6. AIR TEMPERATURES

Note: Spool pieces arranged in 3-2-1 order in the direction of flow.

No.	Parameter	Location	Station	Range/Units
1	TAF-S10A	Model Aft (Spool Piece #1) at 0 deg	80.5	-50 to 100 deg F
2	TAF-S10K	Model Aft (Spool Piece #1) at 135 deg	80.5	-50 to 100 deg F
3	TAF-S30A	Model Forward (Spool Piece #3) at 0 deg	44.6	-50 to 100 deg F
4	TAF-S30K	Model Forward (Spool Piece #3) at 135 deg	44.6	-50 to 100 deg F

Table 7. ASRM Igniter Discharge Port Test Measurement Labels

Field 1 Quantity	-	Type	Location	Specific Location	Circumferential Location	-	Field 3 Quantity
3	-	L	N/S		A-Z	-	3
3	-	A	A/B/C/D		A-Z	-	3
3	-	H	A/B/C/D...		A-Z	-	3
3	-	M	A/B/C/D...	U/D/T	A-Z	-	3
3	-	C			A-Z	-	3
3	-	S	1/2/3		A-Z	-	3
3	-	T		T/E	A-Z	-	3
3	-	D	0/1/D/T	0/2/4/6/E/S	A-Z	-	3
3	-	F	V	U		-	3

Symbol Desciption

L = Leg
A = Arm
H = Header
M = Manifold
C = Adapter Chamber
S = Spool Piece
T = Test Model
D = Diffuser
F = Facility

N = North
U = Upstream
D = Downstream
T = Throat
E = Exit
V = Venturi
S = South for Legs/Spacer for Diffuser

* All other Symbols represent Letters

Figure 1. Solid Rocket Motor Air Flow Test Equipment

Fill Connection

Manual Ball Valve, 12 inch, 900 lb.

Manual Ball Valve, 12 inch, 900 lb.

Mixer Temperature Control, 12 inch Butterfly Valves

Mixer

Building 4777

Control Room

Filter

Carbon Steel

Stainless Steel

Manifold System

Exhaust Diffuser

Vertical Exhaust Duct

Venturi

Relief Valve

Checkout Model

Air Storage
• 9,100 Cubic Feet Storage Capacity
• 1,960 psi, Maximum

Quiet Control Valve 16 inch, 1,500 lb.

ROV Ball Valve 12 inch, 1,500 lb.

Heater
• Temperature Range: 70° F - 740° F
• Maximum Pressure: 1,960 psi

891122-6123-1350-188

Figure 2. ASRM Igniter Discharge Port Test Names of Model Components

Manifold Leg (2, typ.)

Metering Nozzle (4, typ.)   (A,B,C,D)

Test Model Throat

Diffuser Exit

Spool Piece 1

Diffuser

Test Plate

Spool Piece 2

Spool Piece 3

Test Model Exit

Adapter chamber

Diffuser Transition Duct Exit
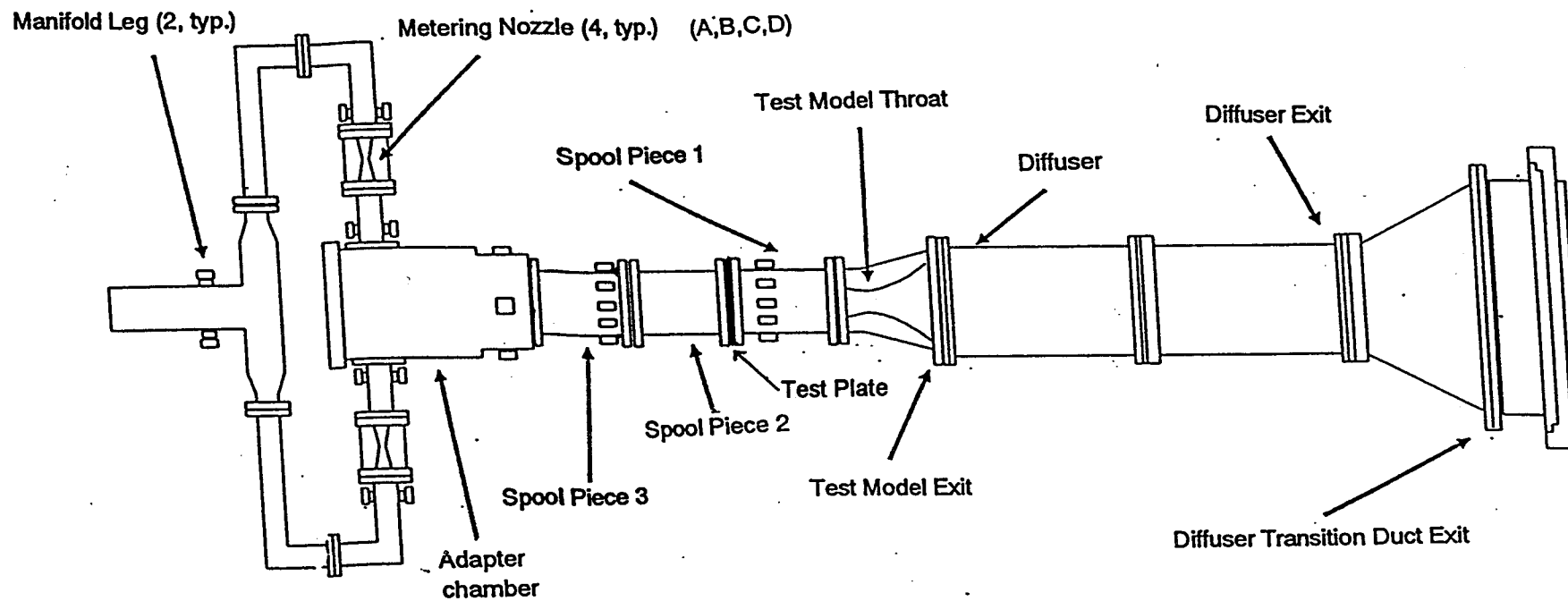
SCHEMATIC ONLY - NOT TO SCALE

MICRO CRAFT

Figure 3. Checkout Model Axial Stations and Angle Designations

LOOKING
UPSTREAM

(AFT LOOKING
FORWARD)

STATION NUMBER, INCHES
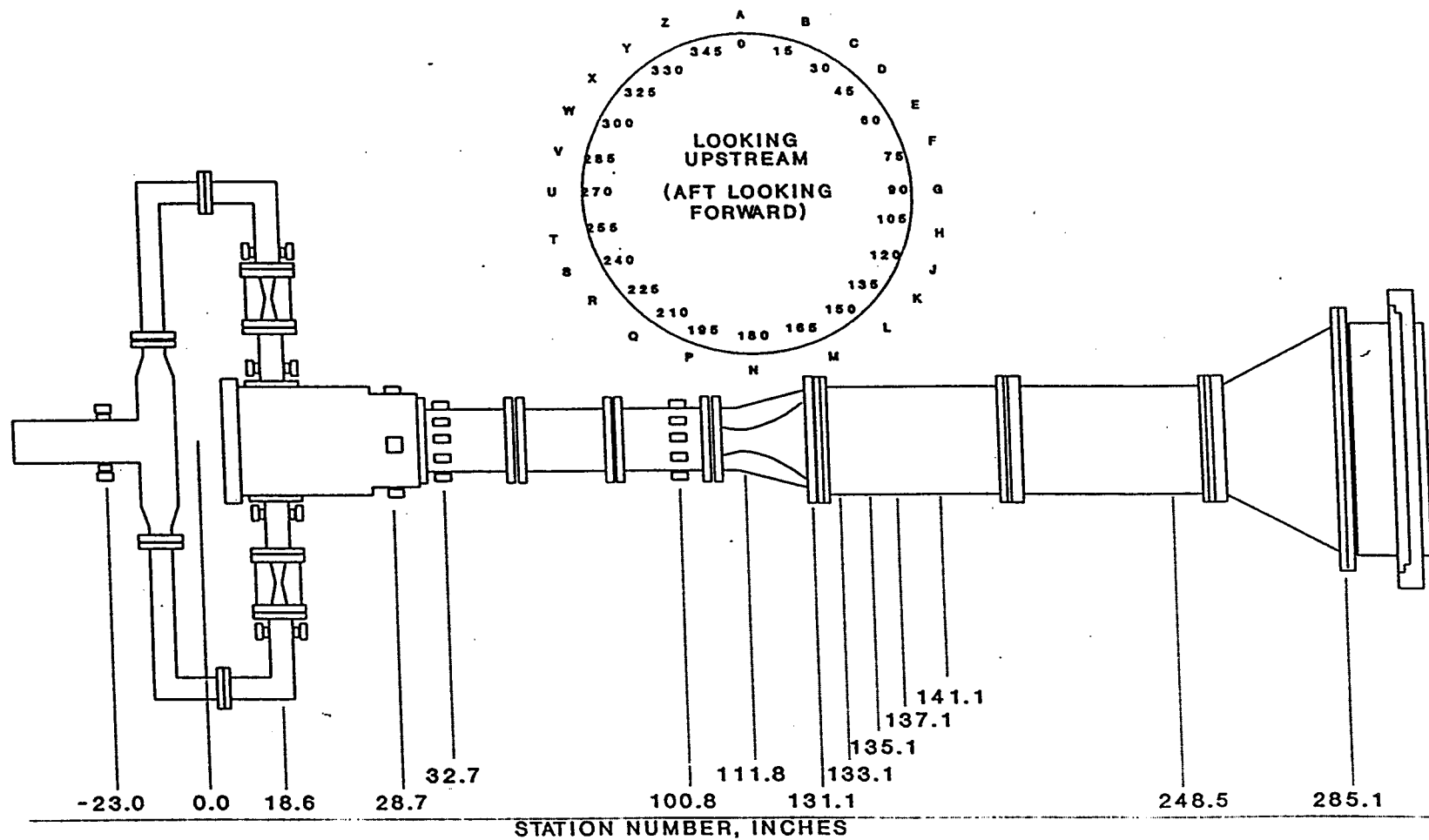
RSRM Nozzle Slag Ejection Precursor Tests Analysis

In past firings of the Redesigned Solid Rocket Motor (RSRM), both static test motors and flight motors have shown pressure anomalies primarily between 65 and 80 second burn times. These pressure anomalies result in a thrust imbalance between the solid rocket boosters (SRB) and an increase in the external tank loads. Films of the motor firings have shown the ejection of debris presumed to be slag from the motor nozzle coinciding with the pressure anomalies. The purpose of the RSRM Nozzle Slag Ejection Precursor Test was to investigate the effect that slag ejection from the RSRM nozzle has on the chamber pressure and thrust of the SRBs.

The pretest report for the RSRM Nozzle Slag Ejection Precursor Tests included the selection of instrumentation and the creation of a test matrix. Various versions of the pretest report were taken to NASA/MSFC for review by NASA/MSFC personnel and their comments were incorporated into the report.

The primary objective of the RSRM Nozzle Slag Ejection Precursor Tests was to establish the feasibility of using cold flow test techniques to investigate the effects of slag ejection from the nozzle of the full scale motor on the chamber pressure.

Test data was generated at NASA/MSFC and as it became available it was transferred via modem from the NASA/MSFC VAX to ERC. The data was then analyzed and predictions of the pressure spike were made using ERC's analytical model. These predictions were then plotted against the measured pressure spikes taken from strip charts produced at the test facility.

A review of the detailed test matrix of controlled test variables generated an interest in defining a more orthogonal test matrix to enable statistical regression analyses to be performed with the test data without incurring the liability of false correlations relative to the issue of variable interaction. The two injectors chosen were the 0.712 in. diameter, Type 2 and the 0.532 in. diameter, Type 1 injectors. Each one of these injectors was run at three different flow rates for three different model chamber pressures. These three flowrates were held constant for each chamber pressure run. In addition, the 0.712 in. diameter injector was run at the maximum flow rate which could be achieved for each of the three model pressures run. These runs totaled 21, 9 for the 3x3 matrix for the 0.532 in. dia. injector and 12 for the 3x4 matrix for the 0.712 in. dia. injector. These twenty-one runs were completed and the data analyzed. The results of the comparison between the predicted pressure spikes and the measured pressure spikes were comparable to the other test data analyzed to date.

After all the test data was generated a number of studies were performed on varying the drag coefficient and the slag density multiplier in the analysis. This was done in order to better predict the pressure spike value as a function of model pressure and water flowrate through the model. A parametric study was performed by running the analytical model over a range of values for these variables and comparing to the

experimental data. A set of values was arrived at which produced the best fit between the experimental data and the analytical model prediction. The final value for the drag coefficient was chosen as 0.5 and the slag density multiplier was selected to be 0.3.

A final report for the RSRM Nozzle Slag Ejection Precursor Tests was completed and review copies were made available to NASA/MSFC personnel. Comments were received and were incorporated into the report which was then copied and distributed. The report is included in this appendix.

FINAL REPORT

RSRM NOZZLE SLAG EJECTION PRECURSOR TEST

29 April 1994

Prepared for:
National Aeronautics and Space Administration
George C. Marshall Space Flight Center
Marshall Space Flight Center, AL 35812

Contract NAS8-39095

Prepared by:
ERC, Incorporated
Huntsville Operation
555 Sparkman Drive, Suite 1622
Huntsville, AL 35816

PREFACE

This report was prepared by the Huntsville Operation of ERC, Incorporated for the Aerophysics Division of the Science and Engineering Directorate, George C. Marshall Space Flight Center, National Aeronautics and Space Administration. This effort was performed under Contract NAS8-39095 with David L. Bacchus/ED34 serving as the Contracting Officer's Technical Representative.

The ERC, Incorporated contributors to this report are David C. Purinton, who served as Performance Data Analyst, and R. Harold Whitesides, who serves as Project Engineer. Fluid Dynamics Division personnel also contributed to model design and test planning. The NASA/MSFC Test Engineer was Jack Hengel/ED34.

TABLE OF CONTENTS

LIST OF TABLES

LIST OF FIGURES

1.0 INTRODUCTION

In past firings of the Redesigned Solid Rocket Motor (RSRM), both static test motors and flight motors have shown pressure anomalies primarily between 65 and 80 second burn times. These pressure anomalies result in a thrust imbalance between the solid rocket boosters (SRB) and an increase in the external tank loads. Films of the motor firings have shown the ejection of debris presumed to be slag from the motor nozzle coinciding with the pressure anomalies. The purpose of the RSRM Nozzle Slag Ejection Precursor Test is to investigate the effect that slag ejection from the RSRM nozzle has on the chamber pressure and thrust of the SRBs.

It should be noted that this was a precursor test. These tests obtained data so that some information on this phenomenon was available in a short amount of time. These tests utilized the Solid Rocket Motor Air Flow Facility (SAF). This facility is capable of testing various solid rocket motor model configurations over a range of chamber pressures and flowrates and is capable of full scale RSRM Reynolds Number simulation of a 10% scale model. This precursor test used Checkout Model 538 which is a 10% scale RSRM model. However, the model nozzle is not of the submerged nose type, rather it is a converging diverging nozzle scaled to 10% RSRM throat and exit diameters. The chamber diameter results in a port Mach Number of 0.24 which represents an earlier burn time than desired. However, later tests will make use of a submerged nose nozzle and a chamber diameter scaled to a burn time of approximately 70 seconds.

2.0 OBJECTIVES

The primary objective of the RSRM Nozzle Slag Ejection Precursor Tests was to establish the feasibility of using cold flow test techniques to investigate the effects of slag ejection from the nozzle of the full scale motor on motor chamber pressure. This was accomplished by measuring the pressure response in the model chamber to a liquid being injected into the model chamber and passing through the model nozzle throat.

Objective 1: Evaluate the effect of varying model chamber pressure and flowrate.

Varying the model chamber pressure allows one to see the effect of the model nozzle blockage over a range of Reynolds Numbers and Weber Numbers. This increases confidence in the analytical model and allow the results of the testing to be applied over a greater motor pressure range with more confidence.

Objective 2: Evaluate the effect of varying the fluid injection rate and velocity.

Varying the rate at which the fluid is injected into the system allows one to determine how the system reacts to blockage in the nozzle model throat as registered by the magnitude of the observed pressure spike.

The injection speed of the water at a given flowrate was also varied. This was accomplished by varying the diameter of the water injector nozzle.

Objective 3: Evaluate the effect of varying the location where the fluid is injected into the system.

Instrumentation ports were available at the upstream end of spool piece #1 and at the downstream end of spool piece #3. In the slag ejection tests the injected fluid was introduced through the instrumentation ports of the spool pieces. Because spool pieces #1 and #3 are interchangeable it allowed four possible axial locations for fluid introduction. These locations are the upstream end of spool piece #1 and downstream end of spool piece #3 with each spool piece in two locations, respectively. However, only the positions available with the spool pieces in the order of 3-2-1 were used.

The radial position of water injection was also varied. The two radial locations were the model centerline and near the model wall.

Objective 4: Experiment with a variety of different fluids to be injected into the system.

The initial slag ejection tests were carried out using water as the injected fluid. However, other fluids may be tried at a later date, such as ethylene glycol, water based gels, or light oils. The different fluids would be tried in order that a Weber number match might be obtained between the RSRM full-scale motor and the RSRM Nozzle Slag Ejection Model while at the same time matching Reynolds Number or another simulation parameter.

Objective 5: Develop a means to measure the injected fluid velocity at the nozzle exit plane.

The purpose of measuring the injected fluid velocity at the nozzle exit plane is to enable the thrust increase due to slag ejection to be calculated. An attempt was made to measure the trajectory of the fluid through the nozzle exit plane by the use of a high speed camera in the model nozzle diffuser. Analysis of a fluid droplet position versus time would enable the velocity of the fluid to be found.

3.0 TEST REQUIREMENTS

The test requirements for the RSRM Nozzle Slag Ejection Precursor Tests were developed using various similarity parameters. The test requirements are summarized in Table 1 and Table 2 gives a detailed test matrix. The first test conditions were drawn up by matching the Reynolds number of the full scale RSRM motor and the Checkout Model 538. In order to obtain the same percentage throat blockage it is necessary to calculate a water injection flowrate. The water flowrate is dependent on the chamber pressure of the model. Once this dependency was calculated, it was possible to arrive at test conditions that would match the full scale RSRM motor. In order to apply the

results to a wider range of cases, tests were also run at 25%, 50%, and 75% of the full scale RSRM motor Reynolds Number.

The next test case in Table 1 was developed using a dynamic similarity parameter. In this case, the ratio of the air momentum to water momentum is set equal to the ratio of combustion gas momentum to slag momentum. By doing this it is possible to calculate the chamber pressure required in the model.

Thirdly, a Weber number simulation was calculated. As was the case for the Reynolds Number, test conditions were calculated to obtain a Weber Number match. Because the test condition required to match the Weber Number are above the facility performance capabilities, a modified Weber Number match was made. This modified Weber Number is identical to the true Weber Number except for the omission of the length parameter. With the length parameter removed it becomes possible to run the calculated test conditions.

The spool piece order of 3-2-1 allows injection of water at model station at two axial locations. The main test location was in the forward end of spool piece #1 and limited testing was done at the secondary location at the aft end of spool piece #3. It should also be noted that the radial position of fluid injection was varied among two locations, the model centerline and near the model wall.

4.0 FACILITY and MODEL DESCRIPTION

The Solid Rocket Motor Air Flow Facility (SAF) Phase I configuration is shown in Figure 1. The air storage for the SAF consists of eight storage tanks having 9100 cubic feet of storage capacity. This air supply is a pressure blowdown system which is discharged through the test model to the atmosphere. The inlet air is filtered through a bonded fiberglass cylindrical canisters filter that is designed for a maximum pressure of 1960 psig and a maximum flowrate of 320 lbm/sec. The ROV isolation valve is downstream of the filter and is rated for a maximum pressure of 1960 psig. This valve can be shut down at maximum speed in case of emergency. The actual test model inlet pressure is controlled by a quiet trim control valve. The valve uses a hydraulic operator for actuation and will hold the test model stagnation pressure constant for each test run. Downstream of the quiet valve, a pilot operated relief valve is located to discharge 100% of the flow operating at 1320 psia. The flowrate will be metered by a venturi, which is stationed downstream of the quiet valve.

Next, the flow is split into the two facility supply legs, as shown in Figure 1. These facility supply legs each feed two manifold arms, for a total of four arms. The pressure sensing location for the quiet valve feedback control is located in these two facility supply legs. Each one of these manifold arms, or header pipes, as shown in Figure 2, includes a metering nozzle. With the metering nozzles installed the facility operates in Mode "A". The facility has the capability to operate in a Mode "B" where the four metering nozzles are removed. The installation of the metering nozzles

3

ensures a constant flowrate through the system which is independent of any nozzle blockage. This series of tests was conducted in Mode "A". The manifold arms feed into an adapter chamber at the head end of the model. From the adapter chamber the flow is passed through the model which is described below.

The mass flow through the system is ducted to atmosphere through the test model diffuser. The diffuser enables the test model to operate at full scale booster nozzle expansion ratio without flow separation. Before the air reaches the atmosphere, it is ducted through an 85 dB Silencer which is located outside of building 4777. For this model an acrylic section of diffuser was added at the nozzle exit. This was done in order to make a visual record of the fluid exiting the nozzle exit in order to measure the velocity of the fluid in this plane.

The Checkout Model 538 consists of three model chamber spool pieces with a converging/diverging nozzle. The nozzle throat and exit diameters are scaled to 10% RSRM/ASRM size at motor ignition. Also, the nozzle includes a conical exit section with the full RSRM/ASRM expansion ratio as shown in Figure 3. The spool pieces numbered 1 and 3 are interchangeable. This design feature was used to vary the location of fluid injection into the system (Objective 3). Figure 2 shows the water injector in the aft location of the model port. After passing through the model port the flow exits the model through the converging/diverging nozzle. All Test Requirements use this model terminology in Figure 2 to describe various calculations at different axial stations along the flow of the Checkout Model 538.

The injector enabled a known quantity of fluid to be injected into the model chamber upon operator command using a Marotta valve. The injector was connected to its own high pressure reservoir which enabled it to operate in the high pressure environment of the model chamber. Two injector types and three sizes were used for these tests. The type 1 injector is an 0.75 inch diameter tube with a contraction section on the end which ends in an orifice of 0.532 or 0.581 inches in diameter. The type 2 injector has 0.75 inch diameter tube with a expanded section of increased diameter followed by a contraction section terminating in an orifice of 0.712 inch diameter. These two injectors are shown in Figure 4.

5.0 INSTRUMENTATION

The RSRM Nozzle Slag Ejection Precursor Tests had approximately 40 model measurements, which were located axially and circumferentially throughout the model at key locations (or stations) in the model. These measurements included total, static and dynamic pressures as well as bulk temperatures. A detailed listing of instrumentation is shown in Tables 4 - 7. Figure 5 shows the model instrumentation location by station location and circumferential location both of which are used in the instrumentation labeling scheme to quantify the measurement.

A total of 40 test measurements were taken for each test and are broken down into individual measurements in the following list:

21   Static Pressure Taps
7   Total Pressure Probes
4   Dynamic Pressure Gauges
8   Temperature Probes
40 Total Measurements

Pressure data was measured using absolute pressure transducers with appropriate ranges connected to an electronic scanning system. This system is a 256 channel unit which has modules that can record ranges of differential and absolute pressures. These measurements were recorded as digital test data on a Hewlett Packard recorder and will be translated into engineering units. The recording method used frames of averaged data per test, at steady state, which was in turn read into the Aero Fluids Analysis System (AFAS) VAX. The AFAS database measurement label standard indicates specific formats to which an instrumentation label can be determined. Table 8 shows the instrumentation label format that was used for RSRM Nozzle Slag Ejection testing. Dynamic pressures were recorded on a strip chart.

In addition to the above instrumentation, a high speed camera set-up was employed to record the characteristics of the injected fluid just downstream of the model nozzle exit plane. Unfortunately, the visual record did not allow the determination of the velocity of the injected fluid as it exited through the model nozzle. The velocity of the water ejected from the nozzle was too high for the camera set up to capture an image from which velocity could be obtained.

6.0 PERFORMANCE REDUCTION PROGRAM

The model performance data was transferred from the NASA AFAS VAX to ERC, Incorporated's Tri-Star 486 computer via a Hayes modem. This data, in turn, was "read" into EXCEL 4.0, which is a spreadsheet program. The data was not statistically analyzed for outlying points because it was determined that the data obtained was of a good enough quality not to warrant the statistical deletion of outlying points. The frames of data were averaged to a single value and this one value was used for calculations to determine the pressure perturbation level and model operating conditions.

A performance program was developed specifically for the RSRM Nozzle Slag Ejection testing. The input data was in terms of averaged frames of data over a period of time at steady state conditions. Ten frames of data per measurement, per test, was obtained. The data was averaged and used in the 1-D equations in Table 3 to describe characteristics of the flow through the required pressure ranges.

The analysis used one-dimensional equations as shown in Table 3. Specific calculations made include local Mach numbers, total pressures, static pressures, total temperatures, local velocities and flowrates. Predicted pressure spike amplitudes were compared with measured pressure amplitudes. The EXCEL 4.0 graphics package was used to provide graphical displays of the results.

A Slag Ballistics Model was used to calculate 1) the relationship between the quantity of slag ejected through the nozzle and the amplitude of the pressure perturbation and 2) the additional thrust due to the ejection of fluid through the nozzle. This additional thrust from the fluid ejection is due to the momentum that the fluid acquired as it passed through the nozzle. A more detailed description of the Slag Ballistics Model is given in the following section.

7.0 SLAG BALLISTICS MODEL

The following is a description of the Slag Ballistics Model which calculates the effect of slag ejection through the nozzle on motor performance. The analysis takes an input pressure versus time history and calculates the slag which is required to be ejected through the nozzle in order to produce the input pressure profile. The analysis has also been adapted for other uses including the prediction of pressure perturbations due to water injection measured with this model.

The analysis is actually two separate programs. The first program is a FORTRAN program which takes the pressure versus time history and predicts the throat area versus time needed to produce the given pressure history. This program solves the continuity equation for the solid rocket motor including the chamber mass storage terms. Thus, the mass produced in the motor is equal to the mass ejected from the motor in addition to the mass stored in the motor to produce the pressure perturbation and fill up the free volume produced as the propellant burns. The equation solved is actually the differential equation form of the continuity equation. Along with the pressure versus time data, inputs to this program include the motor conditions at the time of the pressure perturbation. These conditions include the propellant density, burn rate, initial volume, Cstar, gas temperature, and a surface area versus web thickness table.

Mass Generated = Mass Ejected + Mass Stored

$$dm_g/dt = dm_D/dt + \{P_c(dV/dt) + V(dP/dt)\}/RT$$

$$dm_g/dt = \text{Rate of mass generation}$$

$$dm_D/dt = \text{Rate of mass discharge}$$

$$\{P_c(dV/dt) + V(dP/dt)\}/RT = \text{Rate of mass storage}$$

$$P_c = \text{Motor chamber pressure}$$

$$(dV/dt) = \text{Rate of change of motor free volume}$$

$$V = \text{Motor chamber volume}$$

$$(dP/dt) = \text{Rate of change of motor chamber pressure}$$

$$R = \text{Ideal Gas Constant}$$

$$T = \text{Gas temperature}$$

$$dm_D/dt = A_{t_{effect}} P_c / C^*$$

$$A_{t_{effect}} = \text{Effective throat area accounting for blockage effect}$$

$$C^* = \text{Cstar}$$

Next, the output from the FORTRAN program is input into an Excel 4.0 spreadsheet which has been set up to perform the remainder of the necessary calculations and plot any information needed in a graphical form. The information passed to the Excel spreadsheet includes the chamber pressure versus time and the throat area versus time. A nozzle blockage area is computed from the effective throat area versus time by subtracting it from the nominal throat area without blockage for the motor at the appropriate times.

$$A_b = A_{t_{nominal}} - A_{t_{effect}}$$

$$A_b = \text{Blockage area}$$

$$A_{t_{nominal}} = \text{Nominal throat area}$$

The maximum throat blockage is now input into a trajectory calculation to determine the speed of the slag being ejected from the motor nozzle. A sphere of frontal area equal to the maximum throat blockage is flown down the nozzle from the nose tip plane to the exit plane. In order to make these calculations it is necessary to know the conditions through the nozzle. These conditions are found by using compressible, isentropic, one-dimensional flow equations. The area ratios at a number of nozzle locations are used to calculate the gas velocity, Mach number, density, temperature and pressure at these same locations.

In order to calculate the weight of the sphere it is treated as a cloud of slag. The density of this slag cloud (33 lbm/cu. ft.) is set equal to 0.3 times the density of molten Aluminum Oxide (110 lbm/cu. ft.). This value was chosen after work with the cold flow model was performed and this value was found to produce the best pressure perturbation predictions for that work. A drag coefficient was also needed for the sphere. A value of 0.5 was used, again this value being finalized after predictions were compared with cold flow testing data. This value is also representative of a sphere at high Reynolds number. The values 0.3 and 0.5 for the slag cloud density multiplier and the drag coefficient were arrived at by correlating the prediction made by this program with actual results obtained during the cold flow testing at NASA/Marshall Space Flight Center.

The flight of the slag cloud through the nozzle is dependent upon its speed in relation to the gas flow in the nozzle. In order to calculate the slag cloud velocity the drag on the sphere is needed. However, the drag force is dependent on this velocity differential. The iterative solving capability of Excel is used to solve this circular dependence. An initial guess is made for the slag cloud speed in relation to the gas velocity and then the iterative solving of Excel computes new values until convergence is met. The initial velocity of the slag cloud at the nozzle nose tip plane can be input to any value, although zero initial velocity is predominantly used to simulate slag being spilled from underneath the nozzle nose.

$$D = 0.5 \rho_{gas} V^2_{slag} A_{b_{max}} C_D$$

$$D = \text{Drag force}$$

$$\rho_{gas} = \text{Density of gas in motor}$$

$$V_{slag} = \text{Velocity of slag relative to gas velocity}$$

$$A_{b_{max}} = \text{Maximum blockage area}$$

$$C_D = \text{Drag coefficient (0.5)}$$

$$V_{slag|_{t+\Delta t}} = \text{SQRT}\{(G_F + D/m_{sphere}) 2\Delta L + V^2_{slag|_t}\}$$

$$G_F = \text{G-force motor is subjected to during flight}$$

$$m_{sphere} = \text{Mass of sphere being flown through nozzle}$$

$$\Delta L = \text{Distance between computation locations in the nozzle}$$

$$T_{t+\Delta t} = \Delta L/V_{slag} + T_t$$

$$T_t = \text{Time of flight of sphere in nozzle}$$

Once the velocity of the slag cloud is determined, the flow rate of the slag through the nozzle is calculated. The velocity of the slag cloud at the nozzle throat plane is used to make this calculation. The mass flow is calculated at small time intervals so that it may be summed to determine the total mass of slag discharged through the nozzle during a given time period.

$$m_s = \rho_{\text{slag cloud}} A_b V_{\text{slag}|\text{throat}}$$

$$\textbf{Total Mass of Slag} = \Sigma m_s \Delta t$$

$$m_s = \text{Instantaneous slag flow rate}$$

$$\rho_{\text{slag cloud}} = \text{Density of slag cloud (33 lbm/cu. ft.)}$$

$$A_b = \text{Blockage area}$$

$$V_{\text{slag}|\text{throat}} = \text{Slag cloud velocity at nozzle throat plane}$$

$$\Delta t = \text{Time interval between calculation steps}$$

Finally, the slag thrust is calculated. This thrust component is a result of the momentum that the slag has as it is ejected from the nozzle exit. The slag cloud velocity at the nozzle exit plane is used in order to make this calculation. The thrust due to the combustion products is also calculated and added to the slag thrust to obtain a value for the total motor thrust. The program uses a constant value for the overall thrust coefficient in the computation of the gas thrust. A thrust over pressure time history can be calculated by dividing the total motor thrust by the motor chamber pressure.

$$F_{\text{slag}} = m_s V_{\text{slag}|\text{exit}}$$

$$F_{\text{gas}} = P_c A_{t_{\text{effect}}} C_{FM}$$

$$F_{\text{total}} = F_{\text{slag}} + F_{\text{gas}}$$

$$F_{\text{slag}} = \text{Thrust due to slag ejection}$$

$$V_{\text{slag}|\text{exit}} = \text{Velocity of slag cloud at nozzle exit plane}$$

F_{gas} = Thrust due to exhaust of combustion gases

P_c = Motor chamber pressure

C_{F_M} = Overall thrust coefficient (1.68)

F_{total} = Total motor thrust

$F/P = F_{total}/P_c$

F/P = Ratio of motor thrust to motor chamber pressure

For this series of tests the Slag Ballistics Model was altered so that it was capable of predicting the magnitude of a pressure perturbation for a given mass flowrate of water injected into the model. In order to perform this calculation the model was changed to operate in the reverse stream of logic as that outlined above.

8.0 EXPERIMENTAL RESULTS

Approximately 140 total runs were completed including the investigation of secondary variables and test repeatability. These runs are listed in Appendix A. The last twenty-one runs define the final and primary orthogonal test matrix which is outlined in Table 2. Nine of these runs were performed with an injector diameter of 0.532 inches and the remaining twelve runs were performed with an injector of diameter 0.712 inches. The larger injector nozzle had an additional three runs at higher water flowrates than was possible with the smaller injector. These additional water flowrates ranged from approximately 20 lbm/sec to 22 lbm/sec, depending upon the chamber pressure. The magnitude of model pressure perturbation during water injection ranged from 4.0 psi to 16.5 psi depending on test conditions. The tests were successful in generating data on the relationship between pressure spike amplitude and water flow rate. A typical raw data test result plot is shown in Figure 6. The bottom trace is from a pressure transducer on the water injector supply line and shows when water flow is initiated. The middle trace is from a transducer near the aft end of the model chamber and shows that the model chamber pressure is elevated 6 psi for the entire 1.04 seconds of water flow duration. This information was to be used to calculate the simulated slag thrust needed to ultimately determine an experimental total thrust to pressure ratio.

A summary of the data correlation achieved with the test results is shown in Figures 7 and 8. The parameters plotted are the amplitude of the pressure increase normalized by the model chamber pressure versus the water flowrate. The open symbols connected by solid lines represent the predictions by the Slag Ballistics Model and the solid symbols represent the measured data.

It may be seen that the calibrated Slag Ballistics Model does an excellent job of matching the test data over a wide range of model chamber pressures and water flow rates. Properties of air and water are used along with the model geometry in the model for the experimental data correlation but when the model is applied to RSRM, combustion gas and alumina properties are used along with the full scale motor nozzle geometry. The model matches the data better at the highest pressure which is of more interest since the motor Reynolds number is matched at this condition.

9.0 CONCLUSIONS

At the conclusion of this test series it is possible to make several conclusions from the data gathered. These conclusions are as follows:

1. It is seen that for a given chamber pressure, the magnitude of the pressure perturbation increases as the water flowrate increases. Also, as the chamber pressure is increased that the magnitude of the pressure perturbation decreases for a given water flowrate.

2. There seemed to be no effect on the magnitude of the pressure perturbation when the water injection velocity was changed. This is evident by comparing Figures 7 and 8. These two plots represent two different size injectors and thus different injection velocities. These plots show no difference in the pressure perturbation values for equal chamber pressures and water flowrates.

3. During the test series a few runs were made with the injector located near the wall of the model. The results from these runs showed no difference from the runs made with the injector located at the centerline of the model. This is probably due to the fact that this model does not have a submerged nose nozzle and none of the water can be trapped in the back end of the model.

4. It was found that a high speed video camera set-up would not be satisfactory to measure the velocity of the water as it exited the model nozzle. The water velocity was too high for the camera to obtain pictures of a high enough quality to discern individual droplets of water from which to make a velocity measurement. A dual beam laser will be used in a Plexiglas exhaust duct downstream of the model nozzle to solve this problem in the following test series with a scaled submerged nose RSRM nozzle.

5. It was found that the Precursor Tests definitely support and validate the ability of the Slag Ballistics Model to correctly relate the amplitude of the pressure spike to the slag flow rate.

Table 1. RSRM Nozzle Slag Ejection Tests

Simulation Parameter	Manifold Pressure (psia)	Chamber Pressure (psia)	Air Flowrate (lbm/sec)	Water Flowrate[1] (lbm/sec)
Reynolds No.	797	405	212.5	19.3
75% Reynolds No.	598	304	159.5	16.7
50% Reynolds No.	398	202.5	106	14.9
25% Reynolds No.	199	101[2]	53	10.8
Dynamic Ratio	715	363.5	191	18.2
Weber No.	1381	701.7[3]	187	27.0
Modified Weber No.	138	70.2	18.7	9.0

Notes:
1.) Water flowrate should be varied by +/- 50% for each test condition.
2.) Chamber pressures less than 150 psia may result in flow separation near nozzle exit plane.
3.) Not recommended test condition - Reference only.

Table 2. RSRM Nozzle Slag Ejection Test Matrix

0.532 Inch Diameter Nozzle - Aft Location

Chamber Pressure (psia)	Air Flowrate (lbm/sec)	Water Flowrate (lbm/sec)	Pressure Perturbation (psia)
404.70	218.86	18.30	10
404.69	218.85	12.85	9
405.04	219.20	7.79	5.5
303.30	165.50	18.18	11
305.04	166.29	12.68	8
304.00	164.35	7.75	5.85
202.71	110.02	18.57	10
203.08	110.25	13.00	7.5
202.29	110.26	7.94	5

0.712 Inch Diameter Nozzle - Aft Location

Chamber Pressure (psia)	Air Flowrate (lbm/sec)	Water Flowrate (lbm/sec)	Pressure Perturbation (psia)
402.11	218.77	19.95	11
404.40	220.01	19.27	10
404.57	220.40	14.22	8
404.76	220.01	7.47	5
304.01	165.60	21.17	11.5
304.18	165.52	20.43	10.5
304.01	167.08	13.47	9
304.00	167.22	7.30	5.5
201.91	111.19	21.86	11
202.29	111.34	19.85	9.5
201.89	111.09	13.47	7.5
201.86	111.07	7.60	5

Table 3. Formulas Used in Performance Calculations

Mach Number	$$\frac{A}{A^*} = \frac{1}{M}\left[\left(\frac{2}{\gamma+1}\right)\left(1+\frac{\gamma-1}{2}M^2\right)\right]^{\frac{\gamma+1}{2(\gamma-1)}}$$
Total Pressure (psia)	$$\frac{P_o}{P} = \left(1+\frac{\gamma-1}{2}M^2\right)^{\frac{\gamma}{\gamma-1}}$$
Total Temperature (Deg R)	$$\frac{T_o}{T} = 1+\frac{\gamma-1}{2}M^2$$
Flowrate (lbm/sec)	$$\frac{W}{A^*}\frac{\sqrt{T_o}}{P_o} = 0.53175 \quad (C_D = 1)$$
Reynolds Number (throat)	$$Re = \frac{\rho V d_{throat}}{\mu}$$
Weber Number	$$W = \frac{\rho_a L_{model} V_a^2}{\sigma_w}$$
Dynamic Simulation	$$\frac{\rho_s V_s^2}{\rho_g V_g^2} = \frac{\rho_w V_w^2}{\rho_a V_a^2}$$
Total Thrust (lbf)	$$F_T = P_c A_t C_{F_M} + F_{slag}$$
Slag Thrust (lbf)	$$F_{slag} = m_{slag} V_{slag_{exit}}$$
Thrust/Pressure	$$F_T/P_c$$

Table 4. STATIC PRESSURES

RSRM Nozzle Slag Injection Model

Note: Spool pieces arranged in 3-2-1 order in the direction of flow.

No.	Parameter	Location	Station	Range/Units
1	PS-LS0G	Manifold Pipe (South Leg of 8" Pipe) at 90 deg	-23.0	15 to 800 psia
2	PS-LN0U	Manifold Pipe (North Leg of 8" Pipe) at 270 deg	-23.0	15 to 800 psia
3	PS-T0TA	Model Nozzle Throat Wall at 0 deg	111.8	15 to 220 psia
4	PS-T0TG	Model Nozzle Throat Wall at 90 deg	111.8	15 to 220 psia
5	PS-T0TU	Model Nozzle Throat Wall at 270 deg	111.8	15 to 220 psia
6	PS-T0EA	Model Nozzle Exit Wall at 0 deg	131.1	0 to 100 psia
7	PS-T0EG	Model Nozzle Exit Wall at 90 deg	131.1	0 to 100 psia
8	PS-T0EU	Model Nozzle Exit Wall at 270 deg	131.1	0 to 100 psia
9	PS-D00G	Diffuser Duct Wall Downstream 0" of Nozzle, at 90 deg	131.2	0 to 100 psia
10	PS-D02G	Diffuser Duct Wall Downstream 2" of Nozzle, at 90 deg	133.1	0 to 100 psia
11	PS-D04G	Diffuser Duct Wall Downstream 4" of Nozzle, at 90 deg	135.1	0 to 100 psia
12	PS-D06G	Diffuser Duct Wall Downstream 6" of Nozzle, at 90 deg	137.1	0 to 100 psia
13	PS-D10G	Diffuser Duct Wall Downstream 10" of Nozzle, at 90 deg	141.1	0 to 100 psia
14	PS-DE0G	Diffuser Duct (16.75" Dia.) Exit at 90 deg	248.5	0 to 100 psia
15	PS-DTEG	Diffuser Transition Duct Exit at 90 deg	285.1	0 to 100 psia
16	PS-C00A	Adapter (Aft End of 16" Dia. Section) at 0 deg	28.7	15 to 405 psia
17	PS-S10G	Model Aft (Spool Piece #1) at 90 deg	80.5	15 to 405 psia
18	PS-S10U	Model Aft (Spool Piece #1) at 270 deg	80.5	15 to 405 psia
19	PS-S30G	Model Forward (Spool Piece #3) at 90 deg	44.6	15 to 405 psia
20	PS-S30U	Model Forward (Spool Piece #3) at 270 deg	44.6	15 to 405 psia
21	PS-TACC	Fluid Accumulator Supply Line	80.5	15 to 405 psia

Table 5. TOTAL PRESSURES

RSRM Nozzle Slag Injection Model

No.	Parameter	Location	Station	Range/Units
1	PT-LS0N	Manifold Pipe (South Leg of 8" Pipe) at 180 deg	-23.0	15 to 800 psia
2	PT-LN0N	Manifold Pipe (North Leg of 8" Pipe) at 180 deg	-23.0	15 to 800 psia
3	PT-MAUA	Upstream Metering Nozzle "A" at 0 deg	18.6	15 to 800 psia
4	PT-MBUG	Upstream Metering Nozzle "B" at 90 deg	18.6	15 to 800 psia
5	PT-MCUG	Upstream Metering Nozzle "C" at 90 deg	18.6	15 to 800 psia
6	PT-MDUA	Upstream Metering Nozzle "D" at 0 deg	18.6	15 to 800 psia
7	PT-C00N	Adapter (Aft End of 16" Dia. Section) at 180 deg	28.7	15 to 800 psia

Table 6. DYNAMIC PRESSURES

RSRM Nozzle Slag Injection Model

Note: Spool pieces arranged in 3-2-1 order in the direction of flow.

No.	Parameter	Location	Station	Range/Units
1	PDY-C00G	Adapter (Aft End of 16" Dia. Section) at 90 deg	28.7	see note
2	PDY-S10K	Model Aft (Spool Piece #1) at 135 deg	80.5	see note
3	PDY-S30K	Model Forward (Spool Piece #3) at 135 deg	44.6	see note
4	PDY-I30A	Water Injector Downstream of Marotta Valve	100.8	see note

Note: 1.) All gauges 0 to 800 psia Mean Avg.
2.) Actual expected range of pressure spike, 1-20 psid.

Table 7. AIR TEMPERATURES

RSRM Nozzle Slag Injection Model

Note: Spool pieces arranged in 3-2-1 order in the direction of flow.

No.	Parameter	Location	Station	Range/Units
1	TAF-MAUN	Upstream Metering Nozzle "A" at 180 deg	18.6	-50 to 100 deg F
2	TAF-MBUU	Upstream Metering Nozzle "B" at 270 deg	18.6	-50 to 100 deg F
3	TAF-MCUU	Upstream Metering Nozzle "C" at 270 deg	18.6	-50 to 100 deg F
4	TAF-MDUN	Upstream Metering Nozzle "D" at 180 deg	18.6	-50 to 100 deg F
5	TAF-C00G	Adapter (Aft End of 16" Dia. Section) at 90 deg	28.7	-50 to 100 deg F
6	TAF-S10A	Model Aft (Spool Piece #1) at 0 deg	80.5	-50 to 100 deg F
7	TAF-S30A	Model Forward (Spool Piece #3) at 0 deg	44.6	-50 to 100 deg F
8	TAF-DTED	Diffuser Transition Duct Exit at 45 deg	285.1	-50 to 100 deg F

Table 8. RSRM Nozzle Slag Ejection Model Measurement Labels

This table provides an explanation for the instrumentation labels in the preceding tables. The labels are in the following format:

XXX-YYYY.

The first field denoted by XXX describes the type of instrumentation at the station described. The following letter designations tell what the instrumentation type is at a given station.

PS	Static Pressure
PT	Total Pressure
PDY	Dynamic Pressure
TAF	Bulk (Air) Temperature

The second field denoted by YYYY describes the location of the instrumentation station. The following letter designations describe the different instrumentation location. The first character gives the physical hardware description.

L	Facility Supply Leg		S	Spool Piece
M	Metering Nozzles		D	Diffuser
C	Adapter Chamber		I	Fluid Injector
T	Model Nozzle or Test Equipment			

The second and third character give a more specific location on a single piece of hardware. A zero in either position is used as a place holder. A number following an S or an I designates a particular spool piece or injector. Following a D it gives an axial position in the diffuser.

S	South Leg		A	Top South Manifold Arm
N	North Leg		B	Bottom South Manifold Arm
T	Throat		C	Bottom North Manifold Arm
E	Exit		D	Top North Manifold Arm
TE	Transition Duct Exit		U	Upstream of a metering nozzle
N	Nozzle Nose Entrance		D	Downstream of a metering nozzle

17

The final character gives the circumferential orientation of the instrumentation in degrees form straight up. The correct orientation is facing upstream into the flow with gravity in effect.

A	0	G	90	N	180	U	270
B	15	H	105	P	195	V	285
C	30	J	120	Q	210	W	300
D	45	K	135	R	225	X	315
E	60	L	150	S	240	Y	330
F	75	M	165	T	255	Z	345

Figure 1.   Solid Rocket Motor Air Flow Test Equipment

Fill Connection

Manual Ball Valve, 12 inch, 900 lb.

Manual Ball Valve, 12 inch, 900 lb.

Building 4777

Control Room

Vertical Exhaust Duct

Wall Injection Manifold

Exhaust Diffuser

SRM Model

Wall Injection Manifold

Filter

Carbon Steel

Stainless Steel

Venturi

Relief Valve

Quiet Control Valve 16 inch, 1,500 lb.

ROV Ball Valve 12 inch, 1,500 lb.

Air Storage
• 9,100 Cubic Feet Storage Capacity
• 1,960 psi, Maximum

19

Figure 2. RSRM Nozzle Slag Ejection Test Names of Model Components

Labels in figure:
- METERING NOZZLE
- ACRYLIC SECTION
- WATER INJECTION SYSTEM
- HYPERBOLIC SPIRAL INLET
- DIFFUSER
- NOZZLE
- SPOOL 1
- SPOOL 2
- SPOOL 3
- ADAPTER CHAMBER
- HEADER PIPES (4 TOT)
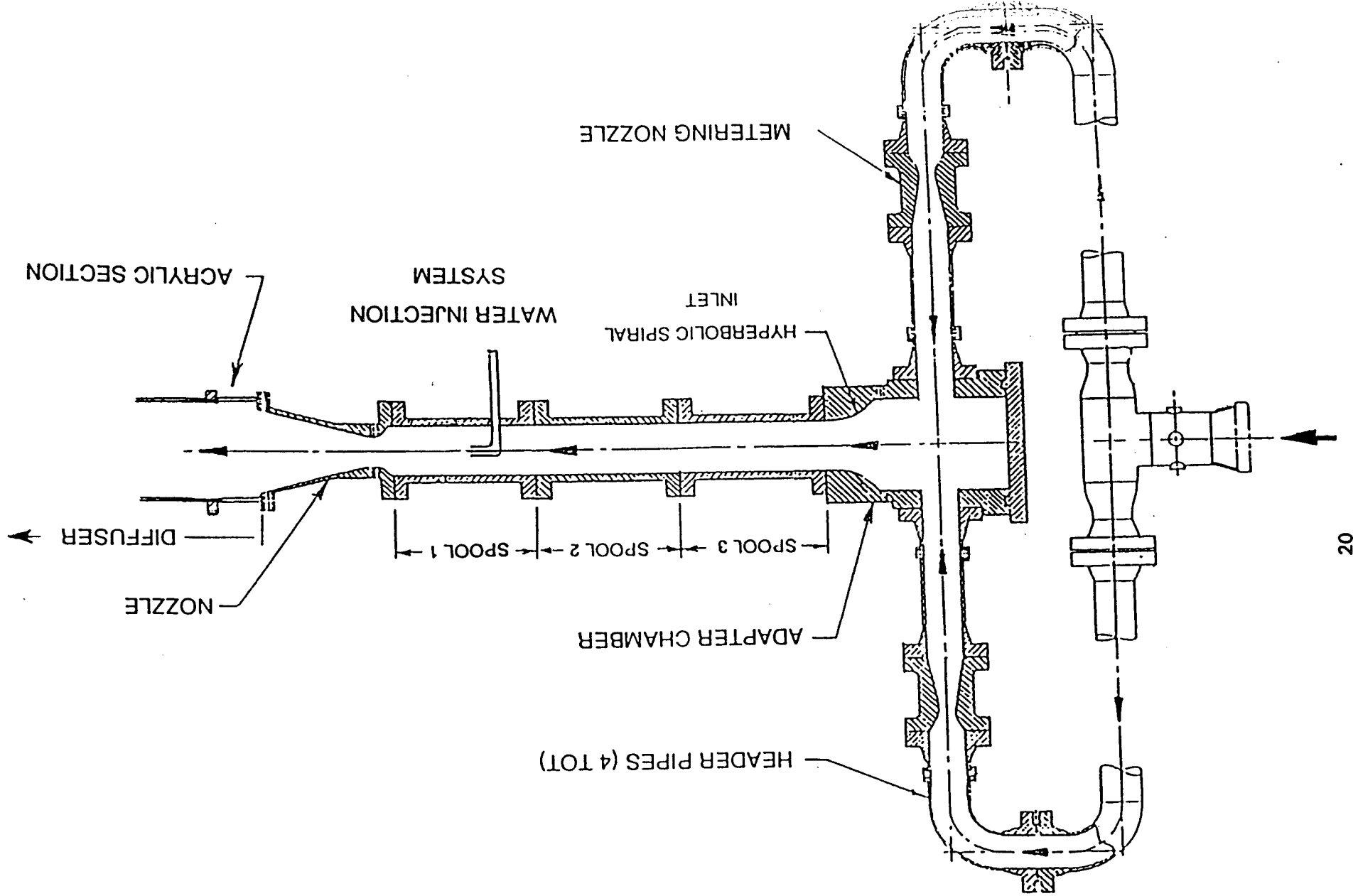
Figure 3. Checkout Model 538 Nozzle
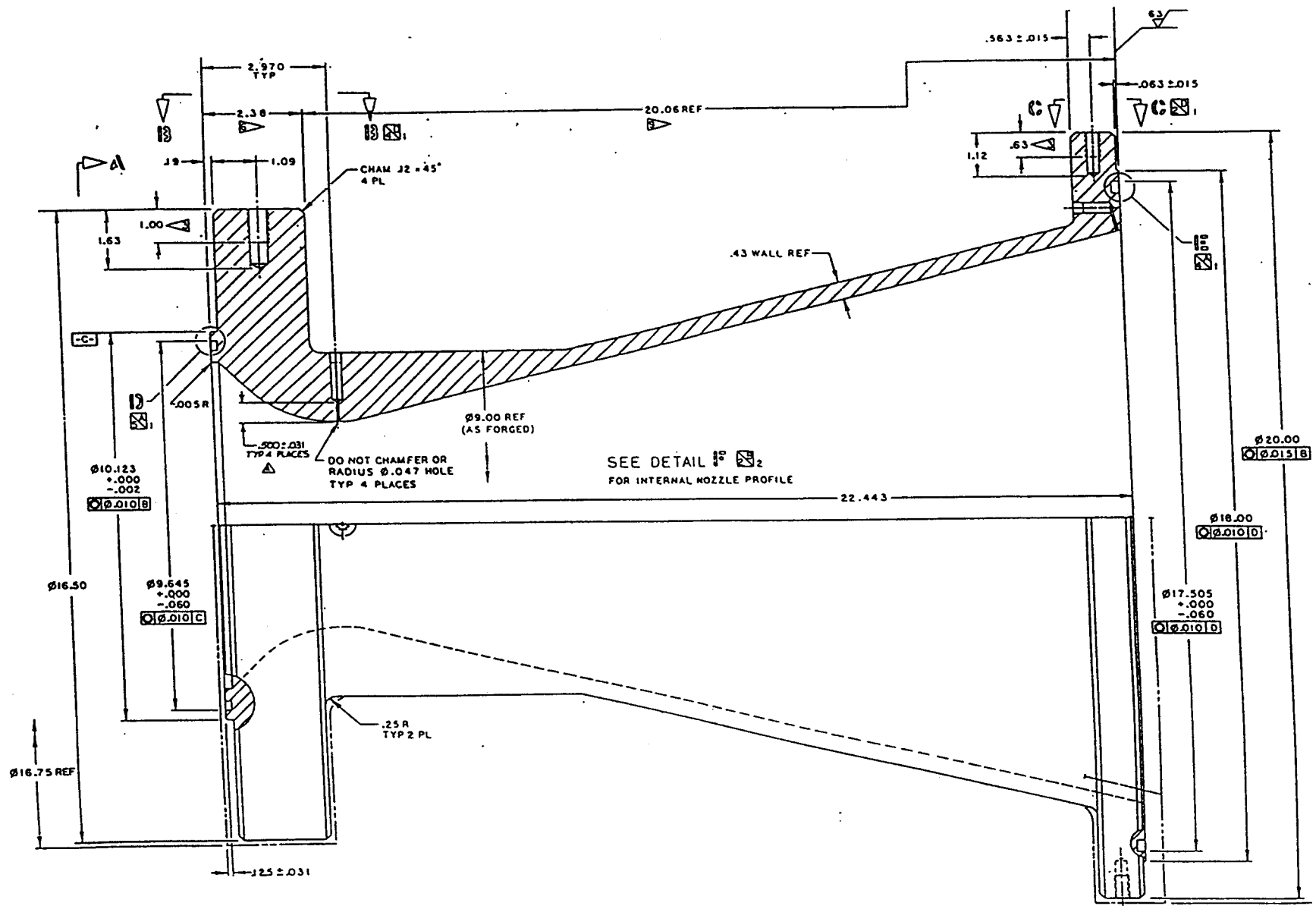
Figure 4. Water Injectors

Dimensions in inches

D_{ex}

0.9225

D_{ex}

0.75

0.75

$D_{ex} = 0.453$
    0.532
    0.581

$D_{ex} = 0.453$
    0.712

TYPE 1

TYPE 2

22
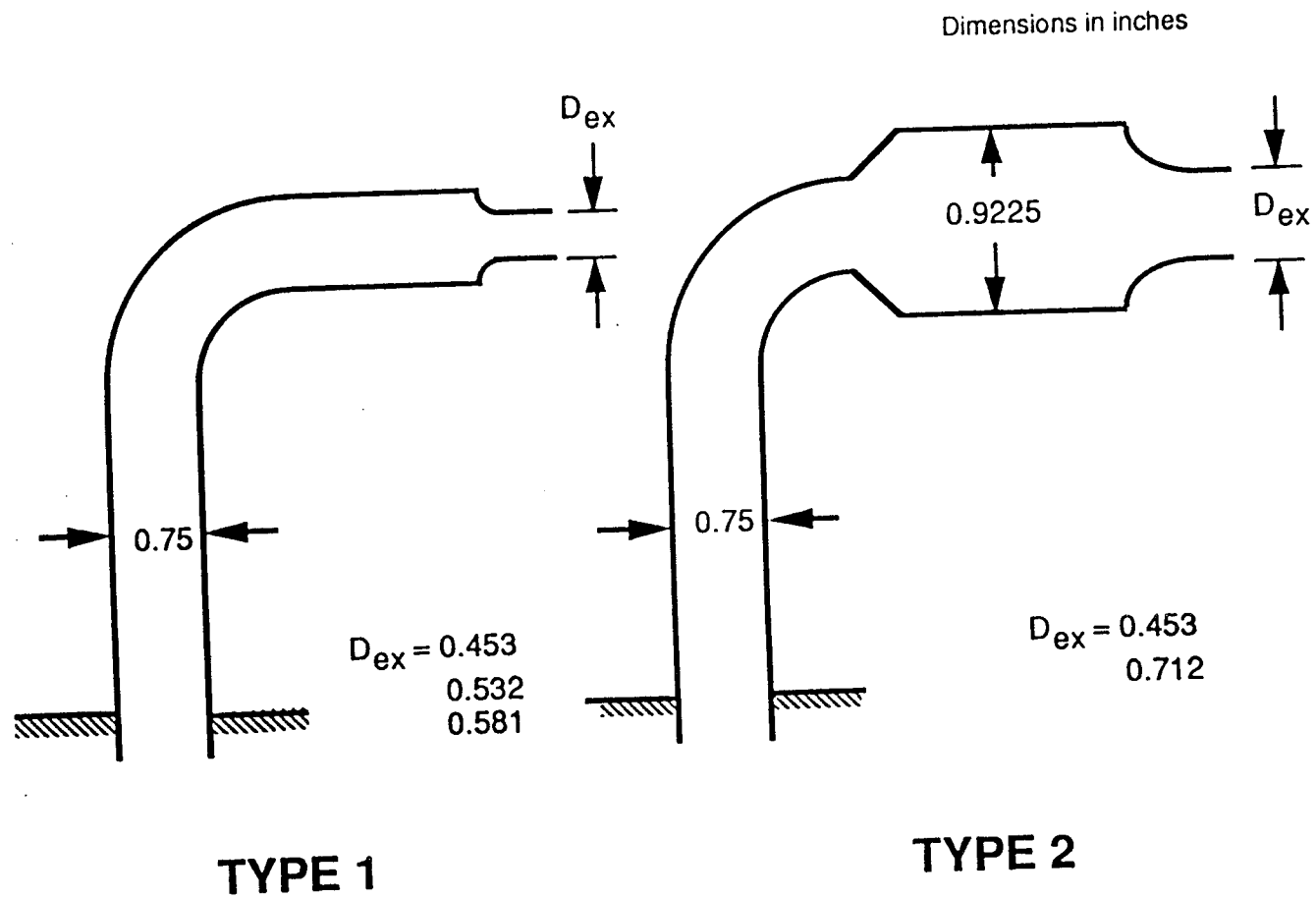
Figure 5. Checkout Model Axial Station and Angle Designations

LOOKING UPSTREAM (AFT LOOKING FORWARD)

STATION NUMBER, INCHES

SCHEMATIC ONLY - NOT TO SCALE

MICRO CRAFT

23

WATER

DOWNSTREAM

UPSTEAM

RUN 7/1
MODEL PRESSURE = 100 PSI
WATER PRESSURE = 300 PSI
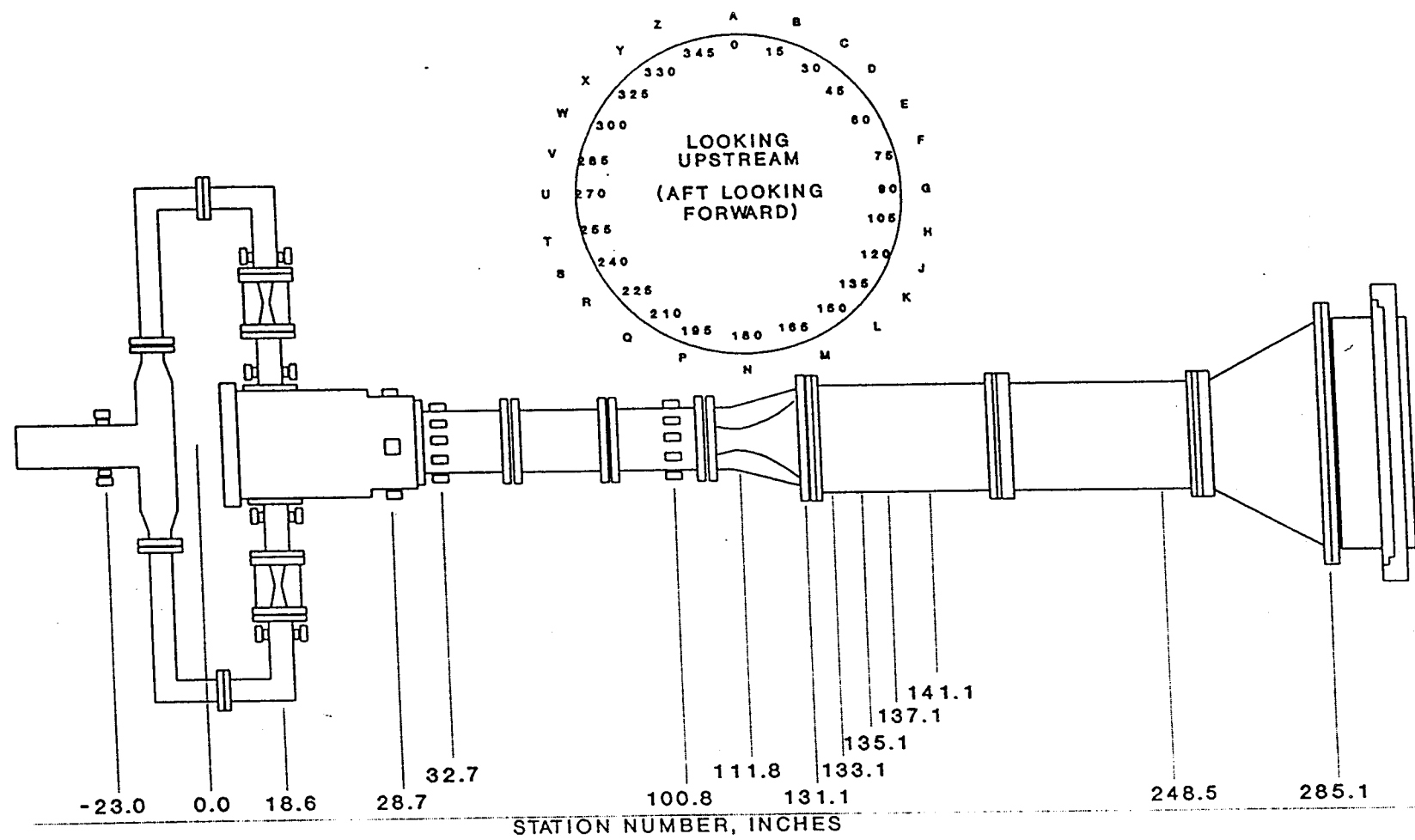
Figure 6. Raw Dynamic Pressure Transducer Data

24
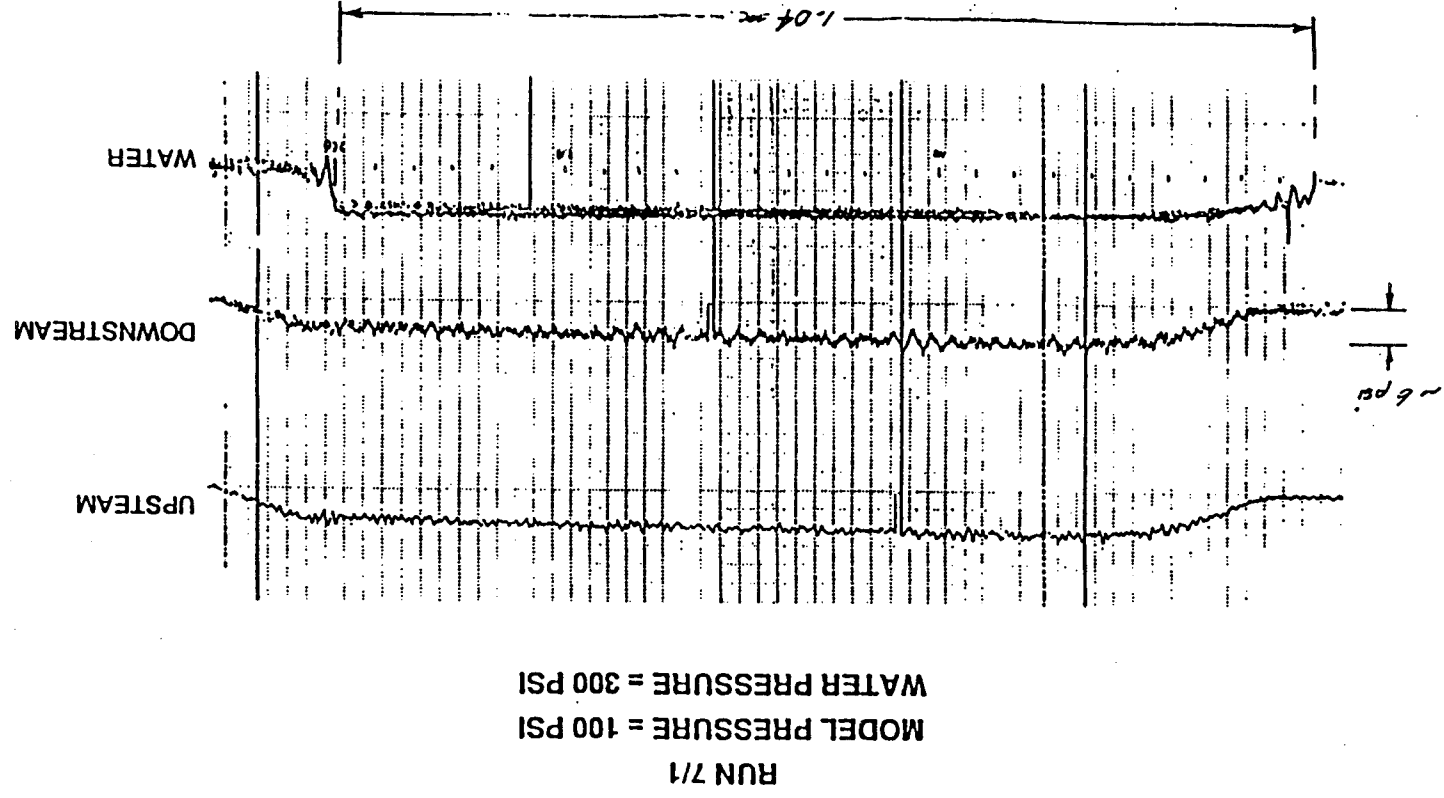
Figure 7. RSRM Nozzle Slag Precursor Tests
Injector Type 1 Dia. = 0.532 Aft Location

ERC, Inc. 10/15/1993
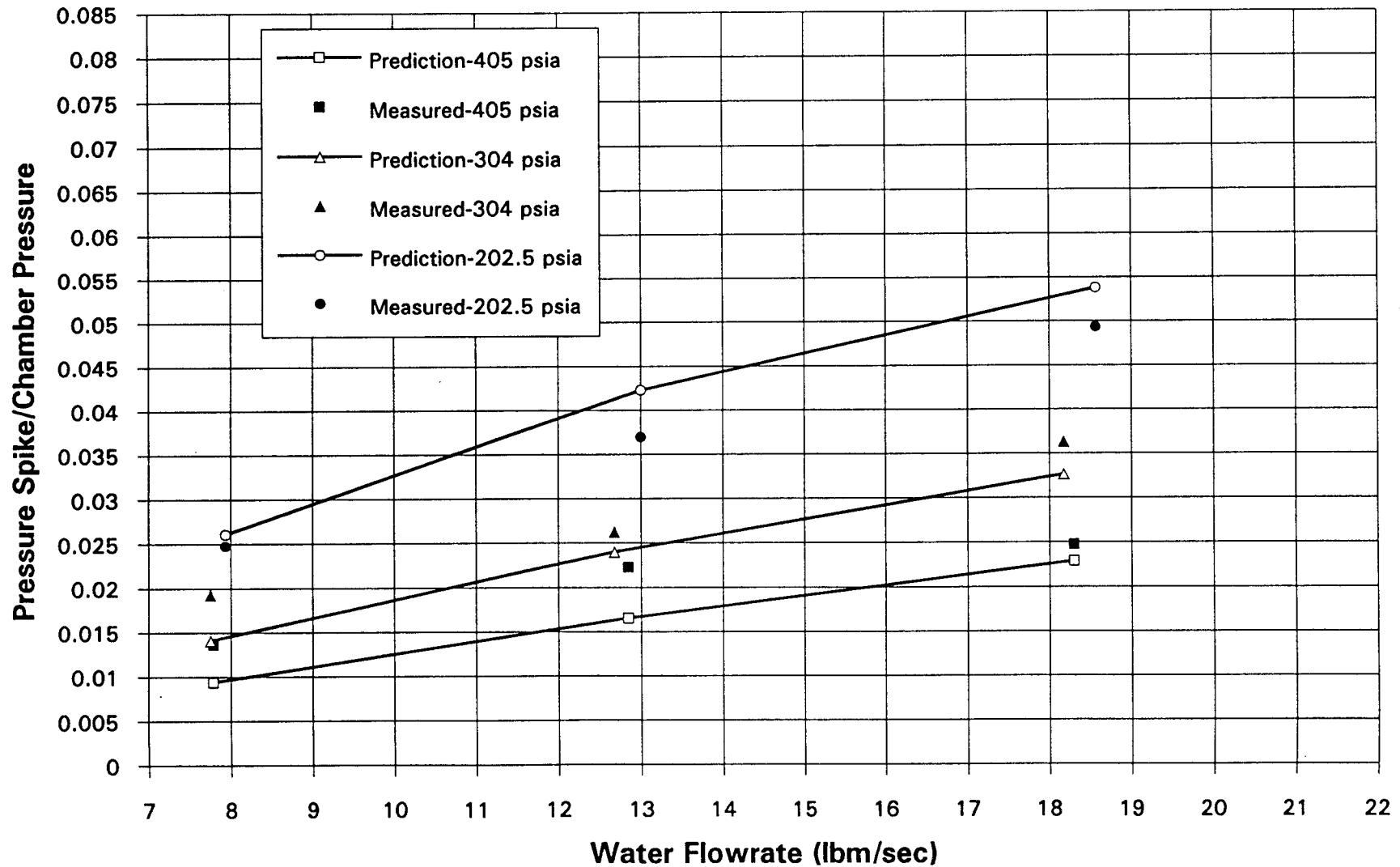
**Figure 8. RSRM Nozzle Slag Precursor Tests
Injector Type 2 Dia.= 0.712 Aft Location**

26
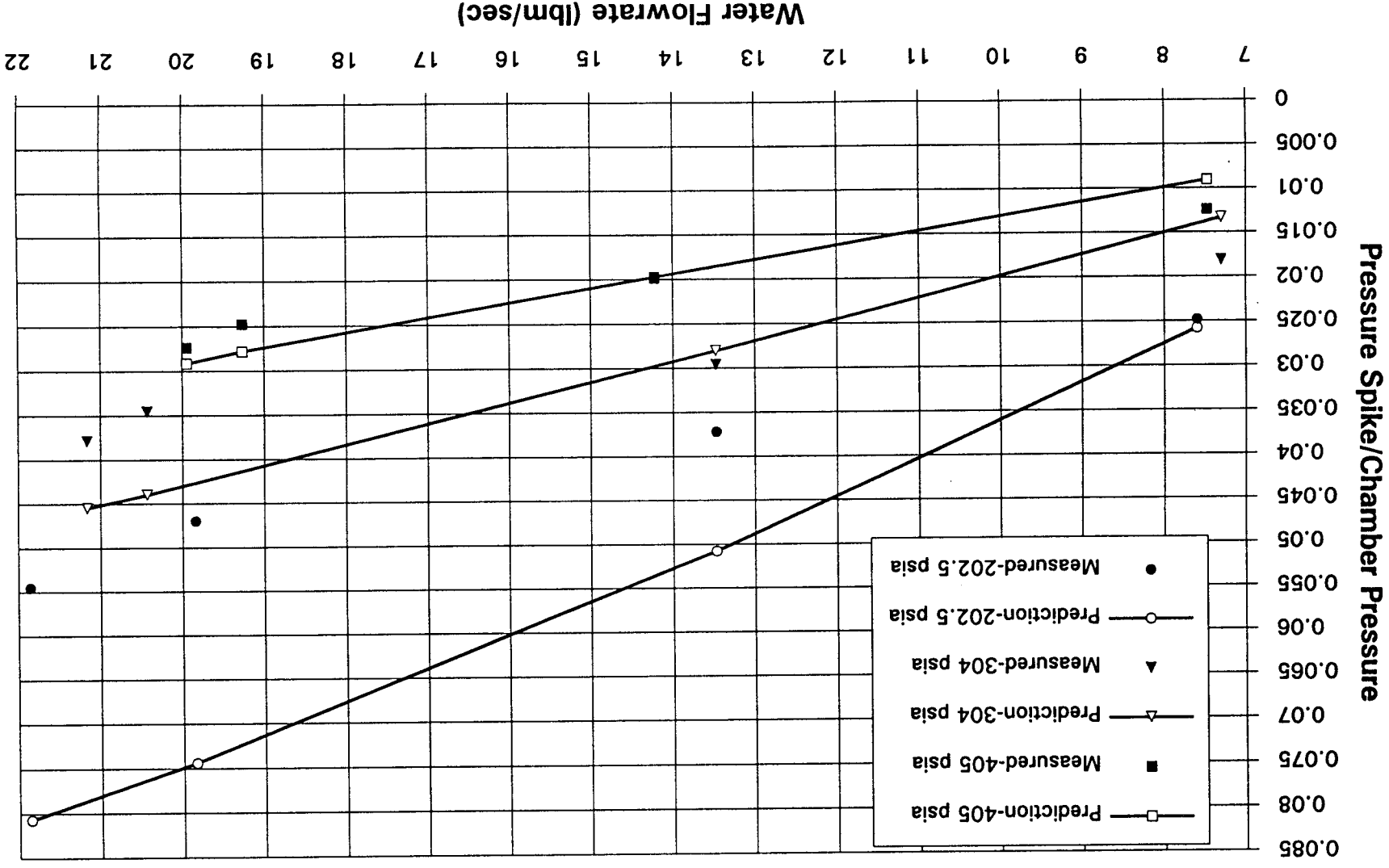
APPENDIX A

RSRM Slag Ejection Precursor Test Runs

PRELIMINARY TEST RESULTS

D = .532 in. Type 1 Nozzle

Forward Location

RUN NO.	MODEL PRESSURE (PSIA)	WATER PRESSURE (PSIA)	WATER PRESSURE (PSID)	WATER EJECTED (GAL)	ΔT (SEC)	FLOW RATE (GPM)	PRESSURE SPIKE (PSI
14/0	150	720	570	1.49	0.93	95.83	9.0
13/0	150	600	450	1.63	1.08	90.80	8.5
4/2	150	300	150	1.20	1.24	57.54	6.5
5/1	150	250	100	0.89	1.17	45.94	6.0
6/0	150	200	50	0.56	1.04	32.29	4.5
7/1	100	300	200	1.11	1.04	63.87	6.0
8/0	100	250	150	0.77	0.84	54.65	5.5
9/0	100	200	100	0.75	0.98	45.75	5.0
15/0	50	720	670	1.53	0.86	107.05	6.5
10/0	50	300	250	1.05	0.88	71.45	5.5
11/0	50	250	200	1.03	0.98	63.00	5.0
12/0	50	200	150	0.92	1.03	53.63	5.0

PRELIMINARY TEST RESULTS

D = .532 in. Type 1 Nozzle

Forward Location

RUN NO.	MODEL PRESSURE (PSIA)	WATER PRESSURE (PSIA)	WATER PRESSURE (PSID)	WATER EJECTED (GAL)	ΔT (SEC)	FLOW RATE (GPM)	PRESSURE SPIKE (PSI
61/0	405	1050	645	1.64	0.77	128.50	14.0
62/0	405	550	145	0.98	0.88	67.02	9.0
63/0	405	800	395	1.17	1.71	98.25	11.5
64/0	304	980	676	1.60	0.76	127.23	14.5
65/0	304	1050	746	1.64	0.75	131.93	14.0
66/0	304	750	446	1.42	0.79	107.80	13.0
67/0	202.5	275	72.5	0.77	0.87	53.00	7.0
68/0	202.5	1050	847.5	1.98	0.84	141.95	13.5
69/0	202.5	560	510	1.27	0.75	101.33	11.0
70/0	101	300	199	1.21	0.85	85.44	7.5
71/0	101	125	24	0.60	0.95	38.05	4.0
72/0	101	525	424	1.42	0.78	108.35	9.5

PRELIMINARY TEST RESULTS

D = .532 in. Type 1 Nozzle

Aft Location

RUN NO.	MODEL PRESSURE (PSIA)	WATER PRESSURE (PSIA)	WATER PRESSURE (PSID)	WATER EJECTED (GAL)	ΔT (SEC)	FLOW RATE (GPM)	PRESSURE SPIKE (PSI
73/0	405	1050	645	1.23	0.61	120.43	9.0
74/0	405	550	145	0.87	0.78	67.61	7.5
75/0	405	800	395	1.08	0.66	97.83	9.5
76/0	304	980	676	1.39	0.67	124.55	10.0
77/0	304	1050	746	1.83	0.88	124.92	10.5
78/0	304	750	446	2.14	1.32	97.48	9.0
79/0	202.5	275	72.5	0.71	0.87	48.93	5.0
80/0	202.5	1050	847.5	1.31	0.58	134.76	10.0
81/0	202.5	560	357.5	1.35	0.80	100.99	7.0
82/0	101	300	199	0.92	0.65	84.82	5.0
83/0	101	125	24	0.29	0.60	29.15	2.5
84/0	101	525	424	1.15	0.63	109.40	7.0

PRELIMINARY TEST RESULTS

D = .532 in. Type 1 Nozzle

Aft Location

RUN NO.	MODEL PRESSURE (PSIA)	WATER PRESSURE (PSIA)	WATER PRESSURE (PSID)	WATER EJECTED (GAL)	ΔT (SEC)	FLOW RATE (GPM)	PRESSURE SPIKE (PSI
85/0	405	1000	595	1.49	0.69	129.82	10.5
86/0	405	900	495	1.29	0.63	122.55	9.5
87/0	405	800	395	1.31	0.73	107.51	10.0
88/0	405	700	295	1.12	0.71	94.71	9.0
89/0	405	600	195	1.04	0.79	78.86	8.0
90/0	405	500	95	0.71	0.78	54.73	6.5
91/0	304	1000	696	1.42	0.63	134.41	10.5
92/0	304	900	596	1.29	0.62	125.73	10.5
93/0	304	800	496	1.39	0.69	121.29	10.0
94/0	304	700	396	1.15	0.65	106.41	9.5
95/0	304	600	296	1.28	0.83	92.34	7.5
96/0	304	450	146	0.81	0.71	68.07	6.5

PRELIMINARY TEST RESULTS

D = .532 in. Type 1 Nozzle

Aft Location

RUN NO.	MODEL PRESSURE (PSIA)	WATER PRESSURE (PSIA)	WATER PRESSURE (PSID)	WATER EJECTED (GAL)	ΔT (SEC)	FLOW RATE (GPM)	PRESSURE SPIKE (PSI
100/0	405	1055	650	1.23	0.56	131.61	10.0
104/4	405	693	288	1.04	0.68	92.40	9.0
105/2	405	505	100	0.69	0.74	56.01	5.5
97/0	304	954	650	1.50	0.69	130.73	11.0
98/0	304	592	288	0.98	0.64	91.17	8.0
99/0	304	404	100	0.71	0.78	54.17	7.5
101/0	202.5	852	650	1.29	0.58	133.54	10.0
102/0	202.5	490	288	1.10	0.71	93.51	7.5
103/0	202.5	302	100	0.67	0.70	57.11	5.0

PRELIMINARY TEST RESULTS

D = .581 in. Type 1 Nozzle

Forward Location

RUN NO.	MODEL PRESSURE (PSIA)	WATER PRESSURE (PSIA)	WATER PRESSURE (PSID)	WATER EJECTED (GAL)	ΔT (SEC)	FLOW RATE (GPM)	PRESSURE SPIKE (PSI
19/0	150	600	450	2.19	1.41	93.16	10.0
18/0	150	500	350	1.87	1.33	84.47	9.0
17/1	150	400	250	1.08	0.89	72.54	8.0
16/0	150	300	150	1.37	1.46	56.60	7.0
22/0	100	700	600	1.98	1.16	102.52	9.0
21/1	100	500	400	1.70	1.16	88.07	8.0
20/0	100	300	200	1.55	1.44	64.72	7.0
23/0	50	700	650	2.30	1.28	107.98	7.0

PRELIMINARY TEST RESULTS

D = .581 in. Type 1 Nozzle

Forward Location

Nozzle Adjacent to Model Wall

RUN NO.	MODEL PRESSURE (PSIA)	WATER PRESSURE (PSIA)	WATER PRESSURE (PSID)	WATER EJECTED (GAL)	ΔT (SEC)	FLOW RATE (GPM)	PRESSURE SPIKE (PSI
24/0	150	550	400	1.42	1.00	85.29	9.0
25/0	100	300	200	1.50	1.46	61.79	6.5

PRELIMINARY TEST RESULTS

D = .581 in. Type 1 Nozzle

Aft Location

RUN NO.	MODEL PRESSURE (PSIA)	WATER PRESSURE (PSIA)	WATER PRESSURE (PSID)	WATER EJECTED (GAL)	ΔT (SEC)	FLOW RATE (GPM)	PRESSURE SPIKE (PSI
27/0	150	550	400	1.55	1.06	87.92	7.0
26/0	100	300	200	1.06	1.09	58.67	4.5

PRELIMINARY TEST RESULTS

D = .712 in. Type 2 Nozzle

Aft Location

RUN NO.	MODEL PRESSURE (PSIA)	WATER PRESSURE (PSIA)	WATER PRESSURE (PSID)	WATER EJECTED (GAL)	ΔT (SEC)	FLOW RATE (GPM)	PRESSURE SPIKE (PSI
29/1	150	300	150	1.12	1.28	52.7	5.0
42/0	100	900	800	1.50	0.76	118.4	6.0
40/0	100	430	330	1.21	0.84	86.3	5.0
30/1	100	600	500	2.36	1.32	107.1	6.0
41/0	100	255	155	0.65	0.72	53.8	4.0
31/1	50	650	600	1.25	0.94	80.00	5.0

PRELIMINARY TEST RESULTS

D = .712 in. Type 2 Nozzle

Aft Location

RUN NO.	MODEL PRESSURE (PSIA)	WATER PRESSURE (PSIA)	WATER PRESSURE (PSID)	WATER EJECTED (GAL)	ΔT (SEC)	FLOW RATE (GPM)	PRESSURE SPIKE (PSI
36/1	405	1000	595	1.35	0.86	94.4	9.5
43/0	405	875	470	1.46	0.66	132.5	11.0
45/1	304	1050	746	1.52	0.60	152.0	11.0
37/0	304	750	446	1.37	0.92	100.5	8.0
44/0	304	720	416	1.92	0.78	148.0	11.0
46/0	202.5	1050	847.5	1.73	0.64	162.0	11.0
38/0	202.5	950	747.5	1.66	0.82	121.1	9.5
47/0	202.5	850	647.5	1.65	0.70	141.0	10.0
39/0	202.5	525	322.5	1.21	0.88	82.3	7.0

PRELIMINARY TEST RESULTS

D = .712 in. Type 2 Nozzle

Forward Location

RUN NO.	MODEL PRESSURE (PSIA)	WATER PRESSURE (PSIA)	WATER PRESSURE (PSID)	WATER EJECTED (GAL)	ΔT (SEC)	FLOW RATE (GPM)	PRESSURE SPIKE (PSI
49/0	405	900	495	1.85	0.96	115.8	13.5
48/2	405	575	170	1.35	1.01	78.7	10.0
48/3	405	550	145	1.19	0.89	79.8	10.0
48/1	405	525	120	0.83	0.83	60.4	7.5
51/0	304	1050	746	2.06	0.86	144.0	16.5
50/0	304	810	506	1.58	0.74	127.6	14.0
52/0	304	750	446	1.83	0.92	120.0	14.0
56/0	202.5	1050	847.5	1.98	0.73	163.0	16.0
53/0	202.5	900	697.5	2.33	1.08	129.6	15.0
55/0	202.5	550	347.5	1.67	0.83	119.5	12.0
54/0	202.5	330	127.5	1.15	0.86	79.9	8.0

PRELIMINARY TEST RESULTS

D = .712 in. Type 2 Nozzle

Forward Location

RUN NO.	MODEL PRESSURE (PSIA)	WATER PRESSURE (PSIA)	WATER PRESSURE (PSID)	WATER EJECTED (GAL)	ΔT (SEC)	FLOW RATE (GPM)	PRESSURE SPIKE (PSI
59/0	101	510	409	1.81	0.90	121.3	11.0
57/0	101	300	199	1.17	0.73	96.1	9.0
58/0	101	200	99	0.97	1.03	56.5	7.0

PRELIMINARY TEST RESULTS

D = .712 in. Type 2 Nozzle

Aft Location

RUN NO.	MODEL PRESSURE (PSIA)	WATER PRESSURE (PSIA)	WATER PRESSURE (PSID)	WATER EJECTED (GAL)	ΔT (SEC)	FLOW RATE (GPM)	PRESSURE SPIKE (PSI
111/0	202.5	1000	797.5	1.98	0.74	159.51	10.5
112/0	202.5	900	697.5	1.17	0.47	148.21	10.0
113/0	202.5	800	597.5	1.58	0.70	136.41	10.5
114/0	202.5	700	497.5	1.15	0.54	127.23	9.0
115/0	202.5	600	397.5	1.31	0.66	119.97	9.0
116/0	202.5	500	297.5	1.12	0.67	100.98	8.0
117/0	202.5	400	197.5	0.83	0.57	87.97	7.0
118/0	202.5	300	97.5	0.77	0.71	65.28	6.5

PRELIMINARY TEST RESULTS

D = .712 in. Type 2 Nozzle

Aft Location

RUN NO.	MODEL PRESSURE (PSIA)	WATER PRESSURE (PSIA)	WATER PRESSURE (PSID)	WATER EJECTED (GAL)	ΔT (SEC)	FLOW RATE (GPM)	PRESSURE SPIKE (PSI
106/0	405	1000	595	1.56	0.72	130.85	11.0
107/0	405	900	495	1.44	0.72	119.05	11.0?
119/0	405	800	395	1.46	0.83	105.10	10.0
120/0	405	700	295	0.98	0.60	97.85	9.0
123/0	405	600	195	0.81	0.57	85.17	7.5
124/0	405	500	95	0.71	0.70	60.68	5.5
124/1	405	500	95	0.87	0.82	63.98	6.0
108/0	304	1000	696	1.60	0.67	143.14	11.0
109/0	304	900	596	1.46	0.65	134.94	10.5
110/0	304	800	496	1.50	0.69	130.73	10.0
121/0	304	700	396	1.02	0.54?	113.35?	10.0
122/0	304	600	296	0.98	0.59	99.85	9.0
125/0	304	450	146	0.85	0.67	76.67	7.5

PRELIMINARY TEST RESULTS

D = .712 in. Type 2 Nozzle

Aft Location

RUN NO.	MODEL PRESSURE (PSIA)	WATER PRESSURE (PSIA)	WATER PRESSURE (PSID)	WATER EJECTED (GAL)	ΔT (SEC)	FLOW RATE (GPM)	PRESSURE SPIKE (PSI
126/0	405	1100	695	1.42	0.59	143.49	11.0
127/0	405	965	560	1.73	0.75	138.61	10.0
128/0	405	640	235	1.19	0.70	102.30	8.0
129/2	405	470	65	0.87	0.98	53.76	5.0
130/0*	304	999	695	1.62	0.64	152.25	11.5
131/0*	304	864	560	1.50	0.61	146.96	10.5
131/1	304	864	560	1.23	0.52	140.65	11.0
132/0	304	539	235	1.12	0.70	96.92	9.0
133/0	304	369	65	0.81	0.93	52.50	5.5
134/0	202.5	898	695	1.52	0.58	157.23	11.0
135/0	202.5	762	560	1.33	0.56	142.77	9.5
136/0	202.5	438	235	1.12	0.70	96.92	7.5
137/0	202.5	268	65	0.65	0.71	54.70	5.0

RSRM Scaled Nozzle Slag Ejection Design and Analysis Work

A requirement drawing of the RSRM Submerged Nozzle Slag Model was prepared as ERC drawing H7002. The model scale factor used was 6.5 percent and uses the initial nozzle geometry contour along with a spool piece of the existing Checkout Model. The scale factor was selected to make the aft chamber mach number match between the model and the motor. Nozzle gimbal angles of 0, 2, 4 and 6 degrees were considered. Preliminary operating requirements were developed based on matching the full scale motor Reynolds number at the nozzle throat. The model nominal chamber pressure was to be 623 psid with a flow rate of 138 lbm/sec. It was determined that the facility would have to be operated with two of the manifold arms blanked-off due to the model scale factor being 6.5 percent compared to the 10 percent for which the manifolds were designed.

The experience gained in conducting the Precursor Nozzle Slag Ejection Tests was evaluated as it applied to planning for the Scaled Submerged Nozzle Slag Ejection Tests. Also, calculations of model and water injection pressure and flow rate operating conditions were made. The requirements for this model were updated and assembled in one package in preparation for the CDR. The updated package was taken to Thiokol to support our presentation of the cold flow work at NASA/Marshall Space Flight Center for the Pressure Perturbation TIM. Information was presented at the CDR by personnel from ERC on the reasoning for the model tests and the design requirements of the model.

A reducer plug was designed for placement in the throat of the scaled submerged nose nozzle for the model. This reducer plug would reduce the throat area in order to achieve a reduction in the chamber Mach number. The reduced Mach number would be necessary to attain a 20 ft/sec velocity required to achieve resonance between the edge tone frequency at the simulated field joint and the chamber first longitudinal mode. This condition is a requirement for the inhibitor dynamic testing.

ERC wrote a pretest report for this model. A review copy of the report was taken to NASA/MSFC and the comments and suggestions received were incorporated into the final version of the report which was distributed to NASA/MSFC personnel.

Early in the test program a meeting was held at NASA/MSFC to discuss some preliminary results from the RSRM 6.5% Scaled Nozzle Slag Model. Presented were traces of the dynamic pressure transducers output for some initial checkout runs of the model. At the meeting suggestions were made to change and add some instrumentation to the model in order to obtain a clearer picture of what was occurring in the model. Shortly after this meeting it was found that some of the valves controlling water flow into the model were defective. These were to be fixed while the instrumentation changes were being made.

Some time was spent on fine tuning the dynamic pressure gauges. The data form these gauges was placed on a magnetic tape. The digital data on the magnetic tape will be analyzed by ED33 personnel and ERC. Leaks in the water valves continued to be a problem and were addressed as they arise. Suggestions made at working level meetings included quantifying the amount of water being leaked into the model, and the amount of water being trapped in the model at the end of each run.

In an attempt to view the slag ejection event form inside the model a boroscope was acquired for a day. It was determined that the light source provided with the boroscope was sufficient to see inside the model. However, the boroscope would not accept the high pressures inside the model chamber. A protective sleeve was needed to make the use of the boroscope a viable option in this model.

The dynamic data from the 6.5% Scaled Nozzle Slag Model was analyzed by using a smoothing technique due to the roughness of the pressure traces. A 100 point moving average was used. This technique serves to smooth the data somewhat so that the general trend of the data is more apparent. The 100 samples per second data was plotted and a water flowrate was calculated. This water flowrate was plotted along with the chamber pressure for a period of time encompassing the water injection event. This data was also analyzed by ED33 personnel to determine the periodicity of the water expulsion from the model. The ERC analysis included the prediction of pressure perturbations given the model conditions using the slag ballistics model

When the test schedule was well underway work was begun on the inhibitors for this model. At one time it was thought that a nozzle throat plug would be required for this model to obtain velocities in the chamber that would cause resonance with the inhibitor edge tone frequencies. The latest calculations show that this plug is not necessary. In addition, it was planned to have an inhibitor that would protrude into the flow field an inch. This inhibitor could then be cut down to obtain data over a range of inhibitor heights. This would help the results of the tests because it will not be necessary to obtain an initial exact match of the port velocity for resonance.

Continuing work was performed with the slag ballistics model. The effort was aimed at improving the predictions made by the model for both the RSRM 6.5% Scaled Slag Model and the full scale RSRM. A new variation of the model was tried. The original model calculated the trajectory of a single globule of slag with an area equal to the total blockage and mass based on the density multiplier. This new model calculated trajectories based on smaller droplets from 0.05 to 0.4 inch in diameter and with a density equal to the water or slag, respectively. This model did indeed produce a better fit with the experimental data in that the slope of the pressure spike/chamber pressure versus water flowrate plots were lower and thus in better agreement with the data. Unfortunately, when the model was used on the full scale RSRM the model predicted a lower thrust to pressure ratio then observed for static motor tests. It was determined to run the original model with a new slag density multiplier based on the latest cold flow data.

During the test schedule the importance of a study of the low frequency oscillations measured in the model chamber during simulated slag ejection became apparent. The following write-up was submitted to state our test objectives and justify additional dynamic pressure gauges on the nozzle exit cone to confirm the periodicity of the slag ejection phenomena.

General: There remains a significant need and interest to determine the triggering mechanism for the periodic discharge of slag from the RSRM. Low frequency oscillations (~ .6 Hz) have been observed in static motor tests and appear to be associated with periods of slag discharge. Our hypothesis is that unsteady vortex phenomena around the nose of the nozzle periodically ingest slag and discharge it through the nozzle causing pressure perturbations. These type of phenomena are difficult to deal with using CFD tools only. It is exciting that the same phenomena appears to be occurring in our slag ejection model at a frequency that can be related to the full scale motor by appropriate scaling. This basic unsteady vortex flow structure has been observed in RSRM water flow models tested at VPI by Woody Waeche during the redesign investigation. Therefore, this division has a unique opportunity to capitalize on a model and test program already in place by discovering and measuring the interaction between an unsteady flow phenomena and slag ejection. An AIAA paper on this topic has recently been accepted for the Propulsion Meeting in July.

Objectives: The objectives of the current testing which relate to the low frequency oscillations are:

> Determine if an unsteady vortex phenomena around the submerged nozzle nose is the source and cause of the very low frequency pressure oscillations observed during slag ejection in both the model and the motor.

> Determine if there is an oscillating flow rate component for the ejected slag (water) that relates to the oscillating component of the model chamber pressure.

Instrumentation: Specific instrumentation tasks required to accomplish these objectives are:

> Develop and implement instrumentation required to determine if there is a periodicity to water ingestion and ejection and measure only the frequency.

> Implement boroscope viewing and recording of the activity of the simulated slag pool underneath the nozzle nose.

It was suggested by the Instrumentation Branch that upstream facing dynamic pressure gauges mounted on a probe which would be positioned downstream of the model nozzle may be able to record the dynamic water impact effect. This may work but there is also a dynamic pressure effect related to the oscillating chamber pressure and we

may not be able to discriminate between the two and thus we will not be able to prove that the water flow is periodic. The shocks from the probe and the model nozzle wall/diffuser wall interaction will generate a complex flow preventing us from being able to predict the pressure effects on the gage as opposed to the water effects.

Another suggestion is to flush mount dynamic pressure gages in the model nozzle wall near the exit plane; one at the top and one at the bottom. We know that during the horizontal motor static firings the slag is ejected near the bottom of the nozzle. This conclusion is supported by circumferentially spaced axial accelerometers, fixed housing strain gages and nozzle mounted radiometers. Higher amplitudes are noted on the bottom side of the nozzle. Also, force analyses of the rock and tilt actuator loads indicate applied nozzle exit cone forces on the bottom half of the nozzle during the slag ejection event.

These data observations are due to slag being ingested into the nozzle flow from the pool on the bottom of the motor. The slag stream moves through the nozzle at a subsonic speed in a supersonic exit cone flow field. This produces shock waves which intersect the nozzle wall and result in higher pressures on the lower nozzle wall. These pressure waves result in forces and strains on the lower half of the nozzle wall.

Since our model is also horizontal, the water expulsion should favor the lower half of the nozzle and having dynamic pressure gages on both the top and bottom of the nozzle will enable us to compare our results with full scale motor data. Simply by comparison of the data from the top and bottom of the nozzle we will know the effect of the water without having to predict magnitudes for both the water impact effect and the oscillating chamber pressure effect. Analysis of the dynamic data from the top and bottom gages will tell us if the water discharge is periodic and matching the frequency of the chamber pressure oscillations.

Recommendation: Install dynamic pressure gages in the nozzle wall near the exit plane at both the 0° and 180° locations. Also, try dynamic gages in an impact probe mounted as close to the exit plane as possible. Proceed with these instrumentation additions with a schedule order that will yield results in the shortest possible time.

Dynamics pressure gages have been installed in the model nozzle wall near the exit plane close to the top and bottom positions. The next phase of testing will concentrate on acquiring data from these nozzle pressure transducers which will hopefully contain the signature of the low frequency periodic entrainment and discharge of slag.

Preliminary data from dynamic pressure gauges installed near the exit plane of the nozzle is showing encouraging signs of matching low frequency oscillations found in the model chamber. Furthermore, the magnitude of these oscillations appears to be quite large as would be expected due to the passage of shock waves from the water globules over the gauges. Also, efforts are continuing on getting camera images

through a boroscope of the motion of the water around the submerged nose of the nozzle.

The technical paper "Effects of Slag Ejection on Solid Rocket Motor Performance" was completed and presented at the 31st AIAA Joint Propulsion Conference in San Diego, July 10-12th. Very significant dynamic data findings, aided by miniature video camera recordings of the dynamic motion of the simulated slag during periodic ingestion and discharge through the nozzle, unfolded immediately before the meeting. A hypothesis was developed to explain the measured and recorded periodic discharge of slag based on unsteady inlet vortices previously observed by other investigations for submerged nozzle type inlets with high flow rates. The video film was shown along with the paper presentation. Significant interest was shown in the paper at the meeting and approximately 100 copies were bought or given out. A copy of that paper is included in Section 3.1.1.1.

RSRM Inhibitor Dynamics Model Design and Analysis Work

A meeting was held on 2 December 1994 with NASA/MSFC personnel to discuss the RSRM NBR Inhibitor Dynamics Model. Topics discussed included test objectives, hardware requirements, the test plan, and a test schedule.

ERC performed a number of calculations pertaining to the RSRM NBR Inhibitor Dynamics Model. These calculations included the chamber pressures at which to run the tests, dynamic pressures on the inhibitors, and the sizes of the inhibitor simulators for the model. The dynamic pressures were calculated such that the dynamic pressure in the model would be the same as the dynamic pressure in the full scale RSRM. This was done so that the deflection angle of the inhibitors in the model would be approximately equivalent to the deflection angle of the inhibitors in the full scale RSRM. In addition, calculations were made to match the edge tone frequencies of the inhibitor simulators with the first longitudinal modes of the model. Due to the physical characteristics of the model there are two first longitudinal mode frequencies. One of these frequencies is 44 hertz which corresponds to an open-closed system and is present due to the model chamber itself. The second frequency is 61 hertz for a closed-closed system which is present due to the model chamber in addition to the adapter chamber located at the forward end of the model chamber.

The inhibitor dynamics testing accomplished in December 1994 was a very abbreviated program designed to acquire a few limited tests on a rush schedule to address a critical flight readiness issue related to stiffer NBR inhibitors. After these tests were successfully completed, it became apparent that follow-on testing would increase confidence in the Strouhal number correlations as well as provide the opportunity to further evaluate other NBR material samples as requested by the Materials Lab. Accordingly, on the Extended Test Plan for the RSRM Inhibitor Dynamics Model was developed as outlined in the pretest report included here. This report also provides a detailed discussion of the model hardware and instrumentation, as well as the planned testing. The RSRM Inhibitor Dynamics Model Pretest (ERC/HSV-TR95-01) report includes final review comments from NASA/MSFC personnel. Copies of the pretest report were made and delivered to Jack Hengel, ED34, for distribution to the appropriate personnel.

A sketch of the model was made showing mass addition piping added to the current model in order to obtain flowrates over the center and aft inhibitor which would be in the correct proportions to match the RSRM. The mass addition piping would be connected to the model through the instrumentation ports in spool pieces #1 and #3. This concept was presented to NASA/MSFC but a subsequent decision was made to delete mass addition modifications from the Inhibitor Dynamics Model and defer this testing to the RSRM 10% Scale Mass Addition Model.

A set of preliminary and operating requirements was completed for this model and presented for review. Comments on dynamic instrumentation and methodology for

sizing the extended length chamber were received from ED33 and incorporated into the requirements. Also, a preliminary test matrix was developed which showed requirements for zero length inhibitors at both the center and aft joints. The scope of work for DEI regarding exact hardware and instrumentation requirements was based on results of this review.

The Preliminary Design Review for this model was held on 6 July 1995. ERC prepared materials to be presented at the PDR, including updated drawings of the model geometry which include clarification's since the last design review of this model.

A pre-test meeting for this model was held on 22 August 1995. The model was installed in the facility and the test instrumentation checked out. The aluminum inhibitor simulators have accelerometers installed on for the first series of tests. This first series of tests was velocity profile survey of the model. A velocity profile rake was installed in the model in the #3 spool piece. This velocity profile survey was being performed to verify the symmetry of the flow field upstream of the inhibitors since the model was being supplied with only two of the four feeder pipes. This data has been analyzed and plots were given to Jack Hengel, ED34.

PRETEST REPORT

RSRM INHIBITOR DYNAMICS MODEL TESTS

8 May 1995

Prepared for:
National Aeronautics and Space Administration
George C. Marshall Space Flight Center
Marshall Space Flight Center, AL 35812

Contract NAS8-39095

Prepared by:
ERC, Incorporated
Huntsville Operation
555 Sparkman Drive, Suite 1622
Huntsville, AL 35816

PREFACE

This report was prepared by the Huntsville Operation of ERC, Incorporated for the Fluid Dynamics Division of the Science and Engineering Directorate, George C. Marshall Space Flight Center, National Aeronautics and Space Administration. This effort was performed under Contract NAS8-39095 with John E. Hengel, ED34, serving as the Contracting Officer's Technical Representative.

The ERC, Incorporated contributors to this report are David C. Purinton, who will serve as Performance Data Analyst, and R. Harold Whitesides, who serves as Project Engineer. Model design, and test planning contributions were also received from Steve Skelley, ED34, and other Fluid Dynamics Division Personnel.

TABLE OF CONTENTS

LIST OF TABLES

LIST OF FIGURES

1.0 INTRODUCTION

In late 1994 it was discovered that the NBR inhibitor material on the newer RSRM motors was significantly stiffer than that in previously flown motors. Concern arose as to the effect that this stiffer material would have on the pressure oscillations in the motor. In addition, information was needed on how the stiffer NBR material would trap slag in relation to the older NBR material. A series of simple tests was run and analysis completed and presented by 23 December 1994. Since those tests there has been an expressed interest by the Chief Engineer's Office in continuing the inhibitor dynamics testing with cold flow models. It is well established that there are significant interactions between inhibitor hole tone frequencies and RSRM acoustic modes which increase the amplitude of dynamic pressure oscillations. Other investigators have analyzed the problem and some cold flow testing has been done, but not with models that are properly scaled to RSRM such that application of results to RSRM is straight forward. The development of cold flow models and correlating analytical models will give NASA/MSFC the capability to evaluate in a timely manner the effect of material property and design changes on the potentially critical issue of thrust oscillations.

These tests will utilize the Solid Rocket Motor Air Flow Facility (SAF) with additional hardware developed specifically for these tests. This facility is capable of testing various solid rocket motor model configurations over a wide range of chamber pressures and flowrates and is capable of full scale RSRM Reynolds Number simulation. This test will use Checkout Model 538 spool pieces to model the motor chamber but will make use of a new chamber length extension spool piece which changes the first longitudinal mode frequency of the model. This model will be a 6.5% scale RSRM model scaled to a burn time of approximately 67 seconds. The model will have provisions to install inhibitors at two locations which will simulate the center and aft joints of the full scale RSRM.

2.0 OBJECTIVES

The primary objective of the RSRM Inhibitor Dynamics Model Tests is to model the acoustic environment of the full scale RSRM and determine the effect of inhibitor geometry and properties such as material stiffness on the pressure oscillations in the RSRM motor chamber. Specific test objectives are as listed below:

Objective 1: Demonstrate the ability to achieve tuning conditions between inhibitor edge tone frequency and model longitudinal modes through the use of empirical models to design inhibitors and set test conditions.

There exist a number of analytical tools for modeling the interaction between the inhibitor edge tone frequency and the model longitudinal modes. By calculating the conditions for resonance and then performing the tests with various parametric variables it will be possible to improve the accuracy of the correlation models used.

1

Objective 2: Determine the effect of inhibitor geometry, inhibitor material modulus, and model dynamic pressure on the oscillating pressure component using both single and double joints with inhibitors.

The effect of inhibitor geometry will be studied by having a number of different inhibitors made of varying heights. The test plan will make use of inhibitors ranging from 0.50 inches in height to 1.75 inches in height.

The effect of material modulus will be studied by using both rigid inhibitors made from aluminum and flexible inhibitors made from NBR material of varying stiffness. The differences in the magnitude of the pressure oscillations can then be correlated to differences in material modulus as it affects the inhibitor geometry in the model.

Finally, the tests will be run at three different levels of dynamic pressure. This pressure scan not only loads the inhibitors differently, but also allows for a Reynold's number correlation to be performed on the data.

Objective 3: Develop and implement instrumentation to measure the frequency (and amplitude if possible) of both the flexible NBR inhibitors and the rigid aluminum inhibitors.

Measuring the frequency and amplitude of the aluminum and NBR inhibitor vibrations with this model will provide a data base of inhibitor performance which can be used with future inhibitor designs and/or materials to predict performance.

Objective 4: Develop an analytical model based on measured critical Strouhal numbers for the scaled model geometry that is applicable to full scale RSRM and can be used to gauge the effect of inhibitor height, thickness, and material changes on the amplitude of the pressure oscillations.

An analytical model will be developed which will correlate the variables studied in the RSRM Inhibitor Dynamics Model Tests. This analytical model will allow for predictions of inhibitor performance in the future should any of the inhibitor variables change.

3.0 TEST REQUIREMENTS

The test requirements for the RSRM Inhibitor Dynamics Model Tests were developed by determining the conditions for resonance between the inhibitor edge tone frequency and the model longitudinal mode. The inhibitor heights were selected by determining what inhibitor heights would have an edge tone frequency near the model longitudinal mode with the given throat diameter which exists with this model. This study is shown in Figure 1 and Figure 2. From Figure 1 it can be seen that for resonance between the inhibitor edge tone frequency and the model first longitudinal

2

mode of 61 Hertz, an inhibitor height of 1.25 inches is required for the aft joint inhibitor. Similarly, Figure 2 shows that for the center joint inhibitor the required inhibitor height is also 1.25 inches with the chamber length extension for a first longitudinal mode of 30 Hertz. The tests will combine these heights along with other heights in a parametric study as shown in the test matrix in Tables 1 - 4. In order to apply the results to a wider range of cases, tests will also be run at 25%, 50% and 75% of the maximum model pressure which can be accomplished in the facility. It should also be noted that the minimum test duration is set at 20 seconds.

The line denoting the model throat with the 2.478 plug was calculated to determine alternate test conditions which could be run with the model. The nozzle throat plug allows resonance between the model longitudinal acoustic mode and the inhibitor edge tone frequency at higher inhibitor heights. The nozzle plug has already been made and is available for testing if required. The nominal throat diameter without the plug for these tests is 3.50 inches.

The test matrix for the RSRM Inhibitor Dynamics Model Tests is divided into three series. The first series outlines the tests to be run with only one rigid inhibitor installed in the model. The tests, denoted as Series IA and shown in Table 1, will use an inhibitor placed between spool pieces #3 and #1 in order to model the aft joint of the RSRM as shown in Figure 4. The tests in Table 2, Series IB, will test a rigid inhibitor between spool pieces #2 and #3 to simulate the center field joint of the RSRM as shown in Figure 5. For this configuration a zero height inhibitor should be installed in the aft joint location along with the chamber length extension.

The second series of tests, shown in Table 3, outlines the tests to be conducted with two inhibitors installed in the model. These are referred to as Series II tests. The rigid inhibitors will be installed between spool pieces #3 and #1 to again model the aft joint of the RSRM and also between spool pieces #2 and #3 to model the center joint of the RSRM simultaneously, as shown in Figure 5. These tests require a chamber length extension to change the model first longitudinal acoustic mode to 30 Hertz.

The Series III tests, outlined in Table 4, are again performed with only one inhibitor simulator installed in the model and the chamber length extension removed. The inhibitor simulator will be installed between spool pieces #3 and #1 to simulate the aft field joint of the RSRM as depicted in Figure 4. This series of tests will differ from Series IA in that the inhibitor simulators for this series of tests will be flexible. The inhibitors will be made from NBR material of varying stiffness.

All of the test series will be run over a range of model pressures and flow rates. This is done to obtain a range of Reynold's Numbers for the tests. In addition, the varying model pressures and flow rates will produce differing air loads on the inhibitors which will vary the deformation of the inhibitors.

Not shown in the test matrix are necessary calibration runs to obtain a baseline measurement of model frequencies with the chamber length extension in place. These runs have previously been performed for the model without the chamber length extension. These additional runs should include not only the chamber length extension but a zero height inhibitor at both the center and the aft joint simulator.

4.0 FACILITY DESCRIPTION

The Solid Rocket Motor Air Flow Facility (SAF) Phase II configuration is shown in Figure 3. The air storage for the SAF consists of eight storage tanks having 9100 cubic feet of storage capacity. This air supply is a pressure blowdown system which is discharged through the test model to the atmosphere. The inlet air is filtered through a bonded fiberglass cylindrical canister filter (0.3μ rating) that is designed for a maximum pressure of 1960 psig and a maximum flowrate of 320 lbm/sec. The ROV isolation valve is downstream of the filter and is rated for a maximum pressure of 1960 psig. This valve can be quickly shut down in case of emergency. The actual test model inlet pressure is controlled by a quiet trim control valve. The valve uses a hydraulic operator for actuation and will hold the test model stagnation pressure constant for each test run as the supply tank pressure decays. Downstream of the quiet valve, a pilot operated relief valve is located to discharge 100% of the flow operating at 1320 psia. The flowrate will be metered by a venturi, which is stationed a minimum equivalent of 10 L/D's downstream of the quiet valve.

Downsteam of the venturi, the flow is split into the two facility supply legs, as shown in Figure 3. These facility supply legs each feed two manifold arms, for a total of four arms. The pressure sensing location for the quiet valve feedback control is located in these facility supply legs upstream of the choked metering nozzles in the manifold arms. Each one of these manifold arms includes a metering nozzle. With the metering nozzles installed the facility operates in Mode "A". The facility has the capability to operate in a Mode "B" where the four metering nozzles are removed. The installation of the metering nozzles ensures a constant flowrate through the system which is independent of any nozzle blockage. The manifold arms feed into an adapter chamber at the head end of the model. From the adapter chamber the flow is passed through the model port and exits the model through the submerged nose nozzle.

The mass flow through the system is ducted to atmosphere through the test model diffuser. The diffuser enables the test model to operate at full scale booster nozzle expansion ratio without flow separation. Before the air reaches the atmosphere, it is ducted through an 85 dB Silencer which is located outside of building 4777.

Testing will be conducted in Mode "A" with a minor modification. Instead of having all four choked metering nozzles installed in each of the four header pipes, two opposing header pipes will employ the choked metering nozzles while the other two header pipes will be blanked off. This is necessary in order to be able to correctly

model the motor Reynolds Number at the burn time chosen. The metering nozzles were designed to choke with a 10% scale model. It is necessary to blank off two of the manifold arms in order to keep the metering nozzles choked with the 6.5% model at the operating pressure and flowrates for these tests. The manifold arms designated B (Bottom South) and D (Top North) will be operational while arms A (Top South) and C (Bottom North) will be blanked off. Again, by operating in test Mode "A", the checkout model flowrate will be independent of any model chamber pressure fluctuations occurring during the test.

5.0 MODEL DESCRIPTION

The RSRM Inhibitor Dynamics Model consists of three model chamber spool pieces from Checkout Model 538, a chamber length extension spool piece, two joint simulators, and a submerged nose nozzle. The spool pieces will be arranged in the order of 2-3-1 in the direction of the airflow with the chamber length extension ahead of the three numbered spool pieces. This will be done to provide instrumentation as close as possible on either side of the aft joint simulator. Wedge shaped gimbal flanges between the nozzle and the chamber would enable the model to be tested at three fixed gimbal angles of 0, 2, and 4 degrees, although these tests will only be run at a gimbal angle of 0 degrees. Figure 4 is a labeled sketch of the original model. Figure 5 shows the model with the chamber length extension spool piece in place. The second configuration will be used to obtain resonance between the model longitudinal acoustic mode and the center inhibitor edge tone frequency. All Test Requirements will use this model terminology to describe locations and axial positions along the length of the RSRM Inhibitor Dynamics Model.

It should be noted that the submerged nose nozzle to be used in these tests is from the RSRM 6.5% Scaled Slag Ejection Model. This nozzle has twelve injection ports in the mounting flange which were used to inject water into the model. These ports will not be used for these tests and should be sealed off.

The RSRM Inhibitor Dynamics Model will have the ability to model the aft field joint and the center field joint of the RSRM motor. This modeling can include flexible inhibitors or rigid inhibitors to simulate the inhibitor in the actual RSRM motor. For a portion of these tests the rigid inhibitors will be made from aluminum so that the geometry of the inhibitors is known. This will make the calculation of critical Strouhal numbers for the model more excat. Flexible inhibitors will also be tested to study the effect of stiffness on the inhibitor edge tone frequency.

6.0 INSTRUMENTATION

The RSRM Inhibitor Dynamics Model Tests will have approximately 38 model measurements, which are located axially and circumferentially throughout the model at

key locations (or stations) in the model. These measurements include total, static and dynamic pressures as well as bulk temperatures. A detailed listing of instrumentation is shown in Tables 5 - 9. A schematic of the instrumentation is shown in Figure 6. The instrumentation for both the configuration without the chamber length extension as well as with the chamber length extension will have the same instrumentation. The only difference will be the station numbers of the instrumentation as the chamber length extension will move all model stations except the adapter chamber a distance of 119.725 inches downstream. Figure 6 shows the planes of the model at which instrumentation is present and also provides a table for quick reference as to the types of instrumentation at various model locations. Tables 5 - 9 provide more detailed location information on the instrumentation.

The accelerometers listed in Table 9 will be used to measure the oscillations of the inhibitor simulators at the center and aft joint simulators. The accelerometers will be mounted as close to the inhibitor simulator tips as possible in order to maximize vibration amplitude. The accelerometers will be mounted on the downstream side of the inhibitor simulators to avoid causing any disruptions in the flow field.

A total of 38 test measurements will be taken for each test and are broken down into individual measurements in the following list. This listing provides the number of measurements required to complete the test objectives. Ranges of all of the measurements are provided in Tables 5 - 9.

22	Static Pressure Taps - Table 5
1	Total Pressure Probe - Table 6
5	Dynamic Pressure Gauges - Table 7
6	Temperature Probes - Table 8
4	Accelerometers - Table 9
38	**Total**

Static and total pressure data will be measured using differential pressure transducers with appropriate ranges connected to an electronic scanning system. This system is capable of measuring 256 channels of data. These measurements will be recorded as digital test data on a Hewlett Packard recorder and will be translated into engineering units. The recording method will use frames of averaged data per test, at steady state, which is in turn read into the Aero Fluids Analysis System (AFAS) VAX. Table 10 shows the instrumentation label format that will be used for the RSRM Inhibitor Dynamics Model. These label formats are compatible with the AFAS database measurement label standard. All the dynamic pressures and accelerometer outputs will be recorded on an FM tape recorder. The output from the thermocouples in the forward and the aft chamber of the model, as well as the adapter chamber, should also be recorded on an FM tape recorder. Both the fluctuating and the mean values, AC and DC components, respectively, from the dynamic pressure gauges and the thermocouples should be recorded. The accelerometers will only have a fluctuaing (AC) component and thus will only require one recorded channel per accelerometer.

7.0 PERFORMANCE ANALYSIS PROGRAM

The model performance data will be transferred from the NASA AFAS VAX to ERC, Incorporated's Tri-Star 486 computer via a Hayes modem or as a backup via computer floppy discs. The backup mode of transfer ensures quick analysis of the data even if problems are encountered with the NASA AFAS VAX. This data, in turn, will be "read" into EXCEL 4.0, which is a spreadsheet program. The data will then be statistically analyzed for outlying points, averaged and used for calculations to evaluate the system performance.

A performance program will be developed specifically for the RSRM Inhibitor Dynamics Model testing. The input data will be in terms of averaged frames of data over a period of time at steady state conditions. Ten to twenty frames of data per measurement, per test, is expected. Sometimes the framed data has a value that is inconsistent with the other values in a particular steady state frame. This anomaly could be caused by a number of reasons, however, in order to have an averaged frame that represents steady state, all anomalies or "outliers" will have to be deleted before an averaged value can be determined from one set of values in a frame. Therefore, the performance program will include a statistical algorithm to delete any extreme points from the steady state data. Extreme points are defined as a point that does not fall in the range of ω/σ or range divided by the population. The algorithm compares each observation with the nearest point in a small sample of data. If one observation is not statistically close to the rest of the sample data, the point is removed. This method is described to be a valid method for a small population of data.[1] The data will then be averaged to provide a single value for each measured parameter for each test.

The program will use one-dimensional equations as shown in Table 11. Specific calculations that will be made include local Mach numbers, total pressures, static pressures, total temperatures, local velocities and flowrates. These parameters will be used along with model dimensions such as throat diameter, inhibitor hole diameter, and the distance between inhibitors and the nozzle throat plane to calculate Strouhal Numbers in an attempt to correlate the vortex shedding frequencies. The Series I and Series II Checkout Model 538 performance analysis programs, as well as the RSRM Nozzle Slag Ejection Precursor Tests, also utilized EXCEL to manipulate the test data. EXCEL 4.0 operates in a windows environment and utilizes a spreadsheet to manipulate data. This software has proven to be powerful in program customization and graphical results. The EXCEL 4.0 graphics package will provide excellent graphical displays of the results.

---

[1]Dixon, Wilfred J. and F. J. Massey, Jr. Introduction to Statistical Analysis, McGraw-Hill, Inc., New York: 1969.

Computational Fluid Dynamic (CFD) calculations will also accompany the one-dimensional performance calculations, since two-dimensional effects will exist in the vicinity of the inhibitors and simulated field joints places in the RSRM Inhibitor Dynamics Model. The Strouhal Number is usually calculated using an average one-dimensional velocity through the inhibitor hole opening; however, it may be that the frequency correlation can be improved by using the actual velocity at the edge of the hole at the point where flow separation and vortex shedding are occurring. This will require a two-dimensional CFD solution of the model port flow field with the single and/or double inhibitors in place.

Also, unsteady CFD solutions modeling the vortex shedding phenomena will be performed to increase understanding of the coupling of the inhibitor hole tone and acoustic mode frequencies. The frequency of vortex shedding can be determined along with transport times and dissipation of vortices in the vortex stream between the inhibitor and the aft model cavity.

Table 1. RSRM Inhibitor Dynamics Model Test Matrix

Series IA. Aft Inhibitor Tuning Test Matrix

Test Number	Aft Inhibitor Height	Hole Tone Frequency	Model Pressure	Mass Flow Rate	Inhibitor I. D.
***	inches	Hertz	psia	lbm/sec	inches
1	1.75	89.7	625	139.8	5.020
2	1.75	89.7	469	104.9	5.020
3	1.75	89.7	313	70.0	5.020
4	1.75	89.7	156	34.9	5.020
5	1.50	74.2	625	139.8	5.520
6	1.50	74.2	469	104.9	5.520
7	1.50	74.2	313	70.0	5.520
8	1.50	74.2	156	34.9	5.520
9	1.25	62.4	625	139.8	6.020
10	1.25	62.4	469	104.9	6.020
11	1.25	62.4	313	70.0	6.020
12	1.25	62.4	156	34.9	6.020
13	1.00	53.2	625	139.8	6.520
14	1.00	53.2	469	104.9	6.520
15	1.00	53.2	313	70.0	6.520
16	1.00	53.2	156	34.9	6.520
17	0.75	45.9	625	139.8	7.020
18	0.75	45.9	469	104.9	7.020
19	0.75	45.9	313	70.0	7.020
20	0.75	45.9	156	34.9	7.020
21	0.50	40.0	625	139.8	7.520
22	0.50	40.0	469	104.9	7.520
23	0.50	40.0	313	70.0	7.520
24	0.50	40.0	156	34.9	7.520

Notes:
1.) Strouhal Number = 0.90, Aft Inhibitor to Throat Distance = 22.937 inches.
2.) Nominal Nozzle Throat Diameter = 3.50 Inches.
3.) Closed - Closed first longitudinal mode for model chamber plus adapter chamber = 61 Hertz.
4.) Rigid inhibitor thickness is 0.100 inch, aluminum.

9

Table 2. RSRM Inhibitor Dynamics Model Test Matrix

Series IB. Center Inhibitor Tuning Test Matrix for Extended Length Chamber

Test Number	Cnt. Inhibitor Height	Hole Tone Frequency	Model Pressure	Mass Flow Rate	Inhibitor I. D.
***	inches	Hertz	psia	lbm/sec	inches
1	1.75	42.4	625	139.8	5.020
2	1.75	42.4	469	104.9	5.020
3	1.75	42.4	313	70.0	5.020
4	1.75	42.4	156	34.9	5.020
5	1.50	35.1	625	139.8	5.520
6	1.50	35.1	469	104.9	5.520
7	1.50	35.1	313	70.0	5.520
8	1.50	35.1	156	34.9	5.520
9	1.25	29.5	625	139.8	6.020
10	1.25	29.5	469	104.9	6.020
11	1.25	29.5	313	70.0	6.020
12	1.25	29.5	156	34.9	6.020
13	1.00	25.1	625	139.8	6.520
14	1.00	25.1	469	104.9	6.520
15	1.00	25.1	313	70.0	6.520
16	1.00	25.1	156	34.9	6.520
17	0.75	21.7	625	139.8	7.020
18	0.75	21.7	469	104.9	7.020
19	0.75	21.7	313	70.0	7.020
20	0.75	21.7	156	34.9	7.020
21	0.50	18.9	625	139.8	7.520
22	0.50	18.9	469	104.9	7.520
23	0.50	18.9	313	70.0	7.520
24	0.50	18.9	156	34.9	7.520

Notes:

1.) Strouhal Number = 0.90, Center Inhibitor to Throat Distance = 48.492 inches.

2.) Nominal Nozzle Throat Diameter = 3.50 Inches.

3.) Closed - Closed first longitudinal mode for extended length model chamber plus adapter chamber is approximately 30 Hertz.

4.) Rigid inhibitor thickness is 0.100 inch, aluminum.

Table 3. RSRM Inhibitor Dynamics Model Test Matrix

Series II. Inhibitor Tuning Test Matrix for Extended Length Chamber - Dual Inhibitors

Test Number	Aft Inhibitor Height	Center Inhibitor Height	Hole Tone Frequency	Model Pressure	Mass Flow Rate	Aft Inhibitor I. D.	Cnt. Inhibitor I. D.
***	inches		Hertz	psia	lbm/sec	inches	inches
1	1.75	1.25	29.5	625	139.8	5.020	6.020
2	1.75	1.25	29.5	469	104.9	5.020	6.020
3	1.75	1.25	29.5	313	70.0	5.020	6.020
4	1.75	1.25	29.5	156	34.9	5.020	6.020
5	1.25	1.25	29.5	625	139.8	6.020	6.020
6	1.25	1.25	29.5	469	104.9	6.020	6.020
7	1.25	1.25	29.5	313	70.0	6.020	6.020
8	1.25	1.25	29.5	156	34.9	6.020	6.020
9	0.50	1.25	29.5	625	139.8	7.520	6.020
10	0.50	1.25	29.5	469	104.9	7.520	6.020
11	0.50	1.25	29.5	313	70.0	7.520	6.020
12	0.50	1.25	29.5	156	34.9	7.520	6.020
13	1.75	1.00	25.1	625	139.8	5.020	6.520
14	1.75	1.00	25.1	469	104.9	5.020	6.520
15	1.75	1.00	25.1	313	70.0	5.020	6.520
16	1.75	1.00	25.1	156	34.9	5.020	6.520
17	1.00	1.00	25.1	625	139.8	6.520	6.520
18	1.00	1.00	25.1	469	104.9	6.520	6.520
19	1.00	1.00	25.1	313	70.0	6.520	6.520
20	1.00	1.00	25.1	156	34.9	6.520	6.520
21	0.50	1.00	25.1	625	139.8	7.520	6.520
22	0.50	1.00	25.1	469	104.9	7.520	6.520
23	0.50	1.00	25.1	313	70.0	7.520	6.520
24	0.50	1.00	25.1	156	34.9	7.520	6.520
25	1.75	1.50	35.1	156	34.9	5.020	5.520
26	1.75	1.50	35.1	156	34.9	5.020	5.520
27	1.75	1.50	35.1	156	34.9	5.020	5.520
28	1.75	1.50	35.1	156	34.9	5.020	5.520
29	1.50	1.50	35.1	156	34.9	5.520	5.520
30	1.50	1.50	35.1	156	34.9	5.520	5.520
31	1.50	1.50	35.1	156	34.9	5.520	5.520
32	1.50	1.50	35.1	156	34.9	5.520	5.520
33	0.50	1.50	35.1	156	34.9	7.520	5.520
34	0.50	1.50	35.1	156	34.9	7.520	5.520
35	0.50	1.50	35.1	156	34.9	7.520	5.520
36	0.50	1.50	35.1	156	34.9	7.520	5.520

Notes:

1.) Strouhal Number = 0.90, Aft Inhibitor to Throat Distance = 22.937 inches.

2.) Nominal Nozzle Throat Diameter = 3.50 Inches.

3.) Closed - Closed first longitudinal mode for extended length model chamber plus adapter chamber is approximately 30 Hertz.

4.) Rigid inhibitor thickness is 0.100 inch, aluminum.

Table 4. RSRM Inhibitor Dynamics Model Test Matrix

Series III. Material Modulus Effects Test Matrix

Test Number	Inhibitor Material	Inhibitor Thickness	Model Pressure	Mass Flow Rate
***	***	inches	psia	lbm/sec
1	Nominal NBR	0.061	625	139.8
2	Nominal NBR	0.061	469	104.9
3	Nominal NBR	0.061	313	70.0
4	Nominal NBR	0.061	156	34.9
5	Stiff NBR	0.061	625	139.8
6	Stiff NBR	0.061	469	104.9
7	Stiff NBR	0.061	313	70.0
8	Stiff NBR	0.061	156	34.9
9	Thick NBR	0.068	625	139.8
10	Thick NBR	0.068	469	104.9
11	Thick NBR	0.068	313	70.0
12	Thick NBR	0.068	156	34.9

Notes:

1.) Strouhal Number = 0.90, Aft Inhibitor to Throat Distance = 22.937 inches.

2.) Nominal Nozzle Throat Diameter = 3.50 Inches.

3.) Closed - Closed first longitudinal mode for model chamber plus adapter chamber = 61 Hertz.

4.) Inhibitor height and hole tone frequency to be determined from Series I tests.

Table 5. STATIC PRESSURES

RSRM Inhibitor Dynamics Model

Note: Spool Pieces in 2-3-1 order in direction of air flow.

No.	Parameter	Location	Station	Max Value/Units
1	Po	Manifold Pipe (South Leg of 8" Pipe) Facility Measurement	TBD	1200 psia
2	PS-T0NA	Model Nozzle Entrance Wall @ 0 deg	108.5/230.0	650 psia
3	PS-T0NG	Model Nozzle Entrance Wall @ 90 deg	108.5/230.0	650 psia
4	PS-T0NN	Model Nozzle Entrance Wall @ 180 deg	108.5/230.0	650 psia
5	PS-T0NU	Model Nozzle Entrance Wall @ 270 deg	108.5/230.0	650 psia
6	PS-T0TA	Model Nozzle Throat Wall @ 0 deg	109.7/231.2	381 psia
7	PS-T0TG	Model Nozzle Throat Wall @ 90 deg	109.7/231.2	381 psia
8	PS-T0TN	Model Nozzle Throat Wall @ 180 deg	109.7/231.2	381 psia
9	PS-T0TU	Model Nozzle Throat Wall @ 270 deg	109.7/231.2	381 psia
10	PS-T0EA	Model Nozzle Exit Wall @ 0 deg	119.7/241.2	15 psia
11	PS-T0EG	Model Nozzle Exit Wall @ 90 deg	119.7/241.2	15 psia
12	PS-T0EN	Model Nozzle Exit Wall @ 180 deg	119.7/241.2	15 psia
13	PS-T0EU	Model Nozzle Exit Wall @ 270 deg	119.7/241.2	15 psia
14	PS-D00A	Diffuser Duct Adapter Wall Downstream 0" of Nozzle, @ 0 deg	119.8/241.3	15 psia
15	PS-D00G	Diffuser Duct Adapter Wall Downstream 0" of Nozzle, @ 90 deg	119.8/241.3	15 psia
16	PS-D00N	Diffuser Duct Adapter Wall Downstream 0" of Nozzle, @ 180 deg	119.8/241.3	15 psia
17	PS-D00U	Diffuser Duct Adapter Wall Downstream 0" of Nozzle, @ 270 deg	119.8/241.3	15 psia
18	PS-C00G	Adapter (Aft End of 16" Dia. Section) @ 0 deg	28.7	650 psia
19	PS-S10G	Model Aft (Spool Piece #1) @ 90 deg	90.8/212.3	650 psia
20	PS-S10U	Model Aft (Spool Piece #1) @ 270 deg	90.8/212.3	650 psia
21	PS-S30G	Model Forward (Spool Piece #3) @ 90 deg	77.0/196.7	650 psia
22	PS-S30U	Model Forward (Spool Piece #3) @ 270 deg	77.0/196.7	650 psia

Note: The first station number refers to the model without the chamber length extension.
The second station number refers to the model with the chamber length extension.

Table 6. TOTAL PRESSURES

RSRM Inhibitor Dynamics Model

Note: Spool Pieces in 2-3-1 order in direction of air flow.

No.	Parameter	Location	Station	Max Value/Units
1	PT-C00N	Adapter (Aft End of 16" Dia. Section) @ 180 deg	28.7	650 psia

Note: Total pressure probe will be a Kiel Probe along the model centerline.

Table 7. DYNAMIC PRESSURES

RSRM Inhibitor Dynamics Model

Note: Spool Pieces in 2-3-1 order in direction of air flow.

No.	Parameter	Location	Station	Max Value/Units
1	PDY-C00A	Adapter (Aft End of 16" Dia. Section) @ 0 deg	28.7	see note
2	PDY-S10A	Model Aft (Spool Piece #1) @ 0 deg	90.8/212.3	see note
3	PDY-S30A	Model Forward (Spool Piece #3) @ 0 deg	77.0/196.7	see note
4	PDY-J01A	Aft Field Joint Cavity @ 0 Degrees	86.8/208.3	see note
5	PDY-J02A	Center Field Joint Cavity @ 0 Degrees	NA/182.7	see note

Notes: 1.) All gauges 0 to 650 psia Mean Avg.
2.) Expected range of fluctuating component, 1-20 psi, 10-500 Hertz.
3.) The first station number refers to the model without the chamber length extension.
The second station number refers to the model with the chamber length extension.
4.) All transducers to be ENDEVCO type.

Table 8. AIR TEMPERATURES

RSRM Inhibitor Dynamics Model

Note: Spool Pieces in 2-3-1 order in direction of air flow.

No.	Parameter	Location	Station	Range/Units
1	TAF-MBUU	Upstream Metering Nozzle "B" @ 270 deg	18.6	-50 to 100 deg F
2	TAF-MDUN	Upstream Metering Nozzle "D" @ 180 deg	18.6	-50 to 100 deg F
3	TAF-C00U	Adapter (Aft End of 16" Dia. Section) @ 270 deg*	28.7	-50 to 100 deg F
4	TAF-S10N	Model Aft (Spool Piece #1) @ 180 deg*	90.8/212.3	-50 to 100 deg F
5	TAF-S30N	Model Forward (Spool Piece #3) @ 180 deg*	77.0/196.7	-50 to 100 deg F
6	TAF-DTED	Diffuser Transition Duct Exit @ 45 deg	273.8/395.3	-50 to 100 deg F

Notes: 1.) The first station number refers to the model without the chamber length extension.
The second station number refers to the model with the chamber length extension.
2.) Thermocouples marked with a * to be recorded on FM tape.

Table 9. ACCELEROMETERS

RSRM Inhibitor Dynamics Model

Note: Spool Pieces in 2-3-1 order in direction of air flow.

No.	Parameter	Location	Station	Range/Units
1	ACC-N01A	Aft Inhibitor Simuator @ 0 Degrees	86.9/208.4	see note
2	ACC-N01G	Aft Inhibitor Simulator @ 90 Degrees	86.9/208.4	see note
3	ACC-N02A	Center Inhibitor Simulator @ 0 Degrees	NA/182.8	see note
4	ACC-N02G	Center Inhibitor Simulator @ 90 Degrees	NA/182.8	see note

Notes: 1.) The first station number refers to the model without the chamber length extension.
The second station number refers to the model with the chamber length extension.
2.) Expected frequency range 10-500 Hertz, low g range, high sensitivity.

Table 10. RSRM Inhibitor Dynamics Model Measurement Labels

This table provides an explanation for the instrumentation labels in the preceding tables. The labels are in the following format:

XXX-YYYY.

The first field denoted by XXX describes the type of instrumentation at the station described. The following letter designations tell what the instrumentation type is.

PS	Static Pressure	PDY	Dynamic Pressure
PT	Total Pressure	TAF	Bulk (Air) Temperature
ACC	Accelerometer		

The second field denoted by YYYY describes the location of the instrumentation station. The following letter designations describe the different instrumentation location. The first character gives the physical hardware description.

L	Facility Supply Leg	S	Spool Piece
M	Metering Nozzles	D	Diffuser
C	Adapter Chamber	I	Fluid Injector
T	Model Nozzle or Test Equipment	J	Joint Simulator
N	Inhibitor Simulator		

The second and third character give a more specific location on a single piece of hardware. A zero in either position is used as a place holder. A number following an S or an I designates a particular spool piece or injector. Following a D it gives an axial position in the diffuser. Following a J or N it denotes a joint in relation to the nozzle.

S	South Leg	A	Top South Manifold Arm
N	North Leg	B	Bottom South Manifold Arm
T	Throat	C	Bottom North Manifold Arm
E	Exit	D	Top North Manifold Arm
TE	Transition Duct Exit	U	Upstream of a metering nozzle
N	Nozzle Nose Entrance	D	Downstream of a metering nozzle

The final character gives the circumferential orientation of the instrumentation in degrees from straight up. The correct orientation is facing upstream into the flow with gravity in effect.

A	0	E	60	J	120	N	180	S	240	W	300
B	15	F	75	K	135	P	195	T	255	X	315
C	30	G	90	L	150	Q	210	U	270	Y	330
D	45	H	105	M	165	R	225	V	285	Z	345

Table 11. Formulas Used in Performance Calculations

Mach Number	$$\frac{A}{A^*} = \frac{1}{M}\left[\left(\frac{2}{\gamma+1}\right)\left(1+\frac{\gamma-1}{2}M^2\right)\right]^{\frac{\gamma+1}{2(\gamma-1)}}$$
Total Pressure (psia)	$$\frac{P_o}{P} = \left(1+\frac{\gamma-1}{2}M^2\right)^{\frac{\gamma}{\gamma-1}}$$
Total Temperature (Deg R)	$$\frac{T_o}{T} = 1+\frac{\gamma-1}{2}M^2$$
Flowrate (lbm/sec)	$$W = \frac{0.53175 \cdot P_o \cdot A^*}{\sqrt{T_o}} \quad (C_D = 1)$$
Reynolds Number (throat)	$$Re = \frac{\rho V d_{throat}}{\mu}$$
Strouhal Number	$$S = \frac{f \cdot L_c}{V}$$
Inhibitor Hole Velocity	$$V = M \cdot \sqrt{\gamma \cdot g_o \cdot R \cdot T}$$
Dynamic Pressure	$$q = \frac{\gamma P_s M^2}{2}$$

Figure 1. RSRM Inhibitor Dynamics Model
Aft Inhibitor with Standard Length Chamber

ERC, Inc. 05/02/1995
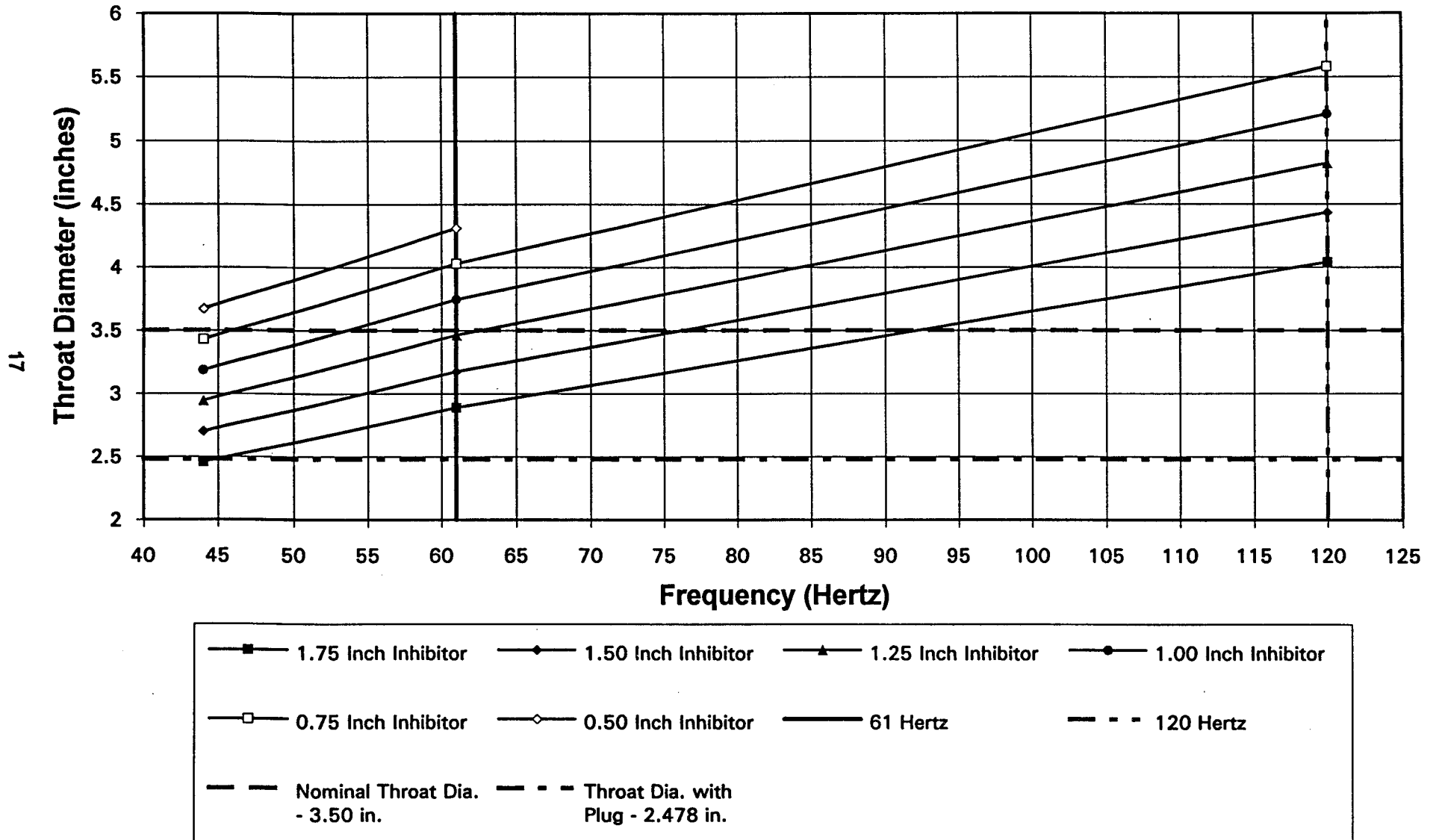
Figure 2. RSRM Inhibitor Dynamics Model
Center Inhibitor with Chamber Length Extension

Legend:
- ■ 1.75 Inch Inhibitor
- ◆ 1.50 inch Inhibitor
- ▲ 1.25 Inch Inhibitor
- ● 1.00 Inch Inhibitor
- □ 0.75 Inch Inhibitor
- ◇ 0.50 Inch Inhibitor
- ── 60 Hertz
- ─ ─ 45 Hertz
- - - - 30 Hertz
- ─ ─ Nominal Throat Dia. - 3.50 in.
- ─ ─ Throat Dia. with Plug - 2.478 in.

ERC, Inc. 04/05/1995

18
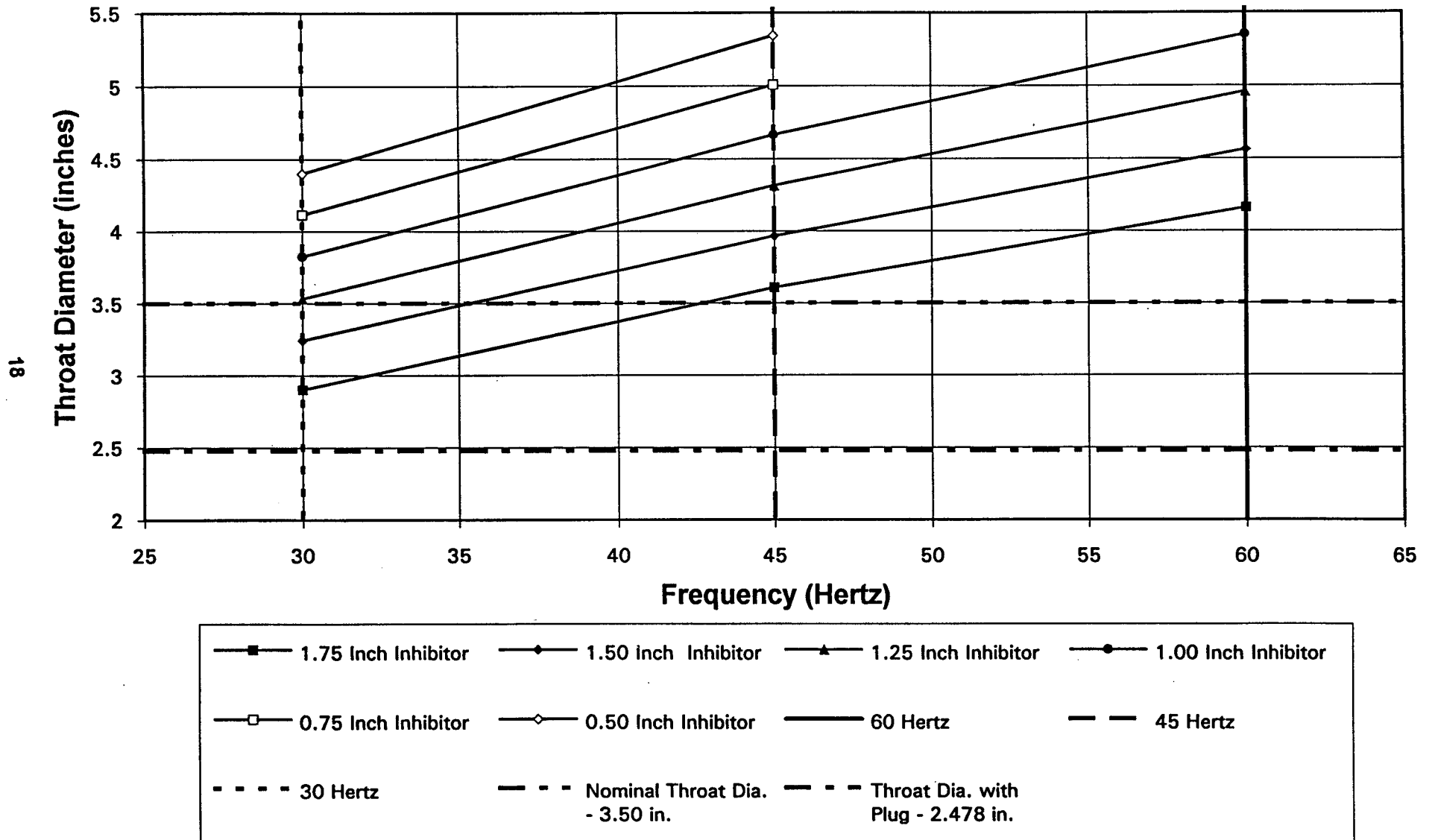
Figure 3. Solid Rocket Motor Air Flow Test Equipment

Fill Connection

Manual Ball Valve, 12 inch, 900 lb.

Manual Ball Valve, 12 inch, 900 lb.

Mixer Temperature Control, 12 inch Butterfly Valves

Mixer

Building 4777

Control Room

Filter

Carbon Steel

Stainless Steel

Vertical Exhaust Duct

Wall Injection Manifold

Plenum

Exhaust Diffuser

SRM Model

Venturi

Relief Valve

Wall Injection Manifold

Air Storage
• 9,100 Cubic Feet
  Storage Capacity
• 1,960 psi, Maximum

Quiet Control Valve
16 inch, 1,500 lb.

ROV Ball Valve
12 inch, 1,500 lb.

Heater
• Temperature Range:
  70° F - 740° F
• Maximum Pressure:
  1,960 psi

Note: This figure shows the heating system which is currently not present at this facility.

891122-6123-1350-188

19

Figure 4. RSRM Inhibitor Dynamics Model Sketch
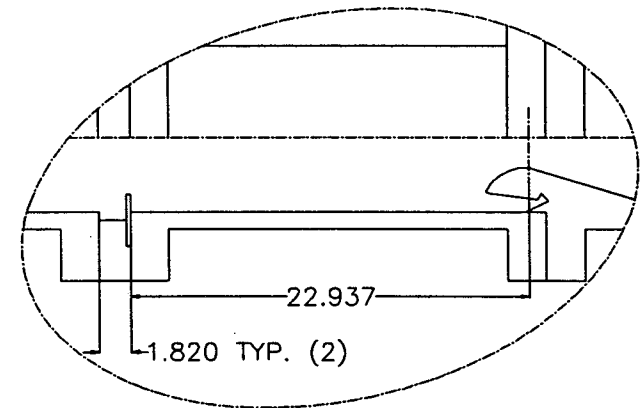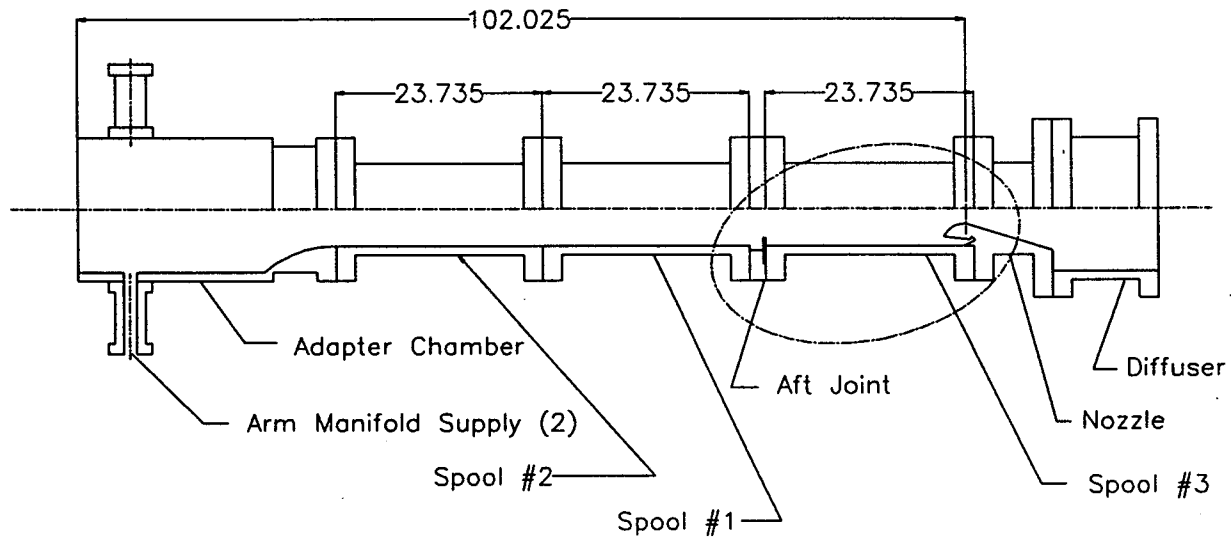
NOTES:

1.) Two manifold arms supply flow to adapter chamber.

2.) Scale 1/20 except where noted.

Scale 1/10

ERC, Inc. 1 May 1995

Figure 5. RSRM Inhibitor Dynamics Model Sketch with Chamber Length Extension
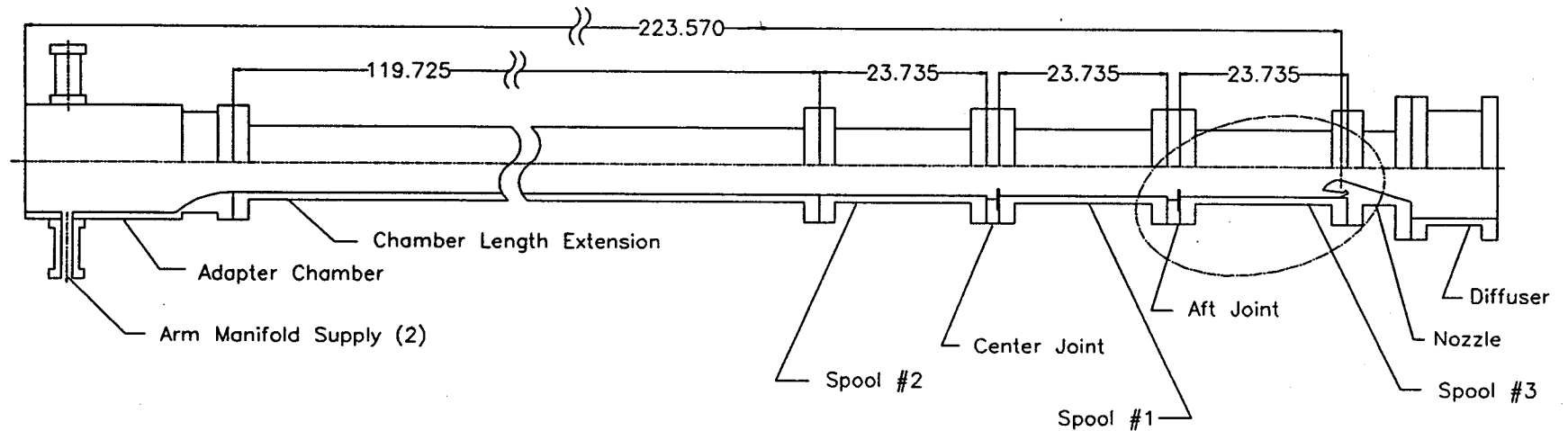
NOTES:
1.) Two manifold arms supply flow to adapter chamber.
2.) Chamber length extension enables resonance for center inhibitor.
3.) Scale 1/20 except where noted.
4.) Chamber length extension I.D. = 8.52 inches nominal. Match I.D. at aft end to existing spool pieces and I.D. at forward end to adaptor chamber. Blend I.D. away from ends to match as received I.D.
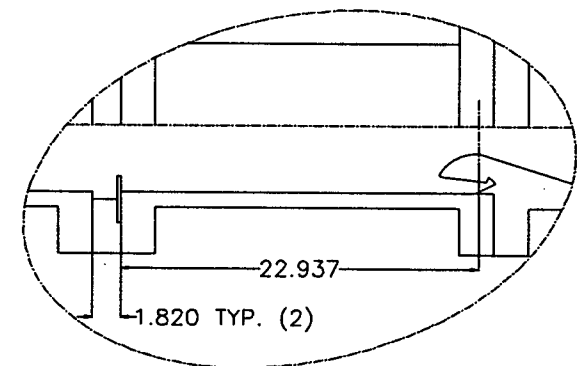
Scale 1/10

Revised
ERC, Inc.   25 April 1995

Figure 6. RSRM Inhibitor Dynamics Model Instrumentation Schematic

Chamber Length Extension

Adapter Chamber

Arm Manifold Supply (2)

Spool #2

Center Joint

Spool #1

Aft Joint

Nozzle

Diffuser

Spool #3
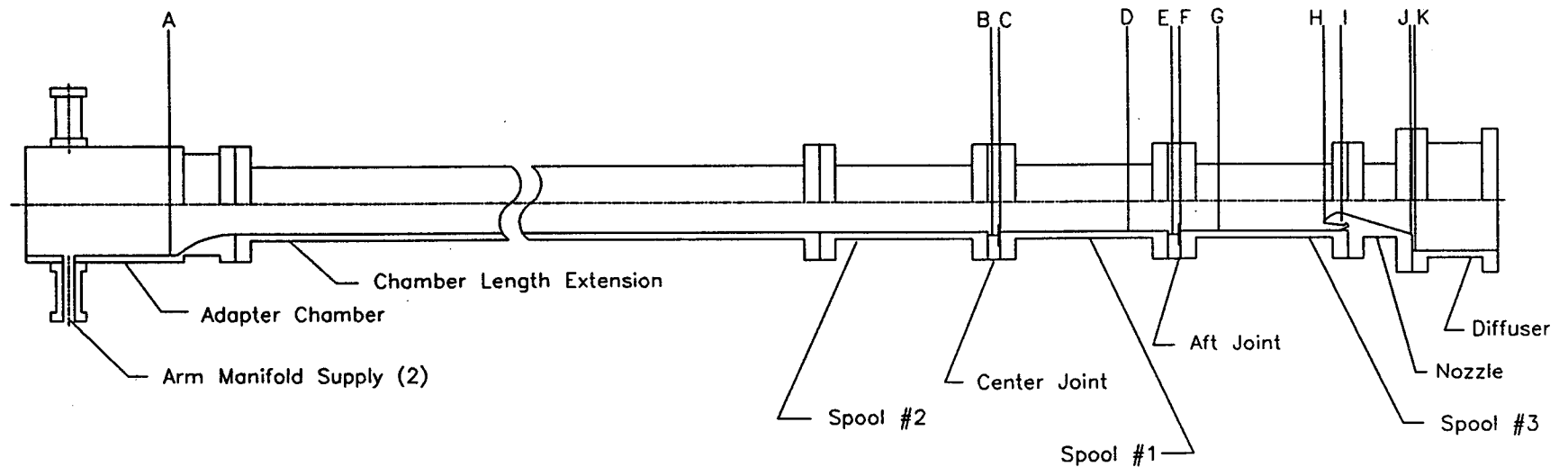
INSTRUMENTATION	A	B	C	D	E	F	G	H	I	J	K	NOTES
Static Pressure Taps	X			X			X	X	X	X	X	Surface
Total Pressure Probe	X											Centerline Kiel Probe
Dynamic Pressure Gauges	X	X		X	X		X					Surface Flush
Thermocouple Probes	X			X			X					Immersed
Accelerometers			X			X						Mounted on downstream face of inhibitor.

STATIONS

Note: Stations B and C only exist when chamber length extension is in place.

RSRM 10% Scale Cold Flow Model Design and Analysis Work

ERC personnel attended a number of meetings to discuss plans for an RSRM Mass Addition Model. Also present at these meetings were personnel from NASA/MSFC and Dynamic Engineering Incorporated. An 80 second burn time RSRM geometry with three joints was provided to Roger Herdy of DEI so that it could be layered over a drawing of the ASRM/Technology Model with two joints which will be modified to produce the RSRM 10% Scale Cold Flow Model.

The basic model description and purpose are stated as:

Model Description: 10% scale model of the entire RSRM including all four segments with mass addition liners and a nozzle assembly with fixed gimbal angle capability from 0 to 8 degrees. Model readily adaptable to burn times from 0 to 85 seconds.

Model Purpose: Provide RSRM Project with test vehicle capable of high fidelity simulation and measurement of the internal flow environment and performance phenomena in the motor and nozzle as related to specific motor design and/ or material upgrades or anomalous conditions.

Candidate testing objectives for the model are as follows:

Inhibitor Dynamics: Evaluate coupling between unsteady flow phenomena at the NBR inhibitors and chamber acoustics at all field joints for various burn times. Frequency coupling and dynamic pressure amplitude enhancement would be investigated with inhibitor geometry and stiffness variations. Results could be scaled directly to RSRM and used to evaluate inhibitor design and/or material changes and improvements under consideration.

Insulation Environments: Measure flow and thermal/erosion environments in all areas of the motor. The change to asbestos-free insulation will warrant the development of higher confidence levels in the thermal and erosion environments for all areas in the motor. Zones of separated flow in the motor at various burn times create uncertainties in the environment which can be measured with heat flux gauges in the simulated insulation surface. This data in terms of heat transfer coefficients can be scaled directly to the full scale motor.

Nozzle Extension Performance: Measure mass discharge coefficients, thrust coefficients, and wall pressure profiles for the extended aft exit cone nozzle. The model nozzle can be configured to represent to proposed nozzle extension and evaluated on the basis of thrust coefficient and wall pressure profile. Thrust coefficients for both the extended nozzle and the existing nozzle can be compared.

Slag Induced Pressure Perturbations: Evaluate and quantify the effect of slag accumulation, entrainment, and nozzle discharge on motor performance using large

scale high fidelity model with mass addition walls. Previous small scale model lacked mass addition walls and instrumentation to measure thrust spike.

Nozzle Gimbal Angle Flow Effects: Evaluate effect of nozzle gimbal angle on chamber/nozzle flow fields and aerodynamic thrust vector alignment. Also measure forces and moments in gimbaled nozzle. Flow field in submerged nozzle region not well understood and this large scale model presents unique opportunity to measure unsteady flow filed using advanced instrumentation techniques.

The general model purpose and candidate model test objectives were presented to and discussed with the Thiokol technical community. After this exchange, the various model test objectives were prioritized and discussed with the RSRM Chief Engineer. Approval was received to proceed with the first priority objective being the inhibitor dynamics experiment at a burn time of 80 seconds. This recommendation along with a very preliminary set of model design and operating requirements were reviewed with Fluid Dynamics Division management and personnel. Directives and various inputs were received to develop and mature the model requirements and target a Preliminary Requirements Review .

A RSRM 10 second burn time geometry was generated and given to DEI to develop a model design. DEI was furnished with a hard copy of ERC drawing H3510 as well as a data file on disk containing the data points for the 10 second as well as the 80 second burn time geometries.

The Preliminary Requirements Review was gave a general overview of the model test objectives as well as the requirements for the model. The following is a summary of the information presented in the review.

The model will be a 10% scale model of the entire Space Shuttle Reusable Solid Rocket Motor including all four segments with wall mass addition liners to simulate the burning propellant surface. The nozzle assembly will include the submerged nose entrance and contoured expansion sections and will have a fixed gimbal angle capability ranging from 0 to 8 degrees. The model will be readily adaptable to burn times form 0 to 80 seconds. Appropriate scaling of model and operating condition will ensure applicability of data to the full scale motor.

The general purpose of the model is to provide the RSRM project with a test vehicle capable of high fidelity aerodynamic simulation and measurement of the internal flow environment and performance phenomena in the motor and nozzle as related to specific motor design and/or material upgrade. The model could be modified as necessary to provide critical and timely data to resolve issues raised by the occurrence of anomalous conditions in the RSRM. The Thiokol technical community strongly supports the argument for having a high fidelity, adaptable RSRM Cold Flow Model readily available for simulation and measurement of flow or performance related phenomena and timely resolution of unexpected anomalies.

There are three specific test objectives for the first Build of the RSRM 10% Scale Cold Flow Model. These objectives are as follows:

- Evaluate coupling between unsteady flow phenomena at the NBR inhibitors and chamber acoustics at all field joints for various burn times. Frequency coupling and dynamic pressure amplitude enhancement would be investigated with inhibitor geometry and stiffness variations. Results could be scaled directly to RSRM and used to evaluate inhibitor design and/or material changes and improvements under consideration.

- Validate effectiveness of currently employed Strouhal number and dynamic pressure scaling methods to predict frequencies and amplitudes of RSRM chamber pressure oscillations.

- Provide data source for validation of unsteady CFD analysis of vortex shedding and acoustic interaction phenomena.

The secondary test objectives for build #1 of the RSRM 10% Scale Cold Flow Model include:

- Evaluate the effect of nozzle gimbal angle on chamber/nozzle flow fields and aerodynamic thrust vector alignment. Also measure forces and moments on the gimbaled nozzle. The flow field in the submerged nozzle region is not well understood and this large scale model presents a unique opportunity to measure unsteady flow field using advanced instrumentation techniques.

- Evaluate extended aft exit cone contour performance by measuring thrust coefficient and wall pressure profile. Model nozzle will include separate add-on extension with sufficient pressure taps on entire nozzle to calculate thrust coefficient for both current and extended nozzle configurations.

The general model requirements state that the model will be a 10% scale, three joint, four segment model. There are three general configurations possible. The first is a 0 to 10 second burn time model in which the star grain in the head end as well as a porous liner would be required. A 20 second burn time geometry would provide a model to perform nozzle gimbal angle tests. The third configuration, an 80 second burn time geometry, would be used to perform inhibitor and slag tests.

The nozzle will be a scaled, submerged nose nozzle and will include the entire contoured expansion section. It will have an optional bolt on extended aft exit cone section. The nozzle will have the ability to be gimbaled from 0 to 8 degrees at fixed gimbal angles. Finally, the nozzle will have full coverage pressure tap instrumentation.

The mass addition liner for the first build of the model will be a drilled hole liner for the late burn times. For follow on builds at earlier burn times the model will have a sintered metal or ceramic powder porous liner. This porous liner will be needed for sub scale characterization flow testing.

The model will make use of a drilled hole flow distribution tube or flow diverters to prevent direct impingement of the flow from the feeder pipes onto the mass addition liner.

Specific requirements for the first build of the model are as follows:

- Motor Configuration - 10% scale length
    - 80 Second burn time - no star grain forward segment
    - Scale factor=9.71% for port diameter only to match area ratio with 10% scale initial nozzle geometry

- Nozzle Configuration - 10% scale
    - Initial time zero geometry - usable at all burn times
    - Extended aft exit cone bolt-on ring
    - Full surface pressure tap instrumentation coverage
    - Zero degree gimbal angle

- Mass Addition Liner
    - Drilled hole liner
    - Porosity 1-2%, Hole diameter=1/16 to 3/32 inch

- Flow Distribution
    - Drilled hole tube (ASRM model requirements)

The design approach for the RSRM 10% Scale Cold Flow Model is to modify the existing three segment ASRM/Technology Model to a four segment RSRM model. The manifold system will require modification and headers added to accommodate the addition model segment. A new RSRM nozzle will be needed which will include the submerged nose and contoured exit section. The existing metering nozzles can be bored out and additional nozzles made for the air supply system. A new liner will need to be made for this model. The liner will be a RSRM 80 second burn time drilled hole liner and flow distribution tube. Some of the axial positions of the model instrumentation will change due to the altered spool pieces. Dynamic pressure gauges at all joints and in the aft nozzle cavity will be added but the hot film flush mounted gauges and heat transfer gauges will be deleted from the required instrumentation.

The material presented above from the Preliminary Requirements Review makes reference to an extended aft exit cone which would be tested to support this add-on to the RSRM nozzle. This project has since been discontinued and thus would not be a part of this model.

In addition, calculations were made to determine the approximate axial locations for flowrate dividers in the model. These axial locations were presented at the Preliminary Requirements Review as a part of ERC, Incorporated drawing H3500.

The ERC, Incorporated drawings H3500 and H3510 were later updated to reflect changes in reference and scaling of the model. The extended aft exit cone was deleted from the model drawings due to the cancellation of this program for the RSRM. The model was also changed from having eight plenum chambers feeding the mass addition liner to having only six feed chambers. This change was a result of having only one feed chamber for each of the two center segments of the model. The need to have only one plenum chamber for each of the two center segments arose from the restriction of only being able to locate feeder pipes in one axial location on the two center segments of the model.

An analysis was performed to calculate the bore pressure gradient down the axial length of the RSRM 10% Scale Cold Flow Model. A FORTRAN computer program was available and the inputs to the program were developed. The geometry of the cold flow model had to be simplified for input into the program. In addition, the mass flow rate for each section of the model was tabulated for input into the program.

Work was also done to determine the locations of the nozzle pressure taps for this model. A table was set up to calculate the area ratios of the pressure taps in the ASRM 8% Aft Section/Nozzle Model. These area ratios were then used to calculate radii for taps in the RSRM 10% Scale Cold Flow Model. Axial stations were then calculated by interpolation in the geometry table for the nozzle. This work included the review of pressure data from the ASRM model so that areas not covered sufficiently in that model can have additional pressure tap instrumentation in this model.

Calculations were also made on the pressure drop across the drilled hole liner for the model. A liner porosity was selected as a result of the analysis and the requirement to have the liner pressure drop significantly more than the bore pressure drop for a given model section. The final selected model liner is 1.5% porosity and holes which are 0.0635 inches in diameter. The associated calculations for this liner are shown in Table I. The section numbers referred to in Table I are shown on ERC drawing H3500. Section 2 corresponds to the cylindrical port section of the forward motor segment. Sections 3 and 4 refer to the forward center and aft center segment of the RSRM, respectively. Section 5 represents the forward portion of the aft segment of the RSRM while section 6 makes up the aft portion of the aft segment of the RSRM. Calculations were also made for the pressure drop across the flow distribution tube for this model. The current flow distribution tube is made up of sections from the ASRM/Technology Model flow distribution tube. This yields varying porosity along the axial coordinate of the model as well as variance in any given model section. The calculations showed a pressure drop across the flow distribution tube from 13 to 65 psid, with a nominal value of 43 psid. This is more pressure drop than is needed for the flow distribution tube and

calculations will be made next month to determine a higher porosity value for the flow distribution tube in order to reduce the pressure drop across it.

The Critical Design Review was held for this model on 18 October 1995. ERC presented the model requirements which included the latest on pressure drops. ERC also took some action items at the CDR. One of these was to develop a test program for drilled hole plates. It was decided to produce some test plates of the same porosity and hole size as the drilled hole liner and the flow distribution tube to determine experimentally the pressure drop across them.

CSD Analysis to Determine the Proper κ-ε Equation Coefficients

A CFD analysis of the internal flow field of a simulated cylindrical port solid propellant rocket motor was completed in May, 1992. The configuration modeled was obtained from a Chemical Systems Division (CSD), United Technologies report, AFRPL TR-86-104. The cold flow test apparatus discussed in the report was nitrogen fed and the report presents experimental data as well as a discussion of the relevant physics of the experiments performed. Both Fluent v4.10 and Fluent/BFC were used in the experimental data comparisons. The original intent of the analysis was to provide a validation case involving a wall mass injection flow for the two Fluent codes. In an unrelated analysis, adjustments to the standard κ-ε model were also shown to improve the pressure drop prediction for the ASRM Technology model.

ERCI has performed several validations of the Fluent/BFC code. The code has produced very good predictions of the experimental axial and radial pressure distributions in the SAF checkout model port without mass injection. No problems with mass or momentum imbalance were noted. However, validation cases worked using Fluent/BFC have not involved mass injection from a simulated cylindrical burning surface. The other Fluent code, Fluent v4.10, is new and although benchmark test comparisons have been made by Fluent Inc., these are the first comparisons made by ERCI between the two codes and experimental data. Therefore this analysis was performed in order to provide a validation case for both Fluent codes and a code comparison between Fluent v4.10 and Fluent/BFC which involved a cylindrical burning motor configuration. Both of the Fluent codes used in this analysis nominally use the standard κ-ε model of turbulence. Both of the codes also employ wall functions in the viscous sublayer.

The standard κ-ε equation used in both Fluent v4.1 and Fluent/BFC utilizes the normal Boussinesq hypothesis and can be written as:

$$\mu_t = \rho C_\mu k^2 / \varepsilon \tag{1}$$

$$\frac{\partial}{\partial t}(\rho k) + \frac{\partial}{\partial x_j}(\rho u_j k) = \frac{\partial}{\partial x_j}\left(\frac{\mu_t}{\sigma_k}\frac{\partial k}{\partial x_j}\right) + \rho(P - \varepsilon) \tag{2}$$

$$\frac{\partial}{\partial t}(\rho \varepsilon) + \frac{\partial}{\partial x_j}(\rho u_j \varepsilon) = \frac{\partial}{\partial x_j}\left(\frac{\mu_t}{\sigma_\varepsilon}\frac{\partial \varepsilon}{\partial x_j}\right) + \rho\frac{\varepsilon}{k}(C_1 P - C_2 \varepsilon) \tag{3}$$

$$P = -\overline{u_i' u_j'}\frac{\partial u_i}{\partial x_j} \tag{4}$$

Equation (1) is the Prandtl-Kolmogorov relation which is obtained from dimensional arguments. The second equation, (2), models the transport of kinetic energy of turbulence. The left hand side of equation (2) represents the convection of kinetic energy while the 1st term on the right hand side of the equation represents the diffusion of kinetic energy. P is the production of kinetic energy term and the last term subtracted from P represents the loss or dissipation of kinetic energy of turbulence. It would be good at this time to note that the kinetic energy of turbulence is defined as the root mean square of the turbulent velocity fluctuations in all spacial directions. Isotropic turbulence is assumed in this model.

$$k = \frac{1}{2}\left(u'^2 + v'^2 + w'^2\right)^2 \tag{5}$$

Also, the dissipation of turbulent kinetic energy is defined as:

$$\varepsilon = \nu\overline{\frac{\partial u'_i}{\partial x_j}\frac{\partial u'_i}{\partial x_j}} \tag{6}$$

Other terms used in the equations are defined as:

t: time

x_j: various spacial coordinate directions representing the problem dimensionality

r: density of the fluid

u_j: velocities in the various coordinate directions

μ_t: turbulent viscosity

n: kinematic viscosity

constants: $C\mu$, C_1, C_2, σ_K, σ_ε

The various terms of equation (3) represent the same convection, diffusion, production, and dissipation phenomena as described for equation (2). The structure of the terms in these equations was not modified in this analysis but the numerical values of the various constant parameters were modified in order to obtain better predictions of the CSD experimental data.

Figure 3 shows the geometry for CSD validation problem analyzed in this work. The experimental apparatus analyzed consisted of a long cylindrical chamber closed at one end and connected to a choked nozzle on the other end. Nitrogen is injected through a porous wall along the cylindrical chamber of the model up to the point where the chamber connects to the nozzle. The dimensions used in this analysis are taken from

the CSD document. The only variation in the setup of the numerical run involves the truncation of the nozzle upstream of the choke point so that the flow remains subsonic. This allows a velocity boundary condition to be used to simulate the mass injection from the porous wall.

The head end pressure in the experiment was 20300pa (29.44 psia). The injectant surface temperature was 278 °K (500.4 °R). The nitrogen injectant has a molecular weight of 28.013. The problem was solved such that the fluid is considered as a compressible gas. The ideal gas law was used in the calculations and the dynamic viscosity used was 1.786×10^{-5}kg/m-sec (1.200×10^{-5}lbm/ft-sec). A specific heat of 1039J/kg-°K (0.248 BTU/lbm-°R) was used and the wall and inlet boundaries were considered to be adiabatic. The injection velocity was determined using the SPP 1-D ballistic code. The value of the injection velocity associated with the conditions stated above was calculated as .662m/s (2.17 ft/s). This value is higher than that stated in the CSD paper, .616m/s (2.021 ft/s). This is cited as a discrepancy in the boundary conditions used in the CSD paper since the chamber pressure, mass injection rate and injection velocity specified do not match. The value of the injection velocity used in this analysis was .662 m/s (2.17 ft/s) as obtained from the SPP code. The experimental run reported in the CSD document had an injection Mach number of .0018 while the CFD solution injection Mach number was .00195. Given the information contained in the CSD report, this was the best match of CFD flow conditions which could be made to the experimental data.

A summary of some general observations about the analysis will be presented before individual steps in the analysis are discussed. The initial data comparisons made between both Fluent codes and the experimental data showed a significant error in the ability to predict both the velocity profile and the kinetic energy of turbulence profile down the model port. A high degree of sensitivity of both the radial velocity and kinetic energy of turbulence profiles to the inlet turbulence quantities used was also noted. This sensitivity to inlet turbulence quantities was also noted in the CSD report. The Fluent codes showed a large variation in the onset of turbulent flow unless the inlet turbulence quantities were highly tuned. This phenomenon was also reported in the CSD document and changes to the k-e model were suggested in the CSD document. This sensitivity to inlet turbulence quantities seems to be associated with the low mass injection rate and low port flow Mach number existing in this cold flow experimental apparatus. The ASRM full-scale motor and the Technology model cold flow simulation of the ASRM motor have much larger port flow Mach numbers and mass injection rates and have shown much less sensitivity to the inlet turbulence quantities. However, this will be investigated further during the continuing analyses of the ASRM Technology model and ASRM full-scale motor. The pressure drop down the model port was very small for the CSD test since the wall mass injection rate was low. Although the experimental pressure drop was over predicted by the CFD code it is difficult to make quantitative judgments with a pressure drop on the order of 1 to 2 psi. However, observations have been made in the past involving the predicted pressure drop down the ASRM full-scale motor port. The Fluent/BFC code has always over predicted the

pressure drop calculation down the ASRM motor port in comparisons made between the CFD code and 1-D ballistic calculations. Since the mass, momentum and energy balance check, the inaccuracy in the prediction of transition and the ASRM full-scale motor pressure drop must be due to the over dissipative nature of the standard κ–ε model used in Fluent/BFC. This has been observed to be especially noticeable in problems involving wall mass injection. This work addresses possible changes to the standard κ–ε model which provide a better estimate of transition onset and the progression of transition down the motor port. CFD predictions using the adjusted κ–ε model will be compared to the CSD experimental data and these changes should also improve the pressure drop prediction down the motor port if the transition phenomena is closely related to the pressure drop down the port. The effect of the adjustments to the κ–ε model constants will be tested using predictions of the ASRM Technology model pressure drop for the CFD codes and a 2-D code which assumes a Culick velocity profile down the model port. The 2-D code has been validated against the 1-D ballistic code discussed in the ASRM Technology Model section of this monthly.

The first subject addressed in this analysis concerns the sensitivity of the flow solution to the inlet turbulence quantities. Two runs were made using the Fluent/BFC code. The runs were identical except for the inlet turbulence parameters.

The two inlet turbulence parameters are the kinetic energy intensity at the inlet, I, and the characteristic length scale of the inlet flow, L. In equation form, the kinetic energy intensity relates the mean flow velocity to the turbulent fluctuating velocities in the following way:

$$k = \frac{3}{2}(\overline{u}I)^2 = \frac{3}{2}(u')^2$$

where

- k: kinetic energy of turbulence
- $\overline{u}$: average velocity associated with the mean flow
- I: turbulent fluctuation intensity
- u': fluctuating velocity component

In the same way, the characteristic length scale, L, is related to the dissipation rate by the following equation:

$$\ell = 0.07L$$

$$\varepsilon = C_\mu^{.75}\frac{k^{1.5}}{\ell}$$

where

ε: dissipation rate

L: characteristic flow length scale

C_μ: constant, C_μ = .09 for the standard k-e equation

The 0.07 is derived from the "average" mixing length in turbulent pipe flow. The value of L was chosen as 100mm which associates the length scale with the size of the porous media used as the surface material of the cold flow apparatus, on the order of 10mm. The value of L was chosen as the same value for both runs. The value of I was set to 1% for one run and 100% for the other run. The run using an inlet turbulence intensity of 1% disagreed with experimental data in the transition of the flow from laminar to turbulent character. The transition to turbulent flow begins much too early and progresses much too fast. Figures 4, 5, 6, 7, 8, and 9 show the transition of the velocity profile down the model port. Figure 4 shows the normalized velocity profile compared with a Culick profile and experimental data at an L/D of 1.8. The velocity profile is laminar. Shortly after this point, the transition begins so that at an L/D of 4.22, the velocity profile has already begun transition. The transition in the experimental data is not noticeable until about at L/D of 6.64. The transition of the flow is also much more rapid than shown in the experimental data. Figure 8 shows that the computed velocity profile is still transitioned more than the experimental data at an L/D of 10.3. After this L/D, the experimental data and the CFD solution agree more closely. Figure 9 shows the velocity profile for an L/D of 12.75. The turbulent kinetic energy is also over predicted as shown in Figures 10, 11, 12, 13, 14, and 15. The CFD run with an inlet turbulence intensity level of 100% also has problems. Figures 16, 17, 18, 19, 20, and 21 show the transition of the velocity profile down the model port for these inlet conditions. The prediction of turbulent flow onset in this run is delayed until an L/D of 10.3, see Figure 20. The transition process is rapid but produces a flatted shape in the velocity profile which still exist at the last experimental measurement station, L/D = 12.75. Figure 21 shows this velocity profile. As has already been said, this illustrated sensitivity to the inlet turbulence quantities has already been reported in the CSD document as well as validation runs for the REFLEX code made by the NASA CFD group.

A journal paper authored by Sabnis and others, "On the Use of the κ–ε Turbulence Model for Computation of Solid Rocket Internal Flows", AIAA-89-2558, provides a method for the adjustment of the inlet turbulence quantities at the propellant surface. As part of this analysis, many runs were made utilizing the Sabnis AIAA paper as a basis for adjusting the inlet turbulence quantities. The paper gives an algebraic equation which adjust nominal inlet kinetic energy of turbulence and dissipation rate according to the ratio of the injection velocity and the friction velocity. The adjustments in the equations made by this paper attempt to decrease the inlet kinetic energy of turbulence and the inlet dissipation rate when the ratio of the injection velocity to the friction velocity is high. This means that when the injection velocity is of the same or

higher order of magnitude as the friction velocity, boundary layer type flow dominates the turbulence phenomena. But if the friction velocity is much larger than the injection velocity, the turbulence phenomena is dominated by the port flow character. The Sabnis paper was used to adjust the inlet turbulence quantities along the cylindrical cold flow porous surface in the axial direction. This was done manually as stated in the paper since an automatic procedure which accurately computes the necessary quantities could not be put in the code at this time. An inviscid solution to the problem with a no-slip boundary condition was used to make axial estimates of the friction velocity along the inlet boundary. This was used to compute the inlet values of kinetic energy of turbulence and dissipation rate used in the code. A better match to the velocity and kinetic energy of turbulence profiles was achieved by using the AIAA paper and this is being kept as a method to be installed in the Fluent code at the first available time. The effect of these κ–ε model updates on the pressure drop calculation down a model with a much larger injection rate was not discussed in this paper and is not known at this time. The changes prescribed in the AIAA paper only adjust the κ–ε model at the inlet and in the viscous sub-layer region of the flow. Since the ASRM motor port calculations have shown little sensitivity to the inlet turbulence quantities, the bulk flow in the port may not be significantly affected by these changes for large mass injection problems. Until changes in the standard κ–ε model used in Fluent can be made, it was decided that in the short term, the best solution to the κ–ε model problem was to attempt to find a set of model constants which better predicted the qualitative and quantitative nature of the port flow in the CSD experiment. These constants will also be tested in both Fluent codes for the ASRM full-scale motor to see if the new set of constants provide a better match with the 1-D ballistic pressure drop calculations.

The standard κ–ε equations have been modified in many different ways for many different kinds of flows in order to obtain a better fit to experimental data. At times, new terms to account for certain physical phenomena have been added to the equations. In some cases, the constants used in the equations have been modified by algebraic equations which make the constants a function of given flow parameters of interest. At other times, the numerical values of the constants themselves have been optimized to match experimental data. All of these are being considered for future incorporation into the κ–ε models of the Fluent code but at the present time, the only feasible method is to attempt to match experimental data better by adjustment of the constants used in the κ–ε equations. A fully automated numerical optimization of the κ–ε model constants was not performed but a large number of runs were made in order to provide the best possible sub-optimal guess of the κ–ε constants within a limited analysis time frame. The constants $C\mu$, C_1, C_2, σ_k, σ_e found in the κ–ε equations already presented were adjusted incrementally in order to determine a set of constants which best match the normalized velocity profiles and normalized kinetic energy of the turbulence profiles down the CSD cold flow port.

Nominal runs were made using an L = 100mm and an inlet turbulence intensity of 1% but runs were also made with various combinations of the κ–ε constants to determine

any effects induced by the inlet turbulence parameters. The set of constants which have given the best fit to the experimental data will now be presented. The standard κ–ε model has the following set of constant parameters.

C_1: 1.44
C_2: 1.92
C_μ: 0.09
σ_ε: 1.3
σ_κ: 1.0

The set of adjustments to the κ–ε constants which gave the best match to the experimental CSD data was:

C_1: 1.44
C_2: 1.65
C_μ: 0.13
σ_ε: 1.3
σ_κ: 1.0

Figures 22, 23, 24, 25, 26, and 27 show the progression of the transition of the port velocity profiles from laminar to turbulent at the various L/D ratios shown on the plots. The kinetic energy of turbulence profiles down the port at various L/D ratios are shown in Figures 28, 29, 30, 31, 32, and 33. The agreement between CFD predictions of the velocity profiles and experimental data is much better for the adjusted κ–ε parameters than the standard κ–ε parameters both before and during transition to turbulent flow. The standard κ–ε model velocity predictions comparable to these predictions are found in Figures 4, 5, 6, 7, 8, and 9. Figures 10, 11, 12, 13, 14, and 15 show the comparable kinetic energy of turbulence profiles.

Fluent Inc. is also testing a new form of κ–ε model which uses renormalized group theory to derive the model constants. This model is referred to as the RNG turbulence model and has shown promise in predicting experimental data on flow separation and heat transfer much better than the standard or modified κ–ε turbulence models. The implementation of this model in the Fluent code was performed by Yakhot and Orszag of Princeton University and documentation of the development of the RNG model can be found in the Journal of Scientific Computing, 1, 3 (1986) and Physics of Fluids, 4, 5 (May 1992). Fluent Inc. will be making some calculations for the CSD model and the ASRM full-scale motor port using the RNG model to determine how well the RNG model can predict the flow in these configurations.

As was previously mentioned, the adjusted κ–ε model constants are also being tested in the ASRM Technology model and full-scale ASRM motor flow field predictions. The calculation of the ASRM Technology model flow field is currently underway using Fluent/BFC. A comparison between the predictions made by the adjusted κ–ε model Fluent/BFC code and the 2-D code shows much better agreement with the pressure

drop calculations down the motor port than between the standard $\kappa-\varepsilon$ model and the 2-D code. Figure 34 shows these preliminary calculations for the standard $\kappa-\varepsilon$ model and an adjusted $\kappa-\varepsilon$ model which has not fully converged
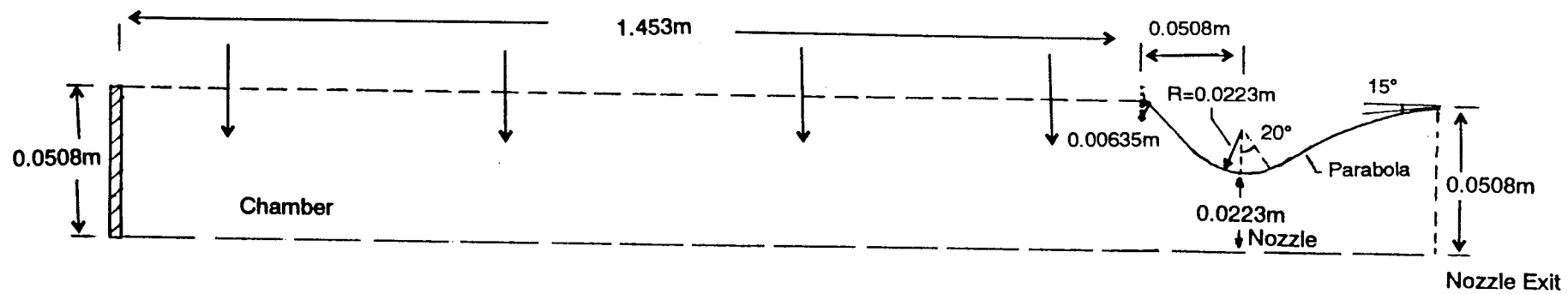
Figure 3. Geometry of the CSD Test Model
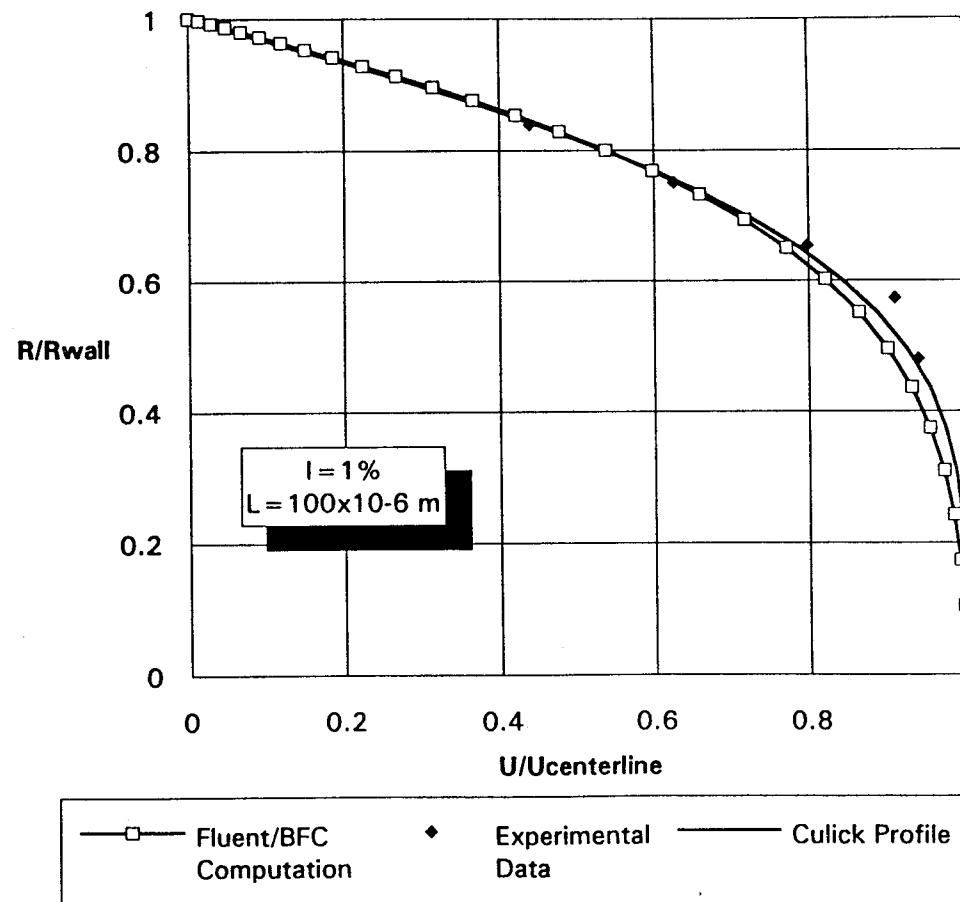
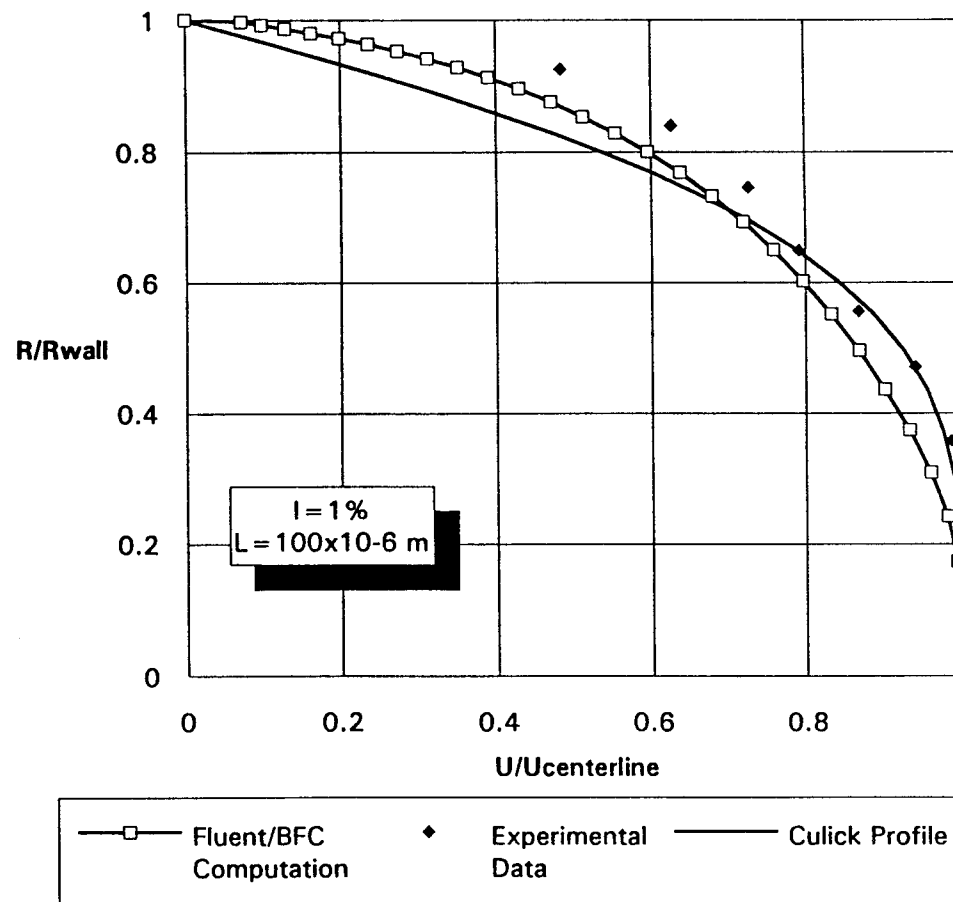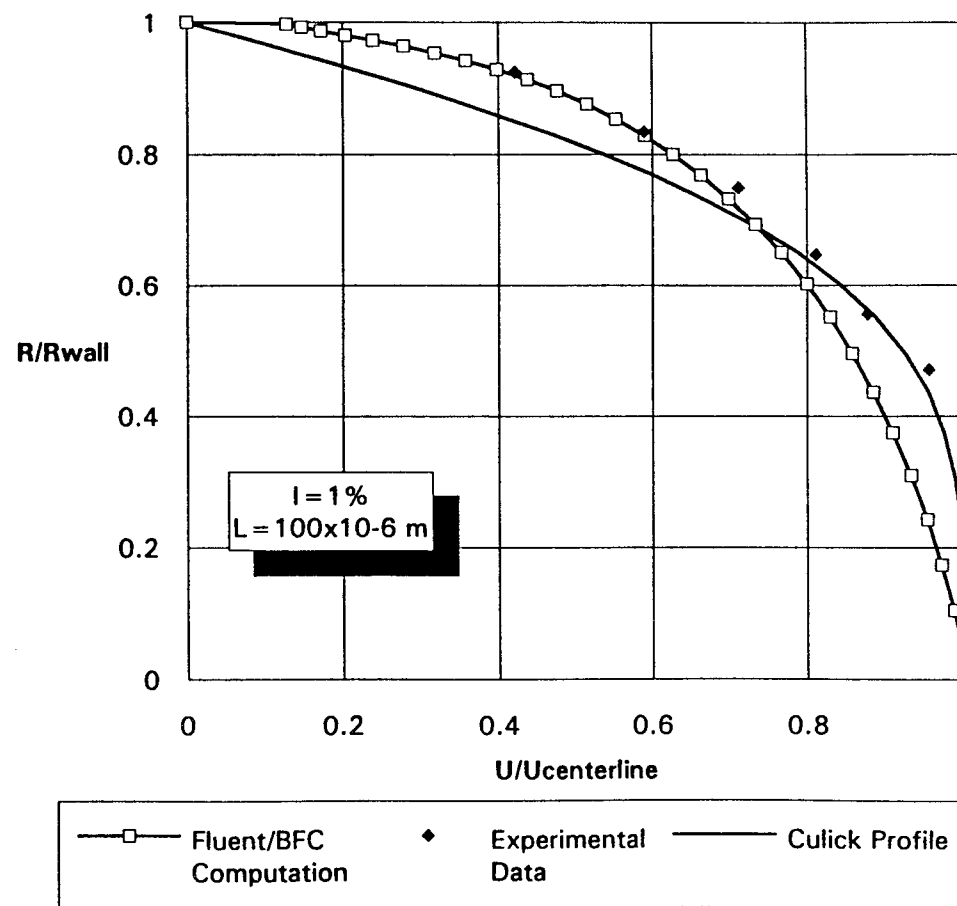# Figure 4. Axial Velocity Profile
L/D = 1.80

R/Rwall

I = 1%
L = 100x10-6 m

U/Ucenterline

─□─ Fluent/BFC Computation   ◆ Experimental Data   ── Culick Profile

Figure 5. Axial Velocity Profile
L/D = 5.46

Chart: X-axis "U/Ucenterline" (0 to 1), Y-axis "R/Rwall" (0 to 1). Inset box: I = 1%, L = 100x10-6 m.

Legend: —□— Fluent/BFC Computation   ◆ Experimental Data   ——— Culick Profile
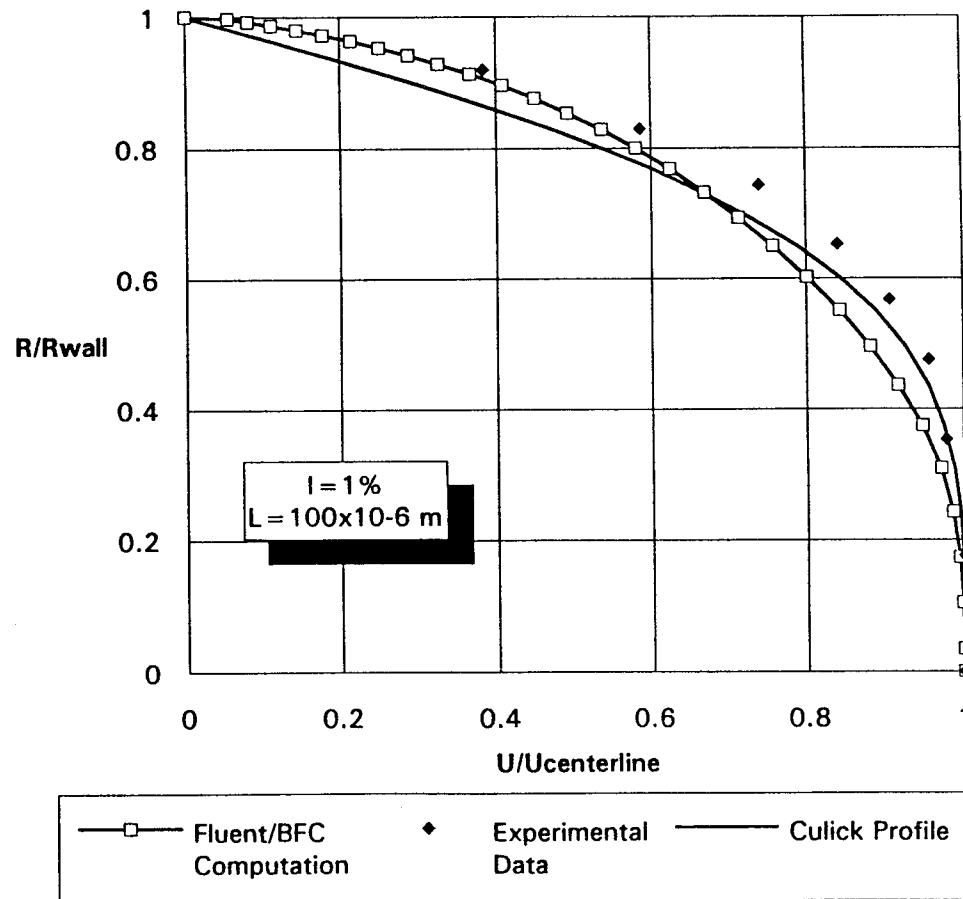
Figure 6. Axial Velocity Profile
L/D = 6.64

I = 1%
L = 100x10-6 m

R/Rwall

U/Ucenterline

—□— Fluent/BFC Computation   ♦ Experimental Data   —— Culick Profile
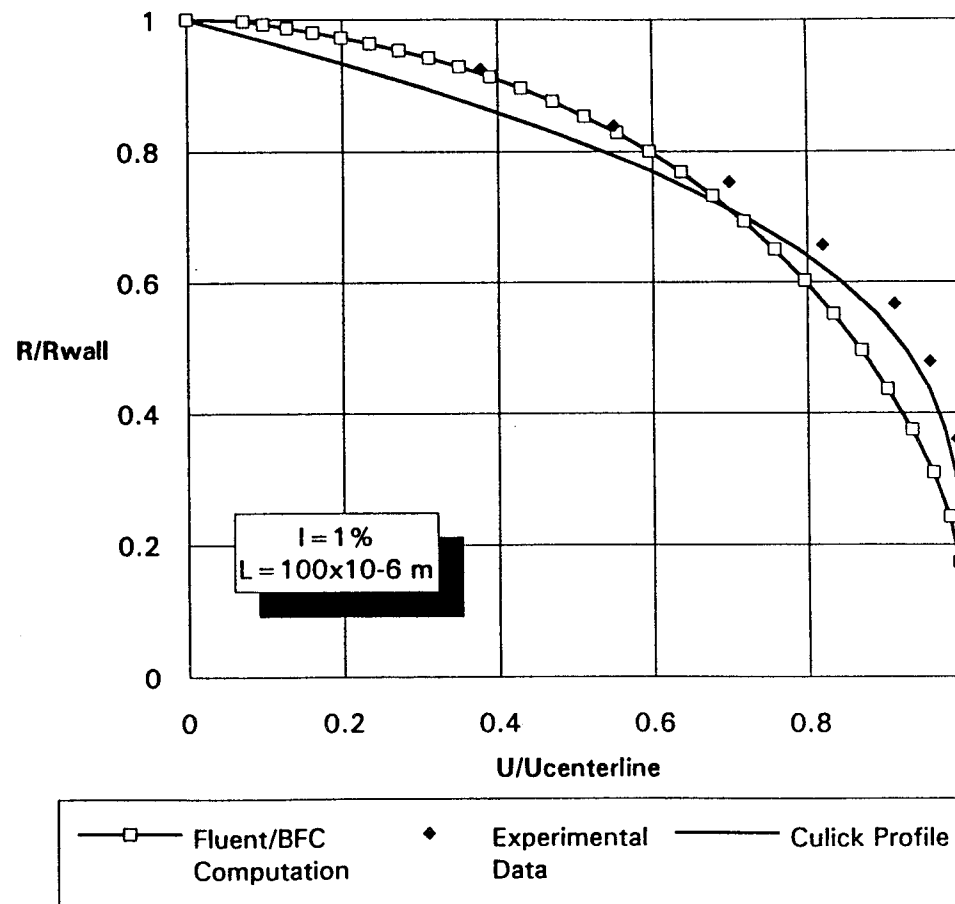
Figure 7. Axial Velocity Profile
L/D = 9.06

I = 1%
L = 100x10-6 m

R/Rwall

U/Ucenterline

—□— Fluent/BFC Computation   ◆ Experimental Data   —— Culick Profile

Figure 8. Axial Velocity Profile
L/D = 10.3

I = 1%
L = 100x10-6 m

R/Rwall

U/Ucenterline

—□— Fluent/BFC Computation   ◆ Experimental Data   —— Culick Profile

Figure 9. Axial Velocity Profile
L/D = 12.75

I = 1%
L = 100x10-6 m

R/Rwall

U/Ucenterline

—□— Fluent/BFC Computation   ◆ Experimental Data   —— Culick Profile
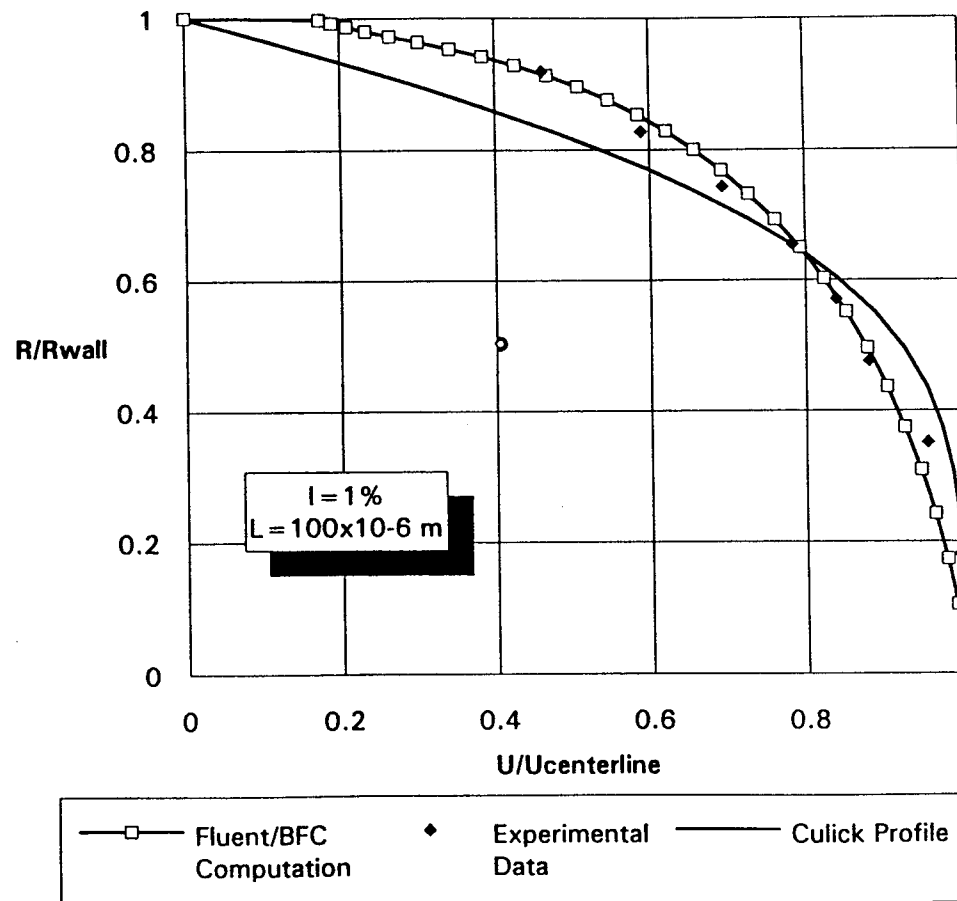
Figure 10. Kinetic Energy of Turbulence L/D = 1.80
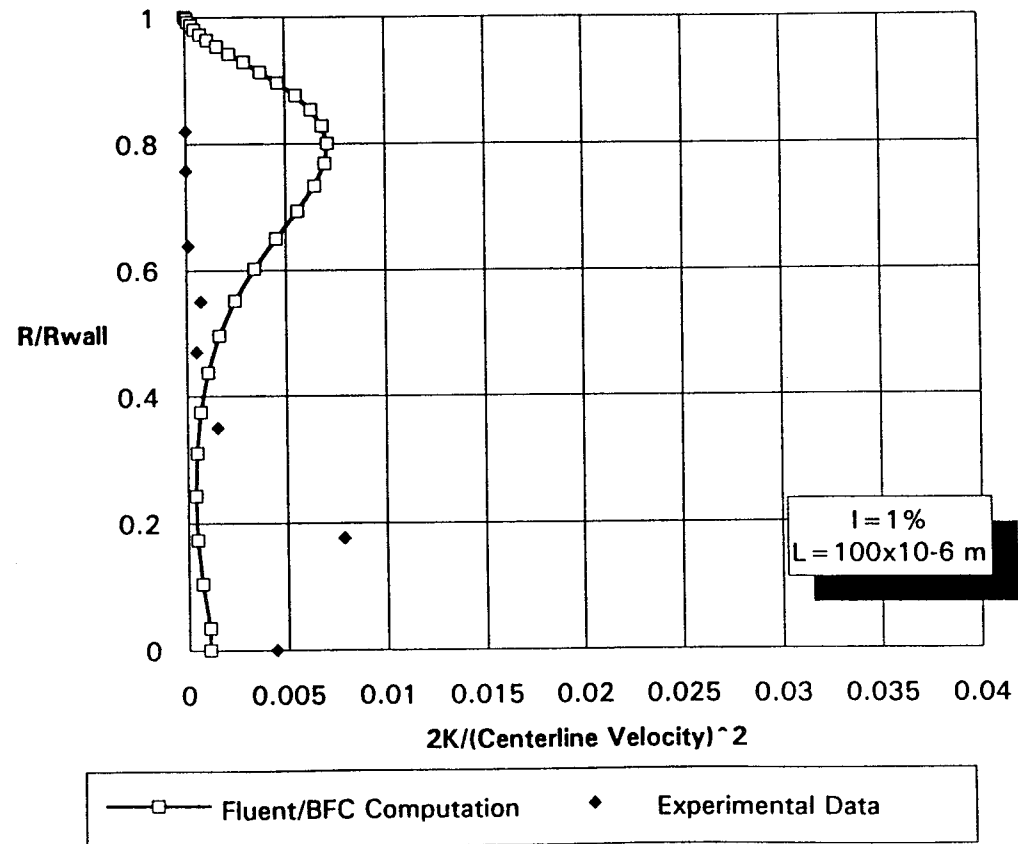
Figure 11. Kinetic Energy of Turbulence
L/D = 5.46

Y-axis: R/Rwall

X-axis: 2K/(Centerline Velocity)^2

Legend box:
I = 1%
L = 100x10-6 m

Legend: —□— Fluent/BFC Computation   ◆ Experimental Data
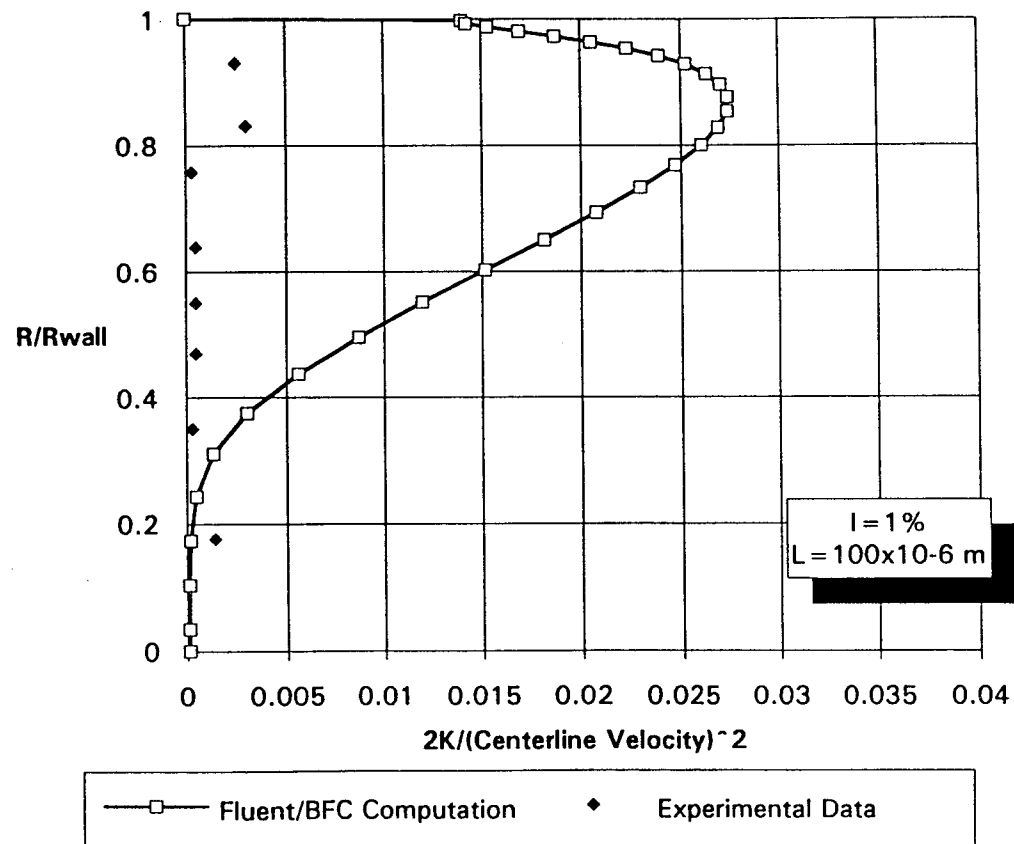
Figure 12. Kinetic Energy of
Turbulence
L/D = 6.64
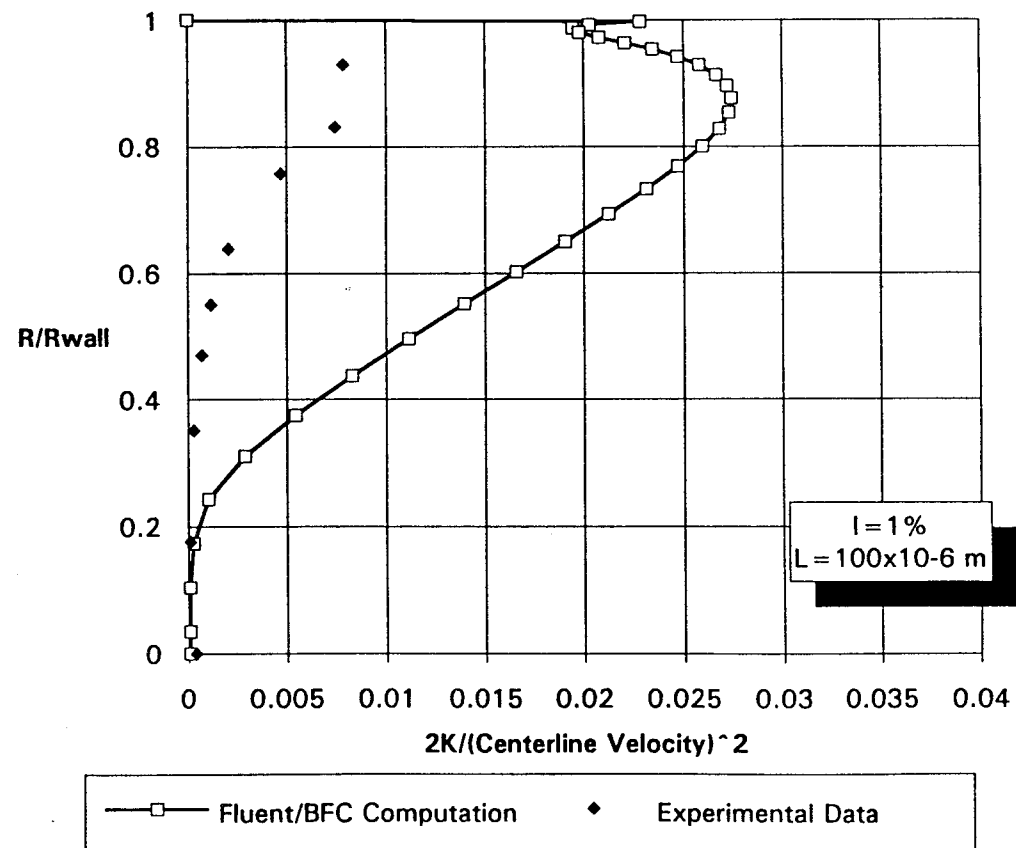
Figure 13. Kinetic Energy of
Turbulence
L/D = 9.06

R/Rwall

2K/(Centerline Velocity)^2

I = 1%
L = 100x10-6 m

Fluent/BFC Computation   ◆   Experimental Data
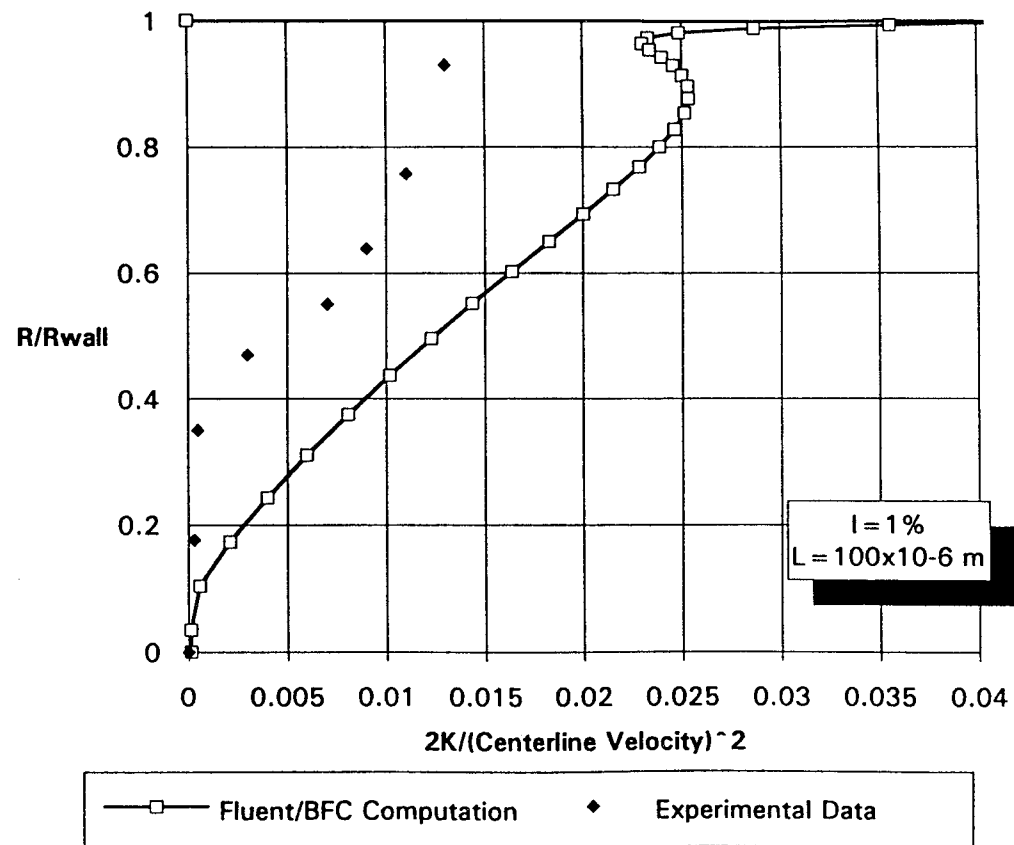
Figure 14. Kinetic Energy of Turbulence
L/D = 10.3

I = 1%
L = 100x10-6 m

R/Rwall

2K/(Centerline Velocity)^2

———□——— Fluent/BFC Computation   ◆   Experimental Data
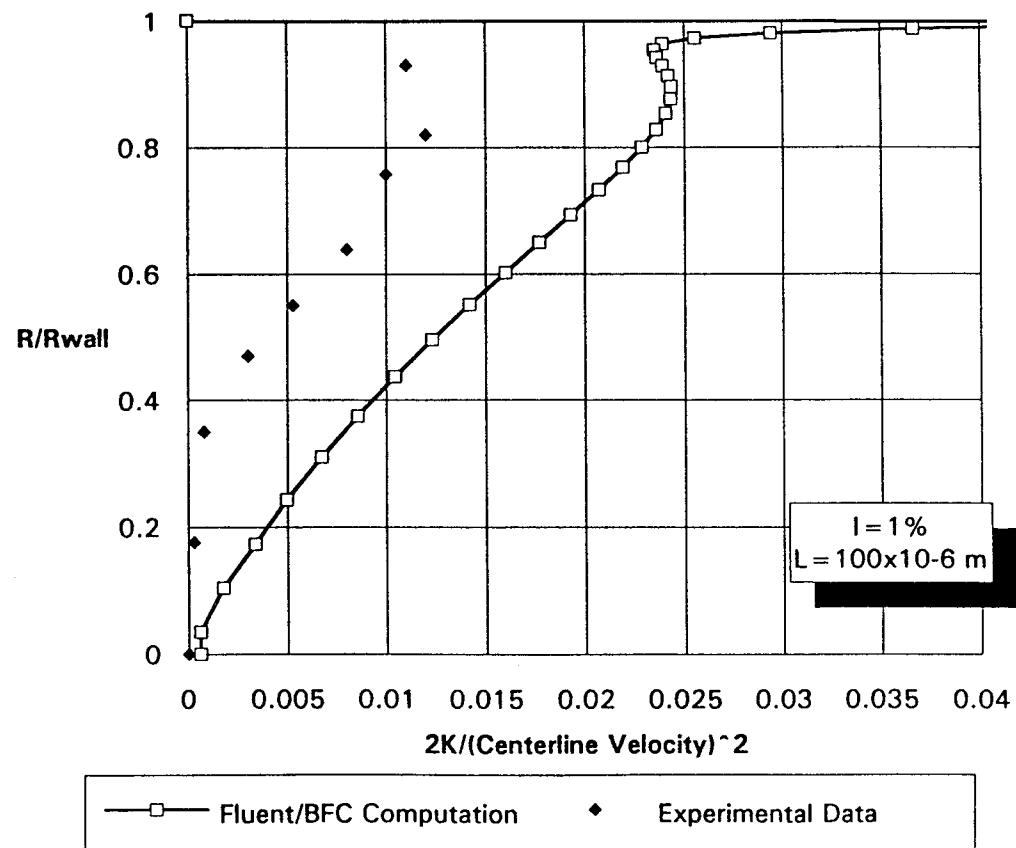
Figure 15. Kinetic Energy of Turbulence L/D = 12.75
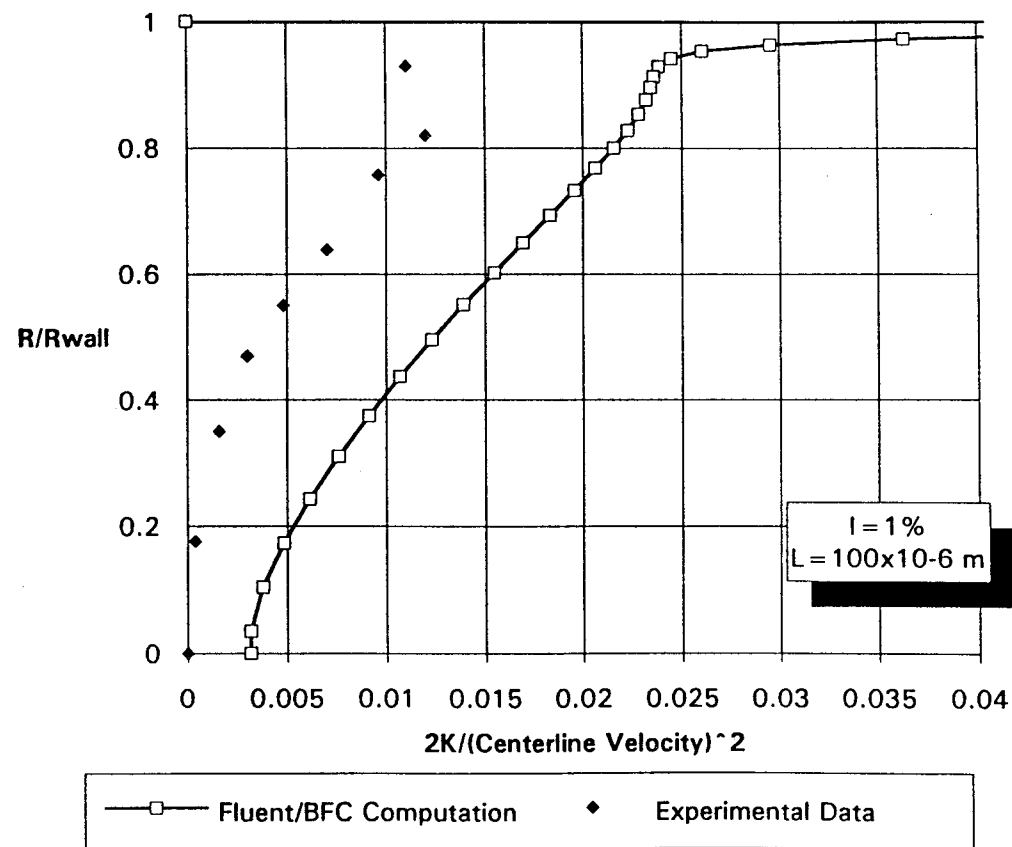
Figure 16. Axial Velocity Profile
L/D = 1.80

R/Rwall

I = 100%
L = 100×10-6 m

U/Ucenterline

─────□───── Fluent/BFC   ◆   Experimental   ─────────── Culick Profile
Computation   Data
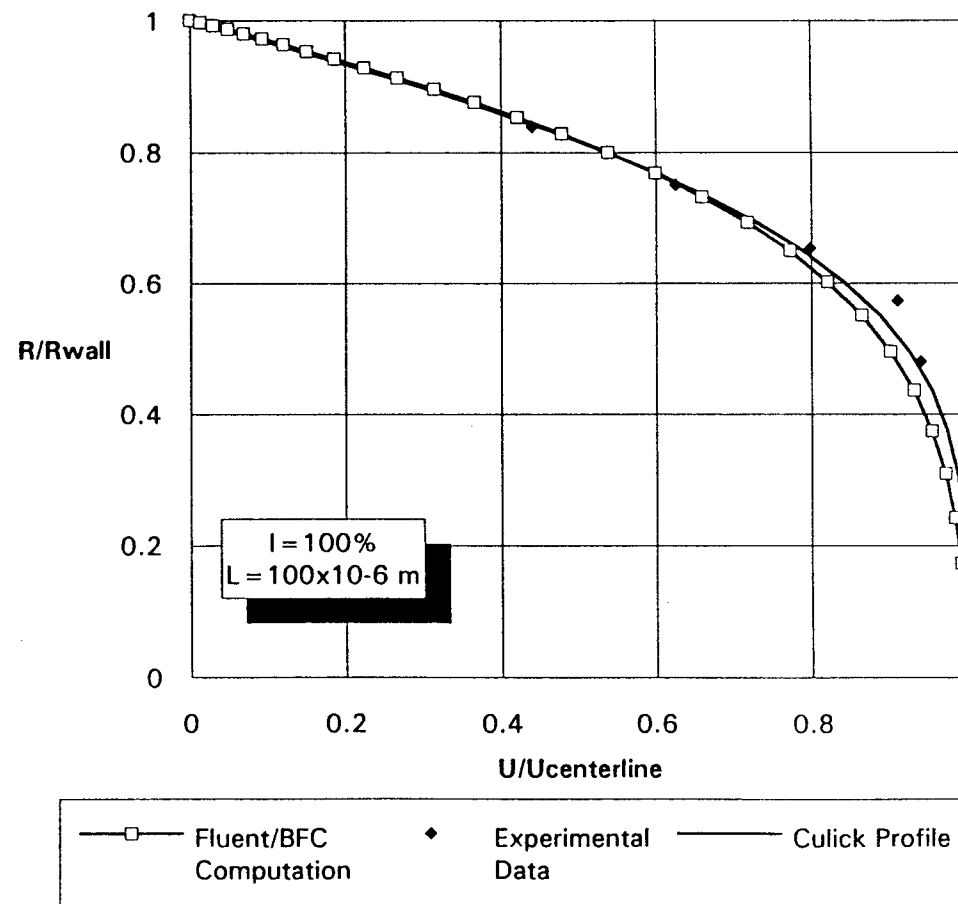
Figure 17. Axial Velocity Profile
L/D = 5.46

I = 100%
L = 100x10-6 m

R/Rwall

U/Ucenterline

Fluent/BFC Computation   ◆ Experimental Data   Culick Profile
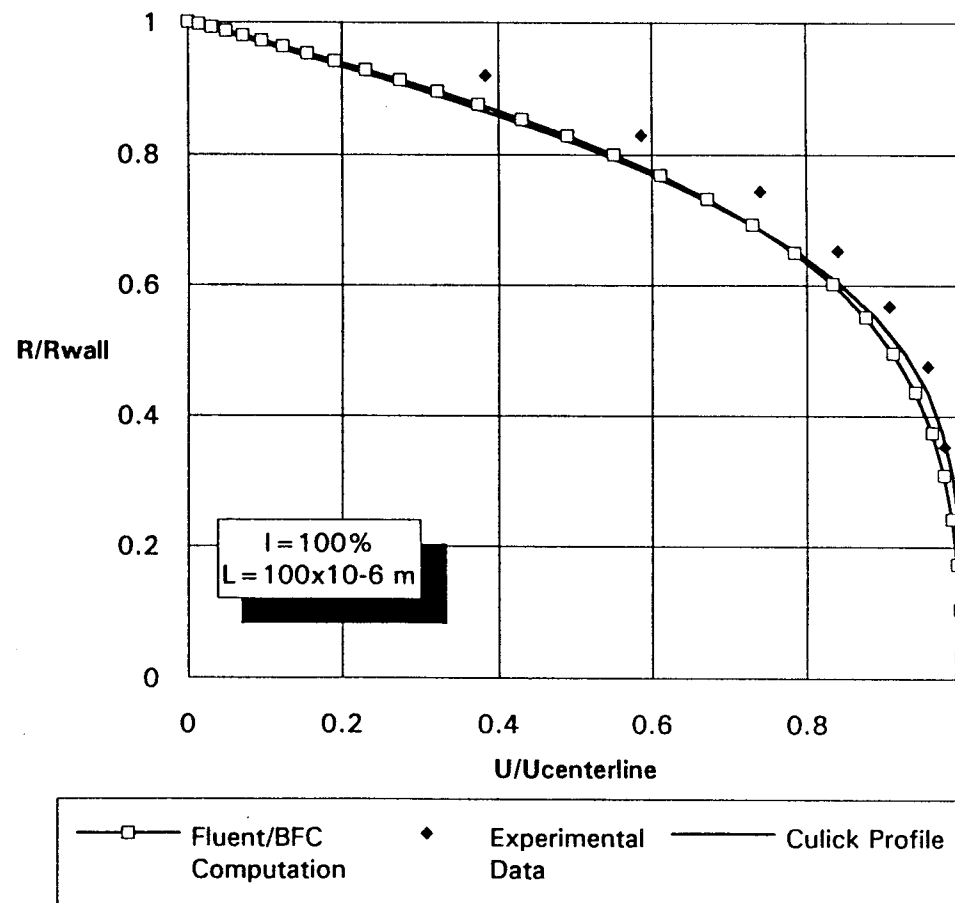
Figure 18. Axial Velocity Profile
L/D = 6.64
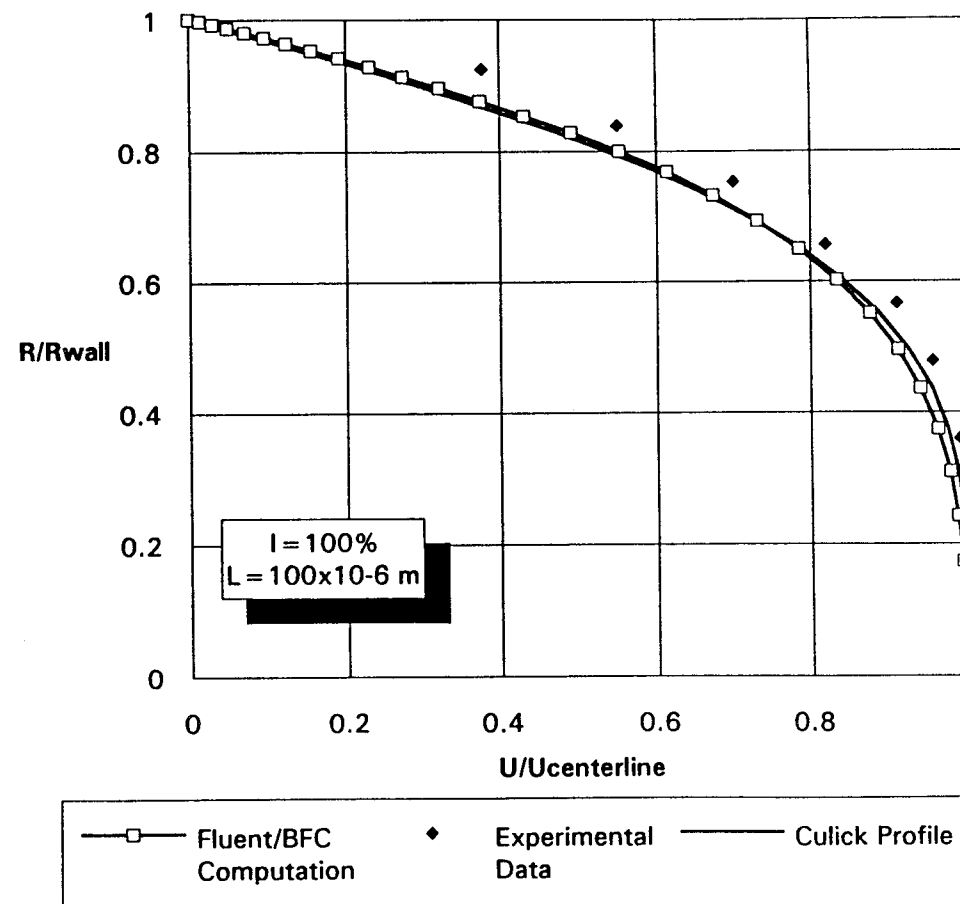
Figure 19. Axial Velocity Profile
L/D = 9.06

R/Rwall

I = 100%
L = 100x10-6 m

U/Ucenterline

—□— Fluent/BFC
Computation   ◆   Experimental
Data   ——— Culick Profile
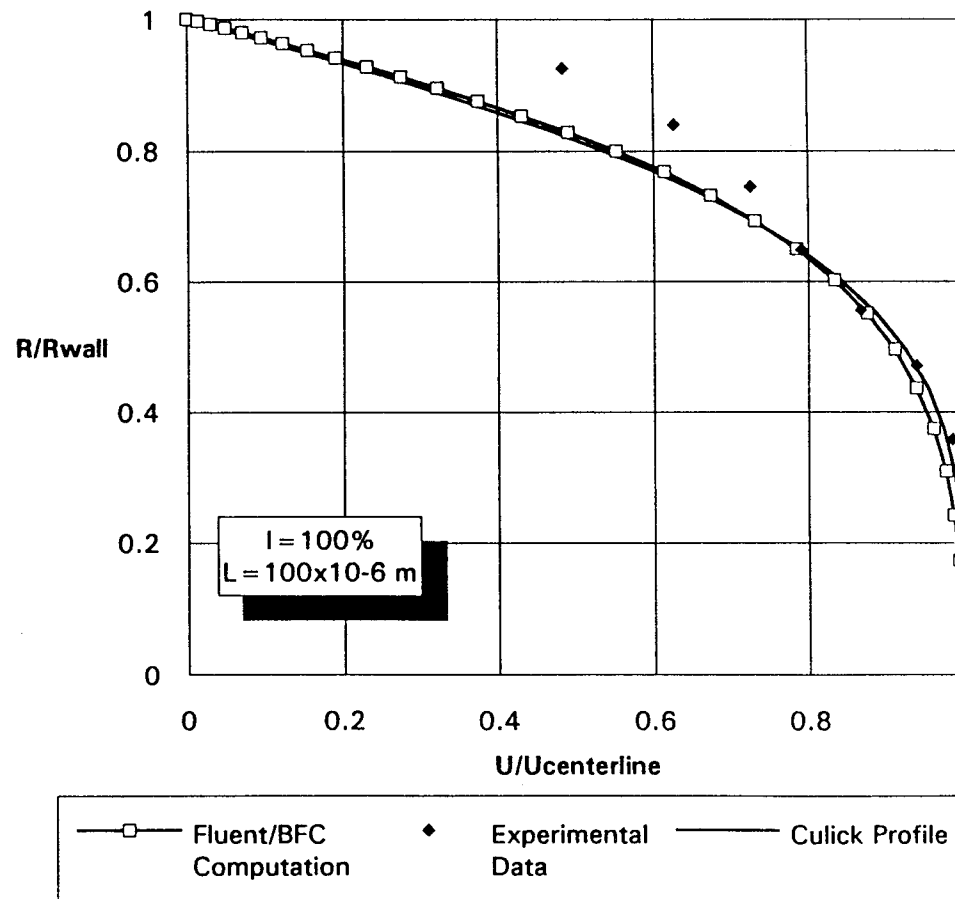
Figure 20. Axial Velocity Profile
L/D = 10.3

I = 100%
L = 100x10-6 m

R/Rwall

U/Ucenterline

—□— Fluent/BFC Computation   ◆ Experimental Data   ——— Culick Profile
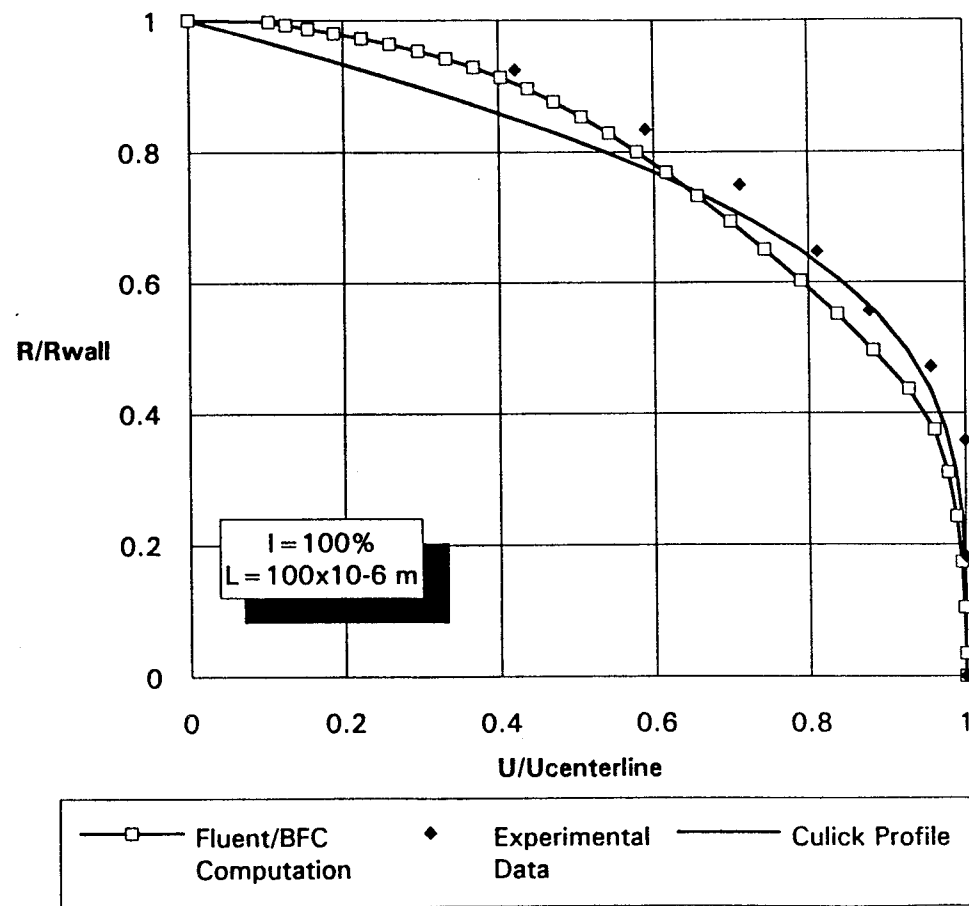
Figure 21. Axial Velocity Profile
L/D = 12.75

I = 100%
L = 100x10-6 m

R/Rwall

U/Ucenterline

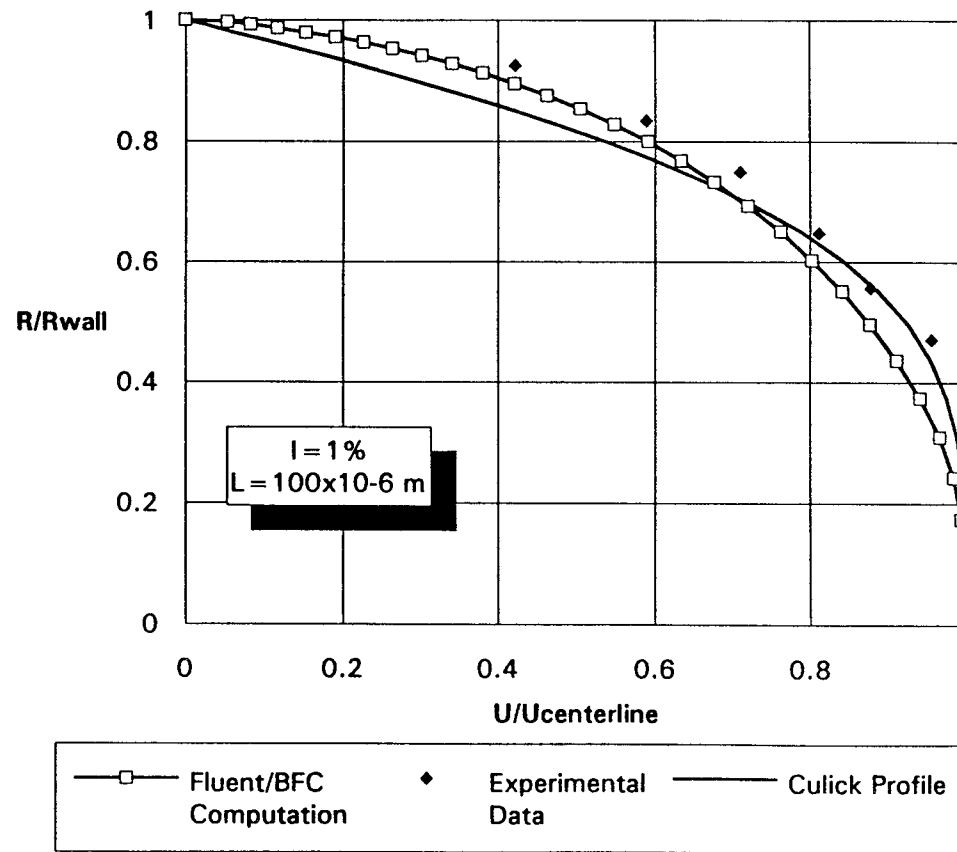☐ Fluent/BFC Computation ◆ Experimental Data ─── Culick Profile
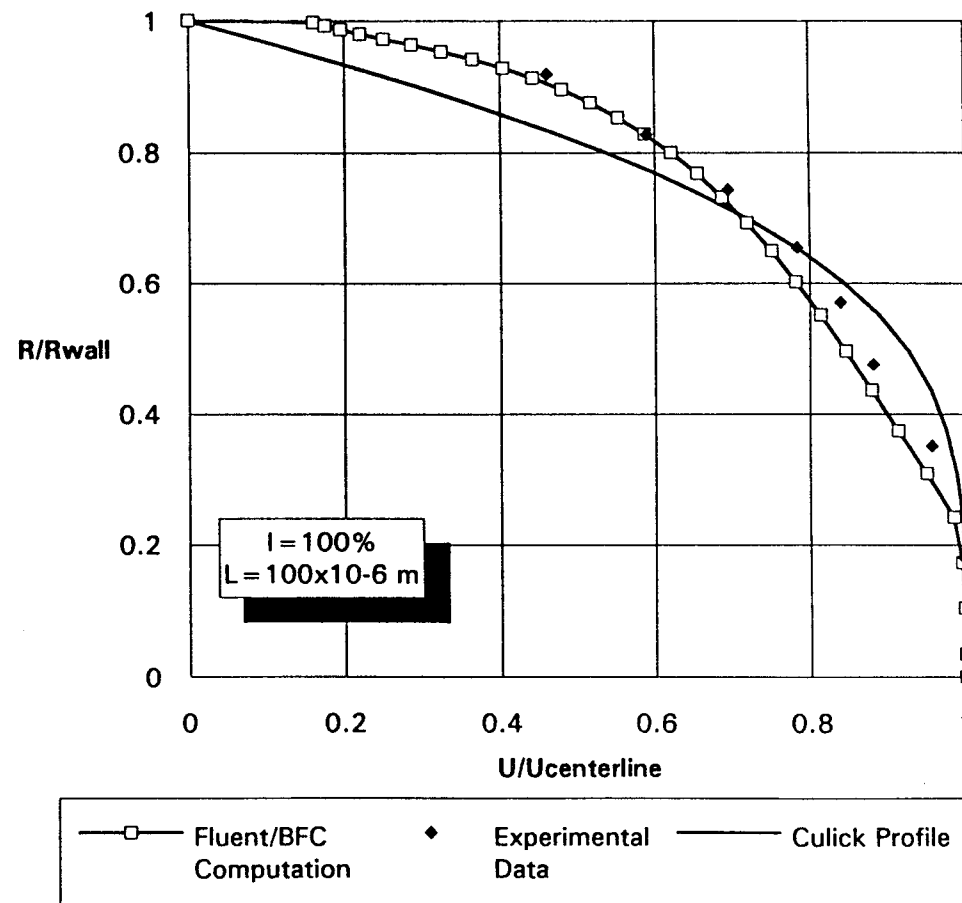
Figure 22. Axial Velocity Profile
L/D = 1.80
Adjusted k-e

I = 1%
L = 100x10-6 m

R/Rwall

U/Ucenterline

——□—— Fluent/BFC
Computation

◆ Experimental
Data

——— Culick Profile
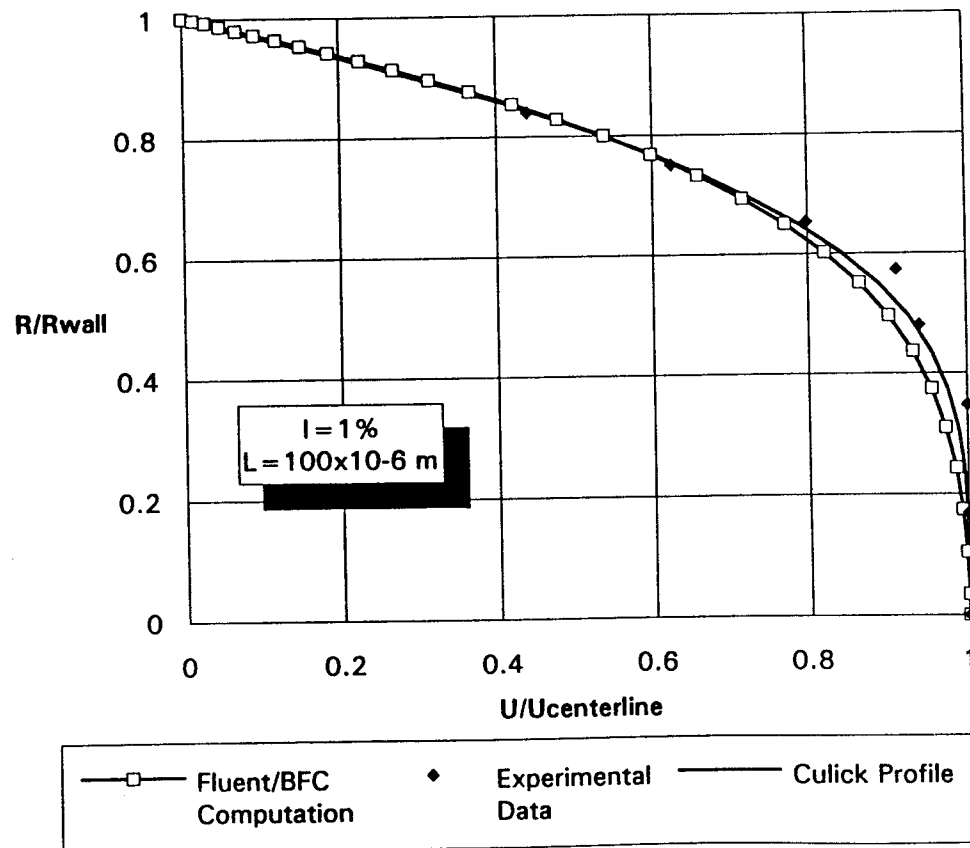
Figure 23. Axial Velocity Profile
L/D = 5.46
Adjusted k-e

I = 1%
L = 100x10-6 m

R/Rwall

U/Ucenterline

———□——— Fluent/BFC Computation   ◆ Experimental Data   ——————— Culick Profile
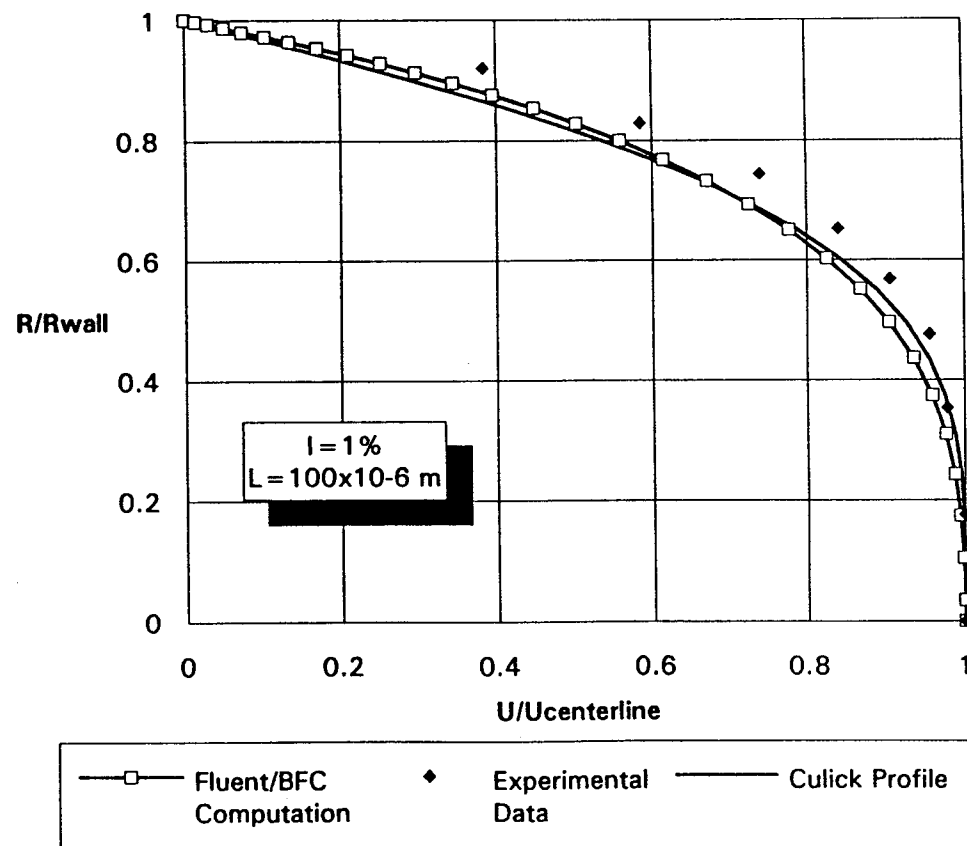
Figure 24. Axial Velocity Profile
L/D = 6.64
Adjusted k-e
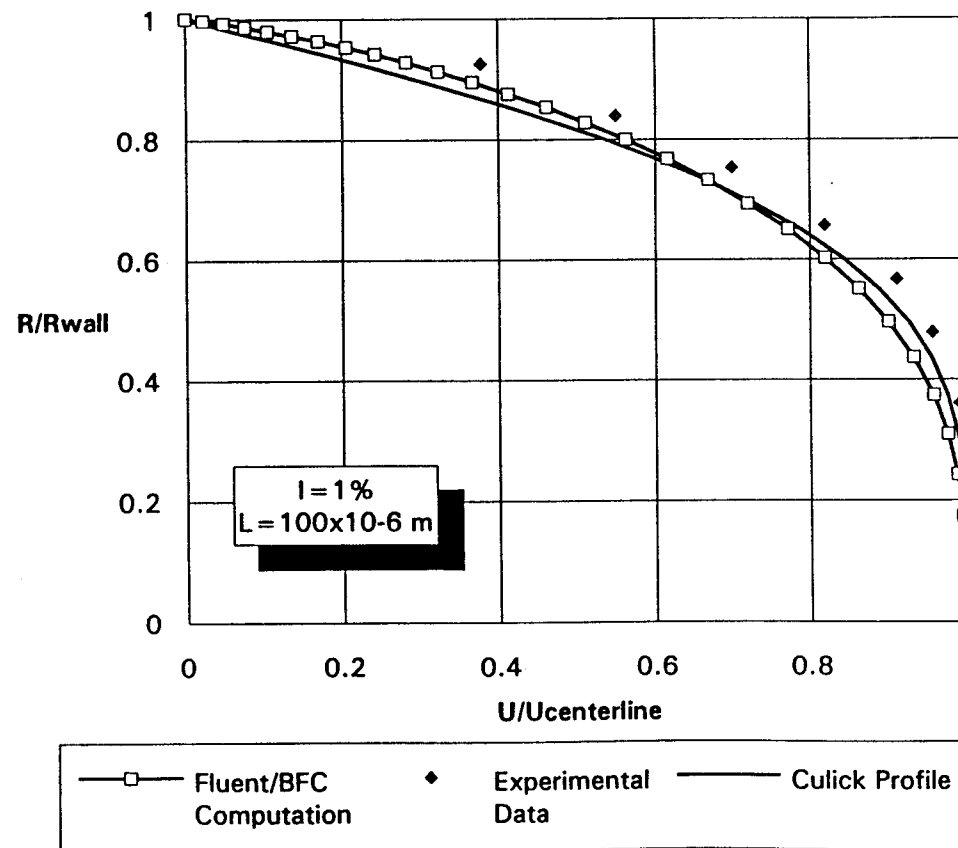
Figure 25. Axial Velocity Profile
L/D = 9.06
Adjusted k-e
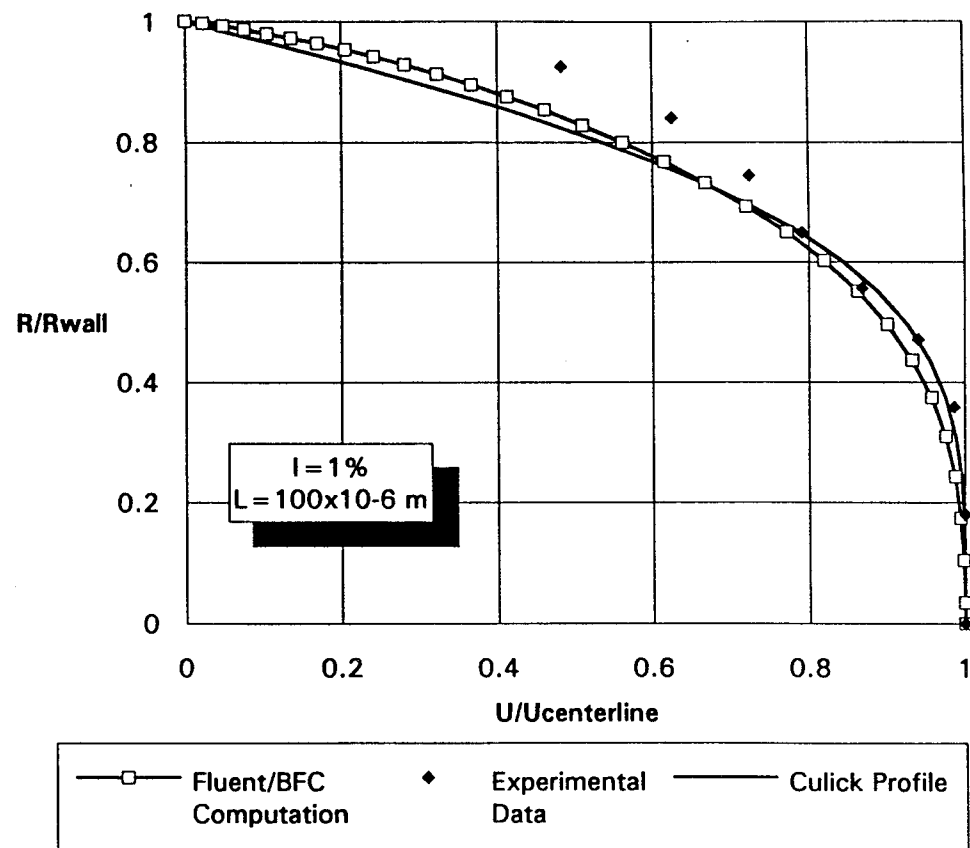
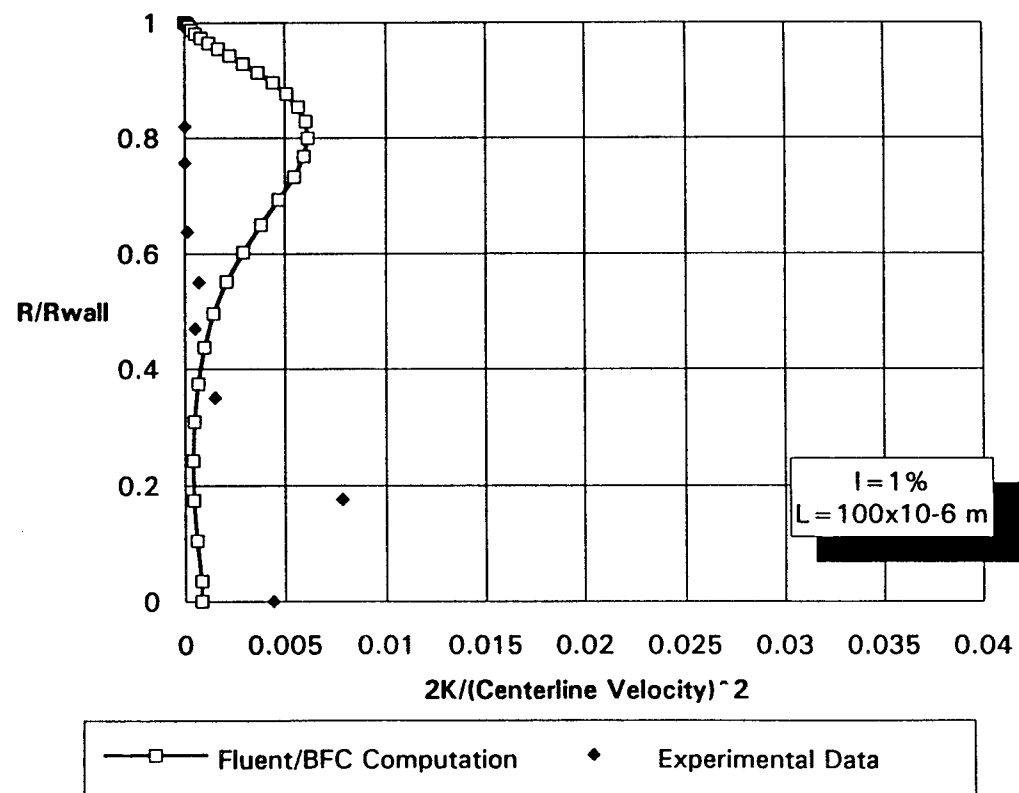# Figure 26. Axial Velocity Profile
L/D = 10.3
Adjusted k-e

Legend:
- □ Fluent/BFC Computation
- ◆ Experimental Data
- —— Culick Profile

Axis labels: R/Rwall (vertical), U/Ucenterline (horizontal)

Inset:
I = 1%
L = 100x10-6 m

Figure 27. Axial Velocity Profile
L/D = 12.75
Adjusted k-e

I = 1%
L = 100x10-6 m

R/Rwall

U/Ucenterline

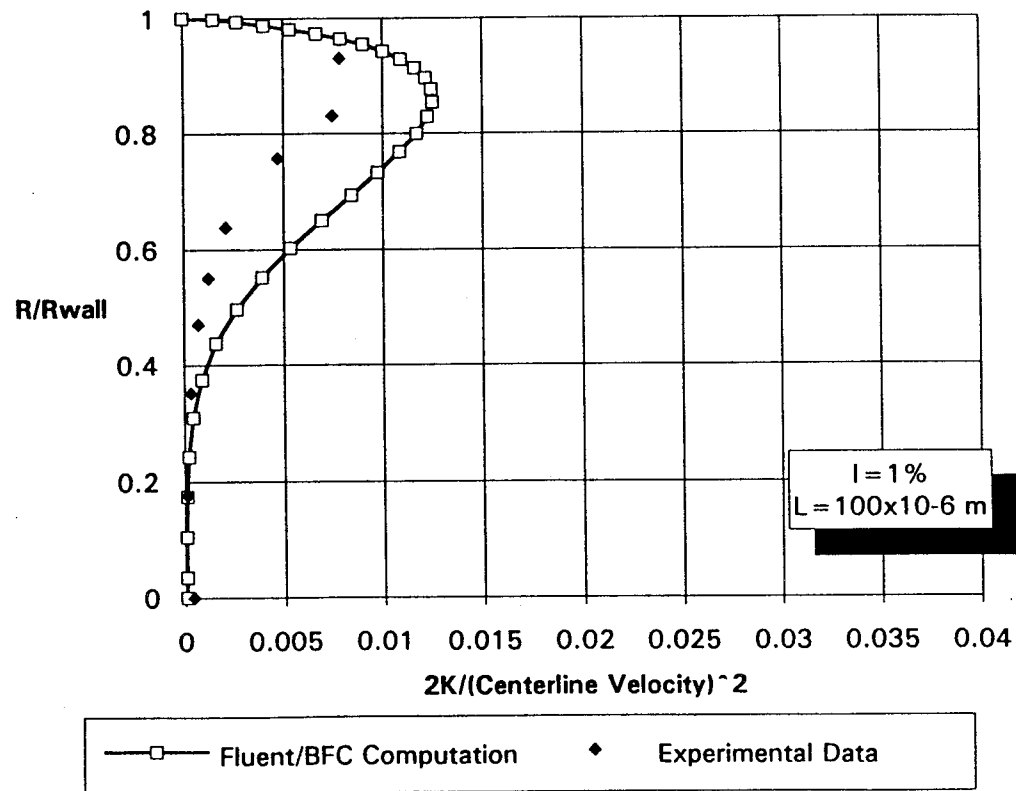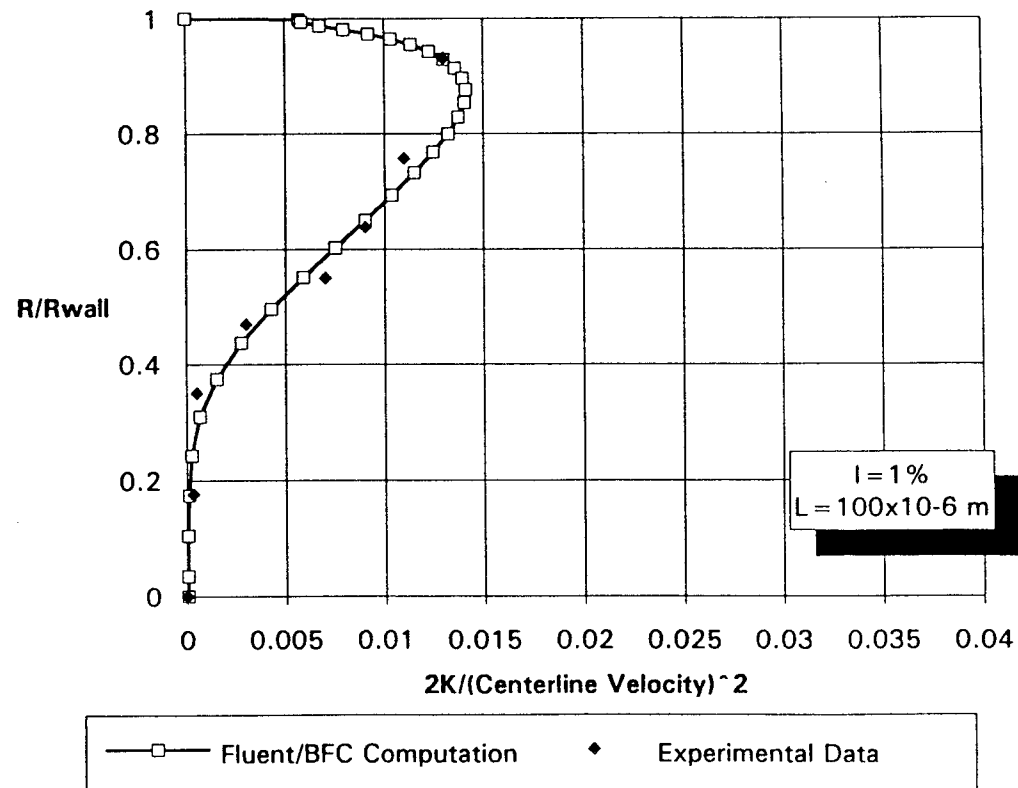| —□— Fluent/BFC Computation | ♦ Experimental Data | —— Culick Profile |
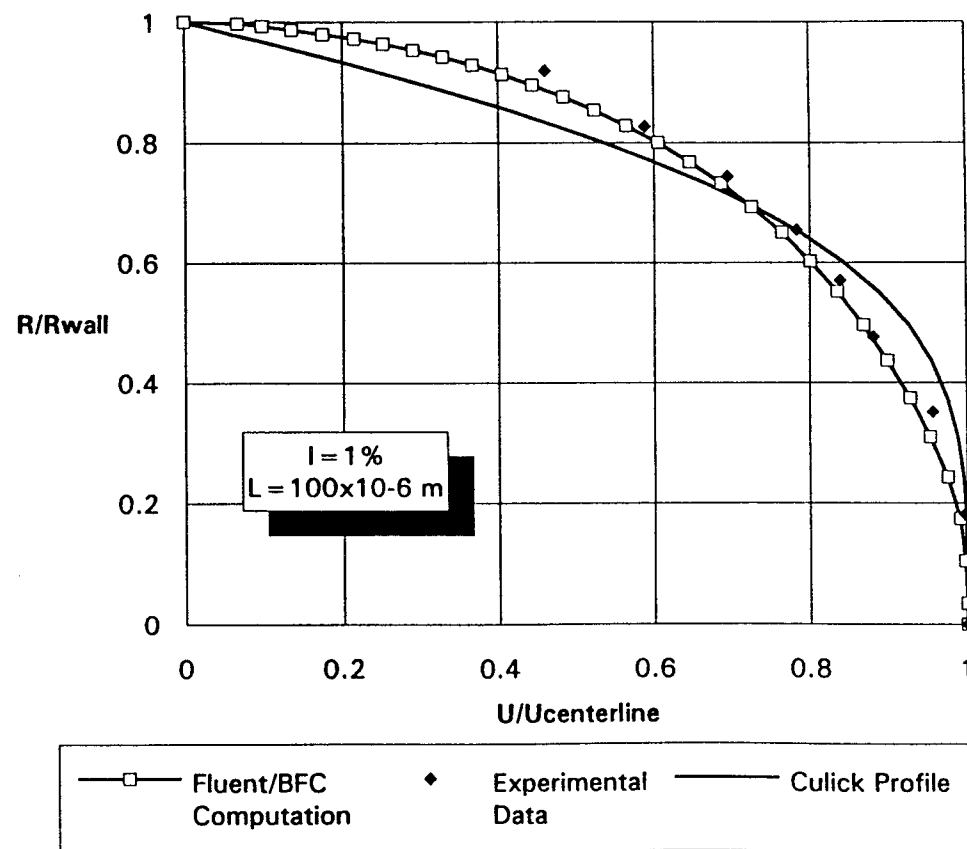
Figure 28. Kinetic Energy of Turbulence L/D = 1.80 Adjusted k-e

Figure 29. Kinetic Energy of Turbulence
L/D = 5.46
Adjusted k-e

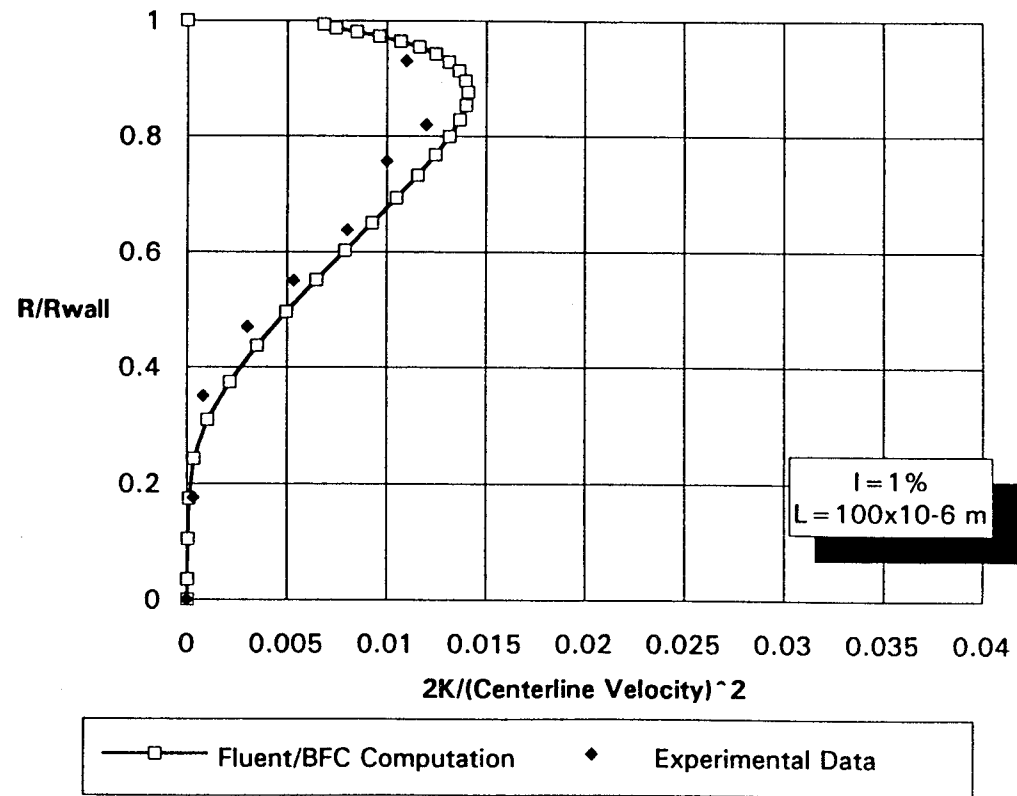2K/(Centerline Velocity)^2

R/Rwall

I = 1%
L = 100x10-6 m

──□── Fluent/BFC Computation   ◆   Experimental Data
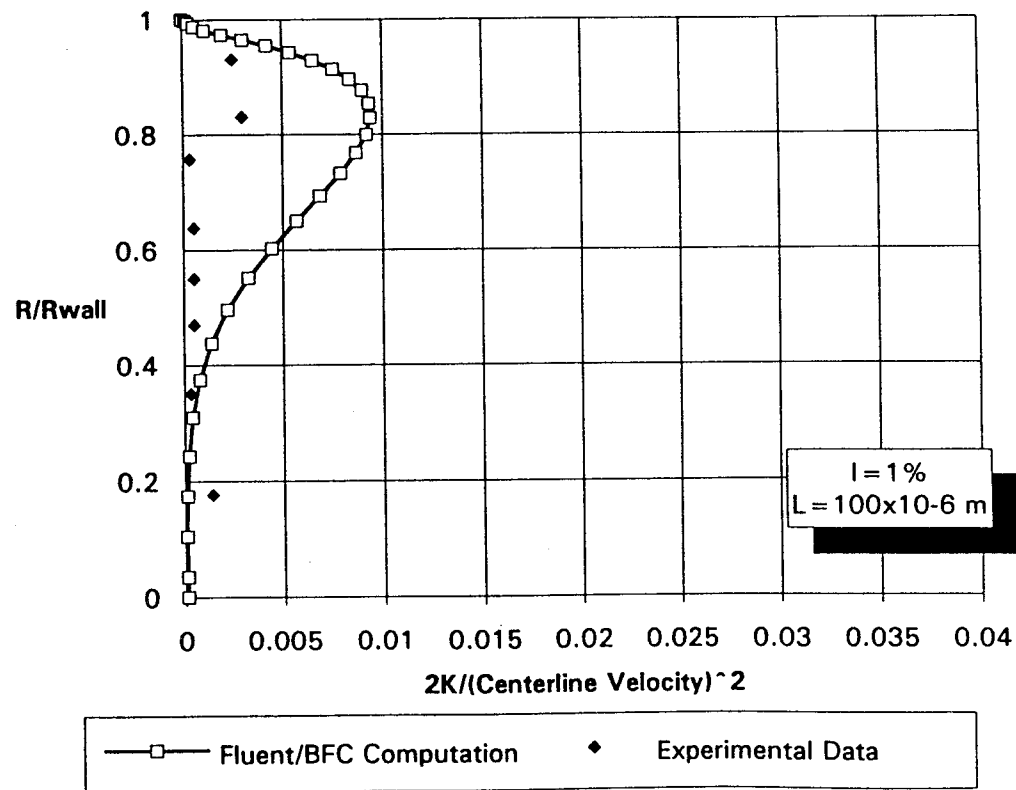
Figure 30. Kinetic Energy of
Turbulence
L/D = 6.64
Adjusted k-e

Figure 31. Kinetic Energy of Turbulence
L/D = 9.06
Adjusted k-e

Legend: Fluent/BFC Computation ◆ Experimental Data

Chart axes: R/Rwall (vertical), 2K/(Centerline Velocity)^2 (horizontal)

Box label: I = 1% L = 100x10-6 m
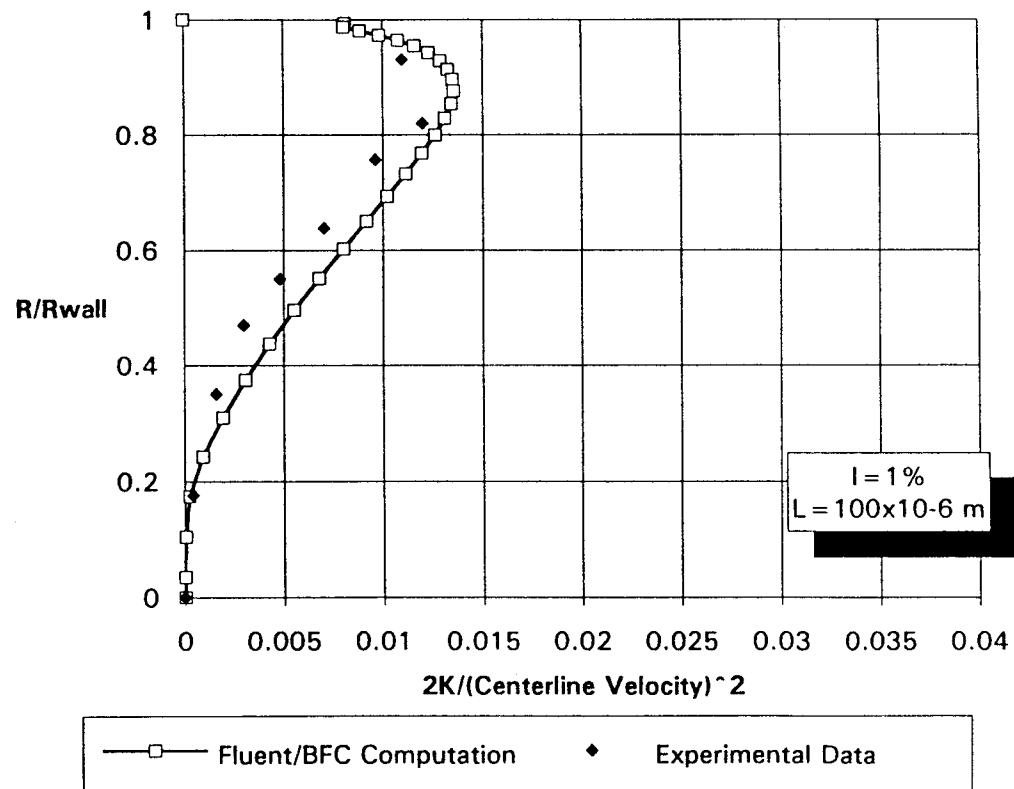
Figure 32. Kinetic Energy of
Turbulence
L/D = 10.3
Adjusted k-e

Figure 33. Kinetic Energy of
Turbulence
L/D = 12.75
Adjusted k-e

Figure 34. Axial Static Pressure Distribution Technology Model

Pressure (psia) vs. Axial Distance (inches)

Legend:
- – – – Standard k-e
- · · · · · · Adjusted k-e
- ——— 2-D (Culick Profile)